

Florida Institute of Technology

Scholarship Repository @ Florida Tech

---

Theses and Dissertations

---

7-2015

## Analysis of Angular Momentum in Planetary Systems and Host Stars

Stacy Ann Irwin

Follow this and additional works at: <https://repository.fit.edu/etd>



Part of the [Astrophysics and Astronomy Commons](#)

---

# Analysis of Angular Momentum in Planetary Systems and Host Stars

by

Stacy Ann Irwin

Bachelor of Science, Computer Science  
University of Houston  
2000

Master of Science, Space Sciences  
Florida Institute of Technology  
2009

A dissertation  
submitted to the College of Science at  
Florida Institute of Technology  
in partial fulfillment of the requirements  
for the degree of

Doctor of Philosophy  
in  
Space Sciences

Melbourne, Florida  
July 2015

© Copyright 2015 Stacy Ann Irwin  
All Rights Reserved

The author grants permission to make single copies

---

We the undersigned committee hereby recommend that the attached document  
be accepted as fulfilling in part the requirements for the degree of  
Doctor of Philosophy in Space Sciences.

“Analysis of Angular Momentum  
in Planetary Systems and Host Stars,”  
a dissertation by Stacy Ann Irwin

---

Samuel T. Durrance, Ph.D.  
Professor, Physics and Space Sciences  
Major Advisor

---

Daniel Batcheldor, Ph.D.  
Associate Professor, Physics and Space Sciences  
Committee Member

---

Darin Ragozzine, Ph.D.  
Assistant Professor, Physics and Space Sciences  
Committee Member

---

Semen Koksai, Ph.D.  
Professor, Mathematical Sciences  
Outside Committee Member

---

Daniel Batcheldor, Ph.D.  
Professor, Physics and Space Sciences  
Department Head

# Abstract

## Analysis of Angular Momentum in Planetary Systems and Host Stars

by Stacy Ann Irwin

Dissertation Advisor: Samuel T. Durrance, Ph.D.

The spin angular momentum of single Main Sequence stars has long been shown to follow a primary power law of stellar mass,  $J \propto M^\alpha$ , excluding stars of  $<2$  solar masses. Lower mass stars rotate more slowly with and have smaller moments of inertia, and as a result they contain much less spin angular momentum. A secondary power law describes the upper bound of angular momenta of these less massive stars with a steeper slope. The Solar System's orbital angular momentum, however, is of the same order of magnitude as the primary law, whereas the Sun's spin angular momentum is consistent with the secondary relationship. This suggests that planets are an important clue to answering questions about stellar angular momentum loss and transfer. With recent advances in exoplanet discovery and characterization, the angular momenta of exoplanetary systems can now be determined. A method is developed to calculate planetary system angular momenta from the spin and orbital angular momenta of a sample including 426 host stars and 532 planets. To maximize the size of the working sample, systems discovered by both the transit and radial velocity methods are included, and the biases of both techniques are identified. Self-consistent stellar moment of inertia parameters are interpolated from grids of stellar evolutionary models.

Main Sequence host stars range from 0.6 to 1.7 solar masses, and their angular momenta are shown to agree well with previous studies of stellar angular momentum, generally falling on or below the appropriate power law, and exhibiting detection method biases. The systems' angular momenta, including both the planetary orbital and stellar spin components, are widely spread above and below the primary power law, but on average agree well with the primary relationship. The results indicate that the primary power law describes angular momenta of stars of  $<2$  solar masses well, when planetary angular momentum is included. This relationship also holds across host star evolutionary classifications.

For 90% of the systems, the angular momentum contained in the planets is greater than the spin angular momentum of the host star, a characteristic shared by the Solar System. Undetected planets contribute significant bias to the system angular momentum as well as to the proportion of angular momentum contained in the planets. This bias is used to identify systems which are likely to harbor additional planets in already known planetary systems, assuming the Solar System's proportions are typical.

# Contents

List of Figures	ix
List of Tables	xi
List of Symbols, Constants, and Abbreviations	xii
Acknowledgements	xv
<b>1 Introduction</b>	<b>1</b>
1.1 Stellar Mass, Rotation, and Angular Momentum . . . . .	1
1.1.1 An Angular Momentum Puzzle . . . . .	2
1.1.2 The Kraft Curve . . . . .	6
1.1.3 Commonalities . . . . .	8
1.2 Star Formation and Angular Momentum Loss . . . . .	13
1.3 The Solar System and Exoplanetary Systems . . . . .	18
1.4 Motivations and Goals . . . . .	24
<b>2 Method</b>	<b>27</b>

2.1	Angular Momentum Defined . . . . .	27
2.2	Angular Momentum and Specific Angular Momentum . . . . .	29
2.3	Stars and Spin Angular Momentum . . . . .	32
2.3.1	Angular Velocity . . . . .	33
2.3.2	Moment of Inertia . . . . .	36
2.4	Planets and Orbital Angular Momentum . . . . .	41
2.5	Planetary Systems . . . . .	44
2.6	Biases . . . . .	47
<b>3</b>	<b>Data</b>	<b>49</b>
3.1	Planet Discovery Techniques . . . . .	49
3.1.1	Overview . . . . .	49
3.1.2	Detection Method Biases: RV and Transit . . . . .	54
3.2	Sources and Selection . . . . .	54
3.3	The Exoplanet Orbit Database . . . . .	58
3.4	Data Cleaning . . . . .	60
3.4.1	Inclusions and Exclusions . . . . .	61
3.4.2	Corrections and Conflicts . . . . .	61
3.4.3	Missing Data . . . . .	63
3.4.4	Other Adjustments . . . . .	65
3.5	Stellar Classification . . . . .	66
3.6	Stellar Properties . . . . .	71
3.7	Planetary Properties . . . . .	74

<b>4</b>	<b>Results and Discussion</b>	<b>78</b>
4.1	Quantified Angular Momentum . . . . .	78
4.1.1	About the Plots . . . . .	78
4.1.2	Stars . . . . .	81
4.1.3	System Totals . . . . .	85
4.1.4	Fitting the Kraft Relation . . . . .	88
4.1.5	Discussion . . . . .	92
4.2	System Distribution of $J$ . . . . .	98
4.2.1	$\mathcal{L}$ and $K$ . . . . .	98
4.2.2	Toward Determination of System Completeness . . . . .	103
4.3	Biases . . . . .	107
<b>5</b>	<b>Summary, Conclusions, and Suggestions for Future Work</b>	<b>112</b>
5.1	Summary . . . . .	113
5.2	Conclusions . . . . .	115
5.3	Suggestions for Future Work . . . . .	117
<b>A</b>	<b>Appendix A: Stellar Inertial Models</b>	<b>120</b>
A.1	PKD Models . . . . .	121
A.2	CG Models . . . . .	125
A.3	Comparison of PKD and CG Models . . . . .	129
A.4	Claret (2004) Models . . . . .	131

<b>B Appendix B: Treatment of Uncertainties and Error Propagation</b>	<b>134</b>
<b>C Appendix C: Stellar Properties</b>	<b>137</b>
<b>D Appendix D: Planetary Properties</b>	<b>148</b>
<b>E Appendix E: System Properties</b>	<b>162</b>

# List of Figures

1.1	Rotation of Low-mass Stars . . . . .	2
1.2	McNally j-M Plot . . . . .	4
1.3	Carrasco et al. j-M Plot . . . . .	6
1.4	Kraft j-M Plot . . . . .	8
1.5	Kawaler J-M Plot . . . . .	9
1.6	McNally and Kawaler J-M Plot . . . . .	10
1.7	Wolff et al. Plots . . . . .	12
1.8	Alves et al. Plots . . . . .	21
1.9	Paz-Chinchón et al. Plots . . . . .	23
2.1	CG $\log m$ and $\log \beta$ . . . . .	39
3.1	Planet Discoveries by Year . . . . .	53
3.2	Planet Mass and Semi-major Axis . . . . .	55
3.3	HR Diagrams . . . . .	70
3.4	Stellar Mass Distribution . . . . .	72
3.5	Host Star Metallicity Distributions . . . . .	73

3.6	Planet Mass Distribution . . . . .	75
4.1	J-M Model . . . . .	79
4.2	$J_*$ Sample Histogram . . . . .	81
4.3	$J_*$ Histograms . . . . .	82
4.4	$J_*$ Results: MS and Non-MS . . . . .	83
4.5	$J_*$ Results: RV and Transit . . . . .	84
4.6	$J_{sys}$ Results: MS and Non-MS . . . . .	86
4.7	$J_{sys}$ Results: RV and Transit . . . . .	88
4.8	Binned Results: All Systems . . . . .	96
4.9	Binned Results: Main Sequence . . . . .	97
4.10	$\mathcal{L}$ Histograms . . . . .	98
4.11	$\mathcal{L}$ Histogram: Detection Methods . . . . .	99
4.12	$K$ Histograms . . . . .	100
4.13	Logarithmic $K$ Histogram . . . . .	101
4.14	Angular Momentum of High- $K$ MS Systems . . . . .	104
A.1	PKD Inertial Evolution . . . . .	123
A.2	PKD Interpolation Equation . . . . .	126
A.3	CG Inertial Evolution . . . . .	127
A.4	CG $\log m$ and $\log \beta$ . . . . .	128
A.5	Plot of MS Interpolation Equation from Model Data . . . . .	133
A.6	Evolution of $\gamma$ for Selected Masses . . . . .	133

# List of Tables

1.1	Angular Momentum Distribution of the Solar System . . . . .	19
3.1	EOD Downloaded Fields . . . . .	60
3.2	Summary of Host Star and System Classifications . . . . .	71
3.3	Summary of System Type and Discovery Methods . . . . .	71
4.1	Kraft Relations for Sample Subgroups . . . . .	102
4.2	$K$ Values of Solar System Planets . . . . .	105
4.3	$K$ Values of HD 10180 Planets . . . . .	105
A.1	PKD Model Ages at ZAMS and Mid-MS $\log I$ . . . . .	124
A.2	Interpolated Inertial Coefficient Equations . . . . .	132
C.1	Stellar Parameters . . . . .	138
D.1	Planetary Parameters . . . . .	149
E.1	System Parameters . . . . .	162

# List of Symbols, Constants, and Abbreviations

$\vec{J}, J$	Angular momentum, magnitude
$j$	Specific angular momentum, $j = J/M$
$K$	Planet to system angular momentum ratio ( $J_p/J_{sys}$ )
$\mathcal{L}$	Planet to star angular momentum ratio ( $J_p/J_*$ )
$\mathbf{I}, I$	Inertia tensor, scalar moment of inertia
$\gamma$	Inertial coefficient ( $I/MR^2$ )
$i_*$	Inclination angle (stellar)
$i_p$	Inclination angle (planetary orbit)
$\lambda$	Sky-projected spin-orbit angle
$\psi$	True spin-orbit angle, obliquity
$\vec{\Omega}, \Omega$	Angular velocity, magnitude (stellar)
$\vec{\omega}, \omega$	Angular velocity, magnitude (orbital)
$M$	Stellar mass
$M_\odot$	Solar mass, $1.9891 \cdot 10^{33}$ g

$R$	Stellar radius
$R_{\odot}$	Solar radius, $6.96 \cdot 10^{10}$ cm
$M_J$	Jupiter mass, $1.8986 \cdot 10^{30}$ g
$m$	Planet mass
$m_{\oplus}$	Earth mass, $5.9742 \cdot 10^{27}$ g
$r$	Orbital radius (circular orbit)
$a$	Semi-major axis
AU	Astronomical Unit, $1.496 \cdot 10^{13}$ cm
$e$	Orbital eccentricity
$P$	Orbital period
$R_p$	Planet radius
$R_{\oplus}$	Earth radius, $6.371 \cdot 10^8$ cm
$G$	Gravitational constant, $6.67384 \cdot 10^8$ cm <sup>2</sup> g <sup>-1</sup> s <sup>-2</sup>
$T_{\text{eff}}$	Stellar effective temperature
$T_{\odot}$	Solar effective temperature, 5777 K
$\sigma$	Uncertainty, error
J-M	Angular momentum-Mass
MS	Main Sequence
PMS	Pre-Main Sequence
ZAMS	Zero-Age Main Sequence
EOD	Exoplanet Orbit Database

EPE ExoPlanet Encyclopaedia

KCP Kepler Confirmed Planet table

## *Acknowledgements*

First and foremost, I offer many, many thanks to my Ph.D. committee members, Dr. Daniel Batchelder, Dr. Darin Ragozzine, and Dr. Semen Koksal. I wish to thank Dr. Darin Ragozzine in particular for the several conversations that generated helpful insights and suggestions in the direction of the thesis. Huge thanks to my major advisor, Dr. Samuel Durrance, who gave me this topic and is a big part of why I started (and finished) in the first place.

The life of a Ph.D. student paradoxically requires both sacrifice and selfishness. And unlike a typical physics problem, a Ph.D. cannot be completed in a frictionless vacuum. The road was not always smooth, but it was ever upward, and I was never truly alone. I acknowledge here the many relationships I've had during my journey. People who supported me through the long days, long nights, and long hauls – R.C., B.R. – I'm humbled by your patience, commitment, encouragement, and insistence on eating proper meals. Several conversations were particularly valuable at turning points along the way – thank you S.V., P.M., A.H., D.S., and J.G. What would the journey be without friends, peers, and the people outside the ivory tower that kept me sane? – S.G.B., J.R.T., M.M.S., A.D.F., R.T., S.S.S., A.A., D. & J.R., K.B., and A.O., you forever have special place in my heart. The Scott Center Running Club at Florida Tech was what got me moving again in 2012, saving my body and soul from the torpor of desk life. Running is now a permanent part of my life, and it has been integral in teaching me how to set and achieve goals, to pace myself, and to have patience during the down times. Thank you C.M., B.W., K.W. and the rest of the club for getting me started and keeping me going. Special thanks to my cousin and

kindred spirit, Janet Berry, for giving me a much needed break in the middle of the last, long push to finish – South Africa was amazing.

This work was made possible by assistance from a NASA Graduate Student Research Program (GSRP) Fellowship, and by grants from the Florida Space Grant Consortium (FSGC).

This research has made use of the NASA Exoplanet Archive, which is operated by the California Institute of Technology, under contract with the National Aeronautics and Space Administration under the Exoplanet Exploration Program. This research has also made use of the Exoplanet Orbit Database and the Exoplanet Data Explorer at [exoplanets.org](http://exoplanets.org), and the Exoplanet Encyclopaedia at [exoplanet.eu](http://exoplanet.eu).

Analysis of the data was performed in the statistical programming language R (v.3.1.3), using several additional packages. All new graphics except those in Appendix A were created with the `ggplot2` package, repeated visits to [StackExchange.com](http://StackExchange.com) and [StackOverflow.com](http://StackOverflow.com), and a little luck. The graphics in Appendix A were made with the `pgfplots` package for LaTeX developed by [Feuersänger \(2010\)](http://www.feyersaenger.com).

R

R Core Team (2014). R: A language and environment for statistical computing. R Foundation for Statistical Computing, Vienna, Austria. URL <http://www.R-project.org/>.

plyr package

Hadley Wickham (2011). The Split-Apply-Combine Strategy for Data Analysis. *Journal of Statistical Software*, 40(1), 1-29. URL <http://www.jstatsoft.org/v40/i01/>.

ggplot2 package

H. Wickham. *ggplot2: elegant graphics for data analysis*. Springer New York, 2009.

scales package

Hadley Wickham (2014). *scales: Scale functions for graphics*. R package version 0.2.4. URL <http://CRAN.R-project.org/package=scales>

*Dedicated to my parents.*

# *Quotes*

It seems impossible until it is done.

—Nelson Mandela

Well-behaved women seldom make history.

—Laurel Thatcher Ulrich

If you are going through hell, keep going.

—Winston Churchill

It does not matter how slowly you go as long as you do not stop.

—Confucius

# Chapter 1

## Introduction

### 1.1 Stellar Mass, Rotation, and Angular Momentum

Stellar rotation rate has been shown to be linked to a number of other stellar properties. Kraft (1967) found that that rotation rates in F and G stars decrease with age, and Skumanich (1972) confirmed the correlation with Wilson’s (1963) decreased Ca II emission line intensity (also an indicator of surface activity) in dwarf stars. Skumanich’s Law relates the decrease in rotation for solar type stars<sup>1</sup> as  $\Omega \propto t^{-1/2}$  where  $t$  is the stellar age. The spin down of low-mass stars<sup>2</sup> especially appears to be tied to active surface convective zones (Schatzman, 1962) and stellar winds produced by chromospherically active surfaces (Mestel, 1968). Most rotational slow-down for all stars appears to occur during Pre-Main Sequence (PMS) contraction, but additional braking occurs for low-mass stars for much of their lifetime on the Main Sequence (Wolff & Simon, 1997; Tassoul, 2000). Figure 1.1 shows how

---

<sup>1</sup>“Solar type” stars are those which have a radiative core and a convective surface layer. This corresponds to spectral types late-F, G, and early-K, or the mass range from 0.5 to 1.5  $M_{\odot}$ .

<sup>2</sup>Here and throughout, “low-mass” refers to stars less massive than about 1.5  $M_{\odot}$ .

equatorial velocities differ both by mass and age. The older field stars represented by the solid line, especially those later than F0 (about  $1.6 M_{\odot}$ ), rotate more slowly than those in open clusters represented by the dash-dotted line.<sup>3</sup>

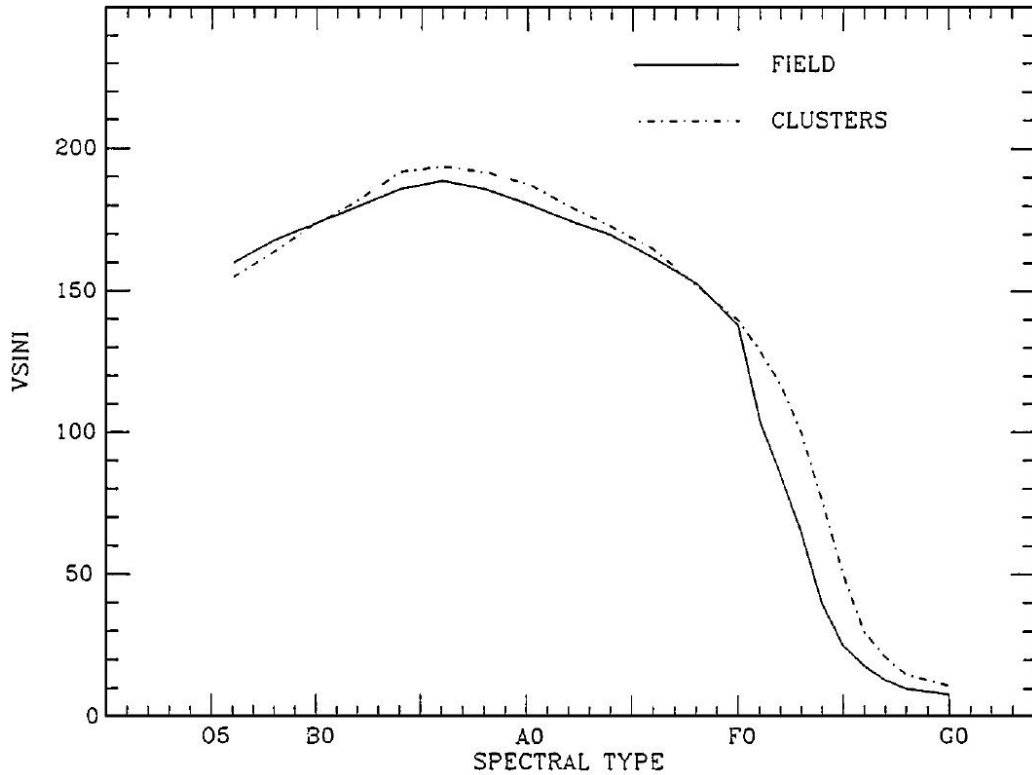


Figure 1.1 Mean projected equatorial velocities for early-type field stars (solid line) and cluster stars (dash-dotted line). (Stauffer & Hartmann, 1986)

### 1.1.1 An Angular Momentum Puzzle

In 1965, McNally published a short letter drawing attention to the angular momenta of Main Sequence (MS) single stars. With only basic assumptions – rigid body rotation and density profiles predicted by the Eddington standard model – he plotted specific angular

<sup>3</sup>Stellar mass and spectral type are very closely correlated, especially for Main Sequence stars. We have attempted to remain true to previous authors' word choice when they describe differences between spectral types, and have included an appropriate approximate mass or mass range when we felt the distinction was helpful and not superfluous.

momentum versus mass for spectral types O5 through G0. Using generalized data found in Allen’s *Astrophysical Quantities* (1963), McNally identified a power law relationship in early-type stars (O5-A5):  $j \propto M^{0.8}$ . There is a break in this power law at around spectral type A5, and stars of later spectral types (and therefore, less massive) follow a steeper power law, or  $j \propto M^{4.7}$ . as in Figure 1.2. He also noted the distinctly different placement of the Sun alone and the Solar System (including the Sun) on the same plot. McNally speculated on possible causes for the break, including planet formation, but ultimately left the puzzle to others. It is now widely accepted that the slower rotation rates of the lower mass stars is responsible for the break. The role of planet formation remained a popular theory well into the 1970’s, but has since been dismissed as a mechanism for slowing the rotation of stars. Indeed, modern evolutionary models which include differential rotation, magnetic braking, and/or stellar winds have adequately produced rotation distributions that agree with those seen in stellar clusters (Tassoul, 2000). Slowed rotation corresponds well with the similar decrease in angular momentum of low-mass *stars* (a.k.a. the “break” in McNally’s plot), but does not consider the role of planet formation on the angular momentum budget of the whole *system*.

The general power law relationship between stellar mass and specific angular momentum has stood the test of time, but the origin of and theory behind the power law itself remained a mystery for years. How and why did a quantity which did not contain mass dimensionally<sup>4</sup> exhibit a clear mass dependence? McNally speculated that the *initial* angular momentum of the system was a sensitive function of the mass, and Herbst et al. (2007) found that rotation period distributions of low-mass young stellar objects (YSOs),

---

<sup>4</sup>Specific angular momentum is defined as angular momentum per unit mass; symbolically,  $j = J/M$  where  $J$  is the angular momentum and  $M$  is the (usually) stellar mass.

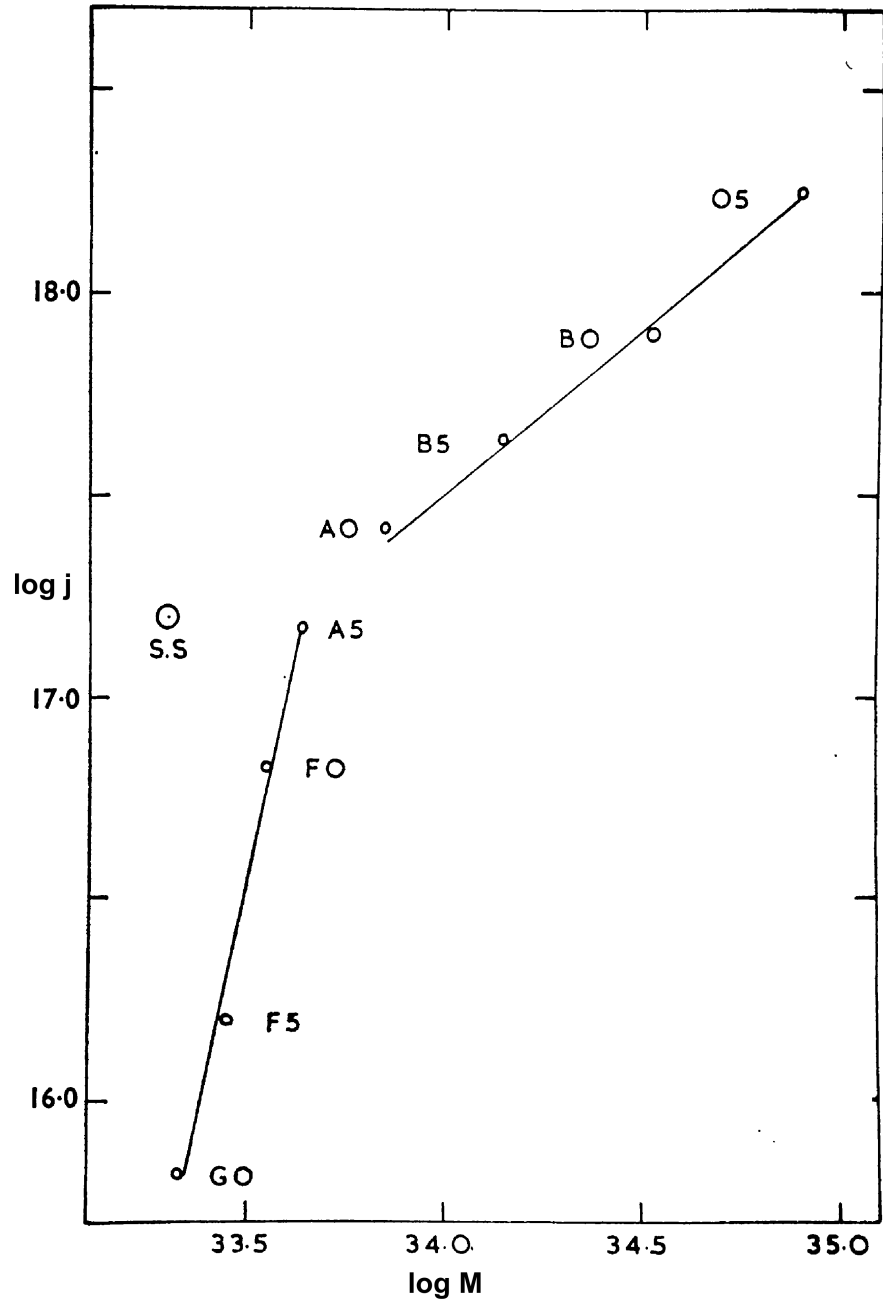


Figure 1.2 McNally's  $j$ - $M$  plot from 1965, showing a graphical bivariate analysis of single, rotating, MS stars. The right-most solid line represents the linear least-squares fit to  $\log j$  as a function of  $\log M$  for less massive, later type stars. The fit corresponds to the power law  $j \propto M^{0.8}$  (Note: This power law is equivalent to  $J \propto M^{1.8}$ .) The left-most solid line with a steeper slope fits McNally's values for later type stars. It is referred to as "the break." The Solar System occupies a position above both power laws. (McNally, 1965)

are strongly mass dependent. Even more broadly, the expression  $J \propto M^2$  is found to describe gravitationally bound astronomical systems across more than 30 orders of magnitude in mass. The masses in the literature range from  $10^{18} - 10^{50}$  g, and include, summarily, asteroids, planets, stars, clusters, galaxies, the local group, and super clusters. This relationship was first derived empirically by Brosche (1963, 1980) while the theory has been debated by Wesson (1979) and Carrasco et al. (1982), among others. Figure 1.3 is an example of one such “universal” J-M plot. From lower left to upper right: the first 4 open boxes represent asteroids, the next 9 open boxes represent Solar System planets with their satellites, small dots are binary star systems, X’s are single MS stars, asterisks (\*) are open and globular clusters, pluses (+) are spiral galaxies while elliptical galaxies and bulges are open triangles, the left-most open circle is the Local Group and the right-most open circle represents super clusters.

Carrasco et al. (1982) in particular determined that if the groups of objects were considered separately from the whole collection, their respective j-M (or equivalently, J-M) relationships are found to agree well with a slope of between  $2/3$  and  $3/4$  (or equivalently for the J-M relationship, between  $5/3$  and  $7/4$ ), assuming constant rotation and relatively similar densities among the group’s objects. For example, in his research, for asteroids, satellites and planets,  $j \propto M^{0.66 \pm 0.06}$ , and for spiral galaxies,  $j \propto M^{0.71 \pm 0.05}$ . They proposed that  $j$  as a monotonically increasing function of  $M$  represents the memory of the initial angular momentum distribution (as opposed to a scale-free j-M power law), and that as the systems age, the slopes of the fitted lines within each sub-grouping also evolve distinctly. Other authors have suggested that the empirical result is not coincidence, and is a consequence of some common law governing the motion of the universe (Godłowski et al., 2003), or is

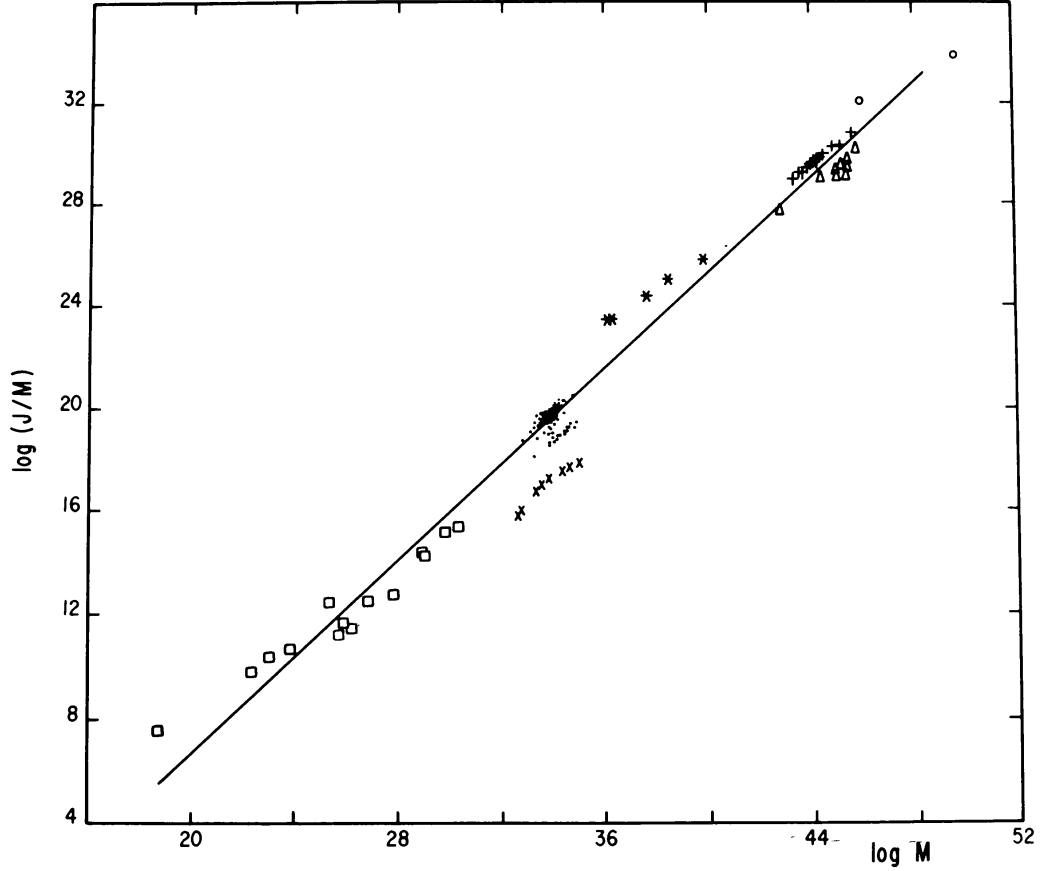


Figure 1.3 Carrasco et al.'s  $j$ - $M$  plot from 1982, showing many different groups of objects. The angular momentum per unit mass ( $j = J/M$ ) as a function of mass on logarithmic scales for a large variety of astronomical objects. The solid line corresponds to a regression line of  $\log j$  versus  $\log M$  with a slope of 0.94. (Note: This power law is equivalent to  $J \propto M^{1.94}$ .) Here,  $j$  is in [ $\text{rad cm}^2/\text{s}$ ] and mass is in [ $\text{g}$ ]. Symbols defined in text above. Carrasco et al. (See 1982, Table 1 for data source references.)

linked to quantum particle physics (Wesson, 1983; Liu et al., 1985). Beyond providing a well-documented baseline to compare the slopes of similar power laws, such theories, while interesting, are without a concrete explanation and are beyond the scope of this work.

### 1.1.2 The Kraft Curve

Investigations into the angular momenta of normal, single, MS stars have yielded interesting results, especially regarding the slope of power laws relating angular momentum and mass.

Kraft (1970) pointed out that more massive stars (those earlier than F5) will rotationally decelerate while on the Hyashi track, or PMS contraction phase, but afterward, due to lack of a convective envelope, retain much of their initial angular momentum. On the other hand, less massive stars that retain their convective envelope slow their rotation at all stages of their evolution. He produced the well known empirically derived “Kraft curve” which described a somewhat smaller mass range than McNally, with  $j \propto M^{0.57}$  (equivalently  $J \propto M^{1.57}$ ) for early-type stars. Figure 1.4 graphically describes this oft-cited landmark analysis. The angular momentum-mass relationship described by  $J \propto M^\alpha$  or  $j \propto M^{(\alpha-1)}$ , where  $\alpha$  is the slope of the power law fit, is called the “Kraft relation.”

Kawaler later revised the Kraft relation in 1987 using a more refined data set, more modern stellar models, and updated rotational velocities for selected spectral types. Most notably, Am and Be stars which Kraft had included in his sample, were excluded here; Am stars are typically slower rotators than other A stars, and Be stars populate the rapidly-rotating tail of the velocity distribution of B stars. Magnetic Ap stars (“peculiar” A stars) are also excluded in Kawaler’s study for their very slow rotation, likely from angular momentum lost by magnetic stellar winds (a trait more common among low-mass stars). Kawaler found  $J \propto M^{2.09 \pm 0.05}$  for MS stars with  $M > 1.5M_\odot$ . The errors listed describe the goodness of the fit of the power law and are not related to intrinsic errors in mass or the calculation of angular momentum. When Am and Be stars are included in the fit of  $\log J \propto \alpha \log M$ , the resulting power law slope is  $\alpha = 2.43 \pm 0.16$ .

It is noted here that  $\alpha = 2$  is near to the slopes determined by McNally and Kawaler, and can serve as a model for comparison of new results. Figure 1.6 displays both McNally’s early-type law (converted to the J-M format), and the updated Kraft curve. It would appear

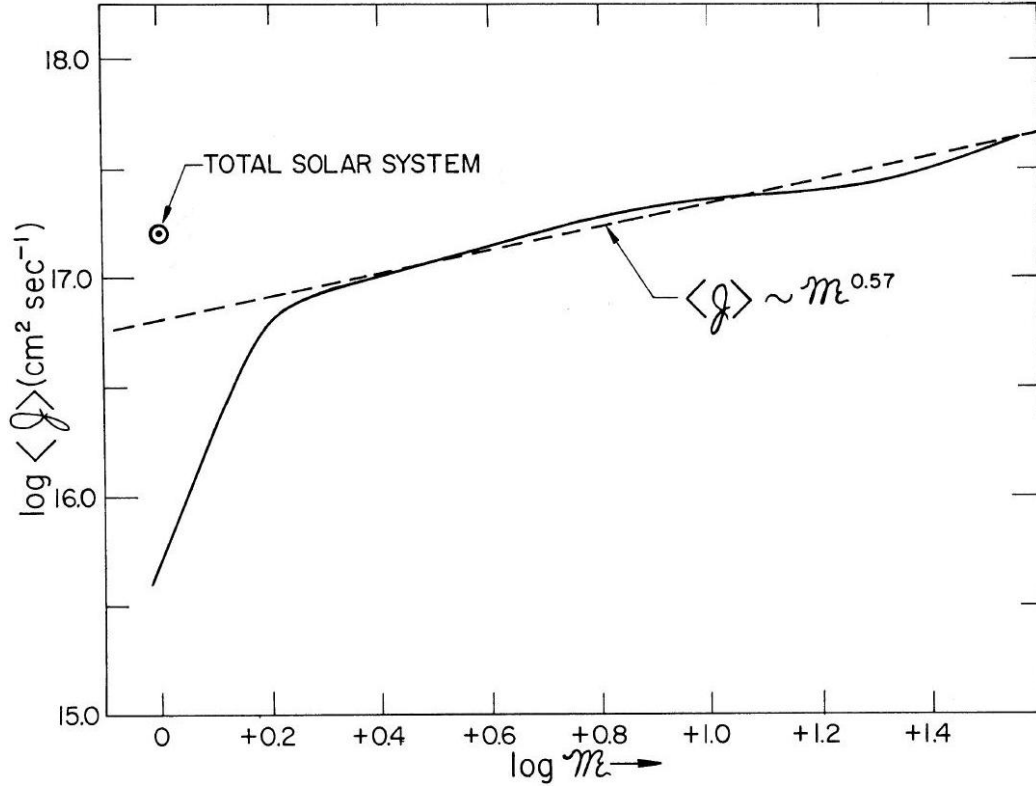


Figure 1.4 Kraft's  $j$ - $M$  plot from 1970, representing 375 MS or near-MS stars of spectral types O to G0. The dashed line represents an unspecified fit to  $\log j$  as a function of  $\log M$  for stars larger than  $2 M_{\odot}$ . The fit corresponds to the power law  $j \propto M^{0.57}$  (Note: This power law is equivalent to  $J \propto M^{1.57}$ .) The Solar System is positioned above an extension of the larger star power law. The solid line corresponds to the distribution of averaged angular momentum per gram for appropriately small mass bins. (abstracted from Kraft, 1970)

that, at least for more massive stars, the stellar  $J$ - $M$  relationship agrees well with Brosche's large scale relation with  $\alpha \approx 2$ .

### 1.1.3 Commonalities

A common feature in many stellar  $J$ - $M$  plots is the break in the power law for low-mass stars. The break itself is considered to be due to differences between stars with radiative versus convective cores, or more precisely, those with convective outer layers and those without.

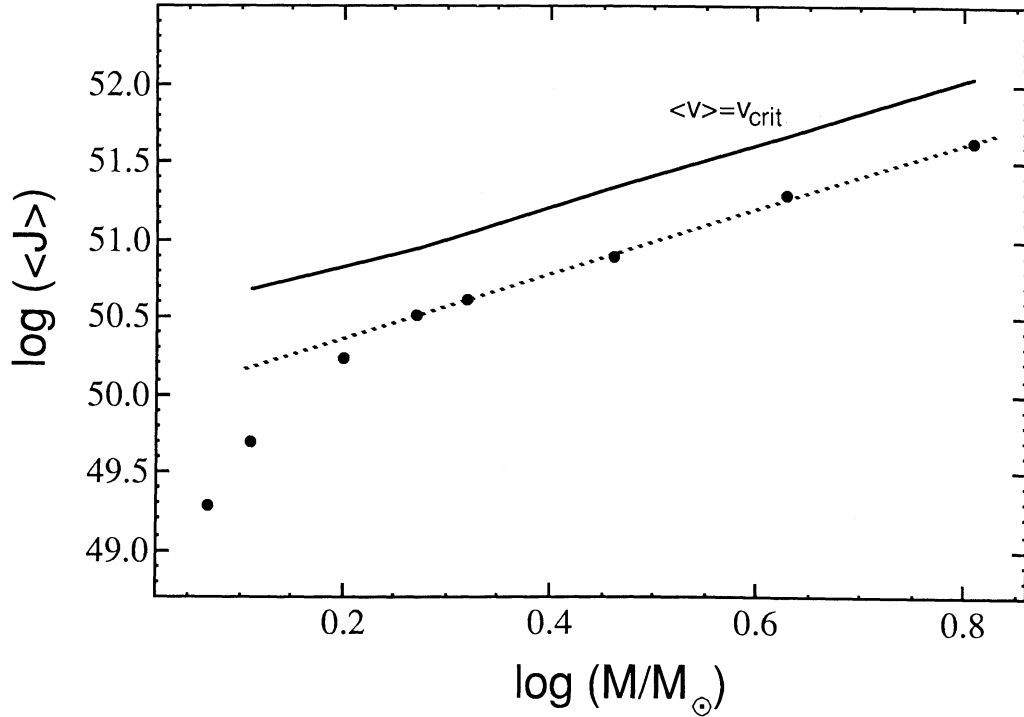


Figure 1.5 Kawaler’s J-M plot from 1987, of single, normal MS stars. The dashed line represents the linear least-squares fit to  $\log J$  as a function of  $\log M$  for stars earlier than F0. The fit corresponds to the power law  $J \propto M^{2.09}$  (Note: This power law is equivalent to  $j \propto M^{1.09}$ .) The Solar System is positioned above an extension of the early-type power law. The solid line corresponds to the angular momentum these stars would have if they were rotating at breakup velocity,  $v_{\text{crit}}$ . (Kawaler, 1987)

The radiative-core stars’ greater loss of angular momentum is popularly thought to be due to stellar winds, magnetic braking, and convection zone ejections, which are characteristic of stars with convective envelopes, and especially those which are fully convective (very low-mass stars,  $M < 0.4 M_{\odot}$ ). A convective envelope is, in fact, necessary for a star to continue losing angular momentum to magnetic braking after reaching the Main Sequence (Tassoul, 2000). Early-type stars, which have a convective outer envelope during their brief PMS contraction, do not remain convective long enough to shed a significant amount of angular momentum, hence they better retain their angular momentum and fast rotation. Radiative and convective core stars differ by their moments of inertia, specifically the inertial

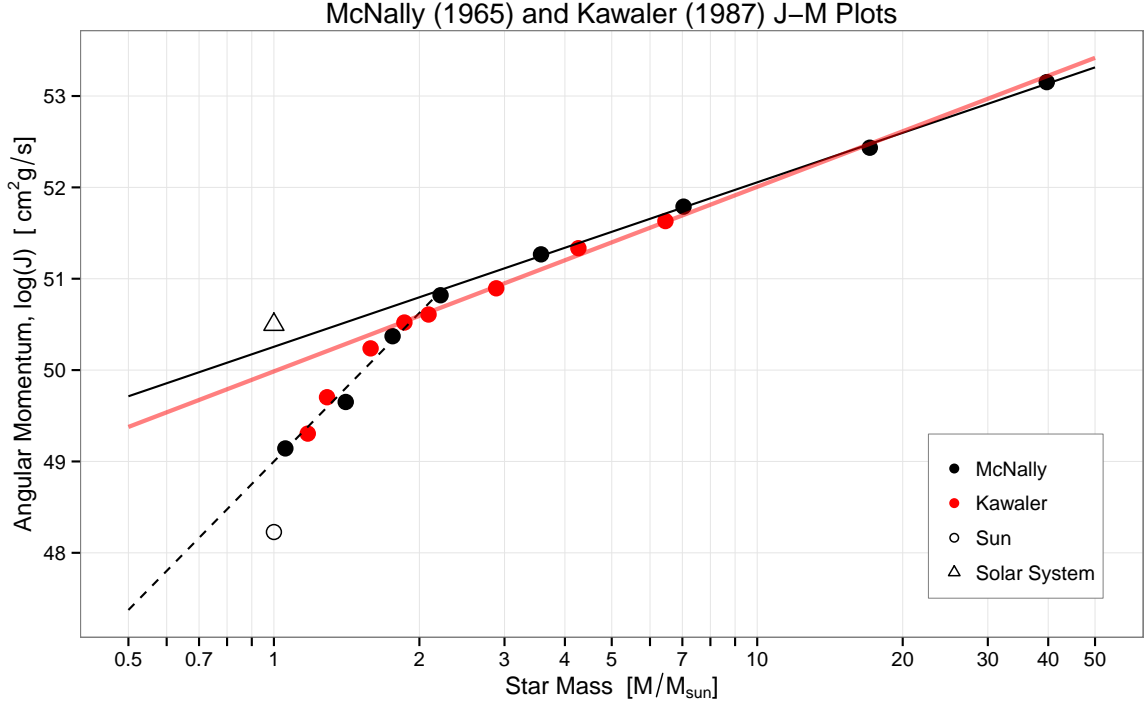


Figure 1.6 The specific angular momentum of single stars is often displayed in a J-M plot similar to the one above. Here, McNally’s original data (black) are compared to Kawaler’s calculations (red) which is updated from Kraft’s (1970) earlier work. For reference, the Sun (open circle) and the Solar System including the Sun (open triangle) are also shown. The solid red line represents a linear fit on  $\log M$  and  $\log J$  for Kawaler’s more massive stars and is extended leftward on the plot. Similarly, the solid black line represents a linear fit on  $\log (J/M)$  as a function of  $\log M$  McNally’s early-type stars, and the dashed black line fits his later type stars, by the same method. The slopes of McNally’s fits have been adjusted to reflect the J-M relationship rather than  $j$ -M. (McNally, 1965; Kawaler, 1987)

coefficient ( $I/MR^2$ ). The inertial coefficient reaches a minimum for stars with radiative cores and very thin convective envelopes.

Some have speculated that the aforementioned power law with slope  $\alpha$ , such that  $J \propto M^\alpha$  as determined by a fit to the more massive, early-type stars, may resemble the initial angular momentum distribution for low-mass stars as well (Kraft, 1970; Kawaler, 1987; Wolff et al., 2004). Kawaler tested the hypothesis by showing that the initial angular momentum of very young low-mass stars was actually greater than that predicted by an

extension of the updated Kraft curve. This suggests that low-mass stars may contain initial angular momentum more consistent with that determined by the rotational breakup velocity than with the Kraft curve. Wolff et al. suggested as much with his eyeball fit of  $\alpha = 1.25$  as an upper bound for a small sample of convective PMS stars, ranging in mass from 1-2  $M_{\odot}$  (right panel of Figure 1.7). A sharp drop in angular momentum for low-mass stars occurs during PMS contraction, once the stars have completed the convective phase of evolution. The trend, or break, then remains for the life of the stars on the Main Sequence. This further confirmed Kraft's proposal that stars earlier than F5V likely lose angular momentum during contraction on the Hyashi track, but retain much of it after reaching, and while residing on, the Main Sequence. These stars do not then have sufficient winds to maintain continued significant angular momentum loss. Stars later than F5V, however, lose angular momentum at all stages of evolution, according to Kraft. Wolff et al. maintain that no conclusions may be drawn between MS stars and their sample of PMS stars for masses  $< 1.4 M_{\odot}$ , but his analysis agrees with Kawaler's statement that initial angular momentum of low-mass stars is greater than that predicted by the Kraft curve. By an eyeball fit to the right panel of Figure 1.7, the placement of radiative-track stars indicate a break in the line representing the upper bound at between  $\log M = 0.2$  and  $0.25$  ( $1.58$ - $1.78 M_{\odot}$ ).

Despite small differences, some conclusions are repeatedly drawn by authors examining the stellar J-M relationship. Stars generally appear to follow a power law relating angular momentum and mass, such that  $J \propto M^{\alpha}$ , also known as the Kraft law or Kraft relation. There is a steep break in the power law indicating that stars less massive than about  $1.5$ - $2.0 M_{\odot}$  have lost a significant amount of angular momentum as evidenced by their much lower spin rates. In all cases, the decrease in  $J$  is greater with decreasing mass

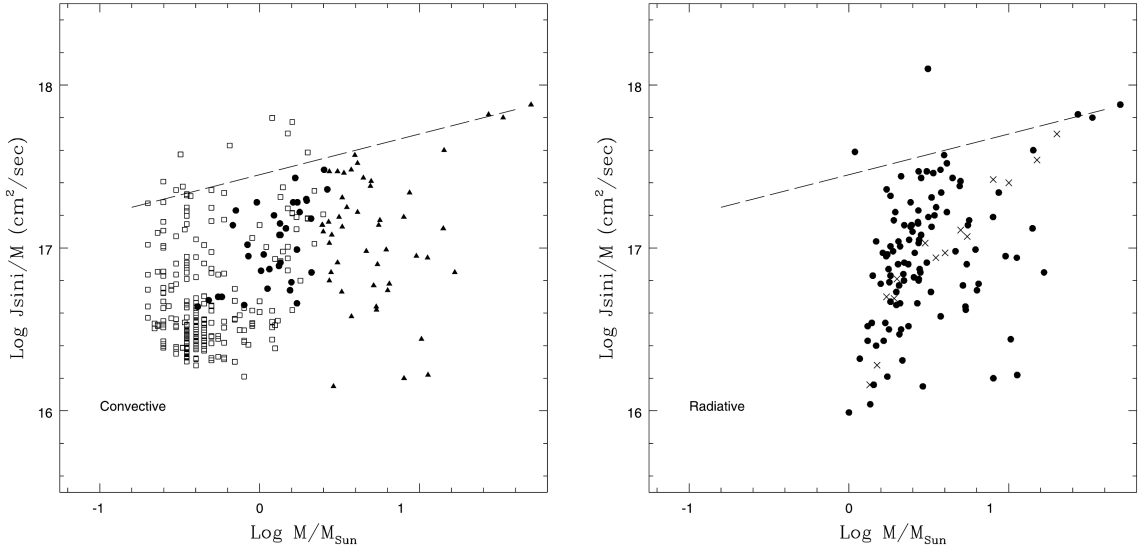


Figure 1.7 Wolff et al.’s  $j$ - $M$  plots, comparing convective PMS stars to ZAMS and MS stars. *Left:* Values of specific angular momentum ( $J \sin i_*/M$ ) as a function of mass for stars on PMS convective tracks. Circles represent Orion stars on convective tracks; squares are primarily lower mass stars in the Orion Nebular Cluster; triangles represent Orion stars with  $T_{\text{eff}} > 10,000$  K, which are already on the Main Sequence. The dashed line is a fit by eye to the upper bound of the data and has slope 0.25. *Right:* Specific angular momentum of stars that have completed the convective phase of evolution. Filled circles represent stars in Orion that are either on radiative PMS tracks or on the ZAMS. Triangles and the dashed line are repeated from the left panel. Crosses represent the average values of  $J \sin i_*/M$  for MS field stars (see Wolff et al. (2004) for references). Note the downturn for Orion and field stars for masses less than about  $2 M_{\odot}$ . This downturn is not seen in convective PMS stars in the left panel.

from that point, producing a steeper slope for power laws fitted to that portion. The break coincides with, and is probably due, directly and indirectly, to differences in overall stellar structure related to mass: the change from radiative to convective core produces different moments of inertia, and the retention of a thick convective envelope produces stellar winds that shed stellar angular momentum on the Main Sequence. It is frequently noted that stellar evolutionary models are needed which include angular momentum conservation/loss as a part of their physics code. Lastly, planet formation is, in general, not considered a likely source of angular momentum loss or redistribution, given the effectiveness of other

angular momentum transport mechanisms driven by subsurface convective layers. Most of these observations and conclusions were made when no confirmed planets had been discovered outside of the Solar System, and it was not known whether planet formation was a common or rare occurrence.

## 1.2 Star Formation and Angular Momentum Loss

Stars form out of cool molecular clouds, which are generally believed to be non-uniform and asymmetric. There are areas of variable density and temperature, creating clumps and cores, such that a giant molecular cloud will not produce just one star, but many stars out of each dense region. These stars are often binary or higher in multiplicity (Duquennoy & Mayor, 1991). Rotation and thereby angular momentum are imparted to the cores by turbulence (Larson, 1981), galactic rotation, interstellar shocks, and magnetic fields (see Cox, 2000, for references therein).

With the onset of the computer age, increasingly complex models of stellar evolution have been developed to explain observed rotation trends in stars, particularly those in clusters. One of the greatest challenges to making realistic models of low-mass stars is the accounting of angular momentum loss throughout the life of the star, from the condensing of a gas cloud core, to a rotating disk, to a hydrogen-burning star. If angular momentum were conserved through the whole process, the star would be rotating much faster than its breakup velocity.  $J_{core}$  turns out to be several orders of magnitude larger than  $J_{crit}$ , the angular momentum of the Sun at breakup velocity.

For example, the minimum angular momentum of a collapsing cloud core could be estimated with the mean particle velocity according to gas theory with simplifications and

assumptions. Here,  $J_{core}$  is a one solar mass isothermal cloud core with  $T \sim 10K$  and  $R \sim 0.1pc \sim 10^{17}cm$ , and  $J_*$  is the angular momentum of a one solar mass star at breakup velocity,  $v_{crit}$ :

$$v_{core} = v_{rms} = \sqrt{\frac{3kT}{m_H}} \quad (1.1)$$

$$\approx 50,000 \text{ cm/s} \quad (1.2)$$

and

$$v_{crit} = \sqrt{\frac{GM}{R_*}} \quad (1.3)$$

$$\approx 50,000,000 \text{ cm/s} \quad (1.4)$$

then

$$\frac{J_{crit}}{J_{core}} = \frac{\mathcal{M}R_{core}v_{core}}{\mathcal{M}R_*v_{crit}} \quad (1.5)$$

$$= \frac{(10^4 \text{ cm/s})(10^{17} \text{ cm})}{(10^7 \text{ cm/s})(10^{10} \text{ cm})} \quad (1.6)$$

$$= 10^4 \quad (1.7)$$

This is known as the “angular momentum problem.” Clearly, cloud collapse models should predict a large amount of rotational braking so that star formation is possible, and stellar evolutionary models must reconcile fast rotating PMS stars with their more slowly rotating ZAMS and MS counterparts. Most MS stars rotate 1-2 dex slower than their breakup velocity, and at most, at only one-half  $v_{crit}$  (Kawaler, 1987). Therefore, one or

more mechanisms must be at work shedding this “excess” angular momentum early in the star’s life.

During the collapse of a molecular cloud core, magnetic fields, ambipolar diffusion, density waves, and ISM gas pressure outside the cloud all affect its collapse rate. Still more mechanisms are at play once a dense core and flattened disk are formed (Carroll & Ostlie, 2006), and the new star is redistributing angular momentum in its interior as it continues to differentiate and contract toward the Main Sequence. From the birth line, stellar spin angular momentum loss is broadly classified into three categories: stellar or disk mass loss, rotational braking via unseen forces (electromagnetic, gravitational, etc.), and mechanical loss/redistribution (such as to planets, disks, or nearby/passing bodies). Many mechanisms overlap in their timescales, and likely interact. Ray (2012) has compiled an overview of mechanisms believed to be responsible for angular momentum loss during star formation, and they are briefly summarized here:

1. *Ambipolar diffusion.* In the presence of a weak magnetic field, cloud core ions spiral around the field lines. This slows the gravitational infall of neutral particles as they collide with the ionized particles, but this has a minor impact on angular momentum.
2. *Binary and multiple star formation.* Giant molecular clouds are not uniform in density or composition, and once collapse begins, multiple dense cores can arise out of a single massive cloud. These cores interact gravitationally with each other to form binary and multi-star systems, which share a larger amount of total system angular momentum than a single star could sustain. For example, wide binaries at  $\sim 1000$  AU contain angular momentum comparable to that in dense cloud cores. Additionally,

a 3-body or higher-order system could eject the lowest mass star, which would take angular momentum with it.

3. *Density, MHD, and acoustic waves.* Axial asymmetries in the circumstellar disk give rise to spiral density waves which carry angular momentum outward while allowing the infall of material to the star. Acoustic and magneto-hydrodynamic waves are also capable of this.
4. *Tidal forces.* Observations of binary systems show that the least massive companion acquires mass more quickly than its counterpart due to tidal disruptions. This causes the total mass distribution to be more equal. That is, the mass ratio of the formed stars is smaller than that of the initial cores. (See Bate 2009)
5. *Disk locking.* Classical T Tauri stars typically have magnetic field lines “frozen into” their surrounding disks. At the radius where the Keplerian rotation of the disk is in phase with that of the star, matter accretes along field lines to the star’s poles, creating a gap in the disk. The frozen-in field lines then carry angular momentum outward in response to the accretion, thus slowing the rotation of the star, despite the mass increase.
6. *Magneto-rotational instability.* In simulations, the magnetic field lines resist the movement of differentially rotating disk material (treated as a fluid). Turbulent instabilities form that shift the net angular momentum outward in the disk.
7. *Collimated jets.* Preliminary Hubble Space Telescope observations by Bacciotti et al. (2002) show that supersonic jets ejecting matter from the poles of classical T

Tauri stars also have a rotational component. The loss of the angular momentum through jets may support continuing mass accretion without spinning the star up to its breakup velocity.

8. *Stellar winds.* According to magnetic dynamo theory, the flux of a star's magnetic field scales with its angular velocity. Winds ejected from the stellar surface have a frozen-in field which either returns it to the star, or tends to drag the field lines away from the star. As a result, the faster the star's rotation, the more effective is the braking.

Currently the most widely accepted theory for the dramatic spin down of late-type stars before the Main Sequence is magnetic disk braking. The theory is attractive because it explains why longer rotation periods are observed in relation to deeper convective envelopes, the source of much magnetic activity on the surface of the star. Recall that a significant drop-off in rotation rates is observed for stars less massive than those at the boundary where internal pressures force fully convective stars to develop radiative cores.

While the list above describes how angular momentum is lost by mass removal or by slowing/resisting the rotation of the star or disk, some angular momentum must be locked into protoplanets and aggregating debris disks. A method of accounting for this redistribution is lacking in contemporary astrophysics. This research puts forth a foundation for such a method, by creating a snapshot of the current spin and orbital angular momentum in mature planetary systems.

### 1.3 The Solar System and Exoplanetary Systems

Thanks to an explosion of available exoplanetary data and ever more precise observational measurements, we are at a point in history where comparisons between our Solar System and other multi-planet systems can be made. According to the NASA Exoplanet archive (<http://exoplanetarchive.ipac.caltech.edu/>), as of 16 April 2015, 1830 planets had been discovered and confirmed, comprised of 662 single-planet systems and 465 multi-planet systems. In the past, most confirmed exoplanetary systems were single-planet and single-host star, but the numbers are rapidly changing, and the single-planet status for discovery does not necessarily imply that only one planet exists in those systems. By comparing the distribution of angular momentum in single and multi-planet systems to that in the Solar System, an estimate how much angular momentum is *expected* to be in planets as compared to their host stars might be made. Further one may identify what characteristics those planets and stars are most likely to have. Ideally, this could in turn be developed into a method to find probable “missing items” in the angular momentum budget, such as undiscovered planets or stellar companions.

As McNally and Kraft noted, the Sun and Solar System occupy interesting placements on any stellar J-M or j-M plot. The Solar System (with the Sun) lies above an extension of the early-type power law fit discussed previously, while the Sun sits below the late-type power law fit, referring again to Figure 1.6. Consider that the Sun contains 99.9% of the mass of the Solar System. When all planets are taken into account, however, the Sun is found to contain less than 0.5% of the total angular momentum. See Table 1.3 for a

Table 1.1. Angular Momentum Distribution of the Solar System

Body	Mass [ $10^{27}$ g]	$a$ [AU]	$e$	$J_{\text{body}}$ [g cm <sup>2</sup> /s]	$J_{\text{body}}/J_{\text{total}}$
Sun	1989100	—	—	$1.69 \cdot 10^{48}$	0.005
Mercury	0.3302	0.3871	0.2056	$8.96 \cdot 10^{45}$	<0.001
Venus	4.8685	0.7233	0.0068	$1.85 \cdot 10^{47}$	<0.001
Earth	5.9736	1.0000	0.0167	$2.66 \cdot 10^{47}$	<0.001
Mars	0.64185	1.5237	0.0934	$3.52 \cdot 10^{46}$	<0.001
Jupiter	1898.6	5.2028	0.0485	$1.93 \cdot 10^{50}$	0.612
Saturn	568.46	9.5428	0.0555	$7.81 \cdot 10^{49}$	0.248
Uranus	86.832	19.1921	0.0463	$1.69 \cdot 10^{49}$	0.054
Neptune	102.43	30.0689	0.0090	$2.50 \cdot 10^{49}$	0.079
Planets total	2668.1			$3.13 \cdot 10^{50}$	0.995
System total	1991800			$3.15 \cdot 10^{50}$	1.000

Note. — All planetary parameters are taken from Yoder (1995). Solar parameters are taken from Yoder (1995) and include inertial coefficient  $I/MR^2 = 0.059$  and  $R_{\text{eq}} = 6.960 \cdot 10^{10}$  cm. Mean solar rotation rate taken from NASA JPL (<http://ssd.jpl.nasa.gov>) as  $\Omega = 2.972 \cdot 10^{-6}$  rad/s.

summary of mass and angular momentum distribution in the Solar System. Note, this table addresses angular momentum ( $J$ ) only, and not specific angular momentum ( $j$ ).

Many questions are raised by this presentation, chief among them, is our Solar System a typical example of such angular momentum distribution, or is it unique? Analysis of a larger sample of planetary systems will surely provide hints to the answer. Moreover, additional constraints should be enforced to make such a comparison meaningful. If other planetary systems' distribution of angular momentum resemble the Solar System's, it would suggest that star formation and planet formation are intimately linked processes, and that stellar rotational braking mechanisms may not be solely responsible for the observed angular momentum “deficit” in low-mass stars.

Recently, two studies of angular momentum related to planetary systems have been conducted. Alves et al. (2010) examined the rotational properties of host stars of planetary systems discovered by the radial velocity (RV) method and compared them to stars without detected planets. They also calculated a rough estimate of stellar angular momentum and plotted it versus stellar mass. Paz-Chinchón et al. (2015) also examined stellar properties of host stars, but only of transiting systems, and only of a subsample of Kepler Objects of Interest (KOIs). In their study, both stellar and system angular momentum are plotted and discussed.

Alves et al.'s (2010) work qualitatively compares rotational differences between stars with and without detected planets with a focus on variations in the samples' stellar and planetary parameters. They first determine with Kolmogorov-Smirnov test on various parameters, that both samples of stars are drawn from the same population. With relation to stellar mass, they found a sudden decline in  $v \sin i_*$  for masses  $1.2 M_\odot$  and less. Their faster rotators have  $T_{\text{eff}} > 6000\text{K}$  and luminosity greater than the Sun. They found the slow rotators are cooler and less luminous than the Sun, in agreement with Kraft (1967). Their calculations of angular momentum assume the stars rotate as constant-density solid spheres, and  $J_*$  is calculated by

$$J_* = \frac{v \sin i_*}{R} I(M) \quad (1.8)$$

where  $R$  is the stellar radius and  $I(M)$  is the moment of inertia, equal to  $\frac{2}{5}MR^2$ . They have fit the Kraft relation to their sample of stars with detected planets but quantify this fit only as a line on the plot of Figure 1.8; they do not explicitly name their value of the slope,

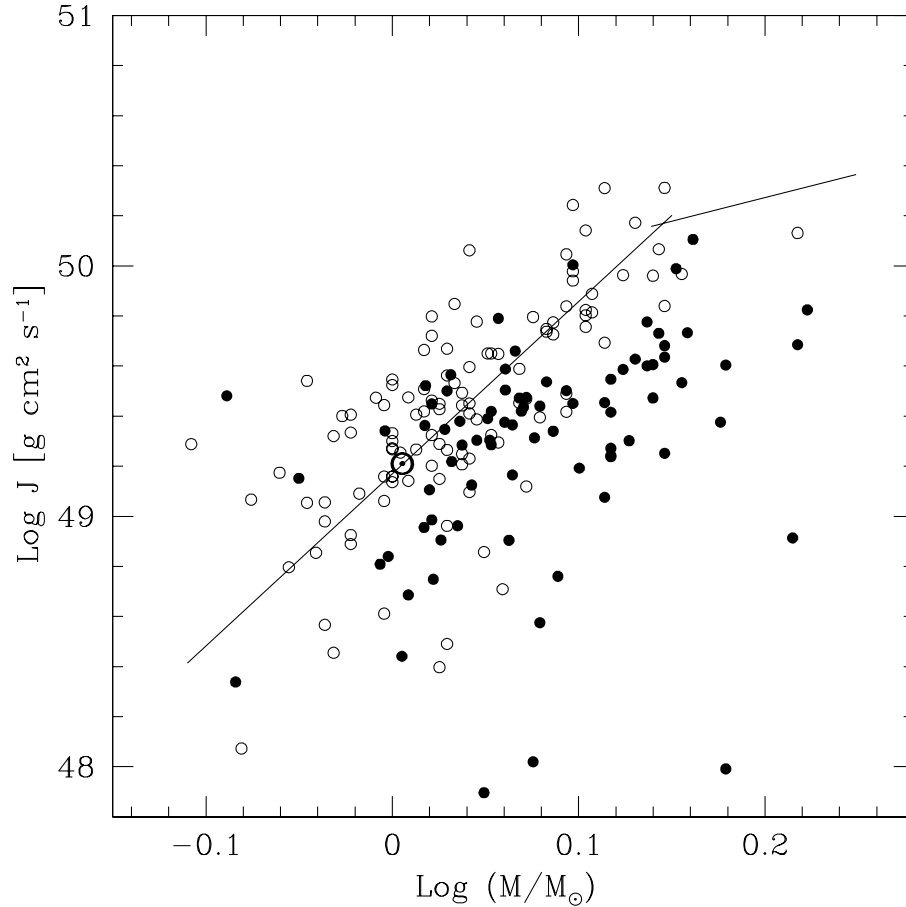


Figure 1.8 Alves et al.'s J-M plot for F- and G-type MS stars, comparing stars with and without detected planets. Open circles represent 118 stars with planets, while filled circles represent 82 without detected planets from Bond et al. (2008). The sun is represented by a dot within a circle. The solid line is assumed to represent Krafts (1970) law, as amended by Kawaler (1987).

$\alpha$ , only stating that their samples are in agreement with the Kraft Law. Further they claim that stars *without* detected planets appear to have an angular momentum deficit compared to those hosting planets, and that host stars with the largest planets have spin angular momentum greater than the Sun.

Alves et al. acknowledge biases introduced by the method of mass determination of the stars, by selection effects of the RV method, and bias due to unknown true masses of

planets. Most attention, however, is given to metallicity bias, as it relates to stellar rotation, occurrence of planet formation, and planetary orbital period. They exclude host stars with transiting planets to avoid possible bias of including fast rotators. The bias of neglecting the stellar inertial coefficient ( $I/MR^2$ ) is absent from their discussion.

Paz-Chinchón et al. (2015) build upon Alves et al.’s (2010) work, and it is noted that the papers have two co-authors in common. Their sample of 131 stars with planets was taken from the Kepler Confirmed Planets table (KCP) and the comparison sample of 409 stars without detected planets was selected from other KOIs. This work is notable since the rotation periods,  $P$ , of the stars were determined from photometric variations in the light curves, and were found to be in agreement with previous measurements and with theory.

Paz-Chinchón et al. (2015) calculate  $J_*$  in the same way as Alves et al. (*i.e.* without regard to the inertial coefficient), but by use of Markov chain Monte Carlo analysis, they do provide a quantitative fit with uncertainty to Kraft’s relation for their stellar sample. The fit, as shown in Figure 1.9, is  $J_* \propto M^{4.9 \pm 1.4}$ . They conclude that the fit is in agreement with Alves et al., and that the power law relation is applicable to the mass range  $0.8 < M/M_\odot < 1.25$ . They do not state agreement with the higher mass power law (for stars more massive than  $1.25 M_\odot$ ) for their stellar sample,  $J_*$ , nor for the 38 systems for which they calculated star-planet system angular momentum,  $J_{sys}$  (method undefined). In fact, system angular momentum is mentioned only fleetingly as having a dependence on stellar mass, and it is noted that “a number” of their calculated system angular momenta are comparable to the Solar System, and that “others” exhibit a deficit compared to the Solar System. Further, they note that the system angular momentum does not show dependence on planet mass, in contrast to the work by Alves et al.

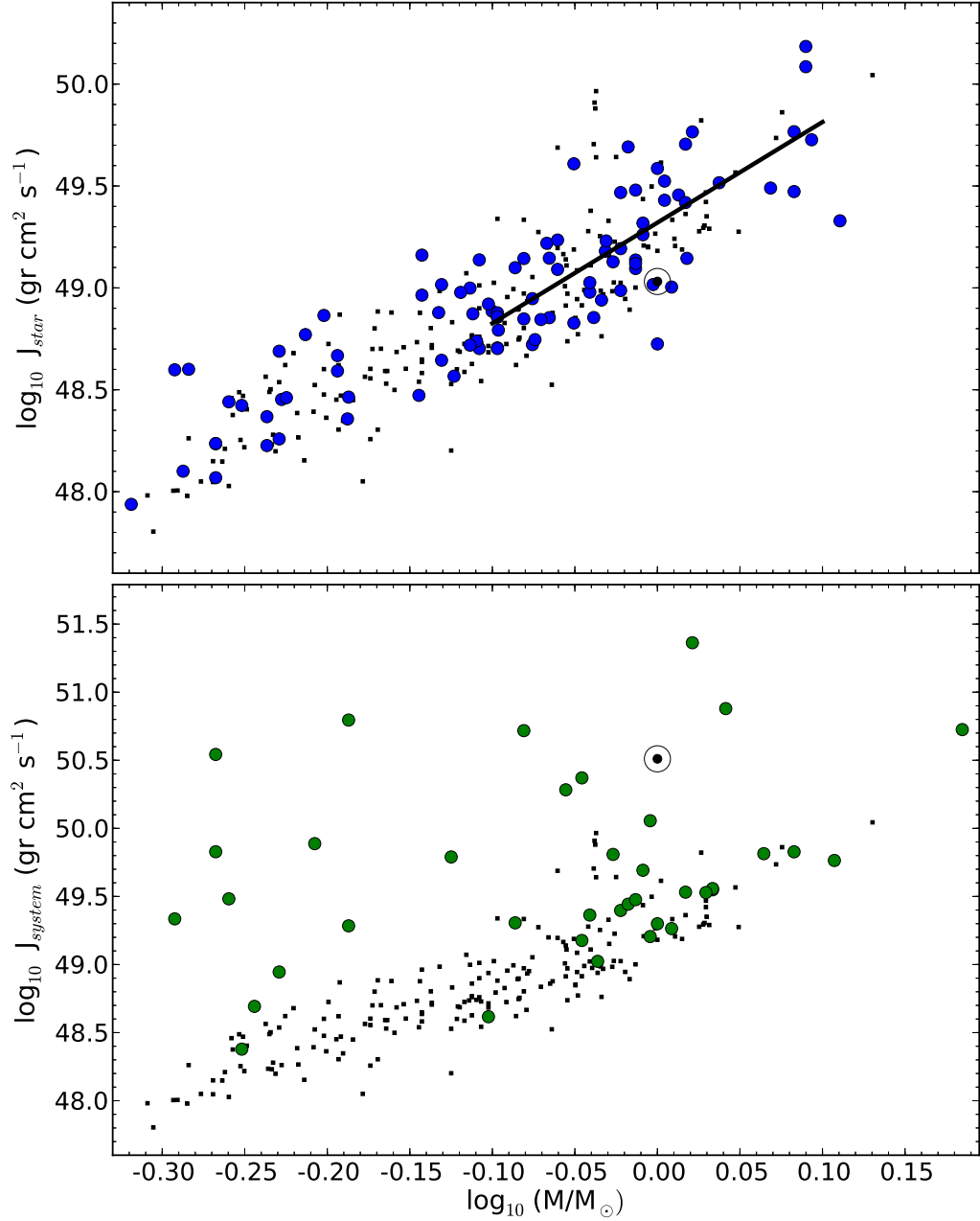


Figure 1.9 Paz-Chinchón et al.’s J-M plots of Kepler Confirmed Planet (KCP) host stars and KOI stars. The Sun is represented by a dot within a circle. *Top*: Stellar angular momentum of 131 KCP host stars (blue circles) and 193 KOI stars (black squares) are plotted versus the stellar mass. The solid line illustrates a best fit of  $J_* \propto M^{4.9 \pm 1.4}$  to their data. *Bottom*: Total angular momentum for 38 (of the original 131) KCP star-planet systems (green circles) and the  $J_*$  of the KOI sample (black squares).

While the use of  $P$  in the calculation of  $J_*$  eliminates some of the uncertainty introduced by using  $v \sin i_*$ , there is still bias inherent in their analysis. They note, correctly, that the disagreement of  $J_{sys}$  dependence on planet mass might be due to the differences between planet detection methods, RV *vs.* transit. They hint that the RV-based sample of Alves et al. was “handicapped” by detections of planets closer to the parent star. They also note the ever-present bias of undetected planets, particularly those at larger orbital radii.

Even considering the studies by Alves et al. and Paz-Chinchón et al., a big picture and all-inclusive study of planetary system angular momentum has not been conducted, and the attempts performed so far have neglected key considerations. As a result, only a superficial description of exoplanetary system angular momentum is known at this time.

## 1.4 Motivations and Goals

In the last 20 years, especially with the success of the Kepler Mission, there has been an explosion of newly discovered planetary systems. To date, Kepler has detected 1022 confirmed planets in over 400 systems and over 4100 candidates (KOI, [http://archive.stsci.edu/kepler/confirmed\\_planets](http://archive.stsci.edu/kepler/confirmed_planets), last accessed Jan 7, 2015) by the transit method. About 800 other planetary systems have been discovered since 1995 by other observations, with significant contributions from ground-based programs, such as SuperWASP, the HATNet Project, the XO Telescope, the Trans-Atlantic Exoplanet Survey (TrES), the Kilodegree Extremely Little Telescope (KELT) Survey, ESO’s High Accuracy Radial velocity Planetary Search (HARPS), the Advanced Fiber-Optic Echelle (AFOE) spectrograph, the CORALIE, SOPHIE, and ELODIE spectrograph programs based out of Geneva Observatory, the Anglo-Australian Planet Search (AAPS) in the southern hemisphere, among many others, as well

as the French-based space telescope, CoRoT (Convection, Rotation, and Transits). To date, the transit and RV methods account for the vast majority of planet discoveries, and yield the most information about new planets, particularly when both can supply information about a system of interest.

At this point in time a unique opportunity exists to examine statistically relevant relationships between planets and their host stars. In this thesis, a method is developed to quantify the angular momentum of planets, their host stars, *and the systems as a whole*. Throughout, there are five main questions that should be answered:

1. What is the best way to quantify the angular momentum of planetary systems?
2. How do these measurements compare to past studies of stars and planetary systems?
3. What are the Kraft relations of planetary host stars and total planetary system angular momenta? *i.e.* What is the value of  $\alpha$  for  $J \propto M^\alpha$  for these groups?
4. Can the results be used to aid in detection of undiscovered planets?
5. Do the results support the the Solar System as unique or typical?

To answer these questions, a large data set is needed, and a variety of analyses must be performed. To quantify the angular momenta, a mass-inertia relationship is developed from published models of stellar evolution to approximate moments of inertia of planetary host stars. Reported stellar mass, stellar radius, and rotational velocity are then used to calculate their spin angular momentum. Up-to-date exoplanet databases provide the orbital parameters needed to calculate the planetary contribution to the system's angular momentum: planet mass, semi-major axis, and orbit eccentricity. Total system angular

momentum is calculated, and ratios of planet-to-system and planet-to-star angular momenta are examined to find specific relationships. The data are divided into various subgroups such as planet classifications, discovery methods, and evolutionary stages of the host star. The stellar and system angular momenta,  $J_*$  and  $J_{sys}$ , are compared to past studies of stellar angular momentum of stars. The possibility of using this analysis to identify systems with potentially undiscovered planets is assessed. These results are compared with the Solar System's angular momentum distribution in the context of the Kraft Curve, the well-known "break" in angular momentum-mass plots for low-mass single stars.

# Chapter 2

## Method

### 2.1 Angular Momentum Defined

In most classical mechanics texts, angular momentum is assigned the symbol  $L$ , and  $l$  or  $\ell$  for specific angular momentum. In astronomy and astrophysics,  $L$  is typically reserved for luminosity, and therefore, the symbols  $J$  and  $j$  are the preferred notation for angular momentum and specific angular momentum, respectively. This notation is also found in most of the reference literature, except when noted. In Newtonian mechanics, the angular momentum is a vector quantity defined by

$$\vec{J} \equiv \vec{r} \times \vec{p} = \vec{r} \times m\vec{v} \quad (2.1)$$

where  $\vec{r}$  is the position vector from some origin, and  $\vec{p}$  is linear momentum of an object with mass,  $m$ , and velocity,  $\vec{v}$ . The direction of  $\vec{J}$  points perpendicular to the plane defined by  $\vec{r}$  and  $\vec{v}$ , and is determined by the right-hand rule.

For a rotating object in an inertial reference frame without external forces acting on it, the angular momentum may be equivalently expressed as

$$\vec{J}_{spin} = \mathbf{I} \cdot \vec{\Omega} \quad (2.2)$$

where  $\mathbf{I}$  is the inertia tensor of degree  $n$  (in  $n$  dimensions), and  $\vec{\Omega}$  is angular velocity. Hereafter the  $\hat{z}$  component of the inertia tensor is taken to represent the scalar moment of inertia for assumed constant rotation about the  $z$ -axis, with the other components being non-contributing. This relation is the basis for the calculation of spin angular momentum of stars. The specific angular momentum is defined as the angular momentum of the system or object divided by its scalar mass:

$$\vec{j} \equiv \frac{\vec{J}}{M} \quad (2.3)$$

The orbital angular momentum of a point mass,  $m$ , revolving in a circular orbit about a fixed axis is derivable from Equation 2.2,

$$\vec{J}_{orb} = I \vec{\omega} \quad (2.4)$$

$$= mr^2 \vec{\omega} \quad (2.5)$$

where  $\vec{\omega}$  is orbital angular velocity, and  $r$  is the distance of the object from the orbital axis. The moment of inertia  $I$  of a point mass is, by consequence of Newton's Second Law of Motion, its mass times the squared perpendicular distance to the rotation axis,  $I = mr^2$ .

In all calculations, symmetry, simplifications, and reasonable approximations are used to avoid complex analysis of misaligned orbits/spins, tidal bulges, precession, and other complications. Therefore, scalar magnitudes of angular momenta are calculated rather than vectors. The magnitude of  $J_*$  computed by this method is sufficient for comparing the angular momentum of single stars with other single stars, and for a general magnitude-based comparison with orbital angular momentum. Justification and implications of this choice for computing total system angular momentum are discussed in Section 2.5. Moreover, the stellar and orbital parameters of exoplanetary systems are reported as scalars (often as projections with systematic errors) since observations via the sky-plane offer only a two-dimensional glimpse of a three-dimensional system.

## 2.2 Angular Momentum and Specific Angular Momentum

In the astronomy field, and regarding stellar spin angular momentum in particular, some authors prefer to calculate and examine specific angular momentum,  $j$  (e.g. McNally, 1965; van den Heuvel, 1966; Kraft, 1965, 1970; Tarafdar & Vardya, 1971; Carrasco et al., 1982; Ruciński, 1988; Bodenheimer, 1995; Wolff et al., 2004; Armstrong & Larson, 2007; Armstrong et al., 2011; Zoghbi, 2013), and some prefer angular momentum,  $J$  (e.g. Wesson, 1979; Brosche, 1986; Kawaler, 1987, 1988; Pinsonneault et al., 1990; Alves et al., 2010; Paz-Chinchón et al., 2015), and both groups refer to the slope of J-M or j-M power laws, confusingly labelled as  $\alpha$  in both cases, without differentiation. Apart from convention or habit, it does not appear that specific angular momentum is any more useful in discussing stellar angular momentum-mass relationships of single rotating stars than simply angular momentum itself. That is, strictly for the single stellar case, if  $J \propto M^\alpha$ , then

$j = J/M \propto M^{\alpha-1}$ . For the latter, a line describing a trend or upper bound to angular momenta of stars as a function of mass is simply translated about 30 orders of magnitude down the plot, and the slope  $\alpha$  is shifted less steeply. Succinctly, Brosche (1969) explains in a one-page letter of critique of van den Heuvel (1966) to *The Observatory*:

One is led to suppose that the division by  $M$  eliminates the dependence on  $M$  and that, consequently, it is possible then to compare  $[j]$  values for different masses without regard to the masses. . . . There is no reason for the  $[j]$  values of different masses to be equal and, therefore, comparisons between such  $[j]$  values have no basis.

It seems that the convention of using  $j$  as opposed to  $J$  is due to wide use in discussions of evolution of binary systems and collapsing clouds; then it was adopted for single stars' spin as a way to remove the dependence of mass, and its uncertainty, from the calculation of angular momentum while still showing a clear (and unexplained) trend with respect to mass. Nevertheless, any identifiable trend regarding the spin angular momentum of single bodies (including the break in the primary power law described by McNally, Kraft, and Kawaler) persists on a J-M plot whether the slope is indicated with  $\alpha$  or  $\alpha - 1$ . Indeed, in the context of planetary systems, the quantity  $j$  has useful function when (a) discussing the relative angular momenta of multiple orbiting bodies about a single central mass, especially if the masses of those bodies is unknown, and (b) comparing the spin angular momenta of a sample of single rotating bodies. This former situation is present as thousands of planet candidates discovered by the transit method are vetted, but most of those systems lack RV measurements to obtain a well-constrained mass. The comparison of their specific

angular momenta may allow some statistical conclusions to be drawn about the distribution of orbital angular momentum within the systems.

For many inhomogeneous multi-body systems, the usefulness of specific angular momentum as a comparative metric breaks down. Angular momentum of an idealized gravitationally bound system is conserved, that is the total angular momentum of the system as a whole remains constant even though the angular momentum may be transferred between  $J_{spin}$  and  $J_{orb}$ . The specific angular momentum in such a case is not conserved. In fact, total system specific angular momentum is not helpful when identifying multiple loss mechanisms in the angular momentum budget, especially if one of those loss mechanisms is redistribution of angular momentum to other bodies.

A simple example demonstrates this. In a two-body system in which  $M \gg m$ , the specific angular momentum of the smaller body at sufficiently large radii will always dwarf that of the primary mass. That is,  $j_m \gg j_M$ . Thus, the specific angular momenta of  $M$  and  $m$ , when divided by their respective masses, appear to have an even greater difference between them – instead of a 2- or 3-order of magnitude difference, there is now a 5- or 6-order of magnitude difference between their specific angular momenta. But by the definition of specific angular momentum, the total angular momentum of the system should be divided by the total mass of the system. The quantity  $J_{total}$  is large, owing mostly to the contribution by  $J_m$ . Dividing this quantity by the total mass, which is now large due to the contribution by  $M$ , will produce a value of  $j_{total}$  which is, counter-intuitively, much less than the minor body's contribution. Clearly, specific angular momentum describing systems with both spin and orbital components is not conserved.

The focus of this research is to quantify the total angular momentum of the planetary system — a host star *and* its planet(s) — therefore, angular momentum,  $J$ , which *is* conserved (in the ideal physical case) regardless of its classification as spin or orbital, is the preferred term in the calculations, comparisons, plots, and discussions herein.

## 2.3 Stars and Spin Angular Momentum

The spin angular momentum of a star, approximated as a radially symmetric sphere with constant rotation,  $\Omega$ , may be expressed as the scalar version of Equation 2.2, that is,

$$J_* = I\Omega \tag{2.6}$$

where the scalar moment of inertia of a rotating body is

$$I = \gamma MR^2 \tag{2.7}$$

where  $\gamma$  is the unitless inertial coefficient<sup>1</sup> describing the distribution of the mass density of the object, and  $M$  and  $R$  are the stellar mass and radius. Stellar mass is determined from a luminosity or temperature relation, as is radius (Hansen et al., 2004), often through various stellar models that take color, temperature, Lithium abundance, etc. as inputs.

A practical and computationally simple method is needed, for calculation of stellar angular momentum from a database of observational values, applicable over a range of

---

<sup>1</sup>The reference literature may refer to this quantity by other names or symbols: represented as  $I/MR^2$  and called the “moment of inertia” by Yoder (1995); the “moment of inertia ratio” by de Pater & Lissauer (2001) and Berget & Durrance (2010); and  $\beta^2$  with  $\beta$  called the “radius of gyration” by Claret & Giménez (1989, 1990).

stellar and orbital characteristics. As they cannot be directly measured, substitutions for variables other than mass and radius must be made.

### 2.3.1 Angular Velocity

Angular velocity is related to the surface velocity by  $\Omega = v/R$ , where  $R$  is the star radius. This is a simplified expression, since there are latitudinal differences in surface rotation rate. Conventionally, equatorial velocity  $v_{eq}$  is taken as the representative surface velocity, assuming rigid body rotation, though rotation rates at other latitudes are generally slower.  $\Omega$  may be determined from rotation periods or surface velocity measurements, but systematic errors or large uncertainties, discussed below, persist in these methods.

**Spectroscopic method:** For stars observed with a rotational axis inclined at some angle  $i_*$ , the stellar surface material is rotating toward and away from the observer. This results in Doppler broadening and flattening of spectral absorption line profiles. The observed quantity is  $v \sin i_*$ , a lower limit for  $v_{eq}$ , with ambiguity due to the unknown projection angle. The expectation value of  $i_*$  of a sample of stars with assumed randomly oriented spin axes is  $\langle i_* \rangle = \frac{\pi}{4}$  (for derivation see Chandrasekhar & Munch, 1950). The expectation value of  $v$  from the spectroscopic measurement and from  $\langle i_* \rangle$ , is then

$$\langle v_{eq} \rangle = \frac{v \sin i_*}{\langle \sin i_* \rangle} = \frac{4}{\pi} v \sin i_*$$

Hence,  $\langle v \rangle$  is useful for statistical purposes (e.g. examining rotation rates of stars in clusters). (Kraft, 1970; Tassoul, 2000)

**Time series photometry:** Observation of periodic photometric irregularities on a star's surface, such as star spots, are indicative of a true rotational period  $P$ , and therefore,  $\Omega$ . This method is limited to stars which exhibit photospheric or chromospheric activity, mostly later types. Ground-based observations require many nights and long viewing windows. Additionally, the rotation period must be less than the lifetime of the star spots. Such precise measurements of rotational periods have been used to further constrain the ages of stars via gyrochronology. (Tassoul, 2000; Barnes, 2007) The spin angular velocity obtained by this method is then just  $\Omega = 2\pi/P$ .

**Rossiter-McLaughlin (RM) effect:** Precision radial velocity spectroscopic measurements can be used to achieve a rotational velocity precision far better than that derived from the Doppler broadening of stellar absorption lines. That is, RV measurements have precision approaching 1 m/s, whereas the spectroscopic method has uncertainties on the order of 1 km/s. The RM precision is achieved because any asymmetry in the absorption lines offset the radial velocity measurements. A periodic asymmetry is produced by a transiting planet or star moving across the stellar disk by partially blocking light from one side of the rotating star and then the other. The apparent change in radial velocity of the star resulting from this is dependent on the alignment between the spin axis of the star and the orbit plane of the occulting object. (Ohta et al., 2005; Schlaufman, 2010) Only a few dozen systems have had RM measurements made, but for those that do, these measurements provide a more accurate value for  $i_*$ , and therefore, a more accurate  $v$  derived from  $v \sin i_*$ .

The most common and most commonly available measurement pertaining to a star’s rotational speed is the projected rotational velocity of the star’s surface obtained from the Doppler broadening of spectral lines,  $v \sin i_*$ , where  $i_*$  is the unknown angle of inclination of the star’s rotation axis with respect to the observer. In this case,  $v \sin i_* \leq v_{eq}$ , where  $v_{eq}$  is the rotational velocity of the star’s surface at its equator. Ignoring the effects of differential rotation, both latitudinal and radial,  $v \sin i_*$  with its systematic bias, does provide a lower bound to  $v_{eq}$  and thereby to  $\Omega$ , as

$$\Omega = \frac{v_{eq}}{R} \tag{2.8}$$

$$\lesssim \frac{v \sin i_*}{R} \tag{2.9}$$

Two problems arise in attempts to reduce uncertainty or account for the bias in  $v \sin i_*$ , as noted by Paz-Chinchón et al. (2015). First, one might expect to divide it by the expectation value of the inclination angle,  $\langle \sin i_* \rangle$  as described above. By the nature of the most common planet detection methods, and with a reasonable assumption about the relationship between orbital and spin axes, is it clear that host stars of detected planets are most likely not a randomly oriented sample of stars. Both main planet discovery methods, Radial Velocity (RV) and Transit, have a significant selection effect on  $i_p$ . The transit method strongly favors systems oriented with the orbital plane along or nearly along the line of sight. This bias is weaker for RV method discoveries, but still persists. At this point in time there is not enough data to know what fraction of planetary systems have small or large angles between the stellar spin axis and the planetary orbital axis. This angle, called  $\psi$ , is covered in more detail in Section 2.5. Second, one might be tempted to assume

that, like the Solar System, the planet orbits are fairly co-aligned with each other and with the star’s spin axis. For transiting planets, the inclination of the orbital axis is known and well constrained. The transit method heavily selects orbital planes along the line of sight. That is,  $80^\circ < i_p \leq 90^\circ$ , with 94% of planets with  $i_p > 82^\circ$  and 80% with  $i_p > 85^\circ$ . For the vast majority of these planets, dividing the stellar  $v \sin i_*$  by  $\sin i_p$  results in a surface velocity that is less than 1% different than the original  $v \sin i_*$ . (For comparison, the mean and median percent uncertainties in all host star  $v \sin i_*$  measurements is 38% and 21%, respectively.) For these reasons  $v \sin i_*$  is left untreated for biases, and it is suggested that its use in place of  $v_{eq}$  is non-fatal, or at least not as significant as the uncertainty in  $v \sin i_*$  itself.

### 2.3.2 Moment of Inertia

Formally,  $I$  involves the integration of the mass density profile over the volume of the object, with respect to a fixed rotational axis coincident with the object’s center of mass. For radially symmetric objects (or approximately so), Equation 2.7 can be used without loss of fidelity, as stellar mass and radius ( $M$ ,  $R$ ) are readily available from the literature, but inertial coefficients must be derived from density profiles, or approximated from stellar evolutionary models. An inertial coefficient of 0.4 corresponds to a solid sphere of uniform density, but stars have centrally condensed cores, yielding a smaller value of  $\gamma$ . The Sun, for example, a G2 star, has a reported  $\gamma$  value of between 0.069 (Yoder, 1995) and 0.073 (Carroll & Ostlie, 2006). Host stars are treated as solid rotating bodies which is sufficient for this kind of time-independent calculation. The effects of oblateness or deformation are

assumed to be negligible, as all but three of the sample host stars are apparent slow rotators ( $v \sin i_* < 25$  km/s).

In previous studies of stellar angular momentum, stars have been assigned a  $\gamma$  value similar to the Sun, about 0.06 (Tarafdar & Vardya, 1971; Berget & Durrance, 2010; Barnes et al., 2013), or the coefficient was set to 0.4, the value used for solid, uniform-density spheres (Alves et al., 2010; Paz-Chinchón et al., 2015). The latter choice is not the best description of the inertia of any population of stars. The stellar masses of this sample range from 0.5 to  $3.1 M_\odot$  and have ages from the birth line to over 10 Gy. Additionally, a significant fraction of the sample may be classified as subgiants or giants (see Section 3.3.5). Based on polytropic models, mostly convective stars, such as very young stars, dwarf stars, and giants (corresponding to polytropic index  $n = 1.5$ ), should be assigned a  $\gamma$  value of approximately 0.15-0.20, while stars with radiative cores and thin convective envelopes (corresponding to  $n = 3$ ) similar to the Sun will have gamma values closer to 0.07. Stars more massive than the Sun are expected to have even smaller values of  $\gamma$ , while subgiants and stars with mass between about 0.4 and  $1.0 M_\odot$  should warrant a value between 0.07 and 0.15. These numbers are consistent with and are borne out by stellar structure theory (Ruciński, 1988; Criss & Hofmeister, 2015) and grids of inertial coefficients such as those by Claret & Giménez, hereafter referred to as CG. With a broad range of masses and evolutionary stages of stars, a simple constant chosen for  $\gamma$  will not suffice, and would produce at least an order of magnitude difference between the tails of the ranges, biasing both ends toward a more inaccurate determination of  $J_*$  and the descriptive power law slope  $\alpha$ .

Stellar evolutionary models were developed by CG (1989; 1990) and Claret (2004) to assist in the study of apsidal motion constants in double-lined eclipsing binaries. The

moment of inertia was determined to be an important aspect of understanding apsidal motion in binaries, and the stellar model delivers outputs with this focus. Specifically, the models produce inertial coefficients (called gyration radius,  $\beta$ , by CG, such that  $\beta^2 = \gamma$ ) for homogeneous ZAMS stars, with a standard composition ( $X=0.70$ ,  $Z=0.02$ ). Other papers and models, not included here, address different compositions.

Grids of model output by CG (1989; 1990) included the mass range 0.6 to 25  $M_{\odot}$ , evolved from the ZAMS to the beginning of helium burning in the core. Mass loss during evolution was not considered. Later grids by Claret (1995, 2004), included the mass ranges of 1 to 40  $M_{\odot}$  and 0.8 to 125  $M_{\odot}$ , respectively, evolved from the ZAMS through carbon burning in the core. These later models included mass loss. Each subsequent set of model grids used updated opacities and improved physics, discussed in detail in their literature.

Claret & Giménez (1989) noted two linear relations between stellar mass and radius of gyration,  $\beta$ ; the slope for  $\log \beta$  versus  $\log M_*$  differed substantially for mass groupings distinguished by having mass either above or below 1.5  $M_{\odot}$  ( $\log 0.18$ ), as shown in Figure 2.1.

The grids from Claret (2004) were downloaded from VizieR (Ochsenbein et al., 2000) as tabular data, one for each mass available that fell within the range of the sample (0.8, 1, 1.12, 1.19, 1.26, 1.33, 1.41, 1.49, 1.58, 1.78, 2, 2.51, and 3.16  $M_{\odot}$ ). Evolved inertial data for the 0.6  $M_{\odot}$  model was taken Claret & Giménez (1990). For each mass modelled, the following procedure was used to identify typical values for  $\gamma$  to be used in interpolation equations. The gyration radius was plotted against age, and the end of hydrogen burning, and therefore the end of the Main Sequence, was identified. The gyration radius did not vary significantly for most MS values, within each model. The mean and range of inertial coefficients from the ZAMS to the end of hydrogen burning was determined, producing

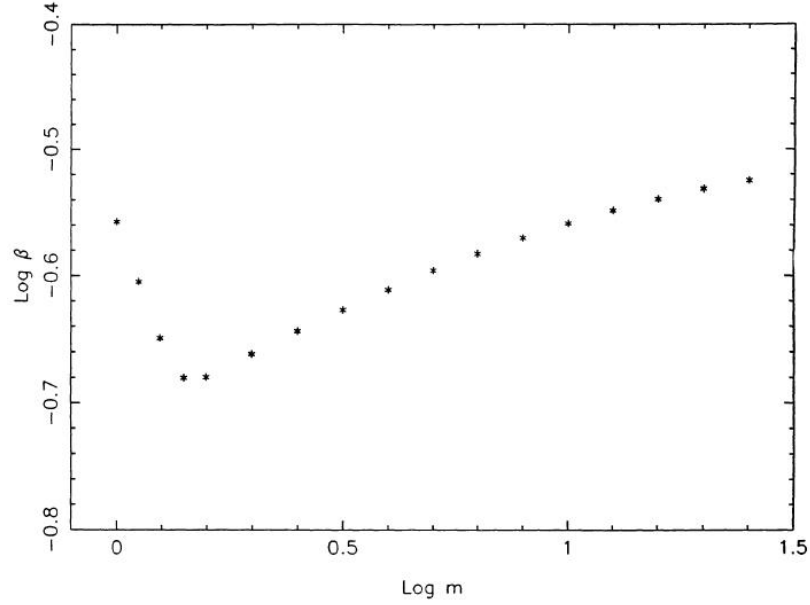


Figure 2.1 The inertial coefficient relation to stellar mass. (abstracted from Claret & Giménez, 1989)

a set of  $\gamma_{MS} \pm \sigma$ . As was demonstrated in Claret & Giménez (1989), a linear regression model fitted the log-transformed values of mass and  $\gamma$  producing an interpolation equation for the mass range 0.6 to 1.5  $M_{\odot}$  with which to determine  $\gamma$  for intermediate masses. The largest host star classified as “MS” had  $M = 1.821 M_{\odot}$  so a second least-squares fit quadratic interpolation equation developed for the five MS host stars with masses between 1.5 to 2.0  $M_{\odot}$ : HAT-P-49, HD 154857, HD 190228, OGLE2-TR-L9 and WASP-79. A third interpolation equation for MS stars with masses from 2.0 to 3.16  $M_{\odot}$  was developed, for the primary purpose of determining the inertial coefficients of Subgiants. Percent error  $\gamma_{MS}$  was set to 0.10, based on the modelled range of values of  $\gamma$  while on the Main Sequence.

A rough calibration to the solar inertial coefficient revealed that the MS fit to the lower masses was better with the mean from the 0.6  $M_{\odot}$  model than without. Without the extra point, the first MS interpolation equation produces  $\gamma = 0.075$  for 1 solar mass, which

is a bit high but not unreasonable. Including the extra data produces an interpolated value of  $\gamma = 0.071$ , which is within the range established for the Sun in Chapter 1.

The method for determining the inertial coefficient for Giants was less precise. The maximum value of the gyration radius was taken as the “typical” coefficient for the Giant classification, for each mass model from 0.8 to 3.16  $M_{\odot}$ . The smallest mass Giant is 0.91  $M_{\odot}$  while the smallest mass Subgiant is 0.7  $M_{\odot}$ , so interpolation equations similar to the first and third developed for the MS host stars were acceptable for this purpose. Again, the slopes of linear regression lines were distinctly different for masses above and below 1.5  $M_{\odot}$ . In general, mean Giant values of  $\gamma$  ranged from 0.125 to 0.150, as would be expected. We are not as concerned about a “bridging function” between the two groupings, as was done for the MS population, since the range of  $\gamma$  is much smaller, and the slopes of the other interpolation equations are not as steep as their MS counterparts. The MS  $\gamma$  means, for comparison, ranged from 0.036 to 0.113 (or, to 0.140, if the mean  $\gamma$  of the 0.6  $M_{\odot}$  model is considered). The percent error for  $\gamma_G$  was set to 0.10, for consistency with  $\gamma_{MS}$ .

Inertial coefficients for Subgiants are probably the least precise, since it is difficult to tell from the stellar radius exactly where the star is evolutionarily, and the change in  $\gamma$  between MS and Giant stages is dramatic and quickly evolved. Subgiants were assigned a value halfway between their interpolated Giant and MS counterparts. The percent uncertainty assigned to  $\gamma_S$  was 0.20, in recognition of the wide range of possible inertial coefficient values of this subtype.

A description of the process used to choose the CG inertial models is given in detail in Appendix A: Choosing an Inertial Model. The interpolation equations developed from the grids of Claret (2004) are also furnished there.

...

With these substitutions for angular velocity and moment of inertia, the practical expression for calculated stellar angular momentum of this sample is

$$J_* = I\Omega \quad (2.10)$$

$$\gtrsim (\gamma MR^2) \left( \frac{v \sin i_*}{R} \right) \quad (2.11)$$

$$\gtrsim \gamma MRv \sin i_* \quad (2.12)$$

## 2.4 Planets and Orbital Angular Momentum

Here is developed an expression for  $J_p$  from Equation 2.5, the angular momentum of an object revolving about a fixed axis. This describes well a planet in orbit about a host star, in which the host star's mass is much greater than the planet's, so that the simplification may be made, that the axis of stellar rotation coincides with the center of mass of the 2-body system. The planet's spin angular momentum is calculated in much the same way as a star's, but its magnitude, regardless of orientation, is negligible compared to its orbital angular momentum, due to the orbital radius being much, much larger than the planetary radius. Moons' contributions, if any were confirmed to exist, are negligible due to their very small orbital radius compared to the planet's. Similarly, it is assumed  $m_{moon} \ll m$ . With these simplifications, planets are treated as point masses in the star-planet system. The magnitude of the planetary orbital angular momentum is then, directly from Equation 2.5.

$$J_p = mr^2\omega \quad (2.13)$$

If the orbit is circular and its period  $P$  is known, the semi-major axis  $a$  is, by the simplification described above, equivalent to  $r$ . Thus,

$$J_p = ma^2 \frac{2\pi}{P} \quad (2.14)$$

Though not all are measured or reported, planets usually have some eccentricity in their orbits, so  $r$  and  $\omega$  cannot be expressed as constants but must be re-expressed in terms of  $M$ , the gravitational constant  $G$ , the semi-major axis  $a$ , and the orbital eccentricity  $e$ . Assuming the planets in question are relatively stable over time, the laws of conservation of energy and conservation of angular momentum are invoked to obtain, for a single planet,

$$J_p = m\sqrt{MGa(1 - e^2)} \quad (2.15)$$

For a planet in circular orbit,  $e \rightarrow 0$ ,  $a \rightarrow r$ , and  $v_{circ} = \sqrt{GM/r}$ . Equation 2.13 is again obtained:

$$J_p = m\sqrt{MGa} \quad (2.16)$$

$$= mr\sqrt{MG/r} \quad (2.17)$$

$$= mrv \quad (2.18)$$

$$= mr^2\omega \quad (2.19)$$

The expression of orbital angular momentum in Equation 2.15 is different from that used by Armstrong & Larson (2007); Armstrong et al. (2011); Alves et al. (2010) and

Paz-Chinchón et al. (2015),

$$J_{star-pl} = \mu \sqrt{(M + m)Ga(1 - e^2)}$$

where  $\mu = Mm/(M + m)$ , the reduced mass. This expression is the *total* orbital angular momentum of each star-planet pair. It is evident that the planetary contribution is nearly equivalent when  $M \gg m$ , and the simplification  $M \approx (M + m)$  produces again Equation 2.15. In the case where  $M \gg m$ , the stellar component of  $J_{orb}$  is non-zero but nearly negligible, and the former expression is preferred so that a discussion of orbital/planetary *vs.* spin/stellar angular momenta is consistent, especially in the context of multiple planet systems.

Here and throughout, the symbol  $J_p$  refers to a planet's orbital angular momentum only. When regarding multi-planet systems,  $\vec{J}_p$  and  $J_p$  represent the sums  $\sum (\vec{J}_p)_i$  and  $\sum (J_p)_i$ , respectively. The assumption is made, with acknowledgement of minor bias, that in multi-planet systems, all planets' orbits are coplanar. This is a safe assumption to make with the data available. Of the 12 multi-planet systems with the projected  $i_p$  measurements available for more than one member, the greatest difference between minimum and maximum projected inclination angles is  $5.25^\circ$  (Kepler-10 b and c), with the remainder of the systems having a maximum difference among their members of  $< 3.2^\circ$ . Additionally, the inclination angles of the Solar System's planets are neglected in the calculation of its angular momentum, with the maximum inclination angle to the ecliptic (Earth's orbit corresponds to  $0^\circ$ ) being Mercury's at  $7^\circ$ . It appears that the known multi-planet systems' planets do not, so far, have grossly misaligned orbital planes.

As  $v \sin i_*$  was used to approximate  $v_{eq}$  for stellar angular velocity (refer to Equations 2.8 and 2.9),  $m \sin i_p$  is used to approximate planetary mass when  $i_p$  is not available. This minimum planetary mass,  $m \sin i_p$ , is obtained from RV measurements, but the measurement of the angle  $i_p$  is obtained from the transit method and is generally well-constrained. In order of decreasing accuracy and precision, mass supplied by EOD has been determined (1) from RV measurements of  $m \sin i_p$  and the transit method measurements of  $i_p$ , (2) from RV measurements of  $m \sin i_p$  alone, (3) as an upper bound in the reported mass or  $m \sin i_p$  uncertainty when neither mass nor  $m \sin i_p$  are present, and (4) by a smoothly varying mass-radius relation described by Han et al. (2014).

## 2.5 Planetary Systems

The total angular momentum of a star-planet system is *not* simply the sum of stellar and planetary angular momenta. The system angular momentum is the vector sum of stellar and planetary momenta,  $\vec{J}_* + \vec{J}_p$ , and its magnitude is the magnitude of that sum. The sum of the magnitudes, on the other hand,  $J_* + J_p$ , introduce a systematic error into the calculation of system angular momentum, which is potentially significant when the stellar spin and planetary orbital axes are not aligned, and  $J_*$  is within an order of magnitude of  $J_p$ . The triangle inequality from geometry states that

$$\|\vec{J}_* + \vec{J}_p\| \leq \|\vec{J}_*\| + \|\vec{J}_p\| \quad (2.20)$$

For our purposes, the scalar  $J_*$  is sufficient for comparing the angular momentum of single stars with other single stars.  $J_p$  is also acceptable for a general magnitude-based

comparison of orbital angular momenta of planets with their host stars. The planets' orbital axes and the stars' spin axes cannot be assumed to be aligned and non-opposing. There is growing evidence that obliquities exist in many of the discovered planetary systems.

For example, a true obliquity angle of  $|\psi| \geq 90^\circ$  would result in a system  $J$  magnitude which is less than the planetary magnitude. This is not cause for alarm, however, since only nine planets (<2%), all of which are in single-planet systems, are affected by this condition.

Even the Sun's spin axis is about  $7^\circ$  from the ecliptic. There are to date 55 single-planet systems and a 3-planet system (Kepler-30) in EOD that meet the data selection requirements and have  $\lambda$  measurements reported, where  $\lambda$  is the sky-projected spin-orbit angle determined by the Rossiter-McLaughlin technique. The actual angle between the spin and orbit axes is called the spin-orbit angle, or  $\psi$ , and is generally impossible to measure. Nonetheless some statistical conclusions have been drawn about the probability of observing  $\lambda$  given a model with a particular value of  $\psi$ . According to Fabrycky & Winn (2009), a small value of  $\lambda$  (less than about  $10^\circ$ ) for a transiting system with an edge-on or nearly edge-on orbital plane (between  $80^\circ$  and  $90^\circ$ ) provides a lower limit to  $\psi$ , but determining an upper limit is problematic. Additionally a large  $\lambda$  would generally imply a large  $\psi$  which could be taken as a lower limit if the rotational velocity is not small. Such estimations introduce more uncertainty and confound the discussion of total system angular momentum, and neglect the fact that the vast majority of planets in this sample lack a measurement for  $\lambda$  altogether.

For simplicity, neither the spin-orbit angle,  $\psi$ , nor the projected spin-orbit angle,  $\lambda$ , is considered for this analysis and instead the focus is on general trends in the sample. The scalar  $J_{sys}$  is produced by the simple sum of component magnitudes to describe the overall

system angular momentum. It is acknowledged that the sum of magnitudes is likely larger than the true magnitude of the vector sum,  $\|\vec{J}_{sys}\|$ , noting that its components also contain lowering biases in their own computation – that is,  $v \sin i_*$  is a lower bound for  $v_{eq}$  in the calculation of  $J_*$  and  $m \sin i_p$  is a lower bound for the planetary mass in the calculation of  $J_p$ . This limitation in accuracy is accepted as nonfatal to the overall analysis of what is otherwise a statistically significant sample.

A new quantity  $K$  is introduced which describes relatively how much of the total system angular momentum is contained in the planet(s). This is the ratio of orbital angular momentum to total system angular momentum,

$$K \equiv \frac{J_p}{J_{sys}} \quad (2.21)$$

This is a helpful metric which describes the relative magnitudes of  $J$  in the host star and its planets. It is used to identify possible trends in these systems, as a potential marker for systems that could harbor undiscovered planets, and to compare exoplanet systems to our own Solar System, especially regarding the distribution of angular momentum. It should not be assumed that host stars' spin angular momentum contributes to the system total on the same scale as the Sun in the Solar System (<0.5%).

Lastly, another ratio which describes relative distribution of angular momentum between planets and host star is  $\mathcal{L}$ :

$$\mathcal{L} \equiv \frac{J_p}{J_*} \quad (2.22)$$

It also has the added benefit of sidestepping some of the uncertainties posed by unknown spin-orbit alignments. The relative amount of angular momentum in the planets versus the host star may be discussed without concern for  $\vec{J}$  directions. These results, especially those of multi-planet systems, are compared to the well-studied Solar System.

## 2.6 Biases

Several systematic biases in the data measurements are propagated to the calculations of  $J_*$ ,  $J_p$ ,  $J_{sys}$  and their derivatives,  $K$  and  $\mathcal{L}$ . In summary, there are listed below.

1. Since  $v \sin i_*$  serves as a lower limit for  $v_{eq}$  and therefore for  $\Omega$ , the stellar angular momentum is generally underestimated. That is, the calculation being made is actually  $J_* \sin i_*$ .
2. In the case of transit observations,  $i_p \approx 90^\circ$ . If it is assumed  $i_* \approx i_p$ , then  $v \sin i_* \approx v_{eq}$  is valid and the effect of the bias is on the order of the uncertainty in  $v \sin i_*$ . For non-transiting planets,  $i_p$  is unknown or known to less certainty, and therefore  $\Omega$  is underestimated.
3. If  $i_* \neq i_p$  then both transiting and non-transiting systems will have  $\Omega$  underestimated to varying degrees.
4. The measurement  $m \sin i_p$ , determined from radial velocity measurements, is also an underestimation of the true planet mass  $m_p$  in the absence of transiting data. Therefore  $J_p$  is also underestimated and the actual calculated quantity is  $J_p \sin i_p$ . When  $i_p$  is known and well-constrained, as is the case for transiting planets, the bias is absent.

5. The sum  $J_* + J_p$  underestimates  $\vec{J}_* + \vec{J}_p$ . The difference between  $i_*$  and  $i_p$  ( $\psi$ ) which determine the directions of  $\vec{J}_*$  and  $\vec{J}_p$ , respectively is unknown and unmeasurable. The true magnitude of  $J_{sys}$  would be  $\sqrt{J_*^2 + J_p^2 - 2J_*J_p \cos \psi}$ . The measurement of the sky-projected difference angle ( $\lambda$ ) cannot be substituted, and would produce an underestimate of  $J_{sys}$ . The uncertainties introduced from unknown spin-orbit angles are unknown at this time.
  
6. As  $J_p$  is underestimated for non-transiting planets and  $J_{sys}$  is underestimated in general, the ratio  $K$  is likely skewed to be lower than the true value. Transiting systems may be less affected.
  
7. Since  $J_*$  and  $J_p$  are generally underestimated, the ratio  $\mathcal{L}$  could be relatively unaffected by the measurement biases. However, since the  $m \sin i_p$  bias has a lesser effect on  $J_p$  for transiting systems, it is likely  $\mathcal{L}$  will be not as underestimated for that subset of systems.

The list addresses biases inherent in the measurements of certain quantities, but other biases also exist in the detection methods themselves, to be discussed later.

# Chapter 3

## Data

### 3.1 Planet Discovery Techniques

#### 3.1.1 Overview

Speculation about the existence of extrasolar planets, exoplanets, has captured the imaginations of people for centuries. Only in the late twentieth century were instruments and techniques accurate enough to measure a planet's effect on a star's motion or light. The first planets were discovered around a pulsar, PSR B1257+12, by analysis of variations in precise measurements of the pulsar's rotation period (Wolszczan & Frail, 1992). These types of planets are rare, however, and only one other pulsar planetary system is known, PSR B1620-26 (AB) (Sigurdsson et al., 2003). They are believed possibly to be formed from post-supernova debris. The first planet discovered around a main sequence star, like the Sun, was 51 Pegasi b (Mayor & Queloz, 1995). Thereafter, more and more planets were discovered around MS and Post-MS stars using a variety of techniques, some more fruitful than others. The methods, their history, and relative success are summarized below.

1. *Radial Velocity (RV)*. A star's motion is perturbed by an orbiting planet such that it moves toward and away from an observer, in the observer's line of sight. This is the mutual orbiting of two bodies about a center of mass. The light from the star is Doppler shifted due to this radial motion and provides a minimum mass ( $m \sin i_*$ ) and orbital elements. In particular the eccentricity is measured directly and is well-constrained. The technique requires resolution of the star's velocity on the scale of 1-10 m/s. Until about 2010, this method was primarily responsible for most planet detections. The method is biased to more massive planets at a wide range of separations. Detections are limited by the time scales of the orbital periods, *e.g.* a Jupiter-like planet at 5 AU would need 20+ years of observations to be confirmed.
2. *Transit*. If a planet passes in front of its host star, from the observer's perspective, the light measured from the star will dip in brightness momentarily, and periodically with each orbit. The drop in brightness is small, on the order of 1% or less. The planet's radius, orbital period, and inclination can be determined from multiple transits. When combined with RV measurements, the true mass, density, and all orbital parameters can be found. When only the planet radius is known, some constraints may still be placed on its mass, based on assumptions of composition and distance from the star. The orbital plane of the planet must be nearly edge-on which means that the likelihood of observing a transit (among a randomly oriented population of systems) decreases as the planet-star separation increases. The technique is biased to small orbits but has been effective at detecting both giant planets and smaller icy and rocky ones. After the success of the Kepler Mission, among other transit observing programs, this method has produced the largest number of planet discoveries

to date. The necessary orientation of a transiting system also makes follow-up RV measurements possible.

3. *Timing.* The “timing method” refers to inferred detection by analyzing variations in the periodic measurements of another body. The primary measurement could be pulsar rotation periods, white dwarf pulsation periods, planet transit occurrences, or binary star eclipse variations. Pulsar timing can produce precise detections of very small sub-Earth-sized planets, as well as the orbital elements of multiple planets in the system. Transit timing variations (TTV) provide period/semi-major axis and a maximum mass, favoring more massive planets perturbing the transits of less massive ones. Eclipse timing favors large planets at large separation.
4. *Imaging.* Directly viewing a planet requires blocking or accounting for the light of the star which is far brighter than that emitted or reflected by the planet. Resolving the planet’s light from the star is usually done by observing at cooler wavelengths, such as infrared. Detections made using this method favor nearby stars and large planets at large separations. It is prone to false positives which could be brown dwarfs or sub-brown dwarfs. Over time, the semi-major axis and eccentricity can be determined with varying accuracy dependent on the inclination angle of the orbital plane. A rough estimate of planetary mass may also be inferred by the temperature of the planet. Less than 10 confirmed planets have been discovered by direct imaging.
5. *Gravitational Microlensing.* Two stars are nearly exactly aligned in the line of sight of an observer; the light of the background star is magnified by the gravity of the foreground star and its planet(s). The additional magnification from the planet’s

gravity gives information about its mass, while separation distance can be constrained, but only loosely as inclination angle and eccentricity are unknown. Unfortunately, such lensing events are rare and brief (lasting days or weeks), disallowing repeated measurements of the system over a long period of time. Nearly 20 planets have been discovered with this method.

6. *Astrometry.* The angular position of the star in the plane of the sky is measured with great accuracy over time to chart its movement. In theory, a star accompanied by a massive planet would wobble back and forth or in a circle or ellipse, depending on orientation of the orbit. Despite great advancements in accuracy and precision, no claims of exoplanets from ground searches using this technique have been confirmed. The planet's mass could be determined from such an observation if it were successful.

Of the methods described above, Transit and RV together account for over 95% of all confirmed exoplanet discoveries and have dominated the most recent discoveries (Figure 3.1). These methods are well-established, and in general cover a broad range of star and planet masses. Transiting planets can often provide RV data, and some RV detected planets can also transit. When both methods are able to be used, they provide more complete and accurate information about the system.

Detections from Microlensing and Imaging do not have  $v \sin i_*$  reported, and therefore  $J_*$  cannot be calculated. Orbital periods are not consistently available for these two types and are very large when they are, precluding an accurate assessment of  $J_p$ . For those detected by Imaging, the stellar mass, planet mass, and uncertainties in planet mass are very large. Conversely, for Microlensing systems, the star mass and planet mass are biased

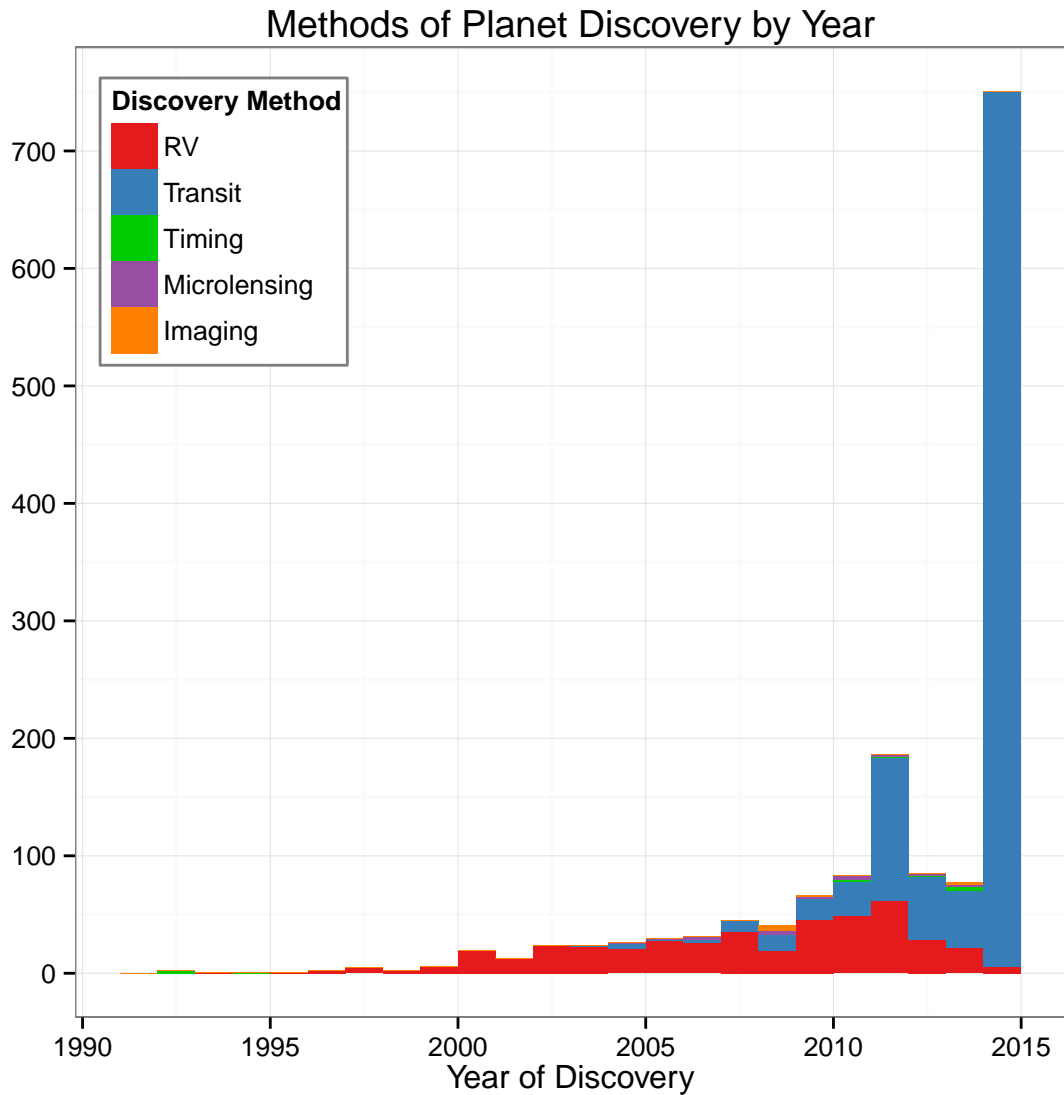


Figure 3.1 The rate of planet discoveries has generally increased since the first two were detected nearly 15 years ago. There has been a recent surge (years 2011-2014) in transit detections from the Kepler Mission. Prior to that, radial velocity was the dominant detection method. Data obtained from EOD and includes all 1523 confirmed planets.

to very small values (about  $0.1-0.6 M_{\odot}$ ). The meager yields of discoveries by these detection methods, along with their lack of a continuous range in both stellar mass and planet mass, make them unsuitable for inclusion in the main data set of this research.

The planets used in this thesis are primarily Transit and RV detections, with some Transit Timing and RV Timing detections. The Timing detections are usually additional planets in multi-planet systems, where the primary detection was either Transit or RV. These planets are classified by their primary method of detection (Transit or RV), instead of as “Timing.”

### 3.1.2 Detection Method Biases: RV and Transit

The RV and Transit methods of planet detection are not free of biases, but both categories represent statistically significant samples across a broad range of stellar and planetary parameters. While others have attempted to avoid bias by excluding planets detected by one method or the other (Alves et al., 2010; Paz-Chinchón et al., 2015), we have included both groups but make note of their tendencies to skew the overall results. General known biases are summarized here, while further biases revealed in the analysis are discussed more fully in Chapter 4. Some biases are complementary, such as the planet mass and semi-major axis relationship, as illustrated in Figure 3.2. This directly affects the calculation of  $J_p$ , as will be shown later.

## 3.2 Sources and Selection

Several reputable databases of exoplanets have been developed in recent years, and most are available to the public. Each database administrator or administrative group strives to include the objects and parameters that they believe are most relevant for their own research and for those who might use the database. While there exists a great deal of overlap in the offerings of these databases, they operate by slightly different criteria, and therefore report

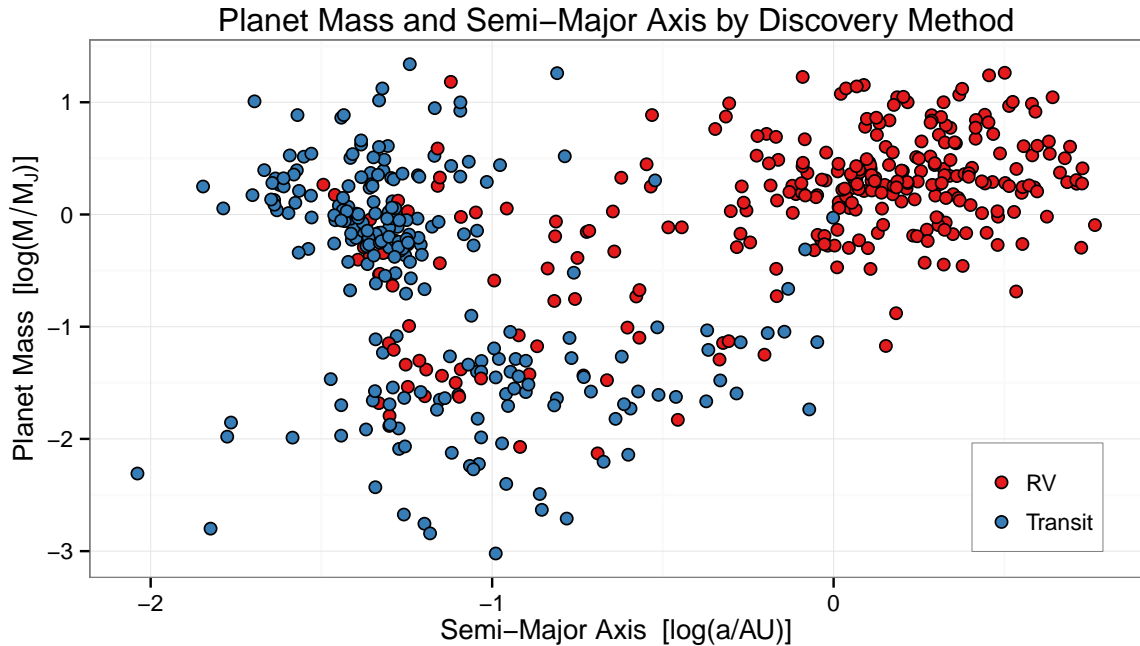


Figure 3.2 Scatter plot showing the biases of the Transit and RV methods of detection as they relate to both planet mass and semi-major axis. Several clusters of planets are apparent.

somewhat different numbers, for example, for total number of planets discovered. Main differences between the databases fall into two categories and are summarized here.

First, the objects themselves are at times the subject of debate:

- Since 28 February 2003, the International Astronomical Union (IAU) has defined a planet to have a maximum mass of  $13 M_J$ , but the major databases include objects with  $m \sin i$  well over  $20 M_J$ , and with differing maximum masses as their cut-off criteria.
- The naming of planets has become standardized with the first planet discovered labelled “b,” the next discovered “c,” and so forth. The host star name, on the other hand, which is generally prefixed to the planet’s designation, may have several different names. Some host stars are well-known members of constellations but may also

be numbered in a stellar survey, with the prefix HD, HIP, or GJ, for example. Some are members of multiple exoplanet search programs, such as WASP-11/HAT-P-10 and HAT-P-27/WASP-40. Databases then use their own preferred method for star naming, resulting in mismatched or slightly different names referencing a single star. It adds some difficulty to the automation of joining, processing, and cross-verifying among databases.

- Confirmation of planet existence and inclusion varies. An online announcement or conference presentation might suffice for one database while another requires refereed journal publications. Some are updated on a daily basis, while others reflect changes quarterly or semi-yearly. Sometimes, planet discoveries are retracted, and the same issues of timeliness of updates produce inconsistencies between databases.

Second, the data fields and values are sometimes inconsistent within and between databases:

- Often the first planet in an exoplanetary system is discovered but its host star properties are not reported or measured. If the star is part of one or more stellar surveys, those parameters, when available, are adopted by some databases. Data admins may prefer one survey's data to another resulting in slightly different reported values, but the method is often not documented in the database help pages.
- Multiple investigations of a planetary system may yield different measurements of its parameters. Their accuracy and precision are dependent on a number of factors, including but not limited to, quality of instrumentation, differences between orbital and stellar parameter fitting models, and skill of the observer.

- New discoveries in systems with confirmed planets can help refine measurements of the primary discoveries, but the values and precision of stellar parameters may differ significantly, especially those which are derived.
- Because all databases are maintained and updated by people, errors, typos, and omissions slip through even in well-maintained databases. The process of collecting of data is subjective and not standardized.

Despite these challenges, most data in each database are correct (*i.e.* consistent with the literature), up-to-date, and self-consistent within each system. The differences in offerings of each database used in this research are summarized below.

The primary source of data was obtained from the Exoplanet Orbit Database (EOD) (see Wright et al., 2011; Han et al., 2014). Additional stellar data was acquired from the NASA Exoplanet Archive (<http://exoplanetarchive.ipac.caltech.edu>, last accessed 9 January 2015), and the Extrasolar Planets Encyclopaedia (EPE) (<http://exoplanet.eu>, last accessed 20 November 2014). Outliers and inconsistencies were checked against EPE and the Kepler confirmed planets table (KCP) hosted within the Mikulski Archive for Space Telescopes (MAST) data archive project, which is derived from a subset of the Kepler Objects of Interest (KOI) catalog by NExSci ([http://archive.stsci.edu/kepler/confirmed\\_planets](http://archive.stsci.edu/kepler/confirmed_planets), last accessed 7 January 2015). This last table is maintained by the Space Telescope Science Institute (STScI) with non-Kepler exoplanets included. Stellar ages, of varying inclusion and agreement, were extracted from EPE and KCP.

Additionally, the Open Exoplanet Catalogue (OEC) is an open source, community-maintained database of exoplanets with open discussion forums (Rein, 2012). It is noted

here for its innovative and collaborative style, but because it is decentralized and alterable by anyone, it was ultimately passed over for inclusion in this research.

EOD was chosen for the framework of the data set because the data is gathered only from peer-reviewed sources, it is regularly maintained (last updated 5 December 2014), reference papers are linked to relevant data sources, and it provides the most complete set of all quantities necessary for the calculation of stellar, planetary, and system angular momentum. In particular, KCP and EPE do not provide  $v \sin i_*$ , a key parameter needed for calculating stellar spin angular momentum. EPE pages were consulted regularly for their more extensive and hyper-linked, recently published reference papers.

### **3.3 The Exoplanet Orbit Database**

The Exoplanet Orbit Database (EOD) provides planetary, orbital, and stellar parameters necessary to calculate planetary system angular momentum. It only contains data from sources that are peer-reviewed, but also optionally includes potential planets from the Kepler planet finding mission, called “Kepler candidates.” EOD contains 1499 planets belonging to 922 unique systems with “good orbits,” (<http://exoplanets.org/>, last accessed 22 March 2015). This is supplemented by 24 planets discovered by direct imaging and microlensing, and over 3300 Kepler candidates. The web interface allows for query-driven access to the whole of the data, which may be displayed in tabular or plot formats. The tabular display format may be downloaded by users as raw text (comma-separated values) in the user’s choice of units, and offers explicit selection of and sorting by columns (data fields). Results may be filtered by various criteria expressed in logical statements. Nearly every datum

is hyperlinked to its published source, and uncertainties may be optionally included or excluded for each field. (Wright et al., 2011)

All numerical quantities accessible for download include general, upper bound, and lower bound uncertainties, when available. For example, the EOD fields containing general, upper, and lower uncertainties for MSINI, would correspond to UMSINI, MSINIUPPER, and MSINILOWER, respectively. Where the upper and lower bound uncertainties are unequal, an average is reported in the general uncertainty field. Only the general uncertainties were used for the error propagation as described in Appendix B. The database was filtered to only include those entries with populated fields for stellar mass, stellar radius,  $v \sin i_*$ , and semi-major axis. At least one of the fields MASS, MSINI, MSINIUPPER, or MASSUPPER were populated for each planet entry. The filter also excluded binary systems. Table 3.3 lists the most important fields downloaded from EOD for analysis, and when pertinent, the corresponding symbols used in this document.

Despite robust offerings, only about a third of the entries in EOD include the necessary quantities to determine  $J_*$  and  $J_p$ . The absent quantity is usually  $v \sin i_*$  (VSINI) or stellar mass (MSTAR). However, special attention was given to table entries which reported uncertainty in, for example, planet mass, but the mass value itself was empty or zero. A simple query requiring the presence of data in the MASS field might miss such a planet, but in fact the planet/system can be used for this research because an upper bound has been reported, and a reasonable approximation for the mass substituted. This is explored in more detail below.

Stellar ages, spectral types, and moments of inertia/inertia coefficients were not contained in the EOD and were obtained elsewhere, inferred, or interpolated from models.

Table 3.1. EOD Downloaded Fields

Symbol, data	Quantity	EOD field name
Stellar Parameters		
TrES-3,WASP-11,...	Star name	STAR
$M$	Mass	MSTAR
$R$	Radius	RSTAR
$v \sin i_*$	Projected surface velocity	VSINI
$T_{\text{eff}}$	Effective temperature	TEFF
[Fe/H]	Metalicity	FE
n	Number of planets	NCOMP
	Multi-planet system? (logical flag)	MULT
Orbital Parameters		
b, c, ...	Planet name	COMP
$m$	Planet mass	MASS
$m \sin i_p$	Projected planet mass (RV)	MSINI
	How is planet mass determined?	MASSREF
$a$	Semi-major axis	A
$e$	Eccentricity	ECC
$i_p$	Orbit inclination	I
$\lambda$	Projected spin-orbit angle	LAMBDA
	Transiting planet? (logical flag)	TRANSIT
	Discovery method of first planet	STARDISCMETH
	Discovery method of planet	PLANETDISCMETH

### 3.4 Data Cleaning

Basic data cleaning was performed on EOD data, and planets or stars with missing or conflicting parameters, or parameters far outside expected or reasonable values were noted and corrections made if necessary. Uncertainties for  $M_*$ ,  $R_*$ ,  $v \sin i_*$ ,  $m$ ,  $a$ , and  $e$  were checked for existence, and if percent errors were zero or greater than unity, they were investigated and adapted.

### 3.4.1 Inclusions and Exclusions

As mentioned earlier, a subset of data was downloaded from EOD with fields containing nonzero values for M, R, VSINI, and A. The original download contained 537 planets in 429 unique systems.

- The two smallest mass host stars were dropped from the sample: GJ 1214 ( $0.157 M_{\odot}$ ), and the 3-planet system Kepler-42 ( $0.130 M_{\odot}$ ).
- WASP-33 with  $v \sin i_*$  of 90 km/s and several stars with masses  $> 2.5 M_{\odot}$  were retained, to be discussed later.
- Binary systems were excluded from this analysis.
- Kepler-410 A b, a circumbinary system, was incorrectly identified with a false binary flag and was excluded from the sample.

The final working sample contains 532 planets in 426 unique systems.

### 3.4.2 Corrections and Conflicts

Early analysis of  $J_*$  and  $J_p$  outliers revealed that some planets/stars did not have reasonable values; they were investigated and corrected. Also, several mismatched fields within multi-planet systems were found and corrected.

- Kepler-407 had a misreported stellar radius ( $0.1 R_{\odot}$ ) which was corrected to  $1.01 R_{\odot}$ . (Marcy et al., 2014)
- The planet masses of Kepler-37 b-d appeared to be mistyped into EOD, as the literature reference URL was incorrect, and also there were no masses reported in

the orbital reference article (Barclay et al., 2013). Instead, the authors explain that masses are calculated by the relation  $m_p/m_\oplus = (R_p/R_\oplus)^{2.05}$ . Using this formula, Kepler-37’s planet masses and uncertainties were corrected.

- Kepler-10 b’s planet mass and error had not been updated in EOD per the most recent literature, and were adjusted to match Dumusque et al. (2014).
- Kepler-10 c had a decimal placement error in the planet mass uncertainty; this, too, was updated to reflect Dumusque et al. (2014).
- Marcy et al. (2014) reported a mass uncertainty for Kepler-102 f over 5 times greater than the value itself. This is apparently due to uncertainty in the RV measurements and fittings. The reported mass is  $0.62 \pm 3.3 m_\oplus$  with an upper bound of  $5.2 m_\oplus$  and a radius of  $0.88 \pm 0.03 R_\oplus$ . It is likely with such a well-constrained radius that the planet is rocky, and therefore, the uncertainty is grossly overestimated. The uncertainty in mass is adjusted to 20% of the value:  $0.12 m_\oplus$ .
- HD 120084 had upper and lower bounds listed for the stellar mass uncertainties in EOD, and these were converted to uncertainties.
- Kepler-27 b and c have differing reported  $v \sin i_* \pm \sigma$  reported for the host star in the literature (Steffen et al., 2012), but EOD has adopted the values reported for planet b:  $0.6 \pm 5.0$  km/s. This produces a percent error over 8 times the value. The  $v \sin i_*$  values for planet c,  $2.76 \pm 1.52$  km/s, are adopted for the star.

- The stellar mass reported for HD 204313 d ( $1.020 M_{\odot}$ ) differed from HD 204313 b ( $1.045 M_{\odot}$ ), and the former lacked  $R_*$  and  $v \sin i_*$  data, so the stellar parameters for the latter were used for calculation of  $J_*$ .
- The stellar radius reported for Kepler-26 d-e ( $5.71 R_{\odot}$ ) differed from Kepler-26 b-c ( $5.90 R_{\odot}$ ), and the former lacked  $M_*$  and  $v \sin i_*$  data, so the stellar parameters for the latter were used.
- WASP-50 b had the stellar inclination and its error listed in place of the orbital inclination. This was corrected to  $i_p = 84.74 \pm 0.24^{\circ}$  from the literature (Gillon et al., 2011).
- WASP-71 b had a number of misreported stellar and orbital parameters that appear to be the result of mistakes in data entry. These were corrected to values published in Smith et al. (2013) and Valsecchi & Rasio (2014), with preference given to the more recent parameters when they differed between the two sources.

### 3.4.3 Missing Data

Kepler-20 b-d and Kepler-406 c lacked  $v \sin i_*$  data, so these fields were populated by those from Kepler-20 e-f and Kepler-406 b, respectively.

If fields required for the calculation of  $J_*$  and  $J_p$  lacked uncertainties, or included uncertainties that were set to zero or that conflicted with their parent value in some way, a best guess for new uncertainties, based on uncertainties in existing values for that type of data, was made and these were applied to the data set.

The transiting planets Kepler-62 b-f, Kepler-100 c, Kepler-102 b, Kepler-407 b, and WASP-33 b had no planet masses and no  $m \sin i_p$  values reported. There were upper bound uncertainties (MASSUPPER), and MASSREF contained inconsistent descriptions (or in the case of Kepler-62 b-f, MASSREF referred to the discovery paper). Ultimately, the upper bound of the mass was taken as reported. To choose planet masses for angular momentum calculations, the mean percent error was calculated for all transiting planets with nonzero mass and nonzero uncertainty in the mass. The mean was 0.203, so the missing masses were set equal to 0.8 times their upper bounds, with uncertainties set to  $\sigma_m = \pm 0.2$ . It is hoped these new values bracket the true mass, or else overestimate the uncertainties.

When the uncertainty in the stellar mass or radius was unavailable or reported as zero, a new uncertainty was derived in a method similar to that done for the planetary mass uncertainties. The mean percent error in host star mass is 0.063. The new uncertainties  $\sigma_M$  were set to 0.1 times the stellar mass for the 18 affected host stars. The mean percent error in host star radius is 0.045. The new uncertainties  $\sigma_R$  were set to 0.1 times the stellar radius for the 7 affected host stars.

The uncertainty in the semi-major axis was unavailable or reported as zero for 17 planets. Following the method for stellar mass above, the mean percent error for planets with nonzero uncertainty in  $a$  was 0.026, and the new uncertainties were set to 0.05 times the semi-major axis value.

The uncertainty in the orbital period was unavailable for 30 planets. Following the method for stellar mass above, the mean percent error for planets with nonzero uncertainty in  $P$  was 0.0076, and the new uncertainties were set to 0.015 times the orbital period.

EOD did not report, or reported a value of zero for, the uncertainty in  $v \sin i_*$  for 79 host stars. Also, the uncertainty in  $v \sin i_*$  was equal to  $v \sin i_*$  for 30 host stars. Following the method for the stellar mass above, the mean percent error for host stars with nonzero uncertainty in  $v \sin i_*$  and  $\sigma_{v \sin i_*} \neq v \sin i_*$ , and was 0.336, and the new uncertainties were set to 0.33 times the projected rotational velocity.

For 25 planets, the orbital eccentricity reported by EOD was zero, but the upper bound was nonzero. Since eccentricity ranges from 0 to 1, the mean uncertainty in eccentricity for planets with nonzero  $e$  and nonzero  $\sigma_e$  was calculated. This value was 0.051. For the affected planets, the eccentricity was set to equal the upper bound, and the new uncertainty was set to 0.05. About half of the affected planets had a somewhat significant upper bound of  $e \geq 0.1$ .

When the eccentricity was not available or was reported as zero, and its uncertainties were not available or were reported as zero, the angular momentum was calculated with Equation 2.14, and the orbit was assumed to be circular or nearly circular. The semi-major axis  $a$  was used in place of  $r$ , and the orbital period  $P$  was available for all 148 affected planets.

### 3.4.4 Other Adjustments

Because some planetary masses in EOD were incorrectly calculated from  $m \sin i_p$  and  $i_p$ , and the MASSREF field indicated that the mass had been determined by this method, the calculation was performed as a check. If EOD values were significantly different from our result ( $> 10\%$ ), the data were corrected, and the errors for mass were propagated in the usual way.

A check against correctly reported semi-major axis values was also performed with Kepler’s third law and the reported orbital period. Nearly all deviated by less than 2%. Only Kepler-26 d-e were found to have EOD values of  $a$  almost 15% of that calculated by

$$a_{\text{theory}} = \sqrt[3]{M_* P^2} \quad (3.1)$$

where  $a_{\text{theory}}$  is in AU,  $M_*$  is in solar masses, and  $P$  is in years. The periods were verified as correct in Giguere et al. (2012), and the semi-major axis values adjusted to our calculations.

### 3.5 Stellar Classification

Except for the exclusions and corrections already noted, the data set is examined as a whole, with attention focused mainly on main sequence systems. The three foundational papers of this thesis (McNally, 1965; Kraft, 1970; Kawaler, 1987) derive angular momenta from typical or average parameters representative of a bin or range of spectral types or masses. Their findings addressed only main sequence, hydrogen-burning stars. Wolff et al. (2004), on the other hand, examined both MS stars and PMS stars during their contraction phase, and even found the Kraft law for his sample of stars. No Kraft relation, however, has been determined for stars in their post-MS life, as subgiants, giants, and beyond. Since the moment of inertia and stellar radius change rapidly and drastically for solar type stars after their hydrogen is depleted, it is difficult to assign a value for angular momentum with confidence to subgiants in particular. Therefore, main sequence stars are the primary focus of the results in Chapter 4, consistent with focus of much of the background literature.

To this end, the host stars were processed to identify three main sub-groups: Giants, Subgiants, and likely Main Sequence (MS) members. Classification was determined by a combination of several methods. First, stellar spectral and luminosity classes were gathered from the EPE and KCP databases and cross-referenced with the working sample of 426 stars from EOD. This produced several subgroups: Stars with two luminosity classes which are in agreement, stars with two luminosity classes which are in conflict, stars with only one luminosity class, and stars with no luminosity classes supplied by EPE or KCP (“unclassified”). Second, the stars were plotted on a theoretical HR diagram. The theorist’s HR diagram (Luminosity vs.  $T_{\text{eff}}$ ) was used instead of the observer’s version (Magnitude vs. B-V color) because B-V information was not available for 52 stars and magnitude data was not available for 70 stars. Luminosity was not supplied by EOD but  $T_{\text{eff}}$  and  $R_*$  were reported for every star in the sample. The luminosity was then determined by the well-known Stefan-Boltzmann equation for stars:

$$L_* = 4\pi\sigma R_*^2 T_{\text{eff}}^4$$

where  $\sigma$  is the Stefan-Boltzmann constant. For the sun,  $L_{\odot} = 3.839 \cdot 10^{26}$  W (Carroll & Ostlie, 2006), and the log of the luminosity is the abscissa on the HR diagram:

$$\log L = \log \left( \frac{L_*}{L_{\odot}} \right)$$

Zero-age Main Sequence (ZAMS) values were taken from the starting parameters of the MS models by Claret (2004), and from the ending values of Claret’s (2012) PMS models for masses  $< 0.8M_{\odot}$ . To graphically define the boundary between Main Sequence

and Subgiant classification, the stars with two reported luminosity classes in agreement were plotted on the HR diagram. Lines relatively parallel to the ZAMS which roughly divided the groups were fit by eye and overplotted. These became the Subgiant-Main Sequence boundary (S-MS) and Giant-Subgiant boundary (G-S) – guides dividing the evolved states of the stars on the diagram.

Stars with two luminosity classes in conflict were investigated on a case-by case basis by examining literature with the most recent observations. In nearly all of the conflicting cases, EPE had reported the most recently published spectral and luminosity class data, per the literature. EPE also provided an up-to-date list of hyperlinked references for each star/planet. On the other hand, KCP does not clearly indicate how their luminosity class data was obtained. At the time of download, at least for non-Kepler items, the spectral classifications were not up-to-date with the most recent literature. Therefore, EPE luminosity class data were preferred. Even so, two stars classified as Main Sequence, according to EPE, were plotted far above the S-MS boundary. Upon reviewing the referenced literature, these had apparently been misclassified by database administrators and were both reclassified as Subgiants.

Next, unclassified stars were plotted on the diagram. Those which were plotted above the G-S border were classed as Giants. Those plotted above the S-MS border were classed as Subgiants. The remainder were classed as MS dwarf stars. Of these unclassified stars, about 40 fell on or very near the S-MS border. The most recent literature was consulted and clues to stellar activity were used to classify these stars, when available. For example, main sequence stars tend to be more chromospherically active than evolved stars, so those described as “active” were classified as MS, while those described as, for example,

“evolved” or “quiescent,” were labelled Subgiant. The remainder were given a classification in agreement with their position on the HR diagram, with respect to the lines separating those classes.

There are likely several Subgiants that are classed as MS and vice versa. This is due to the fact that stellar mass and radius are derived quantities and not directly measurable. The radius, in particular, is used to determine the luminosity (and therefore its vertical placement) on the HR diagram. The class boundary lines are imprecise rough estimates and ignore metallicity which can shift a star’s relative position on the diagram. Therefore an exact line separating classes cannot be drawn with accuracy. Some Subgiants will undoubtedly lie in the MS area of the diagram. Further, the sample classifications are biased to be more MS-heavy, especially at smaller masses, less than  $1.2 M_{\odot}$ . For these low-mass stars, the evolutionary track on the HR diagram moves more upward than left or right, into areas that may be part of the main sequence of a more massive star. Therefore, two stars might occupy the same position on the diagram but have different masses and evolutionary states. The effect of this slight bias likely has a negligible impact on the overall results, due to the large sample size of the MS group.

The final classifications of all sample stars are represented in Figure 3.3. Appendix C lists all 426 host stars and their parameters with classification of G, S, or MS, for Giant, Subgiant, or Main Sequence, respectively. The sub-grouping resulted in 37 Giant systems (2 multi-planet), 73 Subgiant systems (8 multi-planet) and 316 MS systems (55 multi-planet). Tables 3.2 and 3.3 provide an overview of the basic sub-groupings of host stars and system types in the sample data. The most notable aspect of this classification is that about 20% of the MS and Subgiant stars have multi-planet systems, but only 2 of the 37 Giants host more

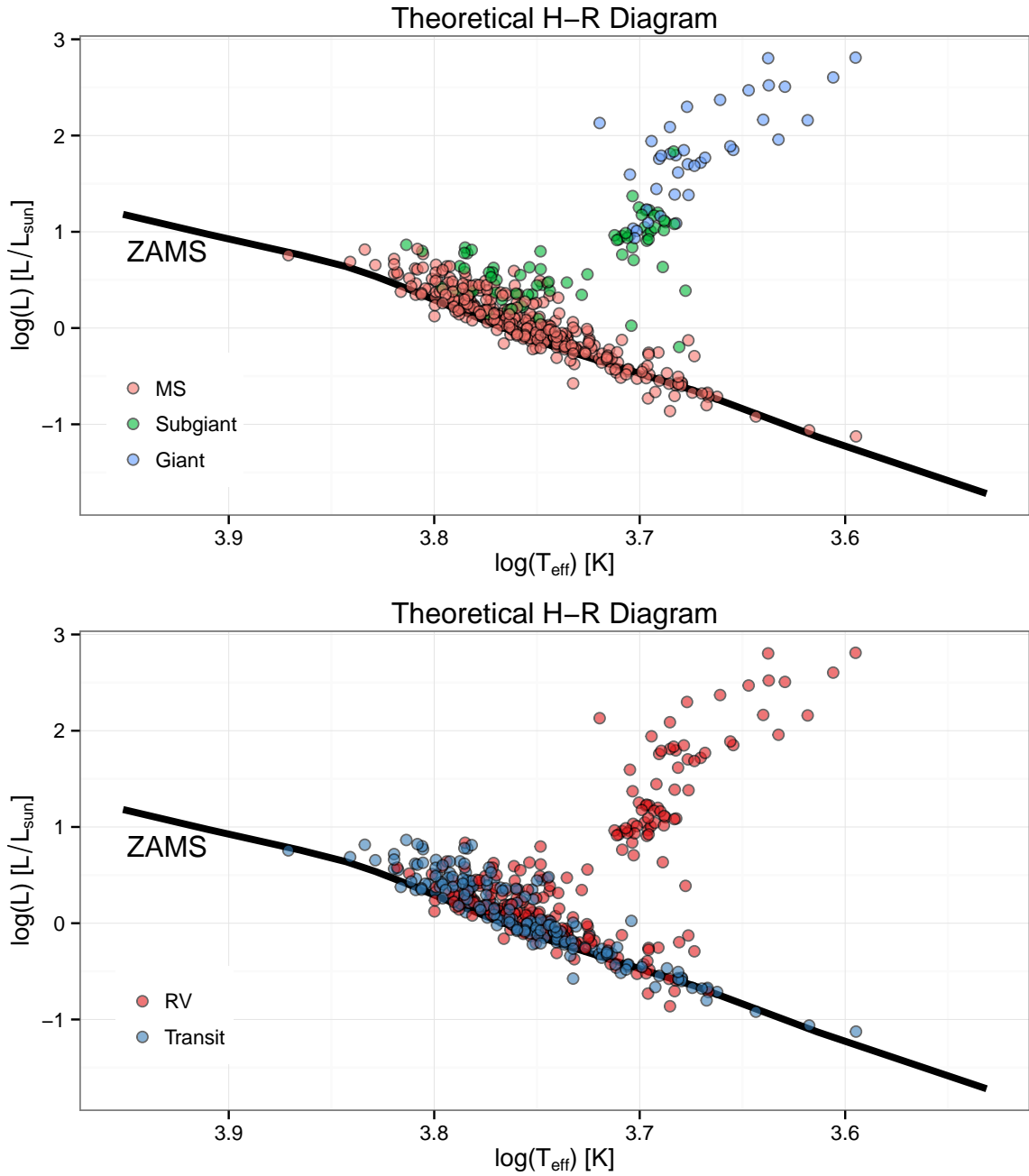


Figure 3.3 The theorist's Hertzsprung-Russell diagrams by stellar classification (top panel) and discovery method (bottom panel). ZAMS line shown for reference with values taken from models by Claret (2004, 2012)

than one detected planet. A bias also exists between the Transit and RV detection methods.

More MS systems have been detected by the Transit method, but more multi-planet systems

Table 3.2. Summary of Host Star and System Classifications

System type	Single-planet systems	Multi-planet systems		<b>Total stars</b>	<b>Total planets</b>
		(stars)	(planets)		
MS	260	56	150	<b>316</b>	<b>410</b>
Subgiant	65	8	18	<b>73</b>	<b>83</b>
Giant	35	2	4	<b>37</b>	<b>39</b>
Totals	360	66	172	<b>426</b>	<b>532</b>

Table 3.3. Summary of System Type and Discovery Methods

	MS Systems			Non-MS Systems		
	Single	Multi	<b>Total</b>	Single	Multi	<b>Total</b>
RV	108	33	<b>191</b>	83	9	<b>92</b>
Transit	152	23	<b>169</b>	17	1	<b>18</b>
Totals	260	56	<b>316</b>	100	10	<b>110</b>

were discovered by radial velocity measurements, regardless of system classification as MS or non-MS. Transits detected by Kepler orbit mainly cooler dwarf stars, which have long life spans and are likely to still be on the Main Sequence when observed. The RV technique has also been in use for over 20 years, so there have been more opportunities to observe and detect multi-planet systems, especially for systems with long-period planets. Transit-based detections started only about a decade ago.

### 3.6 Stellar Properties

The distribution of masses of the host stars in toto appear nearly normal about  $1.15 \pm 0.31 M_{\odot}$ , as seen in Figure 3.4, with 10 out of 426 host stars outside  $\bar{M}_{*} \pm 3\sigma$ . In the subset

of probable Main Sequence stars, the mean stellar mass is  $1.04 \pm 0.19 M_{\odot}$ . Only 2 out of 292 MS host stars have masses outside the  $3\sigma$  limit. The full sample seems to be somewhat biased to larger stars, and the largest stars with mass  $> 2 M_{\odot}$ , are all classified as Giants or Subgiants.

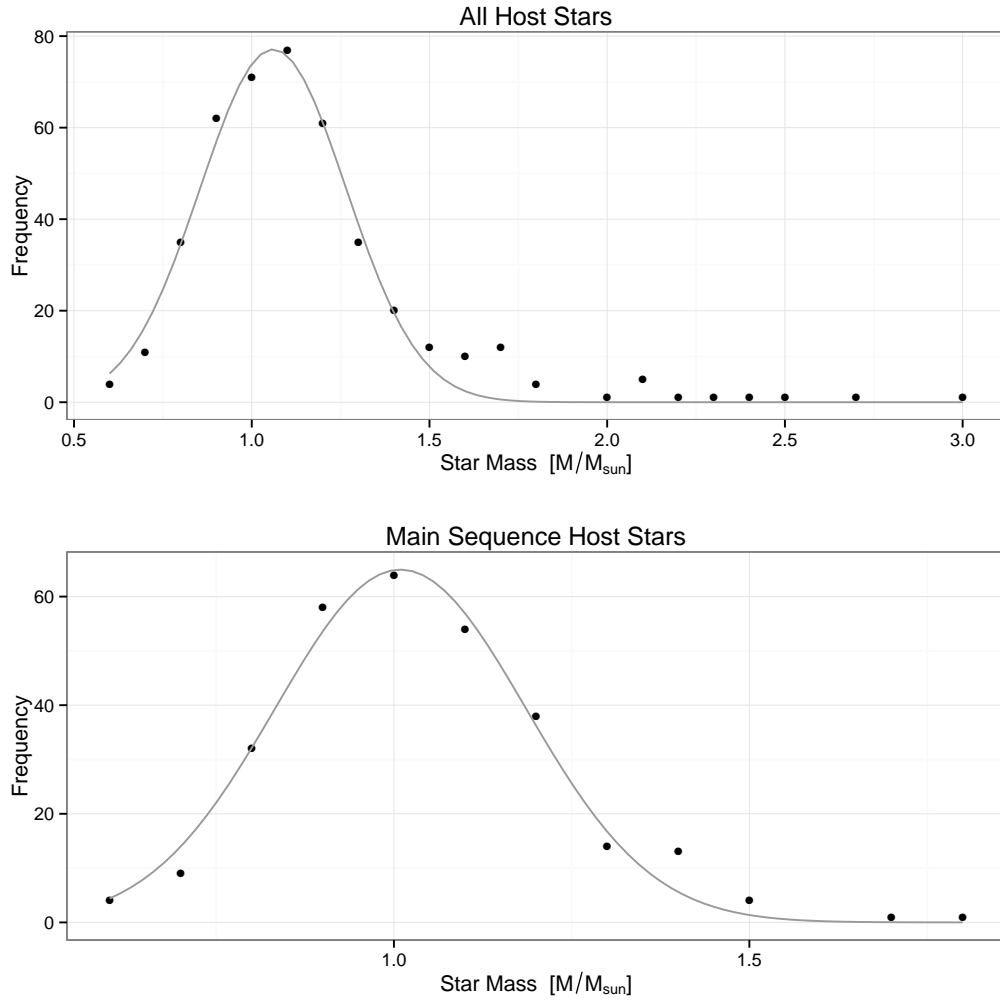


Figure 3.4 Host star mass was binned into  $0.1 M_{\odot}$  groups across the x-axis, and the counts per bin were plotted on the y-axis. Agreement was found for both samples by fitting to normal distribution, with p-values for both with significance levels  $< 0.0001$ . Top: All host stars selected are considered, with a mean of  $1.15 \pm 0.31 M_{\odot}$ . A long tail to the right indicates a paucity of systems in the sample with massive host stars. Bottom: The subgroup of Main Sequence host stars do not include those with masses  $> 2 M_{\odot}$ .

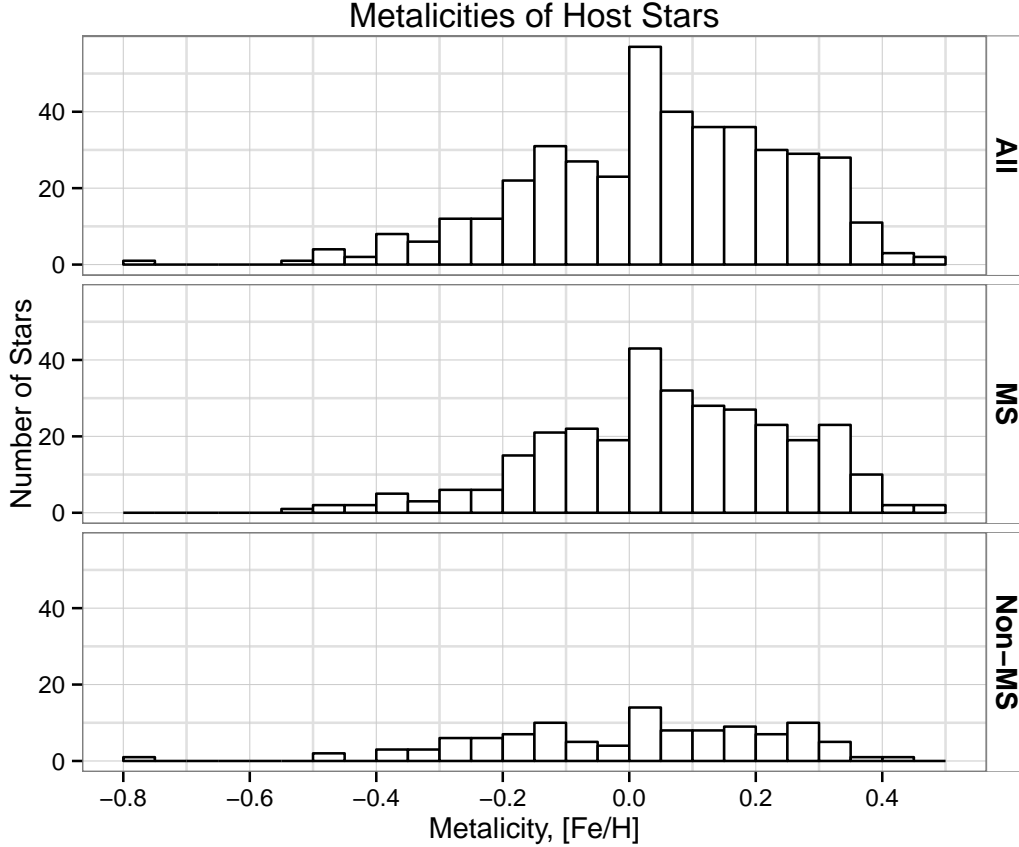


Figure 3.5 Histograms of metallicity in host stars. As expected, the top panel shows planet-hosting stars are skewed to being metal-rich. The middle and bottom panels demonstrate that MS stars with planets are also metal rich but subgiants and giants (non-MS stars) do not exhibit the trend as strongly.

MS host stars with unusual values for at least one of the parameters needed to quantify their angular momentum are noted. “Fast rotators,” stars with large  $v \sin i_p$  were identified: CoRoT-11 and OGLE2-TR-L9 have  $v \sin i_*$  of  $40 \pm 5$  km/s, and WASP-33 is at  $90 \pm 10$  km/s. All other stars have  $v \sin i_* < 25$  km/s. The mean of all host stars’  $v \sin i_*$  is 3.8 km/s, but if the fast rotators are excluded, the mean drops to 3.4 km/s. All three fast rotators are MS single-planet systems with transiting Hot Jupiters (HJ).<sup>1</sup> WASP-33 has a large reported spin-orbit angle,  $\lambda = -109^\circ$  (per EOD). As described before, this will not be used in the

<sup>1</sup>A Hot Jupiter is defined as a planet with a mass of  $\geq 0.1 M_J$  and semi-major axis of  $< 0.1$  AU.

calculation of angular momentum, but is useful to note that the system possibly had a dynamic past.

Metallicity is not reported for five host stars. For the rest,  $[\text{Fe}/\text{H}]$  ranges from -0.790 to 0.460 and is skewed toward higher metallicity. The mean metallicity is slightly higher than solar, at 0.042 with the median value at 0.050. For MS stars, the mean is 0.058, and the median is 0.050. These results are consistent with repeated findings that planet-hosting stars are more metal rich than those without detected planets (e.g. Gonzalez, 1997; Fischer & Valenti, 2005) and that main sequence stars in particular exhibit this correlation while giant stars with planets do not (Pasquini et al. 2007). See Figure 3.5. Metallicities are not used in the analysis, but it is noted that the values are not significantly different from previous findings or the larger population of planet hosting stars.

### 3.7 Planetary Properties

Half the working sample of planets (263) are  $1 M_J$  or less but the majority, about 80%, are greater than  $0.1 M_J$ , which is typically due to bias in detection methods. Both the Transit and RV methods effectively detect large planets, but smaller planets are more difficult to detect. The Doppler shift measured in the RV method is much less for small planets due to the smaller planetary masses. The photometric dip in brightness detected by the transit method, is much less due to smaller planetary radii of planets.

The most useful information about these planetary systems comes from data obtained when both methods have been used to obtain measurements. Transiting planets provide well constrained data about a planet's orbital period, semi-major axis, and inclination angle. RV measurements provides period, eccentricity, and  $m \sin i_p$ , a lower limit on planet

mass. For planets that are both transiting and provide RV data, the true mass may also be determined and is usually found to be about 15% higher than  $m \sin i_p$  (<http://exoplanets.org/help/common/data>), however, this is not necessarily true for RV detections without transits. Analysis of transit timing variations (TTV) can uncover other non-transiting planets in the system and further constrain the properties of transiting planets. At this time, orbital parameters of TTV detections can be determined, but often with large error bars. (Hadden & Lithwick, 2014)

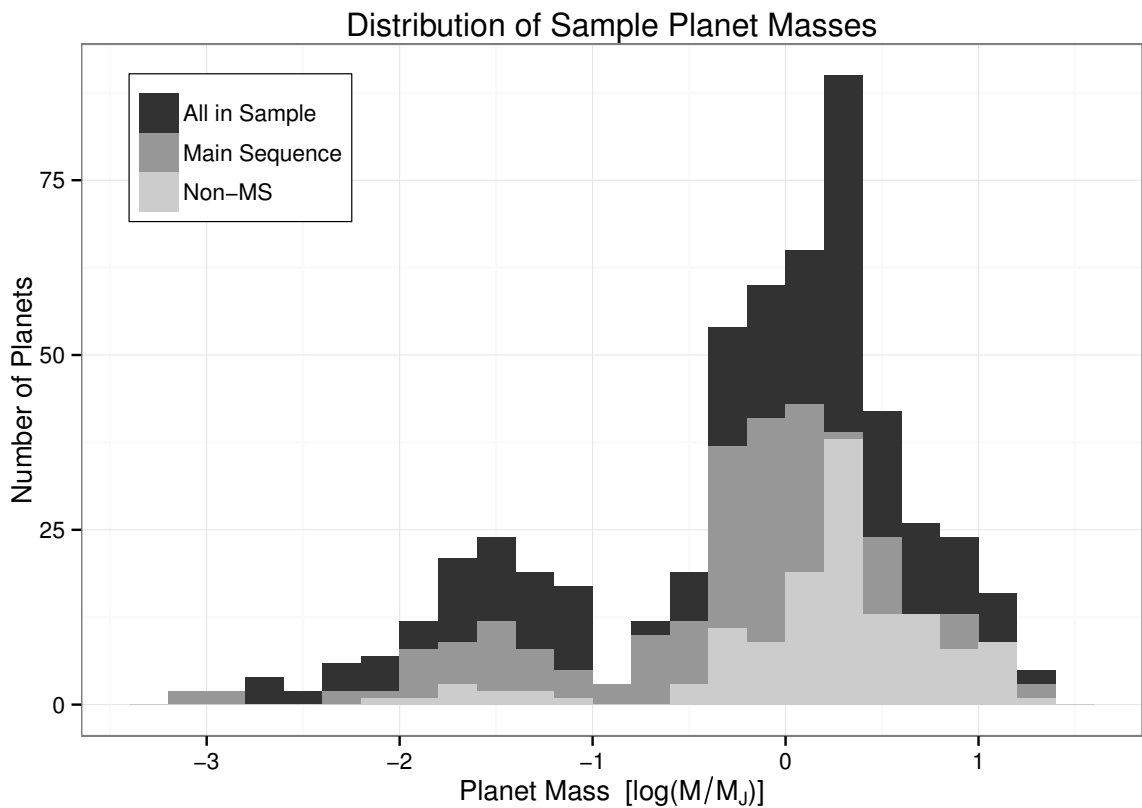


Figure 3.6 Non-stacked histogram of sample planet masses. The bimodal shape of the distributions is independent of stellar classification.

The planet mass distribution of this sample is bimodal and possibly trimodal on a logarithmic scale, an effect that transcends stellar evolutionary classification, as seen in

Figure 3.6. These three modes can be labelled from left to right as Earths (small rocky planets), Neptunes (mid-sized icy planets), and Jupiters (gas giants), a common refrain in exoplanetary categorization. The main split between planet size classifications is at  $0.1 M_J$ . This sample contains a large fraction of hot Jupiters, including 169 HJs in 169 unique systems. Three of the 169 HJs are in multi-planet systems. Of the single-planet HJ systems, 21 were discovered by RV detection, including 2 which also transit. The majority of known HJs are transits. The most recent releases of Kepler data confirm that smaller icy and rocky planets are plentiful (Batalha et al., 2013). Indeed in this sample, only about a quarter of the Kepler systems contain hot Jupiters. Appendix D lists all 530 planets with their orbital parameters, including a code column to flag transiting planets (T), and Hot Jupiters (HJ).

Referring again to Figure 3.2, two distinct populations emerge that are strongly correlated with detection method. In the upper right, mostly planets discovered by the radial velocity method (RV) dominate the area of larger planets in larger orbits, resulting in larger  $J_p$ . In the upper left, large planets with smaller orbits are mostly detected via the Transit method. Lastly, in the bottom half of the figure, smaller planets in small to mid-sized orbits are more evenly represented in both the Transit group and the RV group, but only transits occupy the far left-bottom of the plot: small planets in small orbits. With regards to these metrics, the distribution of planets does not evenly fill the parameter space. Two possible explanations are that (1) planets which would populate the gaps in the plot have not been discovered yet, and/or (2) the groupings are a consequence of planetary system formation and evolutionary architecture. That is, regarding the second explanation, there may exist a tendency for certain masses of planets to form and dominate distributions, or

a tendency for those size-groups to survive dynamic interactions: collisions, migrations, or scattering events during the early life of the system. These speculations are beyond the scope of this thesis, but will be touched on again briefly in the discussion of the distribution of  $J_{sys}$  among planet(s) and host star in Chapter 4.

# Chapter 4

## Results and Discussion

### 4.1 Quantified Angular Momentum

#### 4.1.1 About the Plots

One way to analyze quantified angular momentum is by plotting angular momentum versus mass (J-M) on a scatter plot with logarithmic axes, as others have done (McNally, 1965; van den Heuvel, 1966; Tarafdar & Vardya, 1971; Kraft, 1970; Kawaler, 1987; Ruciński, 1988; Bodenheimer, 1995; Wolff et al., 2004; Berget & Durrance, 2010; Alves et al., 2010; Paz-Chinchón et al., 2015). One can then describe the J-M relationship by the slope of a best fit line to the data,  $J \propto M^\alpha$ , where  $\alpha$  is the slope of the power law.<sup>1</sup> On such plots, this line represents (1) a relationship for representative values of  $J$  across a range of masses or spectral types (Brosche, 1963; McNally, 1965; Kraft, 1970, etc.), (2) an upper bound of  $J$  for many data points in a selected population (Wolff et al., 2004), or (3) a theoretical physical limit, such as rotational break-up velocity (Kawaler, 1987). In the plots presented

---

<sup>1</sup>This power law is referred to as the Kraft Relation or Kraft's Law. In analyses of stellar populations, it is called the Kraft Curve, because of the sudden drop in angular momentum below about  $2 M_\odot$ .

here, we include a “model” Kraft relation with  $\alpha = 2$  for the primary power law, which describes steadily increasing angular momentum with increasing stellar mass. This value is chosen because it lies between the values of  $\alpha$  found by McNally ( $\alpha = 1.8$ ) and Kawaler ( $\alpha = 2.1$ ), and because of the empirical result  $\alpha \approx 2$  for objects across over 30 orders of magnitude (see Figure 1.3). While there is not at present a well-accepted theory for this universal slope, it shall serve as a convenient guidepost and model while reviewing these data.

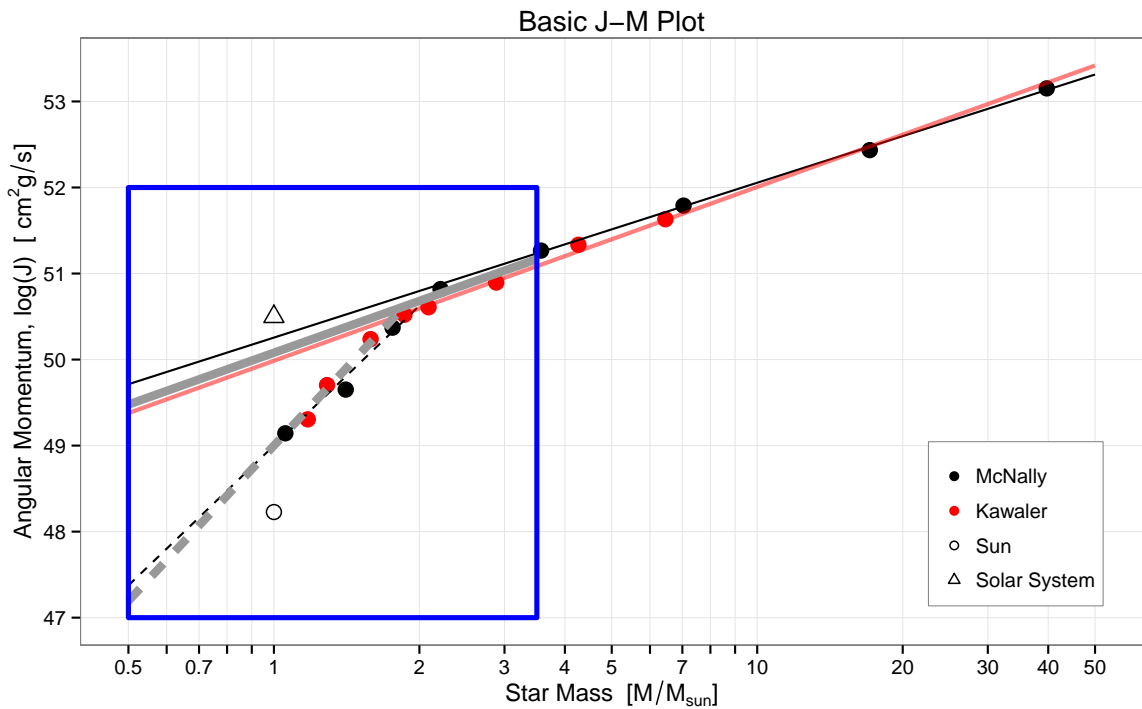


Figure 4.1 Thick grey lines are overplotted on McNally’s (1965) and Kawaler’s (1987) data and fitted lines. The grey lines serve as a reference for all other J-M plots. The blue box represents the working space of the data and the boundaries of all J-M plots hereafter in the thesis.

Figure 4.1 provides further reference to McNally’s and Kawaler’s data and fitted lines. The blue box indicates the axes limits of the plots in this chapter with respect to earlier works. A thick grey solid line represents the primary power law, the Kraft relation, with a

slope of 2, while the dashed line is referential only – a fit to both McNally’s and Kawaler’s data for masses less than  $2 M_{\odot}$ . The slope of this line, referred to as the “break” hereafter, is  $\alpha = 6$ . The break line is not necessarily a model, but an indicator of the general upper bound of past  $J_*$  measurements of MS stars less than  $2 M_{\odot}$ . The value of  $2 M_{\odot}$  was chosen as the intersection of the model and break lines, as it is the most conservative point of angular momentum downturn in the literature. The true *empirical* intersection is near  $2 M_{\odot}$  even though past studies identify a mass value between 1.2 and 1.7  $M_{\odot}$  as the *theoretical* point when structural difference affect the observations. An exact point of intersection is likely non-existent and the bend in the power law more often resembles a smooth curve. These grey lines will be plotted in the background of all J-M plots hereafter.

When possible, all stars/systems relevant to the analysis and discussion are plotted on the J-M plot as points, with their color indicating different groupings. Error bars are included on the first plot for each of Stars and Systems, but are omitted elsewhere for clarity. When overplotting muddles the figure, or trends are not readily apparent, the plot data have been graphically summarized similar to the style of McNally (1965) and Kawaler (1987); for reference see figures in Chapter 1. In some of the plot, the  $J$  values are plotted as bins grouped by stellar mass in relatively equal bin sizes on a logarithmic scale.<sup>2</sup> For points representing bins, error bars represent the standard deviations of the bin.

---

<sup>2</sup>Breaks occur at  $\log M_* = -0.24, -0.16, -0.08, 0, 0.08, \dots$ , etc.

### 4.1.2 Stars

The range and distribution of the entire sample of  $J_*$  (Figure 4.2) do not appear to be biased by the multiplicity of planets, but it is clear that non-MS stars contain more angular momentum than MS stars generally, and that stars with planets detected by RV contain more angular momentum than those with Transit detections. These effects are a consequence of the size of the stars dominating the right side of the histograms (Figure 4.3). Larger stars contain more spin angular momentum because they are more massive and rotate faster. This is apparent when considering biases already discussed in Chapter 3. Planets around larger stars were detected more often by RV than the Transit method, and most of the large stars ( $M_* > 1.5M_\odot$ ) are evolved, *i.e.* they are classified as non-MS (Giants or Subgiants). The most massive MS star in the sample is  $1.718 M_\odot$ . Therefore, the systems of the 20 most massive host stars in the sample will not be considered for parts of the analysis.

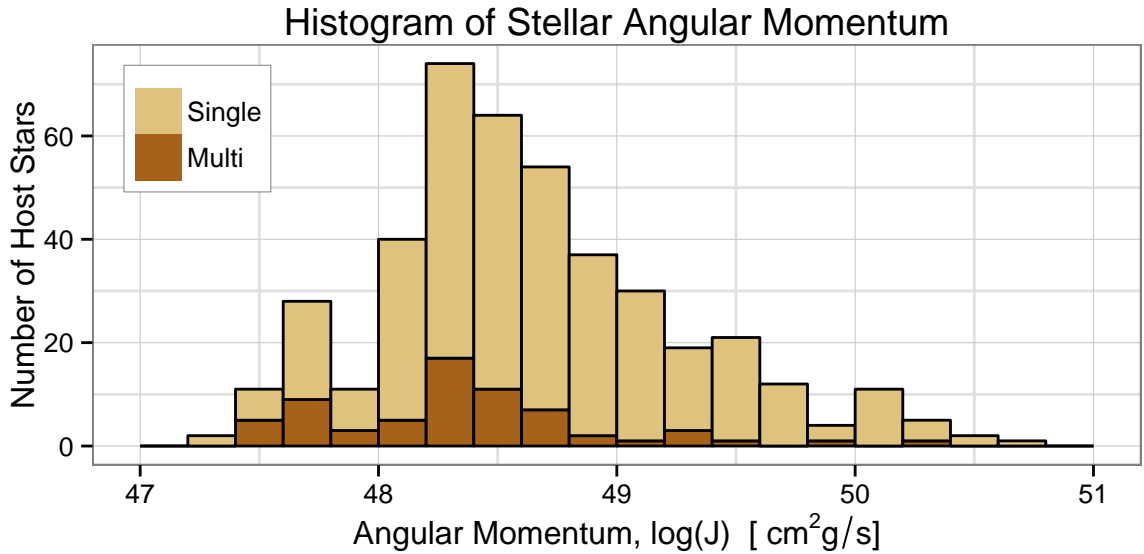


Figure 4.2 Stacked histogram of calculated stellar angular momentum of all sample host stars. Dark brown are host stars of multi-planet systems, while light brown represents single-planet systems.

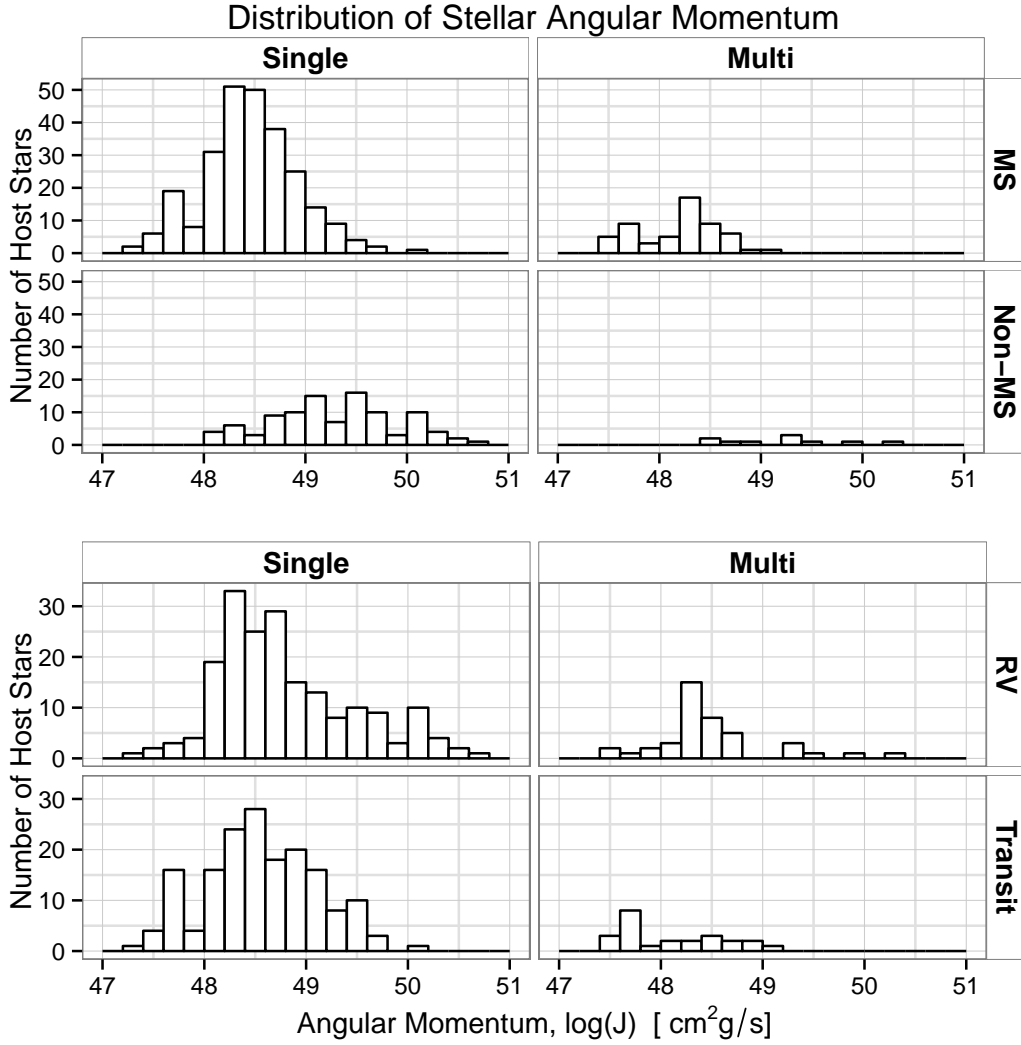


Figure 4.3 Histograms of calculated stellar angular momentum with single-planet system stars on the left and multi-planet system stars on the right. The differences between the histograms for stellar evolutionary classification (top) and planet detection method (bottom) are visible.

Figure 4.4 displays the individual  $J_*$  calculations of the 426 host stars, grouped into main sequence systems and non-main sequence systems. There is little difference between host stars of single planets and those with multiple planets. There is little spread among the results as a whole, and all but two, HD 208527 and HD 220074, fall below the main power law relation (solid grey line). These two stars are classed as giants with very large

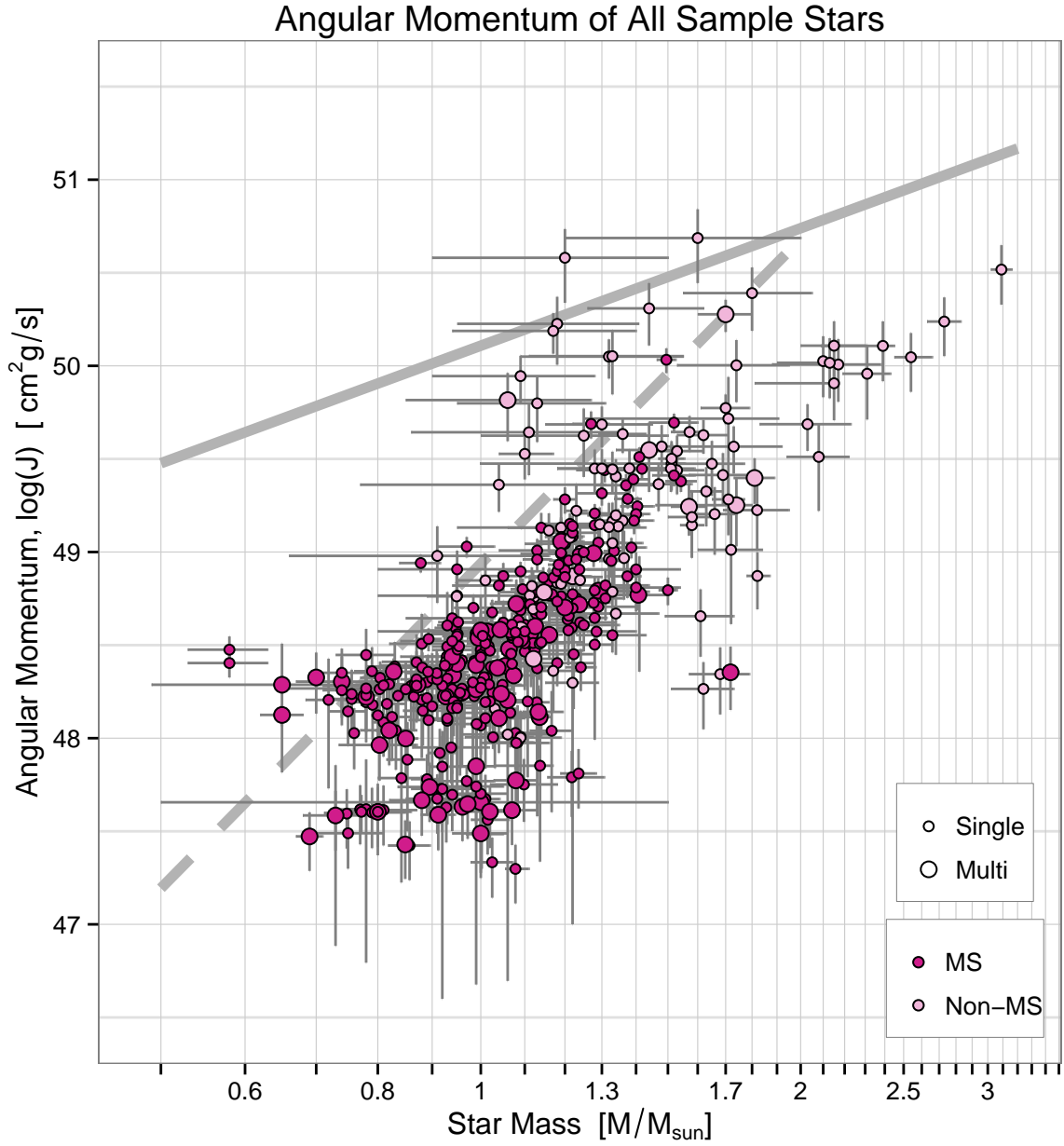


Figure 4.4 The spin angular momentum of host stars is plotted with with model lines and the break in grey for reference. Main sequence, and non-main sequence systems are represented by dark and light pink filled circles, respectively. Horizontal error bars indicate uncertainty in stellar mass, and vertical error bars are propagated errors in  $J_*$

radii,  $41 R_{\odot}$  and  $55 R_{\odot}$ , respectively. In fact, it is apparent that many of the non-MS stars are graphically outliers, as they are positioned above the break.

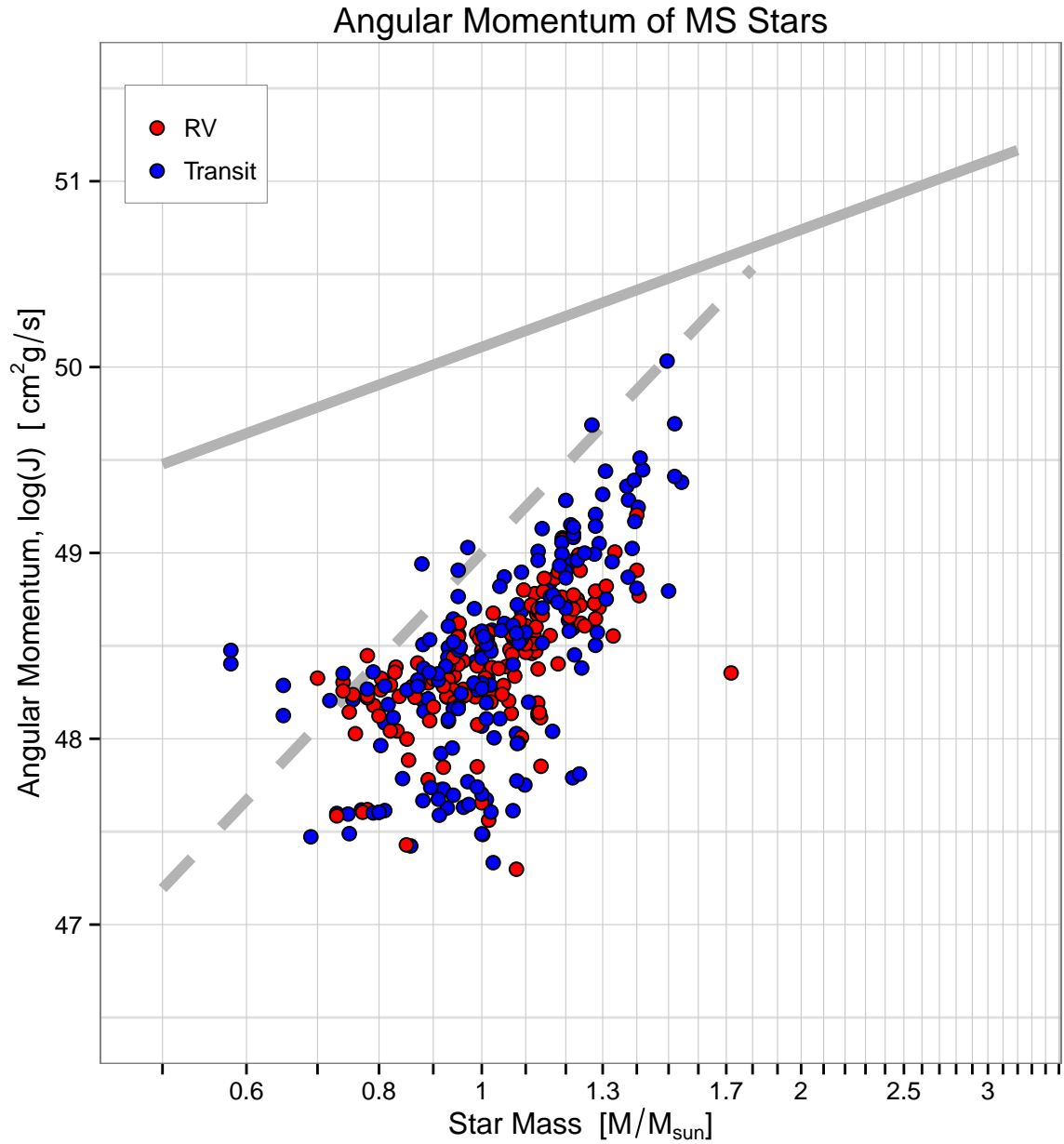


Figure 4.5 The spin angular momentum of MS host stars, with detection method indicated by color. Red indicates RV-detected systems, while blue represents transit detections. Error bars are omitted for clarity.

When examining only the MS systems, as in Figure 4.5, the upper range of host stars disappears from the J-M plot. Interestingly, the stars with the greatest angular momentum (compared to their nearest mass neighbors) are Transit detections (blue). This is likely due

to the RV detection method favoring slow rotators; transit detections, which are detected photometrically, rather than spectroscopically, are not sensitive to stellar rotational velocity.

While several of the MS host stars have  $J_*$  above the break, except for the two lowest mass stars, their position is not more than a 0.5 dex from the line. These two  $J_*$  outliers, WASP-43 and WASP-80, will be discussed in the next subsection, as they are outliers in  $J_{sys}$  as well. A third egregious outlier exists at  $1.7 M_\odot$  at just below  $\log J_* = 48.5$ : HD 154857. It is a rather old (over 5 Gy) MS star with relatively low metallicity,  $[Fe/H] = -.22$ . The rotation is somewhat low, at  $v \sin i_* = 1.4$  km/s, the most likely explanation for its position far below either the break line or the power law. The two non-MS stars near it in Figure 4.4, HD 98219 and HD 102956, are subgiants, but are very slow rotators, both at 0.3 km/s. It is possible that HD 154857 is also a subgiant (misclassified) or is in the process of evolving.

### 4.1.3 System Totals

Figure 4.6 shows the values for  $J_{sys}$  of each unique system, again color coded as MS and non-MS systems. This plot shows an overall increase in magnitude of  $J$  for the group, as well as a greater spread for all sub-populations. The cause of the increased spread is unclear, but as will be discussed later, nearly 10% of the systems exhibit a total orbital  $J_p$  that is *less than* the stellar contribution. Still the sample as a whole now lies above the break, with 199 systems positioned below a line parallel with the model line, shifted -0.5 dex; 217 systems lie above this line, hinting that a Kraft relation of the entire sample of systems may lie close to or slightly below the model line. Planetary angular momentum is clearly an important contributor to the total system angular momentum.

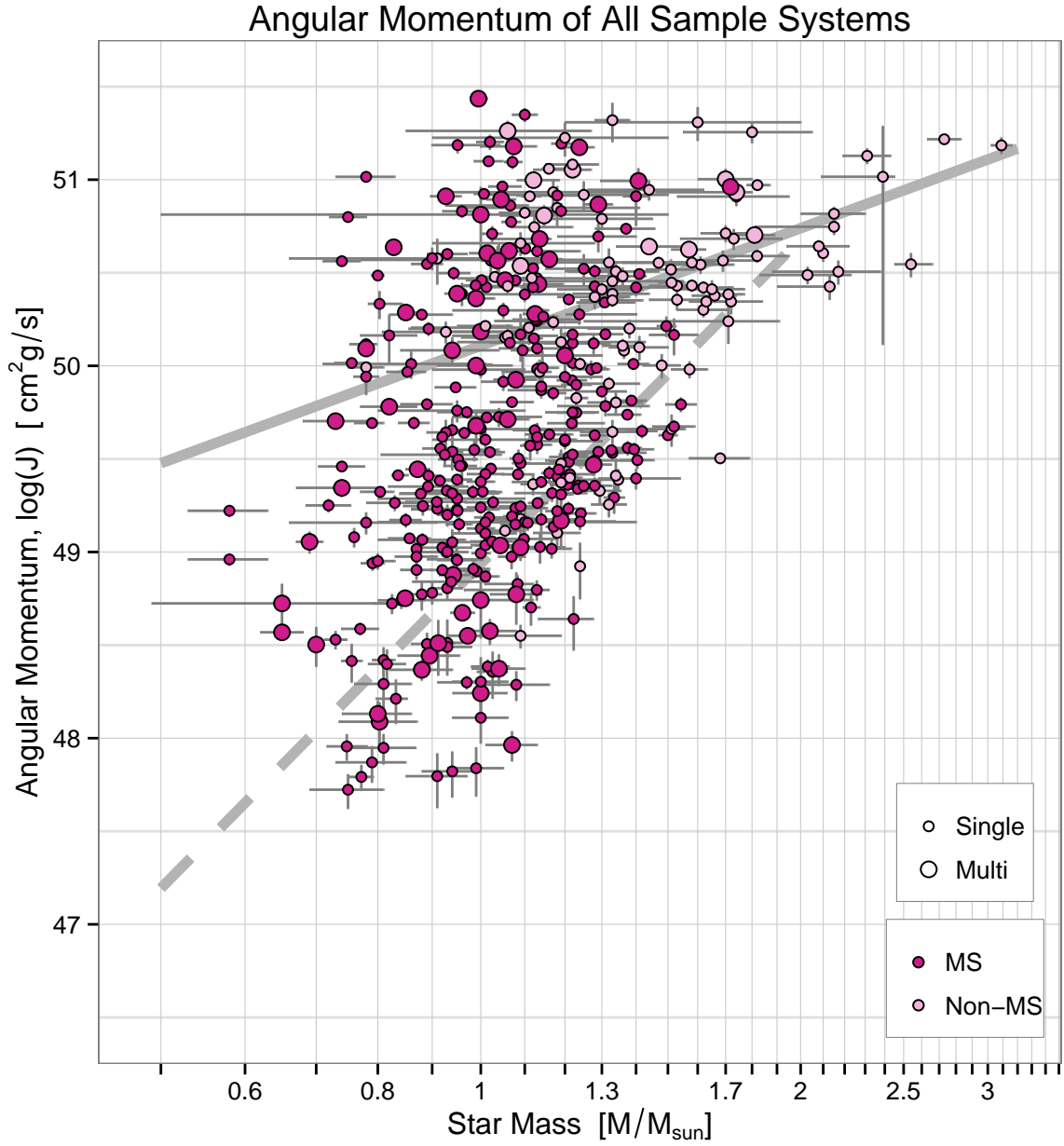


Figure 4.6 The angular momentum of planetary systems, the sum of the host stars and their planets angular momenta, is plotted. Main sequence and non-main sequence systems are represented by dark and light pink filled circles, respectively. Horizontal error bars represent uncertainty in stellar mass, and vertical error bars represent propagated errors in  $J_{sys}$ .

The two small-mass ( $M_* = 0.58 M_\odot$ ) high-valued outliers in  $J_*$ , WASP-43 and WASP-80, are now low-valued in  $J_{sys}$ . The difference between their stellar and system angular

momenta ( $dJ$ )<sup>3</sup> is only about 0.5 dex, and the distance between their position on the J-M plot in the preceding subsection and the power law is over 1 dex. Their nearest neighbors in mass, Kepler-26 and Kepler-27, both with  $M_* = 0.65 M_\odot$ , had  $dJ$  of about 0.5 dex as well. Their reason for their positioning is simply a result of their small, close-in planets. There may be other undetected planets but the sample size of stars in this mass range is not large enough to put too much weight into their results.

Moreover, several of the solar-type stars with  $\log(J_*) < 48$  are not positioned higher than 48 on the  $J_{sys} - M$  plot. The large spread now seems likely explained by characteristics shared by most of these stars: They have only one low-mass ( $< 0.1 M_J$ ) planet detected, which is close to the host star ( $< 0.1$  AU). If these so-called “Hot Neptunes” were identified in each plot, there would be 45 of them on or below the break line in the  $J_*$  plot. Very few moved upward on the  $J_{sys}$  plot, leaving 32, the majority, still below the break line. Furthermore, 20 of these are single-planet systems. These small-mass, close-in planets simply cannot contribute significant angular momentum to  $J_{sys}$  so their position between the  $J_*$  and  $J_{sys}$  plots does not vary much, and their presence skews the low-mass tail of the distribution down in  $J$ .

Another likely culprit for the large spread of  $J_{sys}$  values, small  $J_{sys}$  values, and the reporting of small  $dJ$  for a significant portion of the sample, is the non-inclusion of  $J_p$  from undetected planets. The impact of the speculative absence of these planets on the system angular momenta are discussed more fully in the last two sections of this chapter.

---

<sup>3</sup>Visually determined.

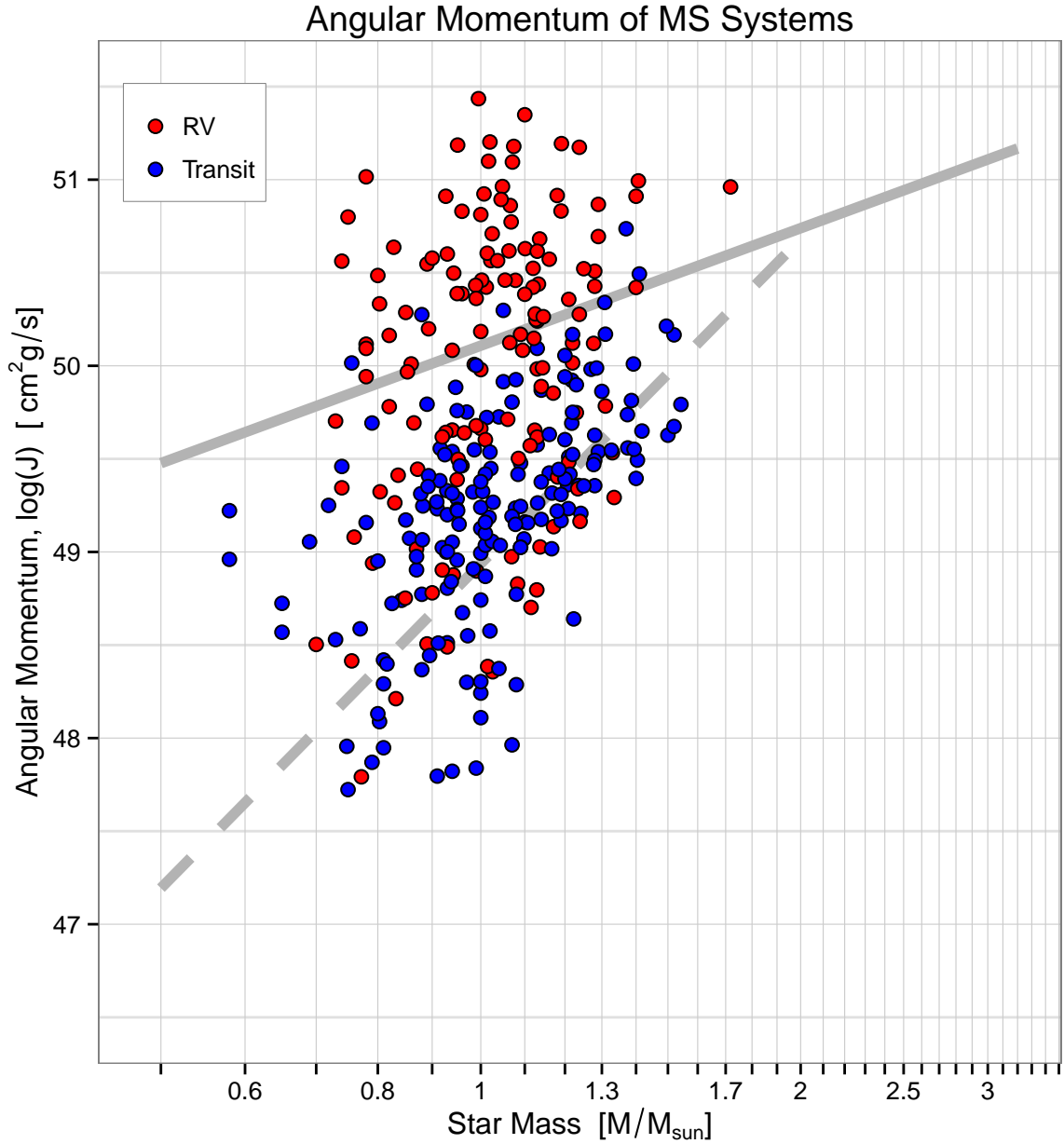


Figure 4.7 The total system angular momentum of MS host stars, with detection method indicated by color. Red indicates RV-detected systems, while blue represents transit detections. Error bars are omitted for clarity.

#### 4.1.4 Fitting the Kraft Relation

After attempting to fit a “straight” line to the results in J-M plots, as others have done (McNally, 1965; Kraft, 1970; Kawaler, 1987; Alves et al., 2010; Paz-Chinchón et al., 2015),

finding the Kraft relation for the results became a complicated ordeal. While it appears that McNally had fitted his points by a simple linear regression on the log-transformed data on both axes, Kawaler had fitted a non-linear least-squares model to his results. Paz-Chinchón et al. did not specify their method, but the problems with their results in  $J$  have already been discussed. The range and criteria for data selection varied among these authors as well. McNally adapted data considered representative of spectral classes, as compiled in a handbook of astronomical constants. These could be considered generalized data based on many observations. Kawaler binned and averaged the various parameters needed for calculation of  $J_*$ , from measurements by Fukuda (1982), then derived moments of inertia for each approximated bin mass from models. Kawaler acknowledged the biases of the bins’ “edges” but felt they did not compromise the overall results.

Neither of these approaches may be taken when planetary systems are considered because of their multi-body nature. The quantity  $J_p$ , and thereby  $J_{sys}$ , is heavily influenced by orbital radius and planet mass. While loose correlations has been found between these planetary parameters, eccentricity, and stellar mass, they are by no means well-constrained, and taking an average value of  $J_p$  in calculation of  $J_{sys}$  would be neither accurate nor precise. Therefore, when fitting a line representing a power law to the data obtained here, one must consider all data points individually. Certain traits among sub-groupings of systems, planets, or host stars may show interesting relationships between the biases in the groups and their affect on the slope of the line. However, a precise fit is not hoped for, since maximizing the coefficient of determination,  $R^2$ , or minimizing Chi-squared has dubious meaning for a nonlinear model regressions on  $J = M^\alpha + b$ , and the data violate all assumptions required for the linear regression on  $\log J = \alpha \log M + q$ .

Regarding this data as a sample from a larger population, which it is, then a nonlinear least squares fit to the entire data set might seem a good choice. But this sample exhibits heteroskedasticity (the tendency for a predictor or its resultant to have non-uniform variability, such as with log-normal distributions or other skewed populations) the data and its errors, as well as multiplicative uncertainties in  $M$ , and the results  $J_*$ , and  $J_{sys}$ . This is common in astronomy and astrophysics where it is often required to plot data on logarithmic axes so it may be uncluttered and easily read. When the non-linear fit was used for this sample, large  $J$  values dominated the fit, and the resulting “best fit line” did not evenly bisect the data points, but sat high on the body of the sample. That is, the non-linear fit produced a high value of  $p$  and  $\alpha$ . The non-linear expression used for the fit was

$$J = p M_*^\alpha \tag{4.1}$$

where  $p$  and  $\alpha$  are free parameters.

Linear model fitting on log-transformed data is often used for fitting power laws in other disciplines, because it takes into account heteroskedasticity of the errors and produces a more plausible model (Xiao et al., 2011). Still, there is broad variability in error, and there are multiple sources of significant systematic error in the data and results. When using a simple linear fit to the data, slopes of between 4 and 9 were consistently obtained for  $J_*$  and  $J_{sys}$  in their various subgroups. A more robust fitting method was needed. These challenges are non-fatal to a fitting method which can give more significance in the fit to data that is well-characterized. Therefore, a *weighted* least-squares fit to the log-log-transformed data was used and provided sensible fits to both stellar angular momentum and system totals.

The linear expression chosen to fit the data was

$$\log(J) = \alpha \log(M_*) + q \quad (4.2)$$

where  $\alpha$  and  $q$  are free parameters, and  $q$  is simply an offsetting variable (the counterpart of  $p$  in the nonlinear version, Equation 4.1).

The weights are determined by

$$w_i = \frac{1}{\sigma_i^2} \quad (4.3)$$

such that the predictor  $y$  and independent variable  $x$  are related by the slope  $B$  and intercept  $A$  by a minimized sum of squares:

$$WLSS = \sum_{i=1}^N w_i (y_i - A - Bx_i) \quad (4.4)$$

This assumes a that the errors in  $X$  are negligible. Here,  $x$  corresponds to sample  $\log M$ , and  $y$  corresponds to calculated  $\log J$ , and  $B$  is the slope  $\alpha$ . In this case, some reported uncertainties in  $M$  (or  $\log M$ ) are substantial, but for over 92% of the sample,  $\sigma_{\log M} < 0.05$ . This is a small effect when compared to stellar  $\sigma_{\log J} \sim 0.2$  and system  $\sigma_{\log J} \sim 0.1$ , and when considering  $J$  range over 5 dex, and  $M$  range for less than 1 dex.

The uncertainties in  $J$  are calculated as described in Appendix B, but the log-uncertainty used for the weighted fitting is calculated in an unsophisticated and slightly asymmetric method, but results in a reasonable counterpart to the raw uncertainties. First the upper and lower bounds of the value are computed by adding and then subtracting

the raw uncertainty from the raw value. The log function is applied to the bounds. The difference between the log-transformed bounds is halved, and this is the log-uncertainty, with as many significant figures as the original measurement. Thus for some value  $J$ ,

$$J_{\text{upper}} = J + \sigma_J \quad (4.5)$$

$$J_{\text{lower}} = J - \sigma_J \quad (4.6)$$

$$\sigma_{\log J} = (\log(J_{\text{upper}}) - \log(J_{\text{lower}})) / 2 \quad (4.7)$$

These statistical issues are not trivial if a precise and objective fit to the data is required, but the focus of this research has been instead on quantifying angular momentum and identifying relationships and biases that affect the results. A sensible choice of a power law fitting procedure for this data set is to perform a weighted least-squares linear fit on log-transformed values. Log-transformed values are preferable when errors or uncertainties are multiplicative with their sources. Least-squares fitting is preferable for values with heteroskedastic errors, and weighted least-squares are used to give less importance to “noisy” measurements and more weight to those in which we have more confidence.

#### 4.1.5 Discussion

Even with the non-MS outliers, the upper bound of the angular momenta of the host stars is consistent with previously calculated angular momentum trends of presumed planetless stars, such as those presented by McNally and Kawaler. The vast majority lie below the break, exhibiting a deficit in  $J_*$  compared to past studies. This is especially true for solar type stars in Figure 4.6, specifically, those with masses between 0.7 and 1.3  $M_{\odot}$ . The reason

for the deficit is not immediately clear. It is possible that systematic biases in calculation or observation, as were listed in Section 2.6 have produced underestimated  $J_*$ , or more probably, the kinds of stars that produce detections are typically less active and slowly rotating, which is a systematic lowering bias of the most popular detection techniques, the RV and Transit methods. Another possibility is that these stars have lost more angular momentum due to age or tidal effects of their close-in planets.

It is possible that the estimated values adopted for  $\gamma$  (inertial coefficient) have produced  $J_*$  results above or below their true value. The maximum range of  $\gamma$  for the sample is 1.2 dex, and the determination of  $\gamma$  is primarily a function of mass, and is sensitive to age, or specifically, the stage of life. Most reported MS stellar masses in the sample have an uncertainty on the order of  $< 0.1 M_\odot$ . For solar type stars, each  $0.1 M_\odot$  change in mass, corresponds to about a 0.01 change in  $\gamma$ . While on the Main Sequence,  $\gamma$  also changes, and for stars less than 1.2 solar masses, this change could be as high as 0.03, or about  $\pm 0.15$  about mean MS values. Therefore, it is unlikely, at least for MS stars, that even an incorrect determination of  $\gamma$  is *grossly* incorrect. The associated uncertainty is definitely not large enough to account for a half dex difference in  $J_*$ . That is not to say, however, that the models on which the calculations are based may underestimate  $\gamma$ , but most models are calibrated to the Sun, the moment of inertia of which is fairly accurate at  $\gamma \sim 0.07$ .

These lower-than-expected values of  $J_*$  will have little effect on  $J_{sys}$  of systems that are similar to the Solar System, with most of their angular momentum in the planets, but it would keep  $J_{sys}$  low for systems which have the converse arrangement ( $J_* > J_p$ ).

To de-clutter the J-M plots and more clearly see stellar and system angular momentum trends with respect to star mass, the sample was binned by relatively equal-sized bins of

stellar mass on a logarithmic scale. The  $M_*$ ,  $J_*$  and  $J_{sys}$  of each group were averaged, and their standard deviations used as error bars (for bins that include only one system, error bars reflect that datum’s uncertainty in  $M_*$  and the propagated uncertainty in  $J$ ). The system and stellar angular momenta averaged for each bin are plotted as black and white circles, respectively, in Figure 4.8. Simple averages were used rather than weighted averages, because these data points are for visually identifying trends, and not fitting the Kraft relations.<sup>4</sup> The black solid and dashed lines do *not* fit the binned values, and in fact, this would be an inaccurate method to determine the Kraft relation of the sample. The number of members per bin vary from under 10 to over 100, so clearly the middle of the mass range is contributing more data to the fit, while those with very high or very low masses should not be given as much significance in the fit. With stellar classification differences, observation bias, and detection method bias, it is more sensible to start broadly and narrow down the population to a subset of particular interest. In our case, the focus is on one Main Sequence host stars and their planetary systems as a whole, with attention paid to detection method bias.

The J-M plot of binned data for all systems, Figure 4.8 is remarkably consistent with the early type power law, excluding the smallest mass bin. The bins exhibit a trend for  $J_*$  which has a shallower slope than the previous studies by McNally and Kawaler. This affect is also reflected in the fitted line. The weighted fit of  $J_{sys}$  for the entire sample nearly

---

<sup>4</sup>Due to the nature of log-log scales, given an nearly even distribution across orders of magnitude, simple means are skewed to the higher end of the sampled values. The weighted means for  $J$  would likely be somewhat less than the standard means.

parallels the early-type law:

$$\log(J_{sys}) = 2.30(\pm 0.32) \log(M_*) + 49.89(\pm 0.03) \quad (4.8)$$

which agrees with the model slope ( $\alpha = 2$ ) within the error of the fit. Listed errors are standard errors of the fit and do not indicate the goodness of the fit. However, there are known systematic biases, some raising and some lowering the values of  $J$ , which have contributed to the fit. The original fits in the literature on which this model is based were for MS stars only.

Figure 4.9 is analogous to the previous plot, but addresses only MS stars and systems. The fit to  $J_{sys}$  for the MS data is

$$\log(J_{sys,MS}) = 1.59(\pm 0.49) \log(M_*) + 49.84(\pm 0.04) \quad (4.9)$$

which also agrees with the model slope ( $\alpha = 2$ ) within the error of the fit. The p-values for all fits described in this section are consistently reported as  $< 0.002$  for the slope ( $\alpha$ ), and  $p < 2 \cdot 10^{-16}$  for the offset value  $q$ . In the absence of a more rigorous statistical analysis, this basic interpretation supports (does not reject) the hypothesis that the variation in system angular momentum is indeed explained by the change in the stellar mass, by the equation above, with greater than 99% confidence level. Unfortunately, the errors on the slopes are very large, which is reasonable considering the huge spread of  $J_{sys}$  in the data set. In this case, a Markov Chain Monte Carlo (MCMC) analysis could have produced a better fit with higher confidence, and would be a “fitting” project for future analyses.

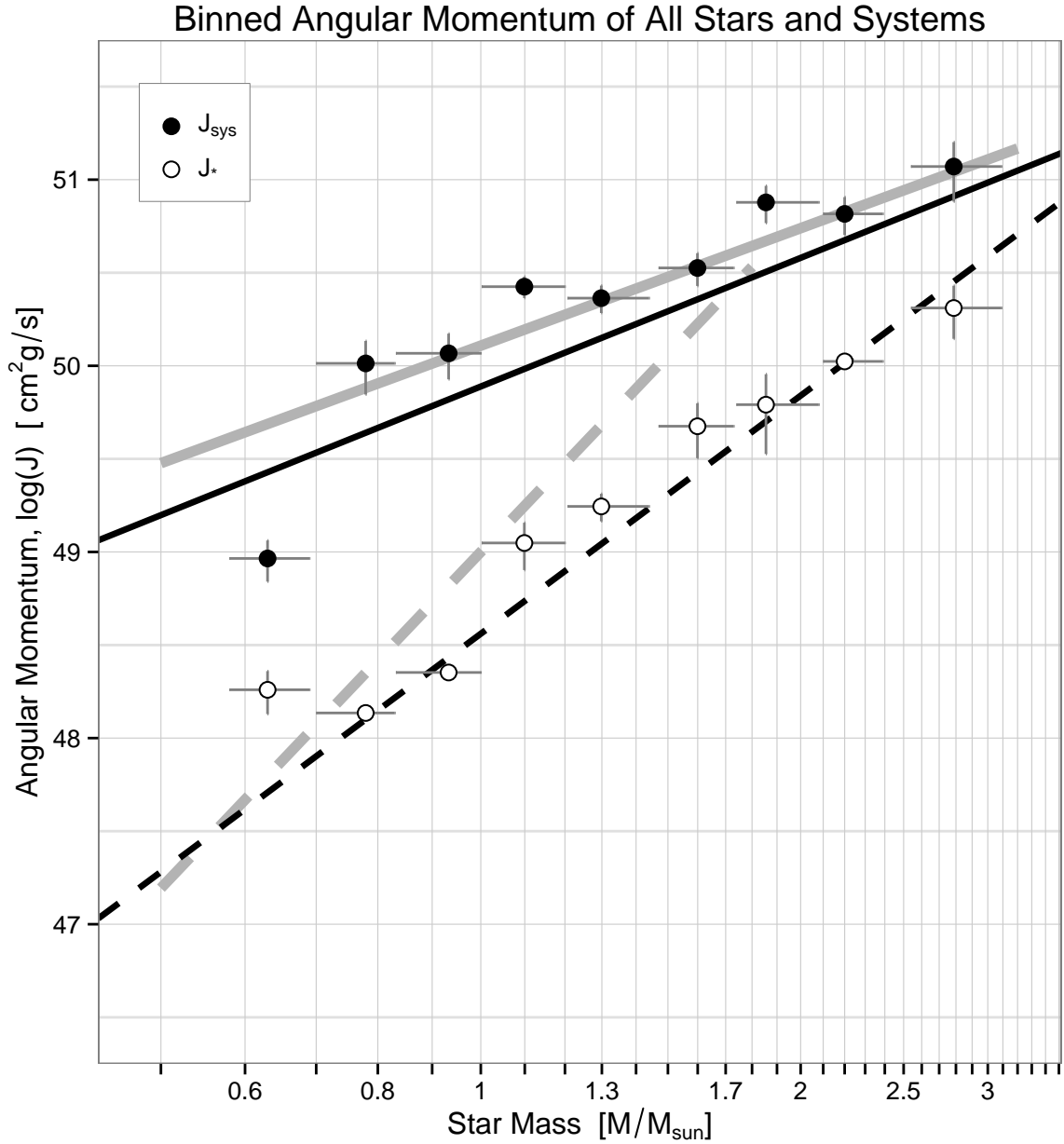


Figure 4.8 The angular momentum of host stars,  $J_*$ , and planetary systems,  $J_{sys}$ , is binned, averaged, and compared to the model J-M plot. The solid grey line represents the power law for early type stars,  $J \propto M^2$ . The solid black line represents the best fit line of  $J_{sys}$  for all systems, with a slope of  $\alpha = 2.30 \pm 0.32$ . The dashed black line represents the best fit line of  $J_*$  for all host stars, and has a steeper slope.

In the next section, the distribution of angular momentum within the systems are examined. This will address the questions about how similar or different the Solar System

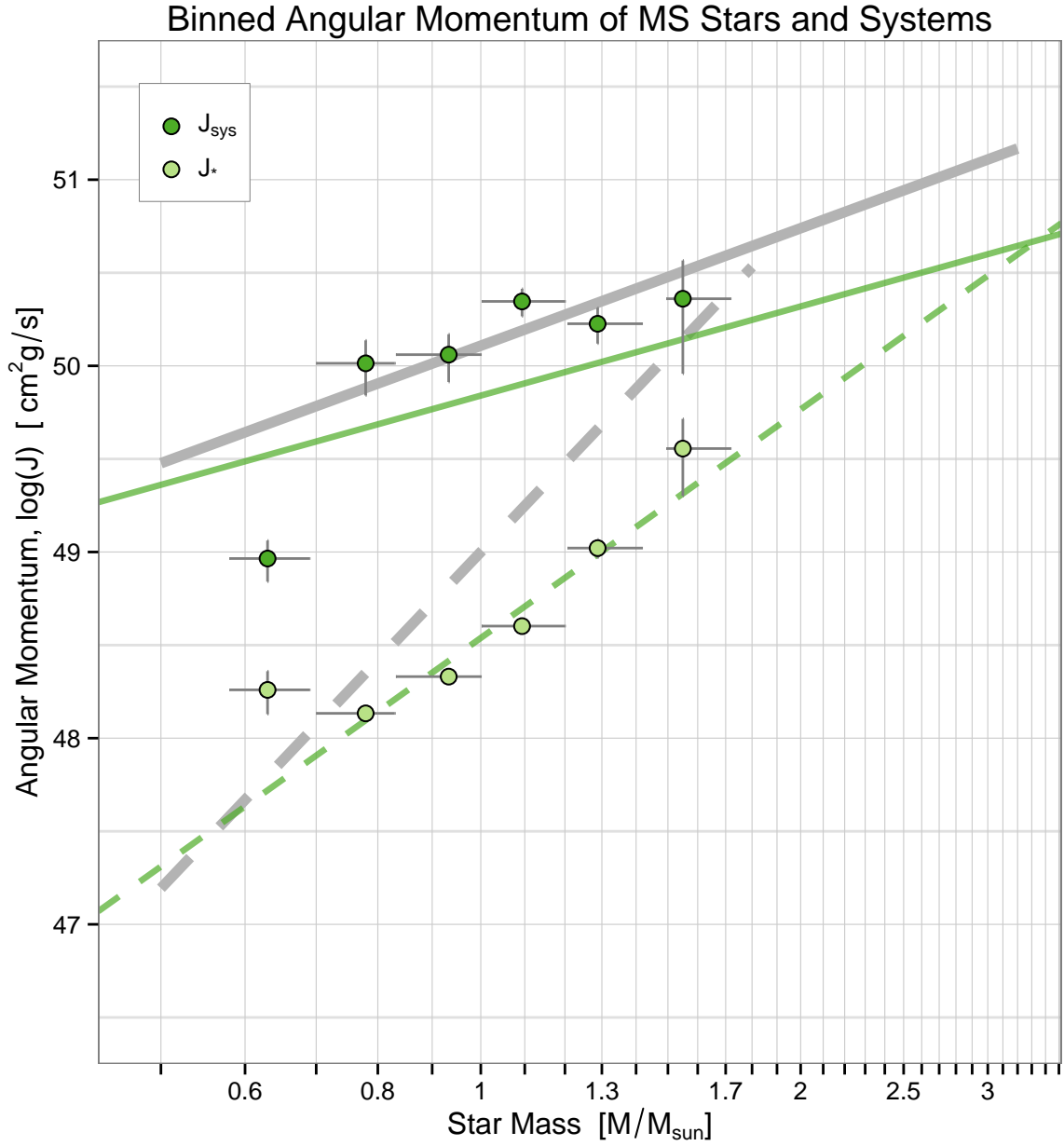


Figure 4.9 The angular momentum of MS host stars,  $J_*$ , and their planetary systems,  $J_{sys}$ , is binned, averaged, and compared to the model J-M plot. The solid grey line represents the power law for early type stars,  $J \propto M^2$ . The solid green line represents the best fit line of  $J_{sys}$  for the MS systems, with a slope of  $\alpha = 1.59 \pm 0.49$ . The dashed green line represents the best fit line of  $J_*$  for MS host stars, and has a steeper slope.

is compared to the larger population while addressing the bias of undiscovered planets on

$J_{sys}$ .

## 4.2 System Distribution of $J$

### 4.2.1 $\mathcal{L}$ and $K$

Others who have examined the angular momentum of exoplanets (Armstrong & Larson, 2007; Alves et al., 2010; Paz-Chinchón et al., 2015) have remarked consistently that Solar System’s orbital angular momentum is two orders of magnitude larger than the spin angular momentum of the Sun. These authors also found a broad range of partitioned orbital angular momenta in their samples, spanning several orders of magnitude. The metric developed in this thesis,  $\mathcal{L}$ , provides a measurement of this ratio directly, as in Figure 4.10.

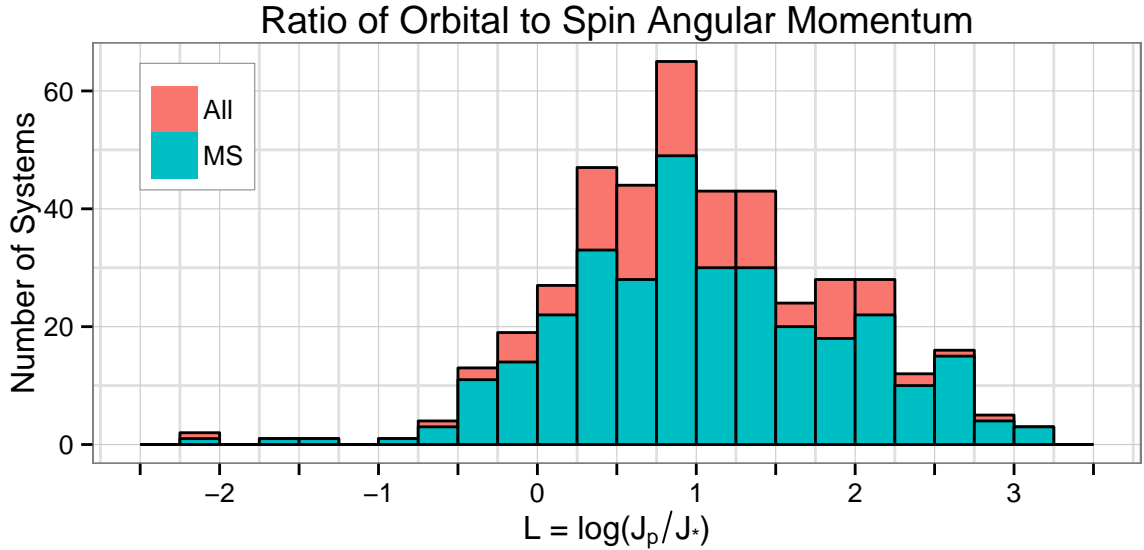


Figure 4.10 Unstacked histogram of  $\mathcal{L}$  for the entire sample of systems, overlaid by the histogram for MS systems only. The distribution of the proportion of orbital to spin angular momentum peaks around 1 order of magnitude.

In general, for this sample, the planetary orbital angular momentum is about 1-2 orders of magnitude larger than the stellar spin angular momentum. Curiously, the distribution is not heavily skewed to the larger end, as might be expected if exoplanetary

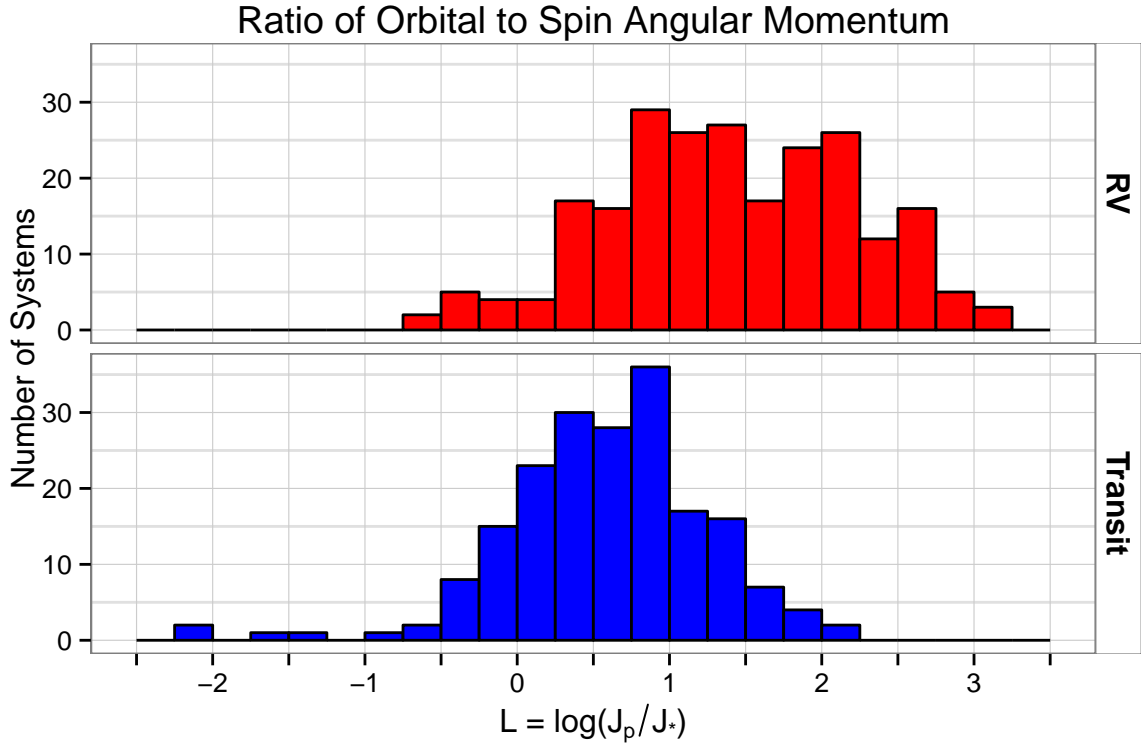


Figure 4.11 Histograms of  $\mathcal{L}$  grouped by detection method.

systems resembled the Solar System. Only 10% of the systems, however, have stellar spin angular momentum greater than the planetary orbital angular momentum. The same is true when considering only MS systems. Over half the systems (224 of 426) have total orbital angular momentum that is at least an order of magnitude larger than the stellar contribution, and the proportion is similar for MS systems as well (164 of 316). The same peaked distribution is found for single- and multi-planet systems as well as Hot Jupiter systems and non-HJ. The trend appears to be classification independent. Only one bias was uncovered in the determinations of  $\mathcal{L}$ : planet detection method. In Figure 4.11, the shift in the peak of angular momentum is directly related to other biases identified with detection method; in general, RV-detected planets have greater angular momentum and greater proportions of angular momentum, owing to the method favoring larger mass planets

at larger orbital radii. A nearly normal distribution of  $\mathcal{L}$  could be the standard. If more planets were detected around known planetary systems, the distribution will take on an even more Gaussian shape.

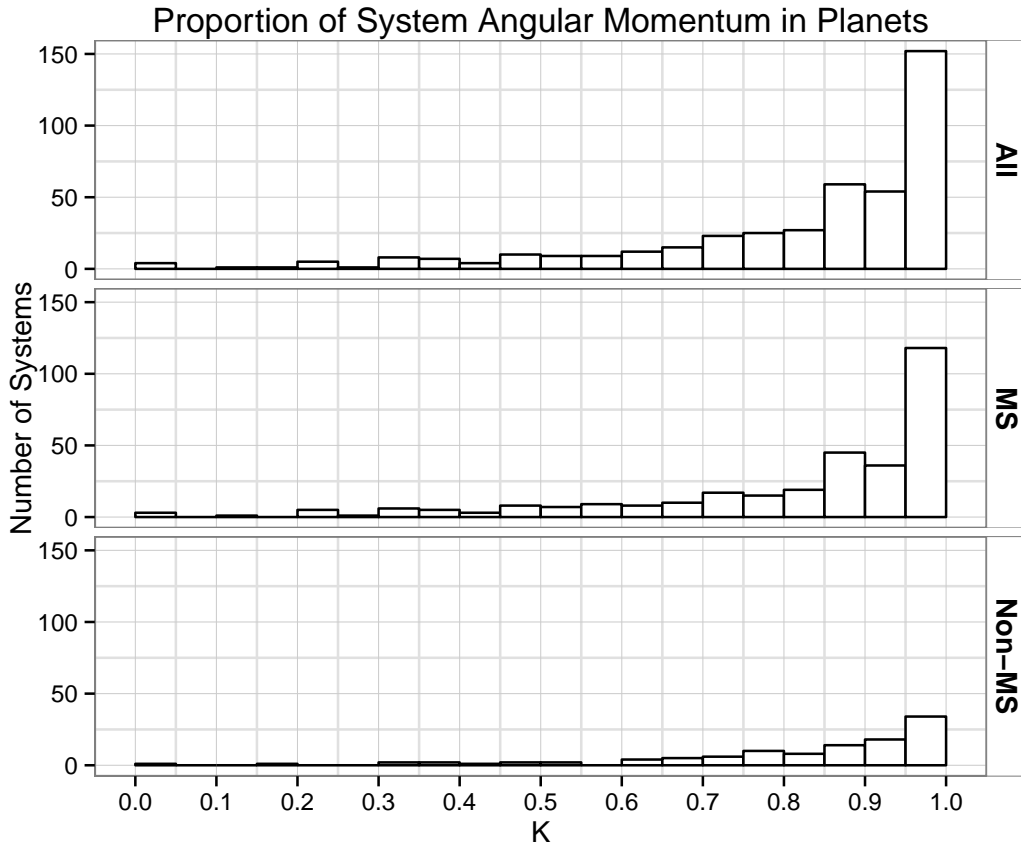


Figure 4.12 Histograms of  $K$  for all systems (top) and the subset of MS systems (bottom).

System angular momentum is now treated as a whole body, made up of parts. Those parts are the stellar and planetary contributions to the total  $J_{sys}$ , and this metric is mathematically related to  $\mathcal{L}$ . That is,  $K$  relates the fraction of system angular momentum that is contributed by the planetary orbital component. Figure 4.12 describes the distribution of  $K$  values for the entire sample, and for MS and non-MS systems. The peak of systems at the far right, indicating  $K > 0.95$  (95% of the angular momentum is contained in the planets)

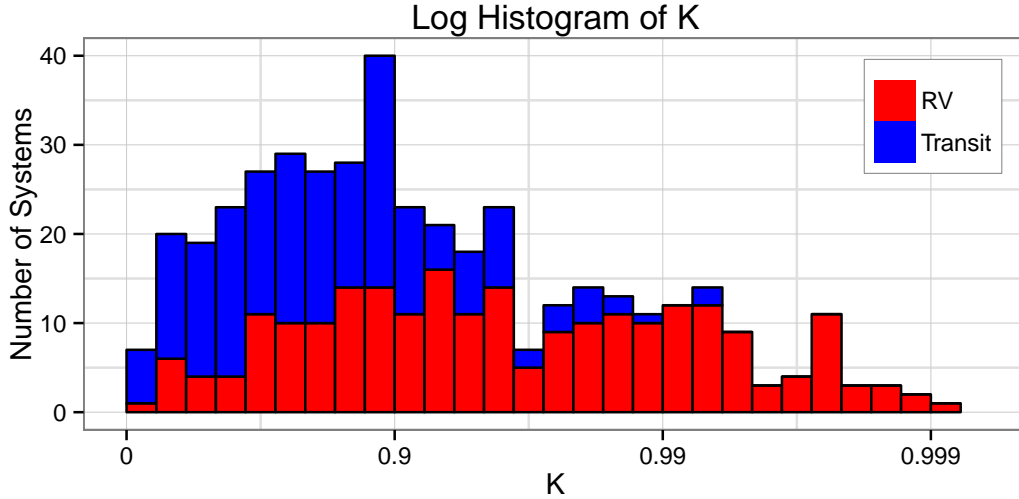


Figure 4.13 Stacked logarithmic histogram of  $K$  values for all systems, colored by detection method.

persists in the MS population but is much less pronounced in the non-MS group. These shall be termed “K-complete” systems, as the addition of new planet discoveries would not significantly change the system’s  $K$ ; these are  $J_p$ -dominant systems. The Solar System, with  $K = 0.995$ , and about a third of the sample systems are K-complete. Notably, half of all systems (206 of 426) and half of the MS systems (154 of 316) have  $K > 0.9$ .

All three system subgroupings reflect bias in  $K$  that was not as readily apparent in studying  $\mathcal{L}$ . By transforming  $K$  to a logarithmic scale, more information about the very high values is seen. The x-axis is transformed by  $K_{\log} = -\log(1 - K)$ . In Figure 4.13 the frequency of systems at higher and higher  $K$  declines. Also the differences between RV and Transit populations is made clear. As usual, the RV-transit group shows exactly which method favors the planet-dominant  $K$  values. Not surprisingly, the multi-planet population reports  $K$  in the top 5%, while the single-planet group is unremarkable compared to the overall sample. Lastly Hot Jupiters, like the transitters, lack a preference for very high  $K$ , and the distribution is proportionally flat in the  $K > 0.5$  region. This is mostly likely due

Table 4.1. Kraft Relations for Sample Subgroups

System Grouping	Slope, $\alpha$		Intercept, $b$		DoF, $n - 2$
All	2.29568	$\pm 0.32138$	49.88885	$\pm 0.03413$	424
RV	1.62082	$\pm 0.35939$	50.26146	$\pm 0.04208$	231
Transit	2.89221	$\pm 0.37118$	49.44697	$\pm 0.03376$	191
MS	1.5919	$\pm 0.4889$	49.8402	$\pm 0.0387$	314
RV	1.92784	$\pm 0.81345$	50.25570	$\pm 0.05513$	139
Transit	2.6553	$\pm 0.3606$	49.4237	$\pm 0.0319$	173
$K > 0.7$	1.86254	$\pm 0.55388$	49.90925	$\pm 0.04226$	248
$K > 0.8$	2.02714	$\pm 0.59310$	49.97319	$\pm 0.04436$	216
$K > 0.85$	1.97999	$\pm 0.61924$	50.01952	$\pm 0.04549$	97
$K > 0.9$	2.42014	$\pm 0.69093$	50.17919	$\pm 0.04822$	152
$K > 0.95$	1.92912	$\pm 0.74716$	50.29821	$\pm 0.05279$	116
$K > 0.98$	2.08886	$\pm 0.72801$	50.54076	$\pm 0.05001$	76

directly to the very small semi-major axis that defines this group,  $a < 0.1$  AU. At small orbital separation, even massive planets do not contribute as much to  $J_{sys}$  as, for example, a Jupiter-mass planet at 5 AU. If large  $K$  is in fact the tendency of most planetary systems, the hot Jupiter systems may have yet undiscovered planets at larger radii, or they may have already dynamically altered the structure of the system via migration, by flinging out or colliding with other lost planets.

The last supposition deserves more attention. If the Solar System is relatively typical and if, in systems with  $K$  values  $> 0.95$ , it can be assumed the dominant planetary contributor(s) to  $J_{sys}$  have been found, and therefore  $K$  would not change substantially upon discovery of more planets – what is the Kraft relation for supposed  $K$ -complete systems? Table 4.1 summarizes Kraft relations with errors and degrees of freedom for system subgroupings and steadily more restricted values of  $K$ . Figure 4.14 is a plot of the group in

the top 15% of  $K$  values. Colors indicate detection method as before (showing the bias persists even at the topmost K-complete systems), and size indicates whether the systems are single or multi-planet. Interestingly, there still exists a spread of 3 dex for even this set of K-complete systems. Of the 6 lowest points on the plot, 4 or multi-planet. All of these are very slow rotators ( $v \sin i_* < 0.5$  km/s) and the three transitters are known to host Hot Neptunes, planets of  $m < 0.1 M_J$  with semi-major axis  $a < 0.1$  AU. While the contribution of  $J_p$  was much larger than their host star's  $J_*$ , the orbital angular momentum was simply not as great as that in most other systems, and their star's spin angular momentum was unusually low compared to other host stars. Thus, this produced a high K-value for these low- $J_{sys}$  multi-planet systems. Most of the other multi-planet systems lie  $\sim 1$  dex higher than these outliers.

#### 4.2.2 Toward Determination of System Completeness

One might be inclined to suggest that systems with small values of  $K$  could harbor more, yet undiscovered planets, if one assumes that a  $K$ -value of  $> 90 - 95\%$  is indicative of a mature, complete systems. If the Solar System is taken as a model of stable multi-planet systems, then one might guess that those systems which have confirmed small inner planets close to the parent star are likely candidates for discovering more exoplanets in that system. In this case, the likelihood of discovery of additional planets would be roughly inversely proportional to the  $K$ -value. However many other factors have been shown to affect planet multiplicity and system stability, such as stellar metallicity, system age, orbit eccentricity, the presence of a Hot Jupiter, large spin-orbit angle, etc. In truth, several decades of observations might need to pass for techniques such as RV and timing methods be able to

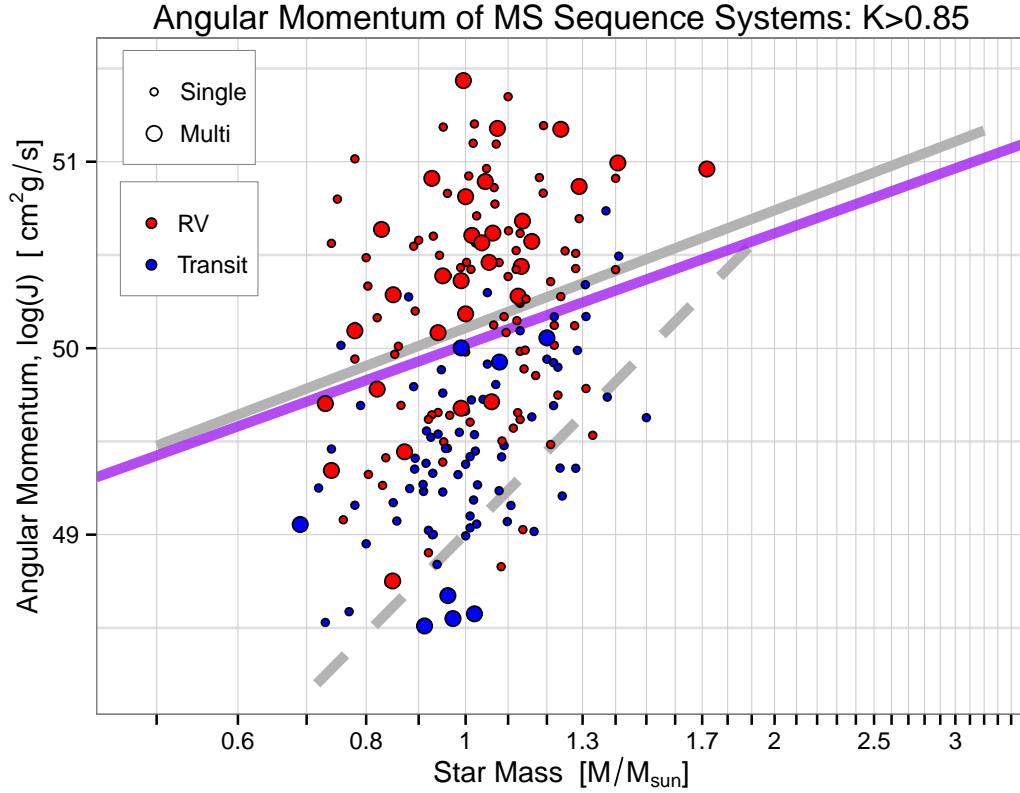


Figure 4.14 J-M plot of high  $K$ -value MS systems. Red points are systems discovered by the radial velocity method, while blue indicates transit detections. The size of the point indicates whether the system is single-planet (small) or multi-planet (large).

discover the most significant planetary contributors to system angular momentum. These first discoveries by Transit and RV methods are indeed low-hanging fruit.

There is hope that systems of short-period transiting planets might have larger companions in orbits farther out, if the  $K$  value of the system so far is sufficiently small. Consider the Solar System as a test case, and refer to Table 4.2. The column of numbers indicates the order of this hypothetical discovery of the planets, assuming the innermost was discovered first and Mars last, and the total number of planets to be tabulated when calculating  $\sum_{i=1}^n J_p$ .  $K_n$  is the value of  $K$  for the system including planets up to the  $n$ th discovery. If the inner-most planets were discovered one by one, or as a group, by the transit method,

Table 4.2.  $K$  Values of Solar System Planets

<i>Inner planets</i>					<i>Outer planets</i>				
n	Planet	$J_{p,n}$	$J_{\odot} + \sum_{i=1}^n J_{p,i}$	$K_n$	n	Planet	$J_{p,n}$	$J_{\odot} + \sum_{i=1}^n J_{p,i}$	$K_n$
1	Mercury	$8.96 \cdot 10^{45}$	$1.70 \cdot 10^{48}$	0.005	1	Jupiter	$1.93 \cdot 10^{50}$	$1.95 \cdot 10^{50}$	0.991
2	Venus	$1.85 \cdot 10^{47}$	$1.88 \cdot 10^{48}$	0.103	2	Saturn	$7.81 \cdot 10^{49}$	$2.73 \cdot 10^{50}$	0.993
3	Earth	$2.66 \cdot 10^{47}$	$2.15 \cdot 10^{48}$	0.214	3	Uranus	$1.69 \cdot 10^{49}$	$2.90 \cdot 10^{50}$	0.994
4	Mars	$3.52 \cdot 10^{46}$	$2.19 \cdot 10^{48}$	0.227	4	Neptune	$2.50 \cdot 10^{49}$	$3.15 \cdot 10^{50}$	0.995

Note. — Units of  $J$  are  $\text{g cm}^2/\text{s}$ . The Sun alone has  $J_{\odot} = 1.69 \cdot 10^{48} \text{ g cm}^2/\text{s}$ . For solar and planetary parameters used in calculations, see Table 1.3.

Table 4.3.  $K$  Values of HD 10180 Planets

Planet	$J_{p,n}$	$J_* + \sum_{i=1}^n J_{p,i}$	$\sum_{i=1}^n K$	$J_{p,n}/J_{\text{total}}$
c	$9.127882 \cdot 10^{47}$	$2.51 \cdot 10^{48}$	0.363	0.018
d	$1.164104 \cdot 10^{48}$	$3.68 \cdot 10^{48}$	0.565	0.023
e	$3.603369 \cdot 10^{48}$	$7.28 \cdot 10^{48}$	0.780	0.070
f	$4.504638 \cdot 10^{48}$	$1.18 \cdot 10^{49}$	0.864	0.087
g	$7.000651 \cdot 10^{48}$	$1.88 \cdot 10^{49}$	0.915	0.136
h	$3.283194 \cdot 10^{49}$	$5.16 \cdot 10^{49}$	0.969	0.636

Note. — Units of  $J$  are  $\text{g cm}^2/\text{s}$ . The star HD 10180 alone has  $J_* = 1.60 \cdot 10^{48} \text{ g cm}^2/\text{s}$  which accounts for 3.1% of the total system angular momentum.

the system  $K$  values would be very small, less than 0.3, even if all 4 were confirmed. On the other hand, suppose astronomers had been taking radial velocity measurements of Sol for 20-25 years, after which they finally were able to confirm Jupiter's signal – with 2 full orbital periods. The resulting  $K$  value would be  $> 0.99$  which satisfies K-completeness, although the system is not yet completely discovered. Perhaps they see secondary effects from Saturn, but cannot confirm its existence. Even so, the  $K$  value would only increase by 0.002. Are there more planets in the system? How is one to know?

Consider also a case study of MS solar-type star HD 10180, hosting at least 6 planets.<sup>5</sup> If planet c were discovered first, before the others, the system would have had a  $K$  value of 0.363. This is very low on the  $K$  scale, and would indicate a promising lead for follow-up observations. Table 4.3 lists a hypothetical planet-by-planet progression of evolving  $K$  values (column 3), as each  $J_p$  (column 2) contributes its angular momentum to  $J_{sys}$  (column 4). Column 5 lists the proportion of total system angular momentum possessed by each planet; notably, planet h contains a similar amount of  $J_{sys}$  in HD 10180 as Jupiter does in the Solar System.

If the true value of  $K$  is assumed to be  $\gtrsim 0.95$  for a K-complete system, then there are already some multi-planet candidates from this research with  $K < 0.4$  that might deserve extra attention: HD 20794, Kepler-25, Kepler-29, Kepler-37, Kepler-100, and Kepler-109. TTV measurements might yield more information about whether more planets exist in the system. Of the single-planet MS systems without Hot Jupiters as they are defined here, several are identified which may also harbor more planets by this criterion: CoRoT-7, Kepler-21, Kepler-78, and Kepler-407, all with  $K < 0.1$ . In addition, HD 1461, Kepler-93, Kepler-97, and Kepler-98 are all single-planet MS systems with  $0.1 < K < 0.3$ . Of all the planets mentioned above, only HD 20794 and HD 1614 are RV-detections. The transiting systems may prove more fruitful for finding extra planets if RV or TTV measurements can be made over a long timescales because the angle of the orbital plane is known.

---

<sup>5</sup>The HD 10180 planetary system was discovered by the radial velocity in 2010/2011 by Lovis et al. (2011) as having up to 7 planets, and further study of the data by Tuomi (2012) indicated the number could be as high as 9. As of 15 June 2015, planet b has been deemed a likely positive detection, though controversial, while planets i and j remain unconfirmed. At the time of this writing, planets b, i, and j are not included in the EOD database, and are therefore, not included in the case study.

Large  $K$  values are not necessarily consistent in determining the “completeness” of discovered planetary systems. The uncertainty lies in the fact that even if a system already has large  $K$ , the addition of a later discovered planet (especially one at a large orbital distance) will significantly increase  $J_{sys}$  but not  $K$ . Consider that for a multi-planet system, each planetary component of  $J_p$  which may be called  $J_b$ ,  $J_c$ , etc., such that the sum of all components equalled the numerator in the the calculation for  $K$  (equation 2.21). In our own system of eight planets, Jupiter’s orbital angular momentum accounts for 61% of the total system  $J$  (*i.e.*  $J_{Jup}/(J_{\odot} + J_{Mer} + J_{Ven} + \dots) = 0.61$ ). When all planets are accounted for, our solar system has  $K = 0.995$ . But if a Jupiter-like planet were the first and only planet detected around a Solar System-like system, probably by the RV method, the planet-system ratio  $K$  would be 0.991 (*i.e.*  $K = J_{Jup}/(J_{\odot} + J_{Jup})$ ), nearly the same as if all planets were known. Therefore, we cannot conclude with any certainty that large  $K$  values are indicators of “complete” systems – that is, systems in which we know of all (or most) of the existing planets. Large  $K$  only indicates whether one of the dominant planetary contributors to the system angular momentum has been discovered. Jupiter-sized planets at  $a > 0.5 - 1.0$  AU will, in general, dominate the distribution of total system angular momentum. Instead, a holistic approach which includes system age, stellar rotation, and/or other factors, is needed to make a worthwhile determination about system completeness for those with large and mid-sized values  $K$ .

### 4.3 Biases

The most consistent problem plaguing this study was observational and selection bias related to detection method. As already pointed out, this sample of exoplanets is biased to large,

Jupiter-sized planets, typically with a small (less than 0.5 AU and in many cases, less than 0.1 AU) semi-major axis. The bulk of planets discovered and all systems' first-discovered planets used in this research were found by the RV or transit methods of planet detection. The RV method is biased to measuring the gravitational effects of large planets on the host stars but the effect is not as noticeable for smaller low-mass planets, for additional planets in orbits significantly misaligned to the first discovered planet, and for very long period orbits. The best RV precision in determining orbital parameters comes from slowly rotating host stars. Further, the transit method only detects planets whose orbits are nearly coplanar with our line of sight, which, again, might miss planets with orbits misaligned to the first discovered planet, or those with long-period orbits. Large planets will cause a greater change in the stars brightness, and close-in planets have a higher probability of transiting, making them easier to detect with transit measurements. Also, large, close-in planets provide the largest change in radial velocity measurements of the host star, making them easier to detect with the RV method. The technology and techniques are improving rapidly, and very small planets are being discovered by both methods. HARPS in particular has achieved sub 1 m/s precision in their radial velocity measurements. With space telescopes, adaptive optics, and the various timing variation methods (RTV, TTV, etc.), more and more planets outside the small-orbit and hot Jupiter classifications are being discovered and confirmed. The Kepler Mission is proving the usefulness of long-term continuous transit method observations, with a significant (200-600%) increase in discovered Earth- and Neptune-sized planets discovered in the latest data set (Batalha et al., 2013). It is this significant increase in the number of small- and medium-sized planets that make this study possible and meaningful.

The true value of the system angular momentum is unknown, but particular values or ranges of values could be given probabilities from Bayesian statistics, as was done for observed obliquities by Fabrycky & Winn (2009). The greatest known uncertainty in the final value for  $J_{sys}$  is inherited from uncertainties in the stellar quantities, most notably  $v \sin i_*$  as determined by Doppler broadening of spectral lines, and the planetary quantity  $m \sin i_p$  except where transit method measurements are available. (The greatest source of unknown uncertainty comes from undetected planets.) The discovery of planets and the measurement of their mass using the RV method is facilitated by slow stellar rotation but the errors in measuring  $v \sin i_*$  are large, and often only the upper bound is reported. The orbital angular momentum of the planets, however, are in general reasonably well constrained, or at least better constrained than the spin angular momentum of the stars.

Bias also exists between the  $J_p$  calculations of the RV and transit method populations. While the distributions of planet masses are relatively similar between the two groups, the plot of planet mass with semi-major axis forms two distinct groups, as in Figure 3.2. In general the RV-detected planets are more massive and in larger orbits – meaning that they possess more orbital angular momentum than the planets (so far) discovered by the transit method. The biases introduced by using only RV discovered planets are covered by Alves et al. (2010) and those that concern the transit method of discovered are discussed in Paz-Chinchón et al. (2015). Put simply, the RV method favors planets and stars with large system angular momenta, while the transit method tends toward smaller stars, smaller planets, and smaller  $a$ , for smaller overall  $J_{sys}$ . Despite these issues, we include all planets regardless of method to include a more continuous distribution of planetary and stellar

characterizations, and to build a more complete picture of angular momentum trends in these systems.

The detection or lack of detection of planets is by itself a source of potentially large systematic error in the  $J_{sys}$  results and the determination of the fit to  $J_{sys} \propto M^\alpha$ . How much the non-discovery of planets affects  $J_{sys}$  and/or the Kraft relation depends on the configuration of the known system, the rotation rate and mass of the star, and the nature of the unknown planets. There are many cases that could be described, and three are identified here.

**Case 1:** When a non-HJ giant planet is present in a system, the orbital angular momentum of that planet alone is on average one to two dex larger than the spin angular momentum of the host star, producing large  $K$ . Whether other planets exist or not, and whether they are detected or not, most of the system angular momentum in such a system has been discovered. The absence of smaller or closer-orbiting planets, of course, negatively biases the angular momentum, but not to a large degree.

**Case 2:** If a hot Jupiter, hot Neptune, or even a “warm” Neptune ( $0.1 \text{ AU} < a < 0.5 \text{ AU}$ ) is known to orbit a star, its orbital angular momentum is small and scales as  $\sqrt{M}$  with stellar mass. If the star has very low mass and/or is a very slow rotator,  $K$  for this system may be high, but overall  $J_{sys}$  may be small compared to other systems of similar stellar mass. Future planetary discoveries in these systems could likely be at greater orbital distances, and would greatly increase  $J_{sys}$  but not  $K$ .

**Case 3:** Consider the known-planet configuration of Case 2 above, but with a more massive and/or faster rotating star.  $J_*$  may have a normal to high placement on a J-M plot, but  $K$  for this system would be small.  $J_{sys}$  would also place high on the plot, due

mostly to the contribution of angular momentum from the star. Other discovered planets might increase  $J_{sys}$  and  $K$  incrementally, raising the overall position of  $J_{sys}$  on the plot.

More discoveries of planets around known systems and more multi-planet discoveries in general are needed before these speculative cases can be considered likelihoods or rarities. A combined analysis of the  $J_p$  and  $K$  values, could then indicate in which groups of stars this is more likely to happen, and how this might affect the slope of the fit for  $J_{sys}$ . At this time, the effect of undiscovered planets on the intercept or slope of the Kraft relations found so far is inconclusive due to many possible system configurations combined with many possibilities of potential planet discoveries.

Lastly, there are a number of stars which have had RV measurements taken for decades, that as yet, do not show evidence of planets, and in particular, no evidence of large planets orbiting at large  $a$  (Cumming et al., 2008). As noted earlier, a detailed comparison of MS stars across a range of spectral types or masses should be undertaken to identify differences, if they exist, between those stars which most likely do not harbor planets and those which do.

## Chapter 5

# Summary, Conclusions, and Suggestions for Future Work

Until now, the moments of inertia and inertial coefficients have not been interpolated and then integrated into the calculation of angular momentum for a sample of stars this large for the purpose of combining  $J_*$  with the orbital angular momentum of  $J_p$ . Similarly, no study of the angular momentum of planetary systems had included planets discovered by both RV and transit methods. The size and range of the sample of planets and host stars (532 planets in 426 systems) has only been available for about a year, and the next release of planet discoveries by the Kepler team will undoubtedly enlarge the sample's parameter space. A summary of the work and results, the major findings of the research, and possible directions for future work follow.

## 5.1 Summary

Several questions regarding the methods and goals of this research were posed at the end of Chapter 1. Here the answers are summarized.

1. **Q:** What is the best way to quantify the angular momentum of planetary systems?

**A:** Given the numerous biases, and without knowing obliquities and spin-orbit angles, a simple addition of  $J_*$  and  $J_p$  is sufficient for calculating  $J_{sys}$ . The moment of inertia of the star is not insignificant.

2. **Q:** How do these measurements compare to past studies of stars and planetary systems?

**A:** With few exceptions and allowing for detection bias, the low-mass Main Sequence host stars exhibit  $J$  consistent with the power law break, but the few larger stars  $> 2 M_\odot$  also fall below the early type power law. Total system  $J$  have wide scatter, are sensitive to detection biases, and are potentially strongly biased by missing data from undiscovered planets.

3. **Q:** What are the Kraft relations of planetary host stars and total planetary system angular momenta? *i.e.* What is the value of  $\alpha$  for  $J \propto M^\alpha$  for these groups?

**A:** In general, the power law fits to the host stars were shallower than expected, even when restricted to the Main Sequence stars only. The systems as a whole, on the other hand, agreed well with  $\alpha = 2$  on average. Various subgroupings of stars and systems revealed biases within the population. The Kraft relations are undoubtedly also affected by the bias of undiscovered bias but the determination of how and by how much is as mysterious as the “missing” planets themselves.

4. **Q:** Can the results be used to aid in detection of undiscovered planets?

**A:** At this time not enough information is available to suggest how much angular momentum *should* be in a planet or the system as a whole, or whether the histogram in Figure 4.12 is representative of all planetary systems, including those with undiscovered planets. Detection methods strongly bias  $K$ , but low  $K$  values could be an indicator of “missing” planets *if* “complete” systems should have  $K > 90\%$ . If that is the case, then longer term studies should reveal more planets in low- $K$  systems over time. The overall distribution of  $\mathcal{L}$ , however, is fairly normal, peaking around 1 dex – but the distribution may be incomplete due to undiscovered planets and/or skewed by biases.

5. **Q:** Do the results support the the Solar System as unique or typical?

**A:** Half the planetary systems have 90% of their angular momentum contained in the planets, and 90% of the systems have  $K > 0.5$ . Most high- $K$  multi-planet systems of solar-type stars contain system angular momentum similar to the amount in the Solar System, and several multi-planet systems resemble the Solar System, with smaller planets closer to the star and larger gas giants further out. But discoveries have been biased to single-planet systems with Hot Jupiters or Hot Neptunes, or those with a single gas giant at large separation. In general, most planetary systems do resemble the Solar System with respect to the amount and distribution of angular momentum, but not with respect to structure. The Solar System type so far is rare, but not unique.

## 5.2 Conclusions

The spread in the J-M plots of  $J_{sys}$ , especially in the region between the model power law and the break line, is likely the result of a couple of several factors. (1) Very slow rotators already displayed an angular momentum deficit, such then even if their planetary contribution was 1-2 dex more than the stellar portion, their  $J_{sys}$  position on the J-M plot did not come near the early type power law model line. This was especially true for the least massive planets which rotated the most slowly, contained the least mass, and had a deficit in  $J_{sys}$  compared to the power law fits to the rest of the sample. (2) While most Hot Jupiters contain more angular momentum than their host stars, the less massive hot Neptunes tended to contain less than their host star. These systems were the most common among the  $J_{sys}$  values still located below the break line. (3) The difference between the stellar and planetary angular momentum, related as a logarithmic ratio,  $\mathcal{L}$ , had a fairly normal distribution. (4) Unknown, undetected planets – specifically, the lack of their contribution to the system total – could be a major source of bias lowering the values of  $K$ ,  $\mathcal{L}$ , and  $J_{sys}$ .

These results support the speculation by Barnes (2001), among others, that planets are likely ubiquitous, that the Solar System is not unique in its structure or formation, and that Main Sequence stars with planets are the norm. These implications are further supported by this sample’s range of host star ages, or more appropriately, the variety in their stages of life, from very young to stars in their Giant and Subgiant stages.

When the ratios of orbital to spin angular momentum are taken into account, and the Solar System is itself held as a model K-complete system, the analysis suggests that low- $K$  systems could harbor other planets. The obvious implication is that stars less massive than

$2 M_{\odot}$  are as likely as not hosting planets. This argument is strengthened by the consistency in the  $J_{sys}$  fitting results — that whether considering the entire sample of systems, those on the Main Sequence, or only K-complete systems – the results repeatedly returned a power law slope for  $J_{sys}$  of  $\alpha \approx 2$ . This value for  $\alpha$  was identified by Brosche (1963) when he found an angular momentum-mass relationship spanning over 30 magnitudes of mass (refer to Section 1.1). But whether this slope will remain consistent with future discoveries is yet to be seen.

With the era of exoplanet discovery still so young, we cannot yet make accurate predictions about which systems have more planets to discover, based solely on the amount of angular momentum in its components ( $J_*$ ,  $J_{sys}$ ) or on the proportion of orbital to system angular momentum calculated ( $K$ ,  $\mathcal{L}$ ). Certainly not enough time has passed with the technology and techniques currently in use to discover a solar-like system with all the outer planets in analogous orbits. To confidently detect two orbits of Jupiter, for example, at least 24 years of observations must be made with the RV, transit, or even TTV methods. (An exception to such lengthy surveys would be the direct imaging technique, but with greatly increased sensitivity.) In the next decades, we may find more long-period planets around sun-like stars, and then the shape of angular momentum distributions to come will be more complete.

It is unclear whether the planetary system power law slope is actually related to the slope of the stellar early type power law. The general increase in system angular momentum can be explained by a combination of factors including biases in measurements, techniques, undiscovered planets, selection effects, and detection methods. So the angular momentum loss problem of stellar formation may indicate that some angular momentum in

the collapsing cloud is put into planet formation, but the existence or absence of planets is not necessarily related to the the rotation rates of their host stars. The angular momentum problem remains unsolved

The agreement between planetary system angular momenta and the power law describing the angular momentum trend for early type stars, could be explained a number of ways. For one, it could be purely coincidence, or the planetary systems follow a power law which is not related to the stellar law. Second, the early type power law describes the “memory” of initial angular momentum imparted on the system during formation, which the early type stars still “remember.” This is problematic, however because a number of solar-type stars that have been observed with the RV method for 20 years have not shown evidence for the existence of planets, and their rotation rates are similar to those stars which have planets.

### **5.3 Suggestions for Future Work**

Binary and multi-star planetary systems were not included in this research. Such a study could (1) support these findings and conclusions, or (2) present another category of planetary systems which follow a different law relating angular momentum and mass, or relating other pertinent quantities. A number of other relationships between stellar evolution and planet formation can and should be explored with the inclusion of quantified *total system* angular momentum, not just the stellar portion. The methods for calculating  $J_*$  would need to be expanded to include the stars’ orbital angular momentum apart from the planets’.

Systems discovered by imaging and microlensing could have their angular momentum similarly studied but their large uncertainties and small sample size make such result prevent

drawing conclusions with great confidence. One could assume  $K > 0.99$  for systems with large  $m$  and/or  $a$  as a starting point and speculate about other components or parameters.

The work of developing a method to determine the inertial coefficient,  $\gamma$ , from a single input variable should be further refined to include  $T_{\text{eff}}$ , metallicity, radius, and age if possible. The group with the greatest uncertainty in this parameter is the Subgiant class of stars. Better determinations could be made for this group, but might need to be undertaken on a case by case basis. Uncertainties in  $\gamma$  were roughly estimated based on the Claret model outputs and did not reflect true propagated error in the interpolation equation, nor with regard to the uncertainties in other stellar parameters.

Missing values and uncertainties in the database were not dealt with in a conservative manner. This was done in order to include the largest possible sample of stars that had data necessary for the angular momentum calculations. The sample could surely be whittled down to a set of systems with well-constrained values, and the results compared to this thesis. Conversely, the sample set could be expanded to include more systems with a greater range of star masses. These would require individual attention to missing parameters that have only upper bounds. For example,  $m \sin i_p$  in particular needs specific treatment when it is missing uncertainties.

The effect of stellar classification (MS, Subgiant, Giant) has been largely neglected in past research on angular momentum in planetary systems. Many questions arose during the course of this research related to stellar evolution: Do evolved stars have a power law describing a J-M relationship? What happens to the planets when the radius of a subgiant or giant star engulfs the planet? When  $J_p$  is substantial, how does this affect the stellar angular momentum?

In the process of quantifying the angular momentum of planetary systems, many more questions were raised than we had started with. The directions the future research could take seem endless, but two are of personal particular interest. On the stellar modelling and physics side, more stars with negative results for planet detection should continue to be observed and compared to the growing number of planetary host stars. On the exoplanet side of the work, the systems identified with low  $K$  values need precision radial velocity measurements done over the course of years to determine if small- $K$  systems are a normal phenomenon, or a red flag indicating more planets at greater distances. Long-term, precision RV measurements are needed as the transit method is less likely to detect planets at large separation distances from their parent star.

## Appendix A

# Stellar Inertial Models

After selecting a sample of host stars and planets, the only piece of data that was not easily obtained from databases or simple equations based on the parameters available, was the stellar moment of inertia. After a thorough literature search, two acceptable sets of models addressing stellar inertial evolution were found. They both published grids or tables of results including stellar inertial data that both (1) described normal stars, (2) covered the range of stellar masses in the sample (at that time, the range was 0.58 to 1.51  $M_{\odot}$ ), (3) included the Main Sequence portion of stellar evolution, and (4) were contemporaries, published at about the same time. Several other models of moments of inertia were found but were not considered because they only included a narrow range of masses, pertained to stars with particular traits – such as relativistic stars, stars with accretion disks, close binaries perturbed by tidal forces – or they only addressed one star, the Sun.

The two models studied in the early stages of the research are described in the following sections. They include the model developed by Pinsonneault, Kawaler & Demarque (1990, hereafter referred to as PKD) which tracked normal stars from the birth line through

the Main Sequence, and that of Claret & Giménez (1989, 1990, hereafter referred to as CG), which evolved models of varying mass from the Zero-Age Main Sequence (ZAMS) through the end of hydrogen burning. Both models generate stellar inertial data as a function of age.

Prior to PKD and CG, Motz (1952) had published inertial coefficients for integral and half-integral polytropes, and a handful of stellar models of the time, now considered outdated. Ilin (1985) calculated ZAMS moments of inertia, among other stellar parameters, for a range of 0.15 to 125 solar masses with composition  $X=0.70$ ,  $Z=0.03$ . But this contribution has not apparently been noteworthy, as it was before the end of the Soviet Union; no citations to the work are documented in the main citation repositories, and it is entirely in Russian. There are also no follow-up works on the same topic, and is mentioned here only in acknowledgement of the effort. A contemporary to CG and PKD, Ruciński (1988), published tables of  $\gamma$  pertaining to various fractional stellar masses and radii, with outputs ordered by polytropic indices; he computed many variations of  $n$  for the core with  $n_{outer} = 1.5$ . The models addressed masses of only up to  $1.2 M_{\odot}$ .

## A.1 PKD Models

The PKD models produced a number of stellar parameters as a function of mass and time, for stellar ages from the birth line to the Main Sequence. The inertial computations were intended for application to stars in open clusters, and includes masses from 0.4 to  $1.75 M_{\odot}$ . The model assumes constant mixing lengths, rigid rotation (though the moments of inertia are determined for a non-rotating model), solar composition/metallicity, total conservation of angular momentum, and a single initial angular momentum for all mass

ranges,  $J_0 = 5 \times 10^{49} \text{ g cm}^2 \text{ s}^{-1}$ . This last assumption may seem unusual at first, but work done by Kawaler (1988), demonstrated that it is valid, and that the effects of magnetic stellar wind on convective envelopes of Pre-Main Sequence (PMS) stars is sufficient to remove excess angular momentum before the star reaches the birth line. Kawaler’s models evolve the surface velocity and internal angular momentum distribution of stars with masses from 0.4 to  $3.0 M_\odot$  with various field geometries. After settling on field geometry parameters that reproduce the empirically derived Skumanich Law of rotational braking, Kawaler examines the dependence of equatorial rotational velocity on initial angular momentum,  $J_0$ . After about 100-300 My, the model’s  $v_{eq}$  loses dependence on  $J_0$ . This describes well how very young stars exhibit a wide range of rotational velocities, while more mature stars populate a much narrower range of velocities and exhibit generally slower rotation rates of  $<20 \text{ km/s}$ .

As seen in Figure A.1, the moment of inertia, or more properly,  $\log I$ , decreases steadily for each modelled mass in its early life, then, once reaching the Main Sequence, continues to decrease more gradually until  $\log I$  reaches a minimum. The moment of inertia begins a gradual, shallow climb upward after this point; that occurs at different ages for each mass but could be called “mid-life.” The models are terminated at 1.7 Gy except for the 1.5 and 1.75 mass models which stop at 0.9 and 1.0 Gy respectively. As such, they do not include “late life,” that is, evolution onto the horizontal branch after the Main Sequence. Since stars lifespans vary inversely with their mass, it should be remembered that the time that passes through the “early life” of one star might be at a time of “near-death” for a more massive one. Therefore references to the early and late life of these models are relative.

For reference, ZAMS has been visually determined from Figure A.1 and tabulated with the  $\log I$  values at the mid-MS or “mid-life” in Table A.1. The minimum moment

Non-rotating stellar moments of inertia

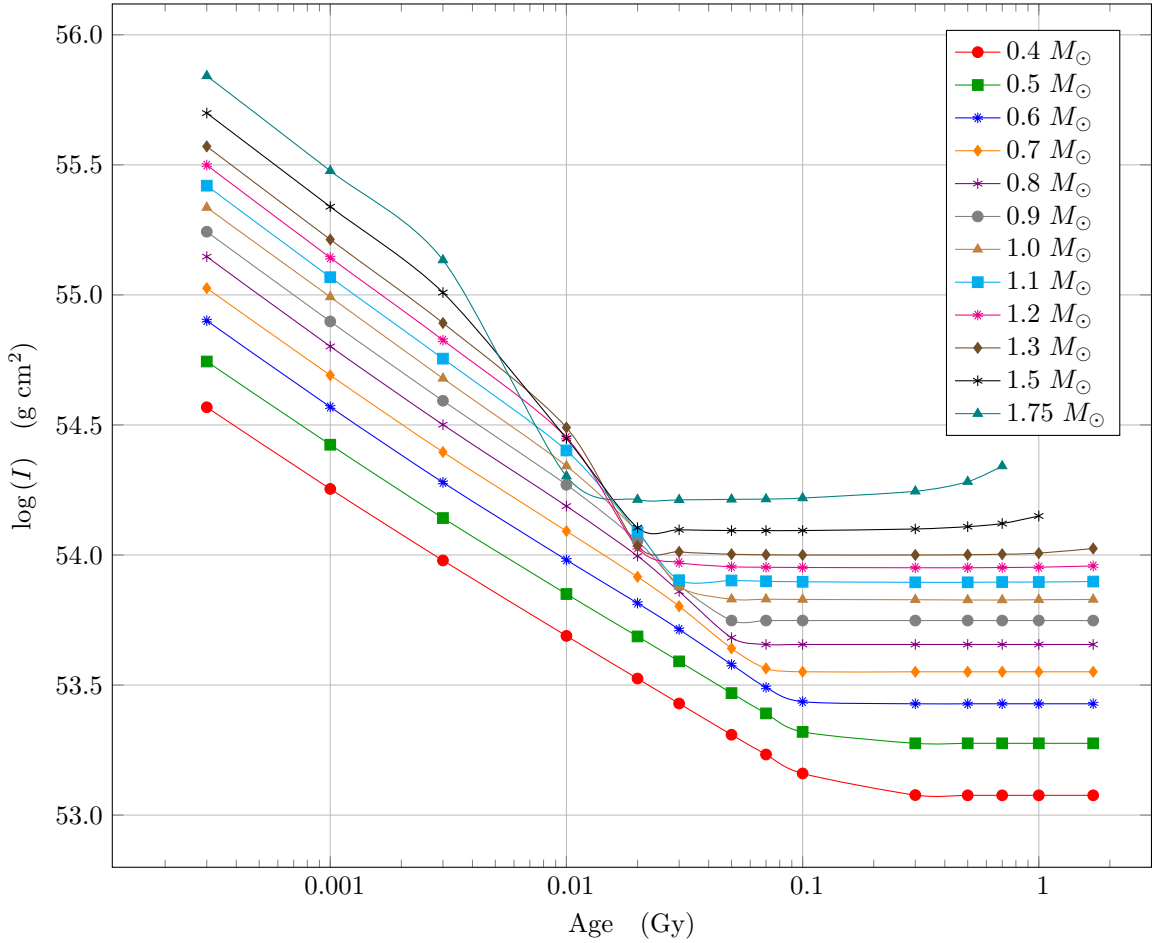


Figure A.1 The moments of inertia (specifically,  $\log I$ ) for host stars in planetary systems were extracted from PKD’s tabulated data of stellar parameters. They are plotted here against age to visually relate the moments of inertia evolving through the Hyashi track through the Main Sequence. Especially for masses less than  $1.5 M_{\odot}$ , the value of  $I$  appears to remain relatively constant once on the Main Sequence. (data from Pinsonneault et al., 1990)

of inertia in this model may be taken as the point where the star has reached maturity, has remained stable over a long period of time, and is no longer contracting its core. At this point it may be treated as a solid rotating body. From this definition, we extract these minimum  $\log I$  values for each mass and develop an interpolation equation for  $I$  as a function of  $M$ . The interpolated moment of inertia needs then only the angular velocity

Table A.1. PKD Model Ages at ZAMS and Mid-MS  $\log I$

Stellar Mass [ $M/M_{\odot}$ ]	ZAMS $\log(\text{Age})$ [Gy]	Mid-MS $\log(\text{Age})$ [Gy]	Mid-MS $\log I$ [ $\text{g cm}^2$ ]
0.4	0.1	1.0	53.076
0.5	0.1	0.7	53.276
0.6	0.1	0.7	53.428
0.7	0.07	0.7	53.551
0.8	0.05	0.5	53.656
0.9	0.05	0.5	53.748
1.0	0.03	0.5	53.827
1.1	0.03	0.3	53.895
1.2	0.02	0.3	53.951
1.3	0.02	0.1	54.000
1.5	0.02	0.07	54.094
1.75	0.01	0.03	54.212

which can be derived from  $v \sin i_*$  and the stellar radius  $R$ , as described in Section 2.3.1.

Then

$$J_* = I_{PKD} \Omega \quad (\text{A.1})$$

The minimum value of  $\log I$  is chosen deliberately with the assumptions about star maturity and stable internal differentiation in mind. Further, the difference between minimum and maximum  $\log I$  of each modelled mass up to and including  $1.5 M_{\odot}$  on the Main Sequence, is comparable to the propagated error from interpolation equations describing the stars' lifetime on the Main Sequence (described in more detail below). A relationship between  $M$  and  $\log I$  is extrapolated for this stable MS period of the stars' lives. A fourth-order polynomial least squares fit for all masses excluding  $1.75 M_{\odot}$  produces good

agreement, as

$$\log(I) = 0.5409M^3 - 2.2108M^2 + 3.4929M + 52.0054 \quad (\text{A.2})$$

The  $\log(I)$  values for mass  $1.75 M_{\odot}$  are not included in the least squares fit, because at the time of this part of the research, there were no host stars with a mass approaching that size in the sample. Exclusion of this mass value also produces a better fit with fewer terms. A secondary check to the fit is given by  $R^2=0.9998$ , confirming correlation. Here,  $R^2$  is the statistical coefficient of determination.<sup>1</sup> This interpolation equation was then used to generate rotational moments of inertia for the sample of exoplanet host stars. Figure A.2 plots the selected MS values of PKD's  $\log I$  against mass (represented by  $\times$ 's), with the interpolation equation overplotted (solid line).

## A.2 CG Models

Contemporary models by CG were developed to aid in the study of apsidal motion in double-lined eclipsing binaries. Their basis for deriving the inertial coefficient, rather than the moment of inertia itself, was to better describe the tidal torques acting on (otherwise normal) stars in circular, synchronized systems. Although their main focus was for binary stars, their tidal and inertial coefficients are included as separate outputs for the models.

These models, may then be used for normal, rotating, single stars.

---

<sup>1</sup>The coefficient of determination,  $R^2$ , is one measure of goodness of fit describing the relative amount of variation in the data that is explained by the model. The  $R^2$  value is determined by  $R^2 = 1 - \frac{\sum (y_i - \hat{y}_i)^2}{\sum (y_i - \bar{y}_i)^2}$ , where  $\hat{y}$  is the resultant predicted by the model-fit. Linear measures of correlation and goodness of fit, such as  $R^2$ , may be used with polynomial models, as their terms are expressed linearly, as opposed to nonlinearly (nonlinear terms would be, for example, exponential, logarithmic, sinusoidal, etc.) (Walpole et al., 2007)

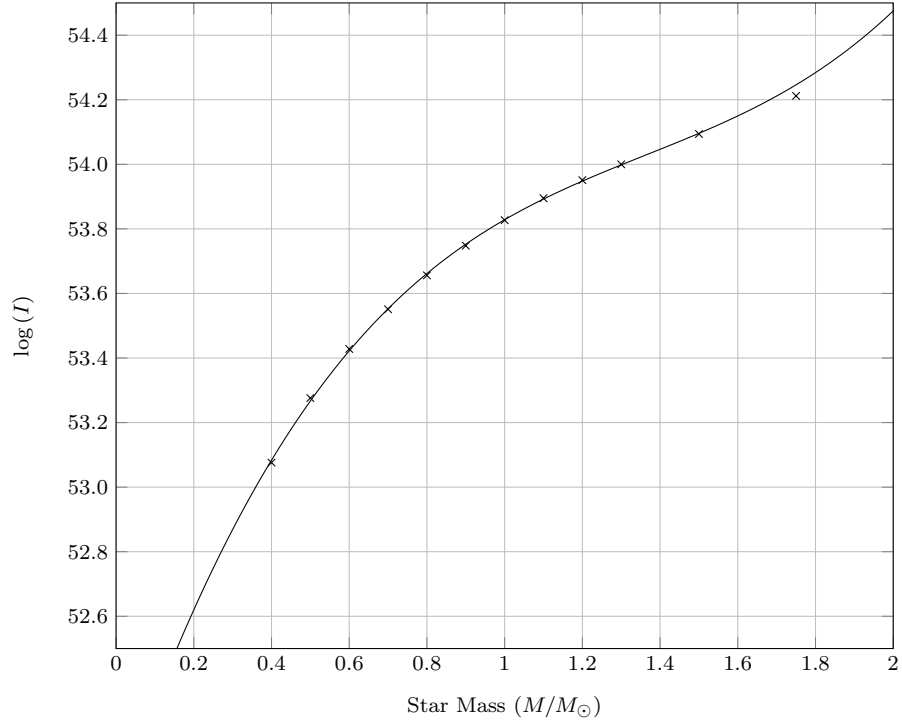


Figure A.2 A best-fit line representing an interpolation equation relating stellar mass ratio to the log of the moment of inertia (minimum value) in MS stars, according to Pinsonneault et al.'s (1990) models.

CG's early models were based on input physics which assumed that stars may be modelled as spherically symmetric objects, stars are homogeneous on the ZAMS, regions of the interior in radiative equilibrium are always stable, and convective zones are fully mixed. These early models did not take into account mass loss. The output included a unitless value called the radius of gyration,  $\beta$ , such that  $\beta^2 = \gamma = I/MR^2$ . Claret & Giménez (1989) evolved models for masses ranging from 1 to 25  $M_{\odot}$ , while Claret & Giménez (1990) modelled low-mass stars, of 0.6 and 0.8  $M_{\odot}$ . Both sets of models begin their evolution at ZAMS and finish at the end of hydrogen burning, so that much of the inertial data pertains to the life of the star while on the Main Sequence. The two low-mass models, however,

do not get evolved far enough in time to leave the Main Sequence. A visualization of the evolution of  $\gamma$  (that is,  $\beta^2$ ) for selected masses is shown in Figure A.3. Colored lines connect data points for ease of reading the plot, and do not represent a mathematical basis. For early times on the Main Sequence, it appears that  $\gamma$  is nearly linearly decreasing. This suggests that, for a given stellar mass and age, the inertia coefficient may be approximated with interpolation equations. This greatly facilitates calculation of a moment of inertia, and therefore angular momentum, when the star's age is known.

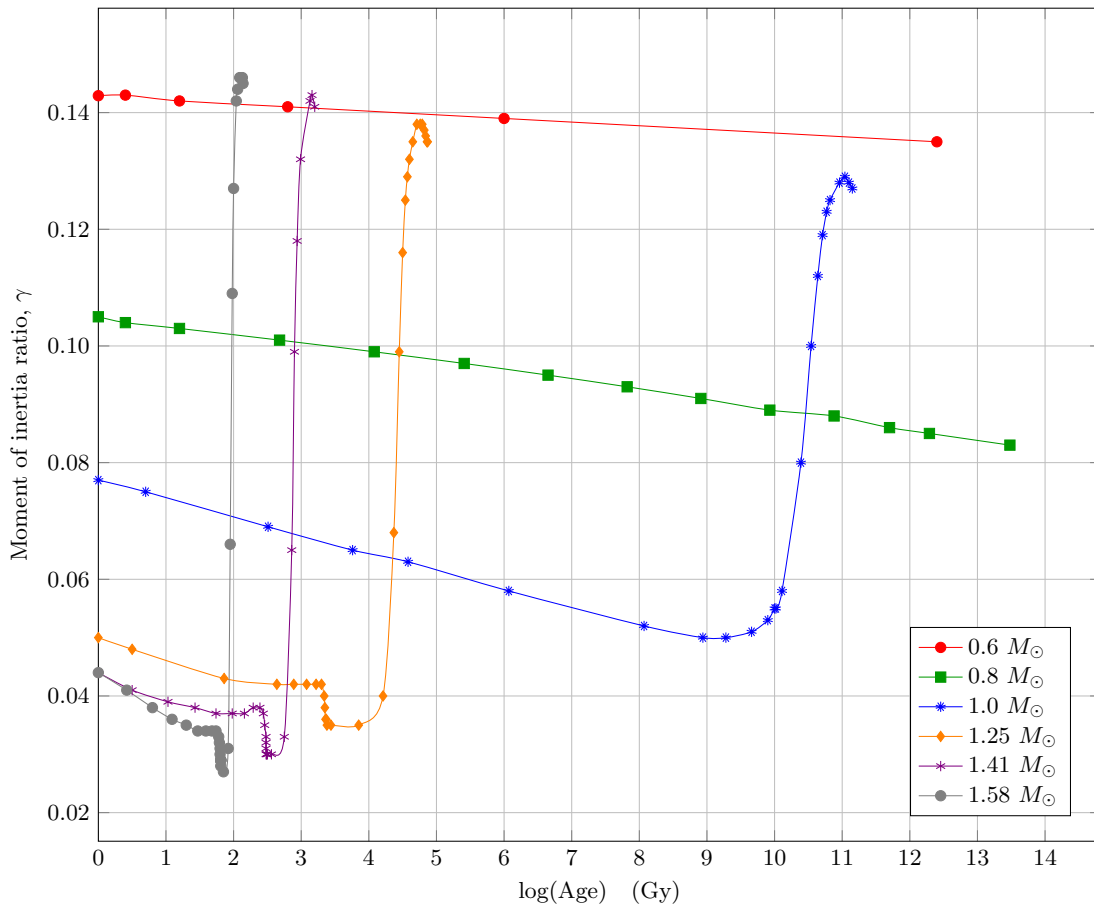


Figure A.3 Evolution of the stellar inertial ratio  $\gamma$  for selected masses according to CG models of ZAMS stars, through MS life to helium core burning. Colored connecting lines are for enhancing readability only. (data from Claret & Giménez, 1989, 1990)

Unfortunately age data is not always available, inconsistent between observers, or contains large uncertainties for many host stars. Initially it was thought these ages could be used to obtain a refined moment of inertia for the stellar spin. But even CG point to a simpler method, as mentioned already in Section 2.3.2, reproduced here for reference (Figure A.4). The ZAMS values for  $\log \beta$  show distinct, nearly linear relationships to  $\log M$  for two groupings of masses divided at around  $1.5 M_{\odot}$ .

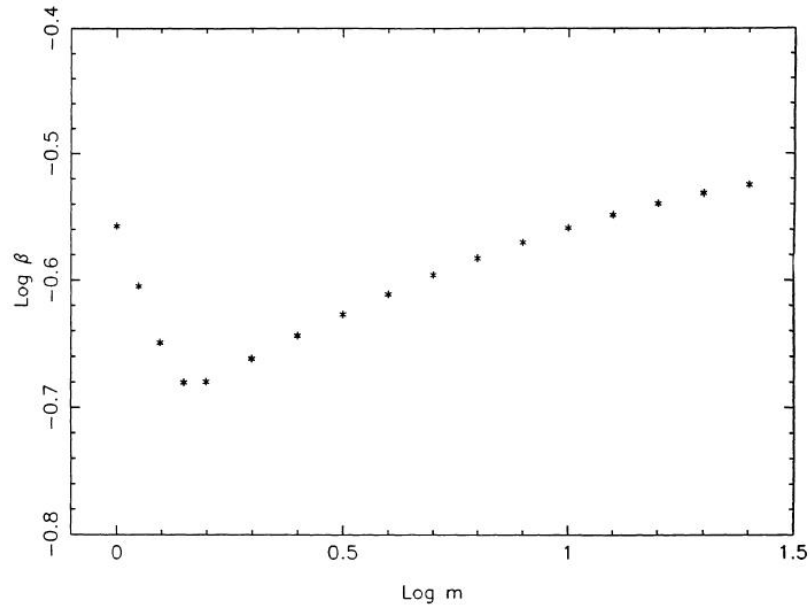


Figure A.4 The inertial coefficient relation to stellar mass. (abstracted from Claret & Giménez, 1989)

Similar to the method of developing an interpolation equation for  $\log I$  in the previous section, the an equation predicting the inertial coefficient  $\gamma$  was derived for ZAMS stars based on these two linear relationships to the log-transformed  $\beta$  and stellar mass. The

equations were:

$$M < 1.46M_{\odot} \quad \log \beta = -0.71318 \log M - 0.56966 \quad (\text{A.3})$$

$$M \geq 1.46M_{\odot} \quad \log \beta = 0.179398 \log M - 0.71561 \quad (\text{A.4})$$

The moment of inertia is then easily obtained with other measurable or derivable stellar parameters. Then,

$$I_{CG} = \gamma M R^2 \quad (\text{A.5})$$

### A.3 Comparison of PKD and CG Models

Both models described above were developed by experts in stellar rotation and evolution, and the main question after examining both models is, *Which model is best suited for describing the sample of planetary host stars in this research?* That is, one model or the other be adopted to accurately describe the inertial properties of the unseen stellar interior of single rotating stars, e.g., this sample of planetary host stars?

Interpolated moments of inertia and  $J_*$  (now referred to as  $J_{CG}$  and  $J_{PKD}$ ) for each of the models was determined with  $M$ ,  $R$ , and  $v \sin i_*$  or  $\Omega$  values used by McNally (1965) (which were obtained from Allen (1963)) and with those used by Kawaler (1987), with  $M$  and  $R$  from Allen (1973) and  $v \sin i_*$  from Fukuda (1982). These were compared, for masses less than  $2 M_{\odot}$ . Both  $J_{CG}$  and  $J_{PKD}$  were consistent with Kawaler's calculated values, but both models underestimated McNally's  $J_*$ . The differences were greater at higher masses,

with CG showing the most deviation. Several explanations are considered: (1) Both models make an assumption about the stellar interior that biases the inertial values at larger masses, (2) McNally’s data or choice of moment of inertia is not as accurate or up-to-date as Kawaler’s, or (3) there are inherent flaws in both models and the matched angular momenta calculations to Kawaler are coincidental. When we check McNally’s  $v \sin i_*$  distribution against  $M$ , we find the velocities are overestimated compared to other published distributions (Kraft, 1970; Tassoul, 2000, etc.), perhaps due to systematic errors in the collection of data by Allen, or simply a bias in the quality of measurements at that time. Whatever the reason, we decide option (2) is the most plausible reason for the deviations, and conclude that both sets of models are in agreement for the mass range of 1 to 2  $M_\odot$ .

Next, the sample (at that time) of about 150 host stars was put through the same calculation of  $J_{CG}$  and  $J_{PKD}$ , and compared. Again, very good agreement was found for low masses, below about 1.2  $M_\odot$ , but the CG model appeared to be consistently higher, now, than the PKD values. The divergence increased for increasing mass, but the values never became unreasonable. (Note: this same divergence was noticed when the sample size increase to over 400 host stars and the maximum mass increased to over 3  $M_\odot$ .) It is perhaps a problem of physical assumptions or differences in time-steps that causes disagreement between these two otherwise reputable inertial models. In an updated version of the CG model, Claret (2004) describes a correction to the input physics that explained why previous models were overshooting  $\gamma$ , especially for the larger masses.  $J_*$  was then calculated for the samples and early literature with the inertial data from Claret (2004), and termed  $J_C$ . Even with the newer models and new interpolation equations for ZAMS (even calculating the mean of MS  $\gamma$ ),  $J_C$  would exhibited higher angular momentum values than  $J_{PKD}$ . The

difference appeared to be due to the inclusion of stellar mass and radius from the samples as opposed to those the models.  $I_{PKD}$  does not take individual stars'  $M$  and  $R$  values into account, since my interpolation equation is a function of mass only. The focus of the models may also have an effect as, PKD was primarily concerned with the moment of inertia as the stars contracted to the Main Sequence, whereas CG modelled their early grids almost entirely on the Main Sequence.

## A.4 Claret (2004) Models

Despite small divergences, the interpolated inertial parameters of both models do appear to be in agreement with each other, for most of the MS mass range up to  $1.5 M_{\odot}$ . As the research progressed, and the sample size was enlarged, it was noticed that many of the more massive host stars (those above  $1.5 M_{\odot}$ ) had underrepresented spin angular momentum calculated with inertial data from both sets of interpolation equations. That is, the angular momenta of stars larger than the point of McNally's "break" did not agree, even with uncertainties, with the early type power laws. This was found to be due to the assumption that all planetary systems' host stars existed on the Main Sequence, which ended up being false. The larger stars had a disproportionately larger population of Giant and Subgiant stars, discussed in Section 3.5, and therefore their moments of inertia were likely larger than their counterparts on the Main Sequence (due to larger  $R$  and also larger  $\gamma$ ). The PKD model only evolved the stars through a mature age on the Main Sequence, but the detailed 2004 models by Claret included inertial data for stars through the helium flash – the Giant stage – and up to carbon burning. After classifying each host star as MS, Giant, and Subgiant, I developed new class-based interpolation equations described in

Table A.2. Interpolated Inertial Coefficient Equations

Stellar Class	$\gamma$ interpolation function	Mass Range [ $M/M_{\odot}$ ]
Main Sequence	$\log \gamma = -1.43257 \log M - 1.14683$	$\leq 1.58$
Main Sequence	$\gamma = 0.0127(M - 1.78)^2 + 0.0364$	1.58-1.86
Main Sequence	$\log \gamma = 0.31481 \log M - 1.52300$	$\geq 1.86$
Giants	$\log \gamma = 0.24918 \log M - 0.87473$	$< 1.55$
Giants	$\log \gamma = -0.06315 \log M - 0.81542$	$\geq 1.55$
Subgiants	$\gamma = (\gamma_{\text{MS}} + \gamma_{\text{Giant}})/2$	(all)

Table A.4. New  $J_C$  agreed well with the early-type power law when applied to McNally and Kraft's data, especially for the more massive stars.

The Main Sequence interpolation equations are shown smoothly transitioning between their mass subgroups in Figure A.5. The thick grey lines indicate the range of values that  $\gamma$  might possess while on the Main Sequence, while the small dark squares indicate the average value of that mass. The interpolation equations are represented by a solid black line.

The models developed by Claret in 2004 included updated opacities, more complicated input physics including mass loss among others, a broader mass range, and a more diverse set of initial compositions. The new research included the standard composition models ( $X=0.70$ ,  $Z=0.02$ ), but it is noted that in the interpolation equations for the inertial coefficient could be refined with ages and metallicities (and uncertainties) as inputs. Time-stepped evolution for selected masses from this newest model are displayed for comparison in Figure A.6.

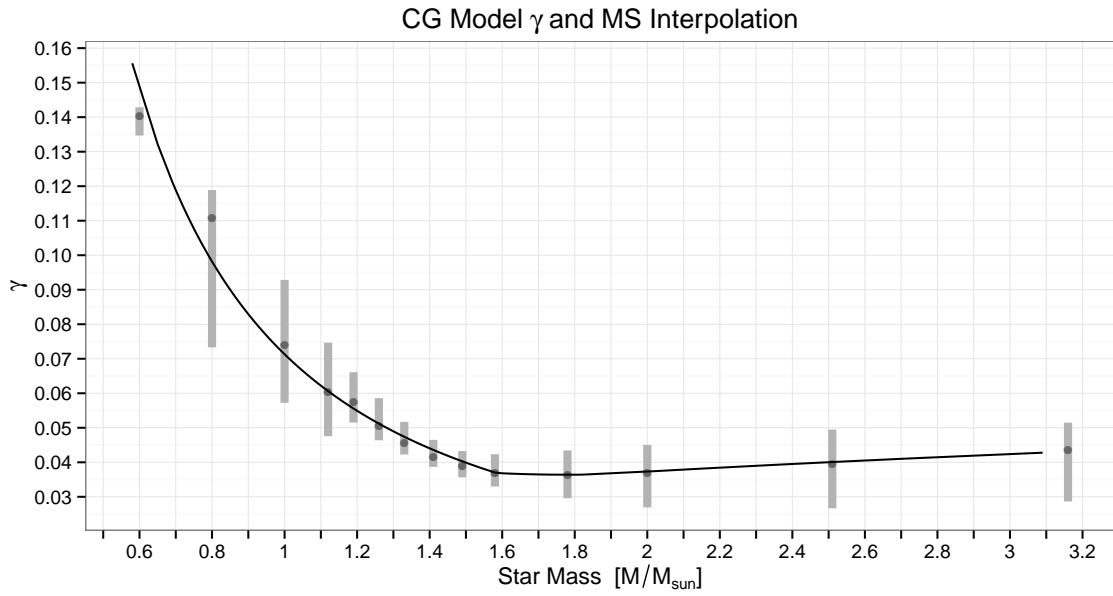


Figure A.5 The inertial coefficient relation to stellar mass. This incorporates the newest grids of stellar evolution from Claret (2004)

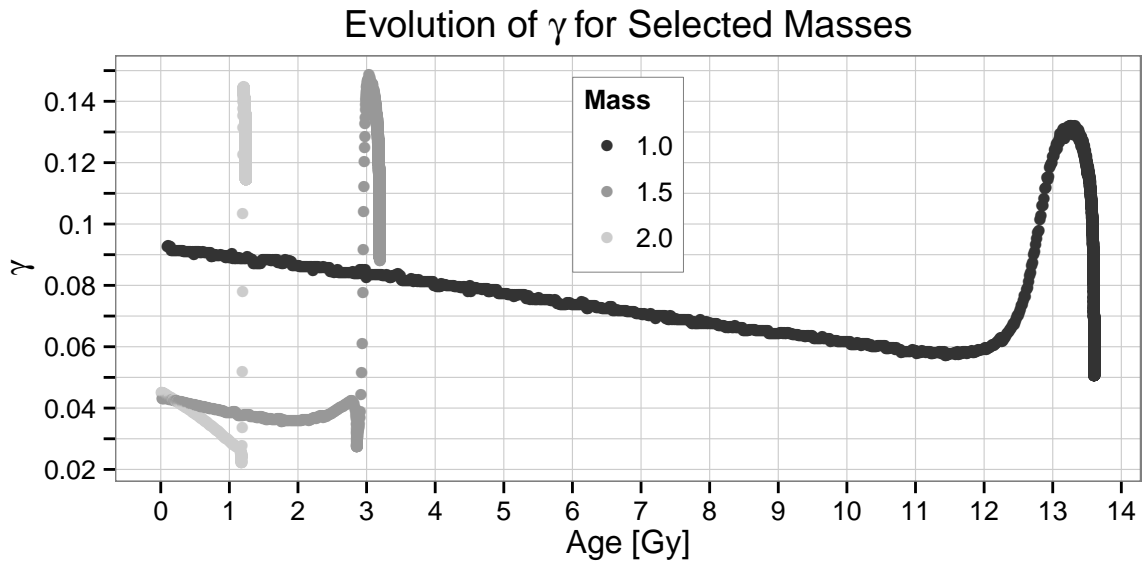


Figure A.6 The time-step evolution of  $\gamma$  for 1, 1.5, and 2  $M_{\odot}$ . Points are plotted individually to show the density of calculation in time. These newer models by Claret (2004) output thousands of time-stepped calculations. Compare to Claret & Giménez (1989) in Figure A.3 which provided <100 points.

## Appendix B

# Treatment of Uncertainties and Error Propagation

In calculating stellar angular momentum,  $v \sin i_*$  has the largest source of uncertainty, with mass and radius also contributing fair amount. In this error propagation,  $\gamma$  is taken from the CG interpolation equation (see Appendix A), and is treated as having 10% error for MS and Giant class stars, and 20% error for Subgiants. Thus,  $J_*$  and its propagated error is

$$J_* = \gamma MR v \sin i_* \quad (\text{B.1})$$

$$\sigma_{J_*} = J_* \sqrt{(0.20)^2 + \left(\frac{\sigma_M}{M}\right)^2 + \left(\frac{\sigma_R}{R}\right)^2 + \left(\frac{\sigma_{v \sin i_*}}{v \sin i_*}\right)^2} \quad (\text{B.2})$$

In the calculation of planetary angular momentum, the major sources of error are in  $M$  and  $a$ . We include the uncertainties in the eccentricity  $e$ , when present, and  $m$  in the error propagation. For single planets orbiting with some eccentricity  $e > 0$ ,  $J_p$  and its

propagated errors are

$$J_p = m\sqrt{MGa(1 - e^2)} \quad (\text{B.3})$$

$$\sigma_{J_p} = J_p \sqrt{\left(\frac{\sigma_m}{m}\right)^2 + \left(\frac{\sigma_M}{2M}\right)^2 + \left(\frac{\sigma_a}{2a}\right)^2 + \left(\frac{2e\sigma_e}{(1 - e^2)}\right)^2} \quad (\text{B.4})$$

In cases where  $m$  has been calculated from  $m \sin i_p / \sin i_p$ , as indicated by the EOD field MASSREF, the propagation to the planetary mass has already been performed by the maintainers of EOD. The uncertainty in  $m \sin i_p$  is taken as the uncertainty in  $m$ .

When eccentricity is zero, or not present in the database and without upper bounds in uncertainty, we use the simpler version of calculating  $J_p$  as if with a circular orbit, from Equation 2.14, as below with its propagated error:

$$J_p = ma^2 \frac{2\pi}{P} \quad (\text{B.5})$$

$$\sigma_{J_p} = J_p \sqrt{\left(\frac{\sigma_m}{m}\right)^2 + \left(\frac{2\sigma_a}{a}\right)^2 + \left(\frac{\sigma_P}{P}\right)^2} \quad (\text{B.6})$$

where  $P$  is the orbital period of the planet.

For a multi-planet system, with planets labeled  $b, c, \dots$  with masses  $m_b, m_c, \dots$ , the angular momentum of each planet respectively is  $J_b, J_c, \dots$ , and their respective uncertainties calculated by Equation B.4 are  $\sigma_{J_b}, \sigma_{J_c}, \dots$ ,

$$J_{p,\text{total}} = J_b + J_c + \dots \quad (\text{B.7})$$

$$\sigma_{J_{p,\text{total}}} = \sqrt{\sigma_{J_b}^2 + \sigma_{J_c}^2 + \dots} \quad (\text{B.8})$$

Propagated errors in system angular momentum include all contributed errors mentioned above for propagating error through  $J_*$  and  $J_p$ .

$$J_{sys} = J_* + J_{p,\text{total}} \quad (\text{B.9})$$

$$\sigma_{J_{sys}} = \sqrt{\sigma_{J_*}^2 + \sigma_{J_{p,\text{total}}}^2} \quad (\text{B.10})$$

The relative amount of system angular momentum contained in the planets' orbital angular momentum,  $K$ , also has associated error.

$$K = \frac{J_{p,\text{total}}}{J_{sys}} \quad (\text{B.11})$$

$$\sigma_K = K \sqrt{\left(\frac{\sigma_{J_{p,\text{total}}}}{J_{p,\text{total}}}\right)^2 + \left(\frac{\sigma_{J_{sys}}}{J_{sys}}\right)^2} \quad (\text{B.12})$$

## Appendix C

# Stellar Properties

The columns of Table C.1, from left to right, are: star name; stellar mass in solar masses, with uncertainties; stellar radius in solar radii, with uncertainties; projected rotational velocity,  $v \sin i_*$ , in km/s, with uncertainties; effective surface temperature,  $T_{\text{eff}}$ ; stellar evolutionary classification (see Section 3.5 for method), MS = Main Sequence, S = Subgiant, and G = Giant; the unitless derived stellar moment of inertia coefficient,  $\gamma = I/MR^2$ ; and log of the calculated stellar angular momentum in  $\text{g} \cdot \text{cm}^2 \cdot \text{s}^{-1}$ , with uncertainties. See Equation 4.7 for method of calculation of log-uncertainties

The foundation of the data sample was query-filtered the 5 December 2014 version of the Exoplanet Orbit Database, the archive of which may be found at <http://exoplanets.org/csv/exoplanets.1417831552.csv.gz>. The filter expression was

```
!BINARY and (A[au] and MSTAR[msun] and RSTAR[rsun] and VSINI[km/s])  
or STAR = 'HD 204313' or STAR == 'Kepler-20' or STAR == 'Kepler-26'  
or STAR == 'Kepler-40' or STAR == 'Kepler-406'
```

The pertinent fields chosen for download are listed in Table 3.3. The following stars had incorrect or inconsistent parameters reported by EOD:

Kepler-20   Kepler-26   Kepler-27   Kepler-406   Kepler-407  
 HD 120084   HD 204313

Corrections and adjustments are detailed in Section sec:clean: Data Cleaning. When a field is blank in the tables that follow, the data were not supplied by EOD. The treatment of missing uncertainties is also described in Section 3.4.

TABLE C.1: Stellar Parameters

Host Star Name	Mass ( $M_{\odot}$ )	Radius ( $R_{\odot}$ )	$v \sin i_*$ (km/s)	$T_{\text{eff}}$ (K)	Class	$\gamma$	$\log J_*$ ( $\text{g cm}^2/\text{s}$ )
11 UMi	$1.80 \pm 0.25$	$44.65 \pm 1.43$	1.5	4340	G	0.147	$50.39 \pm 0.17$
14 And	$2.15 \pm 0.15$	$11.38 \pm 0.26$	2.6	4813	G	0.146	$50.11 \pm 0.16$
14 Her	$1.07 \pm 0.09$	$0.91 \pm 0.03$	$1.6 \pm 0.5$	5388	MS	0.065	$48.14 \pm 0.16$
24 Sex	$1.81 \pm 0.08$	$3.92 \pm 0.13$	$2.8 \pm 0.5$	5069	S	0.092	$49.40 \pm 0.12$
47 UMa	$1.06 \pm 0.03$	$1.12 \pm 0.04$	$2.8 \pm 0.5$	5882	MS	0.065	$48.48 \pm 0.09$
51 Peg	$1.05 \pm 0.04$	$1.02 \pm 0.04$	$2.6 \pm 0.5$	5787	S	0.101	$48.59 \pm 0.13$
6 Lyn	$1.82 \pm 0.13$	$5.50 \pm 0.18$	1.3	4978	S	0.092	$49.23 \pm 0.18$
61 Vir	$0.94 \pm 0.03$	0.98	2.2	5571	MS	0.078	$48.34 \pm 0.16$
7 CMa	$1.34 \pm 0.13$	$2.30 \pm 0.10$	1.1	4761	S	0.095	$48.67 \pm 0.18$
70 Vir	$1.10 \pm 0.01$	$1.60 \pm 0.05$	$2.7 \pm 0.5$	5545	MS	0.062	$48.61 \pm 0.09$
75 Cet	$2.15 \pm 0.18$	$10.50 \pm 1.00$	1.8	4904	G	0.146	$49.91 \pm 0.17$
81 Cet	$1.74 \pm 0.21$	$15.73 \pm 0.50$	1.8	4845	G	0.148	$50.00 \pm 0.17$
91 Aqr	$1.32 \pm 0.23$	$11.00 \pm 0.10$	$3.9 \pm 0.5$	4681	G	0.143	$50.05 \pm 0.11$
alpha Ari	$1.33 \pm 0.22$	$13.79 \pm 0.44$	$3.1 \pm 1.0$	4513	G	0.143	$50.05 \pm 0.17$
BD -08 2823	$0.74 \pm 0.07$	$1.28 \pm 0.07$	1.4	4746	MS	0.110	$48.30 \pm 0.16$
BD -10 3166	$0.92 \pm 0.04$	$0.75 \pm 0.03$	$0.9 \pm 0.5$	5393	MS	0.080	$47.85 \pm 0.27$
BD +14 4559	$0.86 \pm 0.15$	$0.73 \pm 0.03$	$2.5 \pm 1.0$	4814	MS	0.089	$48.28 \pm 0.21$
BD +20 2457	$1.06 \pm 0.21$	$32.96 \pm 1.05$	$1.0 \pm 0.3$	4259	G	0.135	$49.82 \pm 0.18$
BD +48 738	$1.19 \pm 0.24$	$11.79 \pm 0.38$	$0.5 \pm 0.2$	4658	G	0.139	$49.13 \pm 0.18$
CoRoT-1	$0.95 \pm 0.15$	$1.11 \pm 0.05$	$5.2 \pm 1.0$	5950	MS	0.077	$48.77 \pm 0.12$
CoRoT-2	$0.97 \pm 0.06$	$0.90 \pm 0.02$	$11.8 \pm 0.5$	5625	MS	0.074	$49.03 \pm 0.06$
CoRoT-3	$1.37 \pm 0.09$	$1.56 \pm 0.09$	$17.0 \pm 1.0$	6740	MS	0.045	$49.36 \pm 0.06$
CoRoT-4	$1.16 \pm 0.02$	$1.17 \pm 0.02$	$6.4 \pm 1.0$	6190	MS	0.058	$48.84 \pm 0.08$
CoRoT-5	$1.00 \pm 0.02$	$1.19 \pm 0.04$	$1.0 \pm 0.3$	6100	MS	0.071	$48.07 \pm 0.16$
CoRoT-6	$1.05 \pm 0.05$	$1.02 \pm 0.03$	$7.5 \pm 1.0$	6090	MS	0.066	$48.87 \pm 0.08$
CoRoT-7	$0.93 \pm 0.03$	$0.87 \pm 0.04$	$3.5 \pm 1.2$	5275	MS	0.079	$48.49 \pm 0.16$
CoRoT-8	$0.88 \pm 0.04$	$0.77 \pm 0.02$	$2.0 \pm 1.0$	5080	MS	0.086	$48.21 \pm 0.25$
CoRoT-10	$0.89 \pm 0.05$	$0.79 \pm 0.05$	$2.0 \pm 0.5$	5075	MS	0.084	$48.21 \pm 0.13$

Continued on next page

Host Star Name	Mass ( $M_{\odot}$ )	Radius ( $R_{\odot}$ )	$v \sin i_*$ (km/s)	$T_{\text{eff}}$ (K)	Class	$\gamma$	$\log J_*$ ( $\text{g cm}^2/\text{s}$ )
CoRoT-11	1.27 ± 0.05	1.37 ± 0.03	40.0 ± 5.0	6440	MS	0.051	49.69 ± 0.07
CoRoT-12	1.08 ± 0.07	1.12 ± 0.09	1.0 ± 0.3	5675	MS	0.064	48.03 ± 0.16
CoRoT-13	1.09 ± 0.02	1.01 ± 0.03	4.0 ± 1.0	5945	MS	0.063	48.58 ± 0.12
CoRoT-14	1.13 ± 0.09	1.21 ± 0.08	9.0 ± 0.5	6035	MS	0.060	49.01 ± 0.07
CoRoT-16	1.10 ± 0.08	1.19 ± 0.14	0.5 ± 0.2	5650	MS	0.062	47.75 ± 0.17
CoRoT-17	1.04 ± 0.10	1.51 ± 0.05	4.5 ± 0.5	5740	MS	0.067	48.82 ± 0.08
CoRoT-18	0.95 ± 0.15	1.00 ± 0.13	8.0 ± 1.0	5440	MS	0.077	48.91 ± 0.12
CoRoT-19	1.21 ± 0.05	1.65 ± 0.04	6.0 ± 1.0	6090	MS	0.054	48.95 ± 0.09
CoRoT-23	1.14 ± 0.08	1.61 ± 0.18	9.0 ± 1.0	5900	MS	0.059	49.13 ± 0.09
CoRoT-25	1.09 ± 0.08	1.19 ± 0.08	4.3 ± 0.5	6040	MS	0.063	48.69 ± 0.08
CoRoT-26	1.09 ± 0.06	1.79 ± 0.14	2.0 ± 1.0	5590	S	0.100	48.73 ± 0.27
CoRoT-27	1.05 ± 0.11	1.08 ± 0.12	4.0 ± 1.0	5900	MS	0.066	48.62 ± 0.14
epsilon CrB	1.44 ± 0.18	29.12 ± 0.93	2.4	4436	G	0.146	50.31 ± 0.17
epsilon Eri	0.82 ± 0.05	0.74 ± 0.01	2.4 ± 0.5	5146	MS	0.095	48.29 ± 0.10
epsilon Tau	2.73 ± 0.10	12.75 ± 0.41	2.5	4946	G	0.144	50.24 ± 0.16
eta Cet	1.70 ± 0.10	14.30 ± 0.20	3.8 ± 0.6	4528	G	0.148	50.28 ± 0.09
HAT-P-2	1.31 ± 0.08	1.51 ± 0.11	20.8 ± 0.3	6290	MS	0.049	49.44 ± 0.06
HAT-P-3	0.93 ± 0.05	0.83 ± 0.04	0.5 ± 0.2	5185	MS	0.079	47.63 ± 0.16
HAT-P-6	1.29 ± 0.06	1.46 ± 0.06	8.7 ± 1.0	6570	MS	0.050	49.05 ± 0.07
HAT-P-7	1.50 ± 0.03	1.98 ± 0.06	3.8 ± 0.5	6389	MS	0.040	48.79 ± 0.07
HAT-P-8	1.28 ± 0.04	1.58 ± 0.07	11.5 ± 0.5	6200	MS	0.050	49.21 ± 0.05
HAT-P-9	1.28 ± 0.13	1.32 ± 0.07	11.9 ± 1.0	6350	MS	0.050	49.14 ± 0.08
HAT-P-11	0.81 ± 0.02	0.75 ± 0.02	1.5 ± 0.5	4780	MS	0.096	48.09 ± 0.16
HAT-P-12	0.73 ± 0.02	0.70 ± 0.01	0.5 ± 0.4	4650	MS	0.112	47.60 ± 0.49
HAT-P-13	1.22 ± 0.08	1.56 ± 0.08	2.9 ± 1.0	5653	S	0.097	48.87 ± 0.19
HAT-P-14	1.39 ± 0.04	1.47 ± 0.05	8.4 ± 0.5	6600	MS	0.045	49.02 ± 0.06
HAT-P-15	1.01 ± 0.04	1.08 ± 0.04	2.0 ± 0.5	5568	MS	0.070	48.33 ± 0.12
HAT-P-16	1.22 ± 0.04	1.24 ± 0.05	3.5 ± 0.5	6158	MS	0.054	48.59 ± 0.08
HAT-P-17	0.86 ± 0.04	0.84 ± 0.02	0.3 ± 0.1	5246	MS	0.089	47.42 ± 0.16
HAT-P-18	0.77 ± 0.03	0.75 ± 0.04	0.5 ± 0.2	4803	MS	0.104	47.62 ± 0.16
HAT-P-19	0.84 ± 0.04	0.82 ± 0.05	0.7 ± 0.5	4990	MS	0.091	47.79 ± 0.40
HAT-P-20	0.76 ± 0.03	0.69 ± 0.02	2.1 ± 0.5	4595	MS	0.106	48.21 ± 0.12
HAT-P-21	0.95 ± 0.04	1.10 ± 0.08	3.5 ± 0.5	5588	MS	0.077	48.59 ± 0.09
HAT-P-22	0.92 ± 0.04	1.04 ± 0.04	0.5 ± 0.2	5302	MS	0.081	47.73 ± 0.16
HAT-P-23	1.13 ± 0.04	1.20 ± 0.07	8.1 ± 0.5	5905	MS	0.060	48.96 ± 0.06
HAT-P-24	1.19 ± 0.04	1.32 ± 0.07	10.0 ± 0.5	6373	MS	0.056	49.08 ± 0.06
HAT-P-25	1.01 ± 0.03	0.96 ± 0.05	0.5 ± 0.2	5500	MS	0.070	47.67 ± 0.16
HAT-P-26	0.82 ± 0.03	0.79 ± 0.07	1.8 ± 0.5	5079	MS	0.095	48.18 ± 0.14
HAT-P-27	0.92 ± 0.06	0.87 ± 0.04	0.6 ± 0.6	5190	MS	0.080	47.73 ± 0.71
HAT-P-28	1.02 ± 0.05	1.10 ± 0.08	0.2 ± 0.1	5680	MS	0.069	47.33 ± 0.16
HAT-P-29	1.21 ± 0.05	1.22 ± 0.10	3.9 ± 0.5	6087	MS	0.054	48.64 ± 0.08
HAT-P-30	1.24 ± 0.04	1.22 ± 0.05	2.2 ± 0.5	6304	MS	0.052	48.38 ± 0.11
HAT-P-31	1.22 ± 0.08	1.36 ± 0.22	0.5 ± 0.2	6065	MS	0.054	47.79 ± 0.18
HAT-P-33	1.38 ± 0.04	1.64 ± 0.03	13.7 ± 0.5	6446	MS	0.045	49.29 ± 0.05
HAT-P-34	1.39 ± 0.05	1.20 ± 0.11	24.0 ± 0.5	6442	MS	0.044	49.39 ± 0.06
HAT-P-35	1.24 ± 0.05	1.44 ± 0.08	0.5 ± 0.2	6096	MS	0.053	47.81 ± 0.16

Continued on next page

Host Star Name	Mass ( $M_{\odot}$ )	Radius ( $R_{\odot}$ )	$v \sin i_*$ (km/s)	$T_{\text{eff}}$ (K)	Class	$\gamma$	$\log J_*$ ( $\text{g cm}^2/\text{s}$ )
HAT-P-36	1.02 ± 0.05	1.10 ± 0.06	3.6 ± 0.5	5560	MS	0.069	48.58 ± 0.08
HAT-P-37	0.93 ± 0.04	0.88 ± 0.05	3.1 ± 0.5	5500	MS	0.079	48.44 ± 0.09
HAT-P-39	1.40 ± 0.05	1.62 ± 0.07	12.7 ± 0.5	6430	MS	0.044	49.25 ± 0.05
HAT-P-40	1.51 ± 0.28	2.21 ± 0.06	6.9 ± 0.5	6080	S	0.094	49.47 ± 0.13
HAT-P-41	1.42 ± 0.05	1.68 ± 0.05	19.6 ± 0.5	6390	MS	0.043	49.45 ± 0.05
HAT-P-49	1.54 ± 0.05	1.83 ± 0.11	16.0 ± 0.5	6820	MS	0.038	49.38 ± 0.05
HATS-1	0.99 ± 0.05	1.04 ± 0.10	2.5 ± 0.5	5870	MS	0.073	48.41 ± 0.11
HATS-2	0.88 ± 0.04	0.90 ± 0.02	1.5 ± 0.5	5227	MS	0.085	48.15 ± 0.16
HD 1461	1.03 ± 0.04	1.13	1.6	5765	MS	0.069	48.25 ± 0.16
HD 1502	1.47 ± 0.11	4.48 ± 0.14	2.7 ± 0.5	4984	S	0.094	49.36 ± 0.13
HD 1690	1.18 ± 0.23	21.15 ± 0.68	3.5	4364	G	0.139	50.23 ± 0.18
HD 2039	1.12 ± 0.08	1.15 ± 0.04	3.2 ± 0.5	5941	S	0.099	48.76 ± 0.12
HD 2952	2.54 ± 0.10	11.43 ± 0.37	1.9	4844	G	0.144	50.05 ± 0.16
HD 4203	1.13 ± 0.06	1.16 ± 0.04	1.2 ± 0.5	5702	MS	0.060	48.12 ± 0.20
HD 4313	1.53 ± 0.09	4.12 ± 0.13	3.4 ± 0.5	4966	S	0.094	49.44 ± 0.11
HD 4732	1.74 ± 0.17	5.55 ± 0.18	1.4	4959	S	0.092	49.25 ± 0.18
HD 5319	1.28 ± 0.10	4.99 ± 0.16	3.3 ± 0.5	4869	S	0.096	49.45 ± 0.12
HD 5388	1.21 ± 0.12	1.30 ± 0.04	4.2	6297	MS	0.054	48.69 ± 0.16
HD 5608	1.66 ± 0.08	5.50 ± 0.40	1.4	4911	S	0.092	49.20 ± 0.18
HD 5891	1.09 ± 0.19	11.83 ± 0.38	5.0 ± 0.5	4825	S	0.100	49.95 ± 0.13
HD 6718	0.96 ± 0.10	0.96 ± 0.03	1.8 ± 1.0	5746	MS	0.076	48.23 ± 0.29
HD 7924	0.83 ± 0.03	0.76 ± 0.03	1.4 ± 0.5	5177	MS	0.093	48.04 ± 0.18
HD 8535	1.13 ± 0.11	1.04 ± 0.04	1.4 ± 1.0	6136	MS	0.060	48.14 ± 0.40
HD 8574	1.12 ± 0.02	1.42 ± 0.05	4.5 ± 0.5	6050	MS	0.060	48.78 ± 0.07
HD 9446	1.00 ± 0.10	0.92 ± 0.05	4.0 ± 1.0	5793	MS	0.071	48.56 ± 0.13
HD 10180	1.06 ± 0.05	1.11 ± 0.04	1.5 ± 0.5	5911	MS	0.066	48.20 ± 0.16
HD 10647	1.09 ± 0.03	1.19 ± 0.04	5.6 ± 0.5	6105	MS	0.063	48.80 ± 0.06
HD 10697	1.11 ± 0.02	1.54 ± 0.05	2.5 ± 0.5	5680	S	0.099	48.77 ± 0.13
HD 11506	1.19 ± 0.09	1.26 ± 0.04	5.0 ± 0.5	6058	MS	0.056	48.76 ± 0.07
HD 11977	2.31 ± 0.12	8.15 ± 0.26	2.4 ± 1.0	5067	G	0.145	49.96 ± 0.20
HD 12661	1.14 ± 0.07	1.07 ± 0.04	1.3 ± 0.5	5743	MS	0.059	48.11 ± 0.19
HD 13189	1.17 ± 0.23	32.32 ± 1.03	2.1 ± 0.2	4337	G	0.139	50.19 ± 0.11
HD 13908	1.29 ± 0.04	1.67 ± 0.10	4.2 ± 0.5	6255	MS	0.050	48.79 ± 0.07
HD 13931	1.02 ± 0.02	1.22 ± 0.04	2.0 ± 0.5	5829	MS	0.069	48.38 ± 0.12
HD 16175	1.29 ± 0.11	1.20 ± 0.14	4.8 ± 0.5	6080	MS	0.050	48.71 ± 0.09
HD 16417	1.12 ± 0.02	1.46 ± 0.05	2.1	5817	MS	0.061	48.46 ± 0.16
HD 16760	0.78 ± 0.05	0.91 ± 0.04	2.8 ± 1.0	5620	MS	0.102	48.45 ± 0.17
HD 17156	1.28 ± 0.03	1.51 ± 0.01	2.8 ± 0.5	6079	MS	0.050	48.57 ± 0.09
HD 18742	1.73 ± 0.19	5.61 ± 0.18	3.0 ± 0.5	5016	S	0.092	49.57 ± 0.13
HD 20794	0.70 ± 0.07	1.23 ± 0.05	1.5 ± 0.5	5401	MS	0.119	48.33 ± 0.16
HD 20868	0.78 ± 0.03	1.16 ± 0.07	1.1	4795	S	0.114	48.19 ± 0.18
HD 22781	0.75 ± 0.03	0.72 ± 0.02	1.7	5027	MS	0.108	48.14 ± 0.16
HD 23079	1.01 ± 0.04	1.16 ± 0.04	3.0 ± 0.5	5927	MS	0.070	48.53 ± 0.09
HD 23127	1.13 ± 0.08	1.51 ± 0.05	3.3 ± 0.5	5752	MS	0.060	48.67 ± 0.09
HD 23596	1.16 ± 0.04	1.97 ± 0.06	4.2 ± 0.5	5904	S	0.098	49.12 ± 0.11
HD 24040	1.18 ± 0.10	1.15 ± 0.04	2.4 ± 0.5	5853	MS	0.056	48.40 ± 0.11

Continued on next page

Host Star Name	Mass ( $M_{\odot}$ )	Radius ( $R_{\odot}$ )	$v \sin i_*$ (km/s)	$T_{\text{eff}}$ (K)	Class	$\gamma$	$\log J_*$ ( $\text{g cm}^2/\text{s}$ )
HD 25171	1.09 ± 0.03	1.07 ± 0.04	1.0	6160	MS	0.063	48.01 ± 0.16
HD 28678	2.03 ± 0.20	6.34 ± 0.20	3.0 ± 0.5	5052	S	0.092	49.69 ± 0.13
HD 30177	0.95 ± 0.07	1.21 ± 0.04	3.0 ± 0.5	5607	MS	0.077	48.56 ± 0.09
HD 30562	1.28 ± 0.09	1.39 ± 0.05	4.3 ± 0.5	5936	MS	0.050	48.73 ± 0.08
HD 30856	1.36 ± 0.07	5.57 ± 0.18	2.8 ± 0.5	4973	G	0.144	49.63 ± 0.09
HD 31253	1.23 ± 0.05	1.65	3.8	5960	MS	0.053	48.75 ± 0.16
HD 32518	1.13 ± 0.18	24.36 ± 0.78	1.2	4580	G	0.138	49.80 ± 0.17
HD 33142	1.62 ± 0.09	4.30 ± 0.14	3.0 ± 0.5	5049	G	0.148	49.63 ± 0.09
HD 33283	1.24 ± 0.10	1.45 ± 0.05	3.2 ± 0.5	5995	MS	0.052	48.62 ± 0.09
HD 33636	1.02 ± 0.03	1.03 ± 0.04	3.1 ± 0.5	5904	MS	0.070	48.49 ± 0.09
HD 37124	0.85 ± 0.02	0.77 ± 0.03	1.2 ± 0.5	5500	MS	0.090	48.00 ± 0.20
HD 37605	1.00 ± 0.50	0.92 ± 0.03	0.5 ± 0.2	5448	MS	0.071	47.66 ± 0.31
HD 38283	1.08 ± 0.02	1.50	3.0	5998	MS	0.063	48.63 ± 0.16
HD 38801	1.22 ± 0.07	2.25 ± 0.07	0.5 ± 0.5	5314	S	0.097	48.30 ± 0.79
HD 39091	1.07 ± 0.02	1.15 ± 0.04	3.1 ± 0.5	5950	MS	0.065	48.54 ± 0.08
HD 43197	0.96 ± 0.10	1.20 ± 0.04	2.2 ± 1.0	5508	MS	0.076	48.42 ± 0.23
HD 44219	1.00 ± 0.10	1.36 ± 0.04	2.2 ± 1.0	5752	MS	0.071	48.48 ± 0.22
HD 45350	1.05 ± 0.06	1.18 ± 0.04	1.4 ± 0.5	5616	S	0.101	48.38 ± 0.20
HD 45364	0.82 ± 0.05	1.02 ± 0.03	1.0	5434	MS	0.095	48.04 ± 0.16
HD 45652	0.83 ± 0.05	1.13 ± 0.06	2.0 ± 0.7	5312	MS	0.093	48.39 ± 0.16
HD 47186	0.99 ± 0.00	1.13 ± 0.04	2.2	5675	MS	0.072	48.39 ± 0.16
HD 49674	1.01 ± 0.04	0.89 ± 0.03	0.4 ± 0.1	5662	MS	0.070	47.56 ± 0.16
HD 50499	1.28 ± 0.06	1.18 ± 0.04	4.2 ± 0.5	6070	MS	0.050	48.65 ± 0.07
HD 50554	1.02 ± 0.02	1.25 ± 0.04	3.9 ± 0.5	5929	MS	0.069	48.68 ± 0.07
HD 52265	1.17 ± 0.03	1.35 ± 0.04	4.7 ± 0.5	6076	MS	0.057	48.76 ± 0.07
HD 60532	1.44 ± 0.10	2.35	8.0	6095	S	0.094	49.55 ± 0.19
HD 63765	0.86 ± 0.03	0.98 ± 0.03	1.6	5432	MS	0.088	48.22 ± 0.16
HD 68988	1.12 ± 0.09	1.11 ± 0.04	2.8 ± 0.5	5960	MS	0.060	48.47 ± 0.10
HD 69830	0.85 ± 0.01	0.92 ± 0.03	0.3 ± 0.1	5360	MS	0.090	47.43 ± 0.16
HD 70642	1.00 ± 0.04	1.03 ± 0.04	0.3 ± 0.1	5706	MS	0.071	47.48 ± 0.16
HD 72659	1.07 ± 0.02	1.34 ± 0.04	2.2 ± 0.5	5920	MS	0.065	48.45 ± 0.11
HD 73267	0.89 ± 0.03	1.17 ± 0.04	1.6	5317	MS	0.084	48.30 ± 0.16
HD 73526	1.01 ± 0.04	1.46 ± 0.05	2.6 ± 0.5	5584	MS	0.070	48.57 ± 0.10
HD 73534	1.17 ± 0.07	2.90 ± 0.09	0.5 ± 0.2	4884	S	0.098	48.36 ± 0.18
HD 74156	1.24 ± 0.04	1.34 ± 0.04	4.3 ± 0.5	6068	MS	0.053	48.72 ± 0.07
HD 75898	1.28 ± 0.13	1.55 ± 0.06	4.5 ± 0.5	6021	MS	0.050	48.79 ± 0.08
HD 76700	1.13 ± 0.10	1.24 ± 0.04	1.3 ± 0.5	5668	MS	0.060	48.19 ± 0.18
HD 77338	0.93 ± 0.05	0.88 ± 0.04	2.3 ± 0.0	5370	MS	0.079	48.32 ± 0.05
HD 81040	0.96 ± 0.04	0.92 ± 0.04	2.0 ± 1.0	5700	MS	0.076	48.27 ± 0.25
HD 81688	2.10 ± 0.21	20.82 ± 0.67	1.2	4753	G	0.146	50.03 ± 0.16
HD 82886	1.06 ± 0.12	3.84 ± 0.12	0.4 ± 0.1	5112	S	0.100	48.39 ± 0.19
HD 82943	1.13 ± 0.05	1.10 ± 0.04	1.3 ± 0.5	5997	MS	0.060	48.14 ± 0.18
HD 83443	0.99 ± 0.04	0.94 ± 0.03	1.3 ± 0.5	5453	MS	0.072	48.08 ± 0.19
HD 85390	0.76 ± 0.08	0.96 ± 0.04	1.0	5186	MS	0.106	48.03 ± 0.16
HD 86081	1.21 ± 0.05	1.19 ± 0.04	4.2 ± 0.5	6028	MS	0.054	48.66 ± 0.07
HD 86264	1.40 ± 0.04	1.50 ± 0.05	12.5 ± 0.5	6326	MS	0.044	49.20 ± 0.05

Continued on next page

Host Star Name	Mass ( $M_{\odot}$ )	Radius ( $R_{\odot}$ )	$v \sin i_*$ (km/s)	$T_{\text{eff}}$ (K)	Class	$\gamma$	$\log J_*$ ( $\text{g cm}^2/\text{s}$ )
HD 87883	0.80 ± 0.03	0.78 ± 0.04	2.2 ± 0.5	4958	MS	0.098	48.26 ± 0.11
HD 88133	1.18 ± 0.06	1.94 ± 0.06	2.2 ± 0.5	5438	S	0.098	48.83 ± 0.14
HD 89307	0.99 ± 0.03	1.15 ± 0.04	3.2 ± 0.5	5898	MS	0.072	48.56 ± 0.08
HD 92788	1.08 ± 0.03	0.81 ± 0.03	0.3 ± 0.1	5836	MS	0.064	47.30 ± 0.16
HD 95089	1.38 ± 0.12	4.34 ± 0.14	3.6 ± 0.5	4950	S	0.095	49.45 ± 0.12
HD 96063	1.41 ± 0.09	3.66 ± 0.12	0.9 ± 0.5	5131	S	0.094	48.77 ± 0.31
HD 96127	0.91 ± 0.25	23.23 ± 0.74	0.2 ± 0.1	4152	G	0.130	48.98 ± 0.21
HD 96167	1.31 ± 0.13	1.98 ± 0.11	3.8 ± 0.5	5770	MS	0.048	48.82 ± 0.09
HD 97658	0.75 ± 0.03	0.70 ± 0.04	0.5 ± 0.2	5119	MS	0.108	47.59 ± 0.16
HD 98219	1.62 ± 0.11	2.95 ± 0.10	0.3 ± 0.1	5046	S	0.093	48.26 ± 0.18
HD 99109	0.94 ± 0.02	0.97 ± 0.03	1.9 ± 0.5	5272	MS	0.078	48.26 ± 0.13
HD 99706	1.72 ± 0.12	5.26 ± 0.17	0.9 ± 0.5	4932	S	0.092	49.01 ± 0.30
HD 100655	1.71 ± 0.33	9.30 ± 1.20	1.6 ± 1.0	4801	G	0.148	49.72 ± 0.36
HD 100777	1.00 ± 0.10	1.08 ± 0.04	1.8 ± 1.0	5582	MS	0.071	48.28 ± 0.28
HD 102117	1.08 ± 0.06	1.13 ± 0.04	0.9 ± 0.5	5695	MS	0.064	47.98 ± 0.29
HD 102195	0.87 ± 0.09	0.94 ± 0.03	2.6 ± 1.0	5291	MS	0.087	48.41 ± 0.19
HD 102329	1.30 ± 0.15	7.27 ± 0.23	2.6 ± 0.5	4745	G	0.142	49.69 ± 0.11
HD 102365	0.89 ± 0.03	0.83	0.7	5630	MS	0.084	47.78 ± 0.16
HD 102956	1.68 ± 0.11	3.43 ± 0.11	0.3 ± 0.1	5054	S	0.092	48.34 ± 0.18
HD 103197	0.90 ± 0.09	1.02 ± 0.04	2.0	5303	MS	0.083	48.32 ± 0.16
HD 103774	1.34 ± 0.03	1.43 ± 0.05	8.1	6489	MS	0.047	49.01 ± 0.16
HD 104067	0.79 ± 0.02	0.86 ± 0.04	1.6	4969	MS	0.100	48.18 ± 0.16
HD 104985	1.04 ± 0.27	7.10 ± 0.23	1.7 ± 0.1	4819	G	0.135	49.36 ± 0.13
HD 106252	1.01 ± 0.02	1.12 ± 0.04	1.9 ± 0.5	5870	MS	0.071	48.33 ± 0.13
HD 106270	1.33 ± 0.05	2.66 ± 0.09	3.1 ± 0.5	5601	S	0.095	49.17 ± 0.12
HD 107148	1.14 ± 0.07	1.04 ± 0.04	0.7 ± 0.5	5797	MS	0.059	47.85 ± 0.37
HD 108147	1.17 ± 0.02	1.30 ± 0.04	6.1 ± 0.5	6156	MS	0.057	48.86 ± 0.06
HD 108863	2.08 ± 0.14	7.28 ± 0.23	1.1 ± 0.5	4919	G	0.146	49.51 ± 0.23
HD 108874	0.95 ± 0.03	1.12 ± 0.04	2.2 ± 0.5	5551	MS	0.077	48.40 ± 0.11
HD 109246	1.01 ± 0.11	1.01 ± 0.05	3.0 ± 1.0	5844	MS	0.070	48.47 ± 0.17
HD 113337	1.40 ± 0.14	1.50 ± 0.15	6.3 ± 1.0	6577	MS	0.044	48.91 ± 0.10
HD 114386	0.78 ± 0.02	0.64 ± 0.03	0.6 ± 0.5	4820	MS	0.102	47.62 ± 0.55
HD 114613	1.36 ± 0.14	1.92 ± 0.06	2.7 ± 0.9	5729	S	0.095	48.97 ± 0.19
HD 114783	0.85 ± 0.04	0.84 ± 0.03	0.9 ± 0.5	5135	MS	0.090	47.88 ± 0.29
HD 116029	1.33 ± 0.11	5.04 ± 0.16	0.5 ± 0.2	4811	G	0.143	48.79 ± 0.16
HD 117207	1.03 ± 0.04	0.95 ± 0.03	1.0 ± 0.5	5724	S	0.101	48.16 ± 0.25
HD 117618	1.07 ± 0.03	1.17 ± 0.04	3.2 ± 0.5	5964	MS	0.065	48.55 ± 0.08
HD 118203	1.23 ± 0.03	2.15	4.7	5600	S	0.097	49.22 ± 0.18
HD 120084	2.39 ± 0.18	10.95 ± 0.35	2.4	4892	G	0.145	50.11 ± 0.16
HD 125595	0.76 ± 0.02	1.03 ± 0.06	1.5	4908	MS	0.106	48.24 ± 0.16
HD 128311	0.83 ± 0.01	0.58 ± 0.03	3.6 ± 0.5	4965	MS	0.093	48.36 ± 0.08
HD 130322	0.84 ± 0.02	0.99 ± 0.03	1.6 ± 0.5	5308	MS	0.092	48.23 ± 0.15
HD 131496	1.61 ± 0.12	4.56 ± 0.15	0.5 ± 0.2	4927	S	0.093	48.66 ± 0.18
HD 131664	1.10 ± 0.03	1.06 ± 0.04	2.9	5886	MS	0.062	48.47 ± 0.16
HD 134987	1.05 ± 0.06	1.17 ± 0.04	2.2 ± 0.5	5750	MS	0.066	48.39 ± 0.12
HD 136118	1.19 ± 0.02	1.75 ± 0.06	7.3 ± 0.5	6097	MS	0.056	49.07 ± 0.06

Continued on next page

Host Star Name	Mass ( $M_{\odot}$ )	Radius ( $R_{\odot}$ )	$v \sin i_*$ (km/s)	$T_{\text{eff}}$ (K)	Class	$\gamma$	$\log J_*$ ( $\text{g cm}^2/\text{s}$ )
HD 136418	1.33 ± 0.09	3.83 ± 0.12	1.7 ± 0.5	4972	S	0.095	49.05 ± 0.17
HD 141937	1.05 ± 0.04	1.06 ± 0.04	1.9 ± 0.5	5847	MS	0.067	48.29 ± 0.13
HD 142245	1.69 ± 0.12	4.52 ± 0.14	2.7 ± 0.6	4878	S	0.092	49.41 ± 0.14
HD 142415	1.06 ± 0.05	1.12 ± 0.04	3.4 ± 0.5	5902	MS	0.065	48.57 ± 0.08
HD 145377	1.12 ± 0.00	1.00 ± 0.04	3.8	6046	MS	0.061	48.56 ± 0.16
HD 147018	0.93 ± 0.03	1.05 ± 0.05	1.6	5441	MS	0.079	48.22 ± 0.16
HD 148156	1.22 ± 0.12	0.97 ± 0.03	5.7 ± 1.0	6308	MS	0.054	48.70 ± 0.10
HD 148427	1.36 ± 0.06	3.92 ± 0.13	2.1 ± 0.5	4962	S	0.095	49.17 ± 0.14
HD 149026	1.29 ± 0.06	1.37 ± 0.10	6.0 ± 0.5	6160	S	0.096	49.15 ± 0.10
HD 149143	1.20 ± 0.10	1.71 ± 0.06	4.0 ± 0.5	5884	S	0.097	49.04 ± 0.11
HD 152581	0.93 ± 0.12	3.81 ± 0.12	0.5 ± 0.2	5155	S	0.105	48.41 ± 0.19
HD 153950	1.12 ± 0.03	1.15 ± 0.04	3.0	6076	MS	0.061	48.51 ± 0.16
HD 154345	0.89 ± 0.04	1.00 ± 0.05	1.2 ± 0.5	5468	MS	0.084	48.10 ± 0.20
HD 154672	1.06 ± 0.10	1.32 ± 0.04	0.5 ± 0.5	5714	S	0.100	48.02 ± 0.81
HD 154857	1.72 ± 0.03	1.86 ± 0.06	1.4 ± 0.5	5605	MS	0.036	48.35 ± 0.17
HD 156279	0.93 ± 0.04	0.96 ± 0.03	2.5	5453	MS	0.079	48.39 ± 0.16
HD 156411	1.24 ± 0.02	1.86 ± 0.06	3.3 ± 1.0	5910	S	0.097	49.01 ± 0.17
HD 156668	0.77 ± 0.02	0.73 ± 0.04	0.5 ± 0.1	4850	MS	0.103	47.60 ± 0.10
HD 158038	1.65 ± 0.12	5.30 ± 0.17	1.7 ± 0.5	4897	G	0.148	49.47 ± 0.15
HD 159243	1.12 ± 0.03	1.12 ± 0.05	3.8 ± 0.5	6123	MS	0.060	48.60 ± 0.08
HD 159868	1.16 ± 0.04	1.85 ± 0.06	2.1 ± 0.5	5558	MS	0.058	48.56 ± 0.12
HD 162020	0.80 ± 0.01	0.53 ± 0.03	2.3 ± 0.5	4845	MS	0.098	48.12 ± 0.11
HD 163607	1.09 ± 0.02	1.70 ± 0.06	1.5 ± 0.5	5543	S	0.100	48.58 ± 0.18
HD 164509	1.13 ± 0.02	1.06 ± 0.04	2.4 ± 0.0	5922	MS	0.060	48.38 ± 0.05
HD 164922	0.93 ± 0.03	0.90 ± 0.03	1.8 ± 0.5	5385	MS	0.079	48.23 ± 0.13
HD 167042	1.63 ± 0.06	4.22 ± 0.14	1.5 ± 0.5	5028	G	0.148	49.33 ± 0.16
HD 168443	1.00 ± 0.02	1.59 ± 0.05	2.2 ± 0.5	5491	MS	0.072	48.54 ± 0.11
HD 169830	1.41 ± 0.07	1.80 ± 0.06	3.8 ± 0.5	6221	MS	0.044	48.77 ± 0.08
HD 170469	1.14 ± 0.06	1.22 ± 0.04	1.7 ± 0.5	5810	S	0.099	48.51 ± 0.16
HD 171028	1.01 ± 0.06	2.14 ± 0.07	2.3	5671	S	0.102	48.85 ± 0.18
HD 171238	0.94 ± 0.03	1.05 ± 0.05	1.5	5467	MS	0.078	48.20 ± 0.16
HD 175541	1.34 ± 0.08	3.07 ± 0.10	2.9 ± 0.5	5111	S	0.095	49.20 ± 0.12
HD 179079	1.09 ± 0.10	1.34 ± 0.05	0.5 ± 0.2	5724	S	0.100	48.00 ± 0.18
HD 179949	1.18 ± 0.03	1.23 ± 0.04	7.0 ± 0.5	6168	MS	0.056	48.90 ± 0.06
HD 180902	1.53 ± 0.09	3.85 ± 0.12	2.9 ± 0.5	5040	G	0.148	49.54 ± 0.09
HD 181342	1.70 ± 0.09	4.76 ± 0.15	3.6 ± 0.5	4965	G	0.148	49.77 ± 0.08
HD 181433	0.78 ± 0.00	1.01 ± 0.07	1.5	4962	MS	0.102	48.22 ± 0.16
HD 181720	0.92 ± 0.09	1.25 ± 0.05	1.5	5781	MS	0.080	48.28 ± 0.16
HD 183263	1.12 ± 0.05	1.12 ± 0.04	1.6 ± 0.5	5936	S	0.099	48.43 ± 0.18
HD 187085	1.14 ± 0.03	1.31 ± 0.04	5.1 ± 0.5	6075	MS	0.059	48.79 ± 0.06
HD 187123	1.04 ± 0.02	1.14 ± 0.04	2.1 ± 0.5	5815	MS	0.068	48.38 ± 0.11
HD 190228	1.82 ± 0.05	1.74 ± 0.06	1.9 ± 0.5	5348	S	0.092	48.87 ± 0.15
HD 190647	1.10 ± 0.10	1.42 ± 0.05	2.4 ± 1.0	5628	MS	0.062	48.51 ± 0.20
HD 192263	0.80 ± 0.03	0.74 ± 0.03	2.6 ± 0.5	4975	MS	0.097	48.32 ± 0.10
HD 192699	1.58 ± 0.04	3.61 ± 0.12	1.9 ± 0.5	5141	S	0.093	49.14 ± 0.15
HD 200964	1.57 ± 0.06	3.80 ± 0.12	2.3 ± 0.5	5082	S	0.093	49.24 ± 0.13

Continued on next page

Host Star Name	Mass ( $M_{\odot}$ )	Radius ( $R_{\odot}$ )	$v \sin i_*$ (km/s)	$T_{\text{eff}}$ (K)	Class	$\gamma$	$\log J_*$ ( $\text{g cm}^2/\text{s}$ )
HD 202206	1.07 ± 0.06	0.99 ± 0.03	2.3 ± 0.5	5788	MS	0.064	48.34 ± 0.11
HD 204313	1.04 ± 0.03	1.13 ± 0.04	1.6	5767	MS	0.067	48.24 ± 0.16
HD 205739	1.22 ± 0.08	1.46 ± 0.05	4.5 ± 0.5	6176	MS	0.054	48.77 ± 0.07
HD 206610	1.30 ± 0.12	4.98 ± 0.16	3.3 ± 0.5	4821	S	0.096	49.45 ± 0.12
HD 207832	0.94 ± 0.10	0.90 ± 0.06	3.0	5710	MS	0.078	48.44 ± 0.17
HD 208487	1.11 ± 0.02	1.21 ± 0.04	4.6 ± 0.5	6067	MS	0.061	48.72 ± 0.07
HD 208527	1.60 ± 0.40	41.05 ± 1.31	3.6	4035	G	0.148	50.69 ± 0.20
HD 209458	1.13 ± 0.02	1.16 ± 0.02	4.5 ± 0.5	6065	MS	0.060	48.69 ± 0.07
HD 210277	0.99 ± 0.04	0.94 ± 0.03	1.8 ± 0.5	5555	MS	0.073	48.23 ± 0.13
HD 210702	1.71 ± 0.06	5.17 ± 0.15	1.7 ± 0.5	5000	S	0.092	49.28 ± 0.16
HD 212771	1.51 ± 0.08	4.01 ± 0.13	3.6 ± 0.5	5091	S	0.094	49.45 ± 0.11
HD 215497	0.87 ± 0.02	1.11 ± 0.05	1.7	5113	MS	0.087	48.29 ± 0.16
HD 216437	1.12 ± 0.04	1.37 ± 0.05	3.1 ± 0.5	5849	S	0.099	48.82 ± 0.12
HD 217786	1.02 ± 0.03	1.15 ± 0.04	1.4	5966	MS	0.069	48.20 ± 0.16
HD 219828	1.24 ± 0.12	1.47 ± 0.05	2.9	5891	S	0.097	48.85 ± 0.18
HD 220074	1.20 ± 0.30	54.71 ± 1.75	3.0	3935	G	0.140	50.58 ± 0.20
HD 221287	1.25 ± 0.10	1.10 ± 0.05	4.1 ± 1.0	6304	MS	0.052	48.61 ± 0.12
HD 222155	1.13 ± 0.11	1.67 ± 0.07	3.2 ± 1.0	5765	MS	0.060	48.70 ± 0.16
HD 224693	1.33 ± 0.10	1.17 ± 0.04	3.5 ± 0.5	6037	MS	0.047	48.55 ± 0.08
HD 231701	1.14 ± 0.06	1.24 ± 0.04	4.0 ± 0.5	6208	MS	0.059	48.67 ± 0.08
HD 240210	1.25 ± 0.25	17.27 ± 0.55	1.0 ± 0.3	4290	G	0.141	49.62 ± 0.18
HD 290327	0.90 ± 0.09	1.00 ± 0.03	1.4 ± 1.0	5552	MS	0.083	48.17 ± 0.38
HIP 2247	0.74 ± 0.03	1.07 ± 0.07	1.5	4714	MS	0.110	48.26 ± 0.16
HIP 5158	0.78 ± 0.02	0.99 ± 0.06	1.6	4962	MS	0.102	48.23 ± 0.16
HIP 14810	0.99 ± 0.04	1.32 ± 0.04	0.5 ± 0.5	5485	MS	0.072	47.85 ± 0.73
HIP 57274	0.73 ± 0.05	0.68 ± 0.03	0.5 ± 0.2	4640	MS	0.112	47.59 ± 0.16
HIP 91258	0.95 ± 0.03	1.00 ± 0.04	3.5 ± 0.5	5519	MS	0.077	48.55 ± 0.08
iota Hor	1.15 ± 0.03	1.21 ± 0.04	6.5 ± 0.5	6097	MS	0.059	48.86 ± 0.06
kappa CrB	1.58 ± 0.08	5.06 ± 0.04	1.5 ± 0.5	4876	S	0.093	49.19 ± 0.18
Kepler-4	1.22 ± 0.07	1.49 ± 0.08	2.1 ± 1.0	5857	MS	0.053	48.45 ± 0.23
Kepler-5	1.37 ± 0.05	1.79 ± 0.05	4.8 ± 1.0	6297	MS	0.045	48.87 ± 0.10
Kepler-6	1.21 ± 0.04	1.39 ± 0.02	3.0 ± 1.0	5647	MS	0.054	48.58 ± 0.16
Kepler-7	1.35 ± 0.06	1.84 ± 0.06	4.2 ± 0.5	5933	S	0.095	49.14 ± 0.11
Kepler-8	1.21 ± 0.06	1.49 ± 0.06	10.5 ± 0.7	6213	MS	0.054	49.15 ± 0.06
Kepler-10	0.90 ± 0.06	1.06 ± 0.02	0.5 ± 0.2	5627	MS	0.084	47.74 ± 0.16
Kepler-11	0.96 ± 0.02	1.06 ± 0.02	0.4 ± 0.1	5663	MS	0.075	47.63 ± 0.16
Kepler-12	1.17 ± 0.05	1.48 ± 0.03	0.8 ± 0.5	5947	MS	0.057	48.04 ± 0.33
Kepler-14	1.51 ± 0.04	2.05 ± 0.10	7.9 ± 1.0	6395	S	0.094	49.50 ± 0.11
Kepler-15	1.02 ± 0.04	0.99 ± 0.06	2.0 ± 0.7	5515	MS	0.070	48.29 ± 0.16
Kepler-17	1.16 ± 0.06	1.05 ± 0.03	6.0 ± 2.0	5781	MS	0.058	48.77 ± 0.16
Kepler-18	0.97 ± 0.04	1.11 ± 0.05	0.4 ± 0.1	5383	MS	0.074	47.65 ± 0.16
Kepler-20	0.91 ± 0.03	0.94 ± 0.08	0.4 ± 0.1	5466	MS	0.081	47.59 ± 0.16
Kepler-21	1.34 ± 0.01	1.86 ± 0.02	7.8 ± 1.0	6131	S	0.095	49.41 ± 0.11
Kepler-22	0.97 ± 0.06	0.98 ± 0.02	0.6 ± 0.1	5518	MS	0.074	47.77 ± 0.09
Kepler-25	1.19 ± 0.06	1.31 ± 0.02	9.5	6270	MS	0.056	49.06 ± 0.16
Kepler-26	0.65 ± 0.03	0.59 ± 0.03	1.9 ± 0.1	3933	MS	0.132	48.12 ± 0.06

Continued on next page

Host Star Name	Mass ( $M_{\odot}$ )	Radius ( $R_{\odot}$ )	$v \sin i_*$ (km/s)	$T_{\text{eff}}$ (K)	Class	$\gamma$	$\log J_*$ ( $g \text{ cm}^2/\text{s}$ )
Kepler-27	0.65 ± 0.16	0.59 ± 0.15	2.8 ± 1.5	5400	MS	0.132	48.29 ± 0.35
Kepler-29	1.00 ± 0.12	0.96 ± 0.14	4.0 ± 2.0	5750	MS	0.071	48.58 ± 0.26
Kepler-30	0.99 ± 0.08	0.95 ± 0.12	1.9 ± 0.2	5498	MS	0.072	48.26 ± 0.09
Kepler-37	0.80 ± 0.07	0.77 ± 0.03	1.1 ± 0.4	5417	MS	0.098	47.96 ± 0.16
Kepler-38	0.95 ± 0.06	1.76 ± 0.03	2.4 ± 0.5	5623	S	0.104	48.76 ± 0.13
Kepler-39	1.10 ± 0.06	1.39 ± 0.10	16.0 ± 2.5	6260	S	0.099	49.53 ± 0.12
Kepler-40	1.48 ± 0.06	2.13 ± 0.06	9.0 ± 2.0	6510	S	0.094	49.57 ± 0.14
Kepler-41	0.94 ± 0.09	0.97 ± 0.03	4.5 ± 1.5	5660	MS	0.078	48.64 ± 0.16
Kepler-43	1.32 ± 0.09	1.42 ± 0.07	5.5 ± 1.5	6041	S	0.095	49.13 ± 0.16
Kepler-44	1.19 ± 0.10	1.52 ± 0.09	4.0 ± 2.0	5757	S	0.097	48.99 ± 0.27
Kepler-47	1.04 ± 0.06	0.96 ± 0.02	4.1 ± 0.5	5636	MS	0.067	48.58 ± 0.07
Kepler-48	0.88 ± 0.06	0.89 ± 0.05	0.5	5194	MS	0.086	47.67 ± 0.16
Kepler-62	0.69 ± 0.02	0.64 ± 0.02	0.4 ± 0.1	4925	MS	0.121	47.47 ± 0.16
Kepler-63	0.98 ± 0.04	0.90 ± 0.02	5.6 ± 0.8	5576	MS	0.073	48.70 ± 0.08
Kepler-68	1.08 ± 0.05	1.24 ± 0.02	0.5 ± 0.2	5793	MS	0.064	47.77 ± 0.16
Kepler-74	1.40 ± 0.12	1.51 ± 0.14	5.0 ± 1.0	6050	MS	0.044	48.81 ± 0.11
Kepler-75	0.88 ± 0.06	0.88 ± 0.04	3.5 ± 1.5	5330	MS	0.086	48.51 ± 0.21
Kepler-77	0.95 ± 0.04	0.99 ± 0.02	1.5 ± 1.0	5520	MS	0.077	48.18 ± 0.36
Kepler-78	0.81 ± 0.05	0.74 ± 0.09	2.4 ± 0.5	5089	MS	0.096	48.28 ± 0.12
Kepler-89	1.28 ± 0.05	1.52 ± 0.14	7.3 ± 0.5	6182	MS	0.050	48.99 ± 0.07
Kepler-93	0.91 ± 0.06	0.92 ± 0.02	0.5	5669	MS	0.082	47.67 ± 0.16
Kepler-94	0.81 ± 0.06	0.76 ± 0.03	0.5	4781	MS	0.096	47.61 ± 0.16
Kepler-95	1.08 ± 0.08	1.41 ± 0.04	0.7	5699	MS	0.064	47.97 ± 0.16
Kepler-96	1.00 ± 0.06	1.02 ± 0.09	0.5	5690	MS	0.071	47.70 ± 0.16
Kepler-97	0.94 ± 0.06	0.98 ± 0.09	0.5	5779	MS	0.078	47.70 ± 0.16
Kepler-98	0.99 ± 0.06	1.11 ± 0.12	0.5	5539	MS	0.072	47.74 ± 0.17
Kepler-99	0.79 ± 0.06	0.73 ± 0.04	0.5	4782	MS	0.100	47.60 ± 0.16
Kepler-100	1.08 ± 0.06	1.49 ± 0.04	3.7	5825	MS	0.064	48.72 ± 0.16
Kepler-102	0.80 ± 0.06	0.74 ± 0.02	0.5	4903	MS	0.098	47.60 ± 0.16
Kepler-103	1.09 ± 0.07	1.44 ± 0.04	2.5	5845	MS	0.063	48.53 ± 0.16
Kepler-106	1.00 ± 0.06	1.04 ± 0.17	0.3	5858	MS	0.071	47.49 ± 0.18
Kepler-109	1.04 ± 0.06	1.32 ± 0.04	1.0	5952	MS	0.067	48.11 ± 0.16
Kepler-113	0.75 ± 0.06	0.69 ± 0.02	0.4	4725	MS	0.108	47.49 ± 0.16
Kepler-131	1.02 ± 0.06	1.03 ± 0.10	0.4	5685	MS	0.069	47.61 ± 0.17
Kepler-406	1.07 ± 0.06	1.07 ± 0.02	0.4	5538	MS	0.065	47.61 ± 0.16
Kepler-407	1.00 ± 0.06	1.01 ± 0.07	2.0	5476	MS	0.071	48.30 ± 0.16
Kepler-412	1.17 ± 0.09	1.29 ± 0.04	5.0 ± 1.0	5750	MS	0.057	48.77 ± 0.11
KIC 11442793	1.20 ± 0.10	1.20 ± 0.10	4.6 ± 2.1	6080	MS	0.055	48.70 ± 0.23
mu Ara	1.15 ± 0.07	1.25 ± 0.04	3.1 ± 0.5	5784	S	0.098	48.78 ± 0.12
OGLE-TR-10	1.14 ± 0.11	1.17 ± 0.12	3.0 ± 2.0	5950	MS	0.059	48.52 ± 0.37
OGLE2-TR-L9	1.52 ± 0.08	1.53 ± 0.04	39.3 ± 0.4	6933	MS	0.039	49.70 ± 0.05
omega Ser	2.17 ± 0.25	12.30 ± 0.85	1.9	4770	G	0.146	50.01 ± 0.17
omicron CrB	2.13 ± 0.12	10.50 ± 0.70	2.3	4749	G	0.146	50.02 ± 0.16
omicron UMa	3.09 ± 0.07	14.10 ± 0.95	3.8	5242	G	0.142	50.52 ± 0.16
PH-2	0.94 ± 0.02	1.00 ± 0.05	1.4 ± 0.8	5629	MS	0.078	48.16 ± 0.27
Pr 201	1.23 ± 0.03	1.13 ± 0.04	9.6 ± 0.5	6174	MS	0.053	48.99 ± 0.05

Continued on next page

Host Star Name	Mass ( $M_{\odot}$ )	Radius ( $R_{\odot}$ )	$v \sin i_*$ (km/s)	$T_{\text{eff}}$ (K)	Class	$\gamma$	$\log J_*$ ( $\text{g cm}^2/\text{s}$ )
Pr 211	0.95 ± 0.04	0.87 ± 0.08	4.8 ± 0.5	5326	MS	0.077	48.62 ± 0.08
Qatar-1	0.85 ± 0.03	0.82 ± 0.02	2.1 ± 0.8	4861	MS	0.090	48.26 ± 0.18
Qatar-2	0.74 ± 0.04	0.71 ± 0.02	2.8	4645	MS	0.110	48.35 ± 0.16
rho CrB	0.96 ± 0.02	1.10 ± 0.04	1.6 ± 0.5	5823	MS	0.075	48.24 ± 0.15
tau Gru	1.24 ± 0.10	1.55 ± 0.05	5.8 ± 0.5	5999	MS	0.053	48.91 ± 0.07
TrES-1	0.88 ± 0.04	0.81 ± 0.02	10.4 ± 0.1	5230	MS	0.086	48.94 ± 0.05
TrES-2	0.98 ± 0.06	1.00 ± 0.03	2.0 ± 1.5	5850	MS	0.073	48.30 ± 0.43
TrES-3	0.92 ± 0.03	0.81 ± 0.02	1.0 ± 0.3	5650	MS	0.081	47.92 ± 0.16
TrES-4	1.39 ± 0.06	1.82 ± 0.06	9.5 ± 1.0	6200	MS	0.044	49.17 ± 0.07
TrES-5	0.89 ± 0.02	0.87 ± 0.01	3.8 ± 0.4	5171	MS	0.084	48.53 ± 0.06
WASP-1	1.20 ± 0.03	1.52 ± 0.05	5.8 ± 0.4	6110	MS	0.055	48.90 ± 0.05
WASP-4	0.91 ± 0.05	0.91 ± 0.02	2.2 ± 0.8	5500	MS	0.082	48.32 ± 0.17
WASP-5	1.01 ± 0.04	1.03 ± 0.06	3.4 ± 0.7	5880	MS	0.070	48.54 ± 0.11
WASP-6	0.93 ± 0.02	0.87 ± 0.03	1.4 ± 1.0	5450	MS	0.079	48.09 ± 0.40
WASP-7	1.20 ± 0.03	1.24 ± 0.05	17 ± 2	6400	MS	0.055	49.28 ± 0.07
WASP-10	0.79 ± 0.02	0.70 ± 0.01	3.0 ± 1.0	4675	MS	0.100	48.36 ± 0.16
WASP-11	0.80 ± 0.02	0.74 ± 0.04	0.5 ± 0.2	4800	MS	0.098	47.60 ± 0.19
WASP-12	1.28 ± 0.05	1.63 ± 0.08	2.2 ± 1.5	6300	MS	0.050	48.50 ± 0.37
WASP-13	1.09 ± 0.05	1.57 ± 0.05	5.3 ± 0.2	5950	MS	0.063	48.90 ± 0.05
WASP-14	1.31 ± 0.08	1.31 ± 0.07	4.9 ± 1.0	6475	MS	0.048	48.75 ± 0.11
WASP-15	1.18 ± 0.03	1.48 ± 0.07	4.0 ± 2.0	6300	MS	0.056	48.73 ± 0.25
WASP-16	1.00 ± 0.03	0.95 ± 0.05	3.0 ± 1.0	5700	MS	0.071	48.45 ± 0.16
WASP-17	1.19 ± 0.03	1.20 ± 0.08	9.0 ± 1.5	6550	MS	0.056	49.00 ± 0.09
WASP-18	1.22 ± 0.03	1.22 ± 0.06	11.0 ± 1.5	6400	MS	0.054	49.08 ± 0.08
WASP-19	0.93 ± 0.02	0.99 ± 0.02	4.0 ± 2.0	5500	MS	0.079	48.61 ± 0.24
WASP-21	1.01 ± 0.03	1.06 ± 0.04	1.5 ± 0.6	5800	MS	0.070	48.19 ± 0.19
WASP-22	1.10 ± 0.30	1.13 ± 0.03	3.5 ± 0.6	6000	MS	0.062	48.57 ± 0.15
WASP-23	0.78 ± 0.12	0.76 ± 0.04	2.2 ± 0.3	5150	MS	0.102	48.27 ± 0.11
WASP-24	1.18 ± 0.03	1.33 ± 0.03	7.0 ± 0.9	6075	MS	0.056	48.93 ± 0.07
WASP-25	1.00 ± 0.03	0.92 ± 0.04	3.0 ± 1.0	5750	MS	0.071	48.44 ± 0.16
WASP-26	1.12 ± 0.03	1.34 ± 0.06	2.4 ± 1.3	5059	S	0.099	48.69 ± 0.29
WASP-29	0.82 ± 0.03	0.81 ± 0.04	1.5 ± 0.6	4800	MS	0.094	48.11 ± 0.19
WASP-32	1.07 ± 0.05	1.09 ± 0.03	3.9 ± 0.4	6140	MS	0.065	48.61 ± 0.07
WASP-33	1.50 ± 0.03	1.44 ± 0.03	90 ± 10	7430	MS	0.040	50.03 ± 0.07
WASP-34	1.01 ± 0.07	0.93 ± 0.12	1.4 ± 0.6	5700	MS	0.070	48.11 ± 0.22
WASP-35	1.07 ± 0.02	1.09 ± 0.02	2.4 ± 0.6	5990	MS	0.065	48.40 ± 0.12
WASP-36	1.02 ± 0.03	0.94 ± 0.02	3.2 ± 1.3	5881	MS	0.069	48.47 ± 0.19
WASP-37	0.92 ± 0.12	1.00 ± 0.05	2.4 ± 1.6	5800	MS	0.080	48.39 ± 0.37
WASP-38	1.23 ± 0.04	1.35 ± 0.02	7.5 ± 0.2	6180	MS	0.053	48.96 ± 0.05
WASP-39	0.93 ± 0.03	0.90 ± 0.02	1.4 ± 0.6	5400	MS	0.079	48.11 ± 0.21
WASP-41	0.95 ± 0.09	0.90 ± 0.05	1.6 ± 1.1	5450	MS	0.077	48.16 ± 0.38
WASP-42	0.88 ± 0.08	0.85 ± 0.04	2.7 ± 0.4	5200	MS	0.086	48.38 ± 0.09
WASP-43	0.58 ± 0.05	0.60 ± 0.04	4.0 ± 0.4	4400	MS	0.156	48.48 ± 0.08
WASP-44	0.95 ± 0.03	0.93 ± 0.06	3.2 ± 0.9	5410	MS	0.077	48.48 ± 0.14
WASP-45	0.91 ± 0.06	0.94 ± 0.08	2.3 ± 0.7	5140	MS	0.082	48.35 ± 0.15
WASP-46	0.96 ± 0.03	0.92 ± 0.03	1.9 ± 1.2	5620	MS	0.076	48.24 ± 0.33

Continued on next page

Host Star Name	Mass ( $M_{\odot}$ )	Radius ( $R_{\odot}$ )	$v \sin i_*$ (km/s)	$T_{\text{eff}}$ (K)	Class	$\gamma$	$\log J_*$ ( $\text{g cm}^2/\text{s}$ )
WASP-47	$1.08 \pm 0.04$	$1.15 \pm 0.02$	$3.0 \pm 0.6$	5400	MS	0.064	$48.52 \pm 0.10$
WASP-48	$1.19 \pm 0.04$	$1.75 \pm 0.07$	$2.4 \pm 0.6$	5920	S	0.097	$48.83 \pm 0.15$
WASP-49	$0.94 \pm 0.08$	$0.98 \pm 0.03$	$0.9 \pm 0.3$	5600	MS	0.078	$47.95 \pm 0.16$
WASP-50	$0.89 \pm 0.08$	$0.84 \pm 0.03$	$2.6 \pm 0.5$	5400	MS	0.084	$48.36 \pm 0.10$
WASP-52	$0.87 \pm 0.03$	$0.79 \pm 0.02$	$2.5 \pm 1.0$	5000	MS	0.087	$48.32 \pm 0.19$
WASP-54	$1.21 \pm 0.03$	$1.83 \pm 0.09$	$4.0 \pm 0.8$	6100	S	0.097	$49.08 \pm 0.13$
WASP-55	$1.01 \pm 0.04$	$1.06 \pm 0.02$	$3.1 \pm 1.0$	5900	MS	0.070	$48.51 \pm 0.15$
WASP-56	$1.11 \pm 0.02$	$1.11 \pm 0.02$	$1.5 \pm 0.9$	5600	MS	0.062	$48.20 \pm 0.31$
WASP-57	$0.95 \pm 0.03$	$0.84 \pm 0.12$	$3.7 \pm 1.3$	5600	MS	0.076	$48.49 \pm 0.18$
WASP-58	$0.94 \pm 0.10$	$1.17 \pm 0.13$	$2.8 \pm 0.9$	5800	MS	0.078	$48.52 \pm 0.17$
WASP-59	$0.72 \pm 0.04$	$0.61 \pm 0.04$	$2.3 \pm 1.5$	4650	MS	0.114	$48.21 \pm 0.35$
WASP-60	$1.08 \pm 0.04$	$1.14 \pm 0.13$	$3.4 \pm 0.8$	5900	MS	0.064	$48.57 \pm 0.13$
WASP-61	$1.22 \pm 0.07$	$1.36 \pm 0.03$	$10.3 \pm 0.5$	6250	MS	0.054	$49.10 \pm 0.06$
WASP-62	$1.25 \pm 0.05$	$1.28 \pm 0.05$	$8.7 \pm 0.4$	6230	MS	0.052	$49.00 \pm 0.05$
WASP-63	$1.32 \pm 0.05$	$1.88 \pm 0.08$	$2.8 \pm 0.5$	5550	S	0.095	$48.96 \pm 0.12$
WASP-64	$1.00 \pm 0.03$	$1.06 \pm 0.02$	$3.4 \pm 0.8$	5550	MS	0.071	$48.55 \pm 0.11$
WASP-66	$1.30 \pm 0.07$	$1.75 \pm 0.09$	$13.4 \pm 0.9$	6600	MS	0.049	$49.32 \pm 0.06$
WASP-67	$0.87 \pm 0.04$	$0.87 \pm 0.04$	$2.1 \pm 0.4$	5200	MS	0.087	$48.28 \pm 0.10$
WASP-71	$1.57 \pm 0.06$	$2.32 \pm 0.14$	$9.4 \pm 0.5$	6050	S	0.093	$49.64 \pm 0.10$
WASP-72	$1.33 \pm 0.04$	$1.71 \pm 0.12$	$6.0 \pm 0.7$	6250	MS	0.048	$48.95 \pm 0.08$
WASP-75	$1.14 \pm 0.07$	$1.26 \pm 0.04$	$4.3 \pm 0.8$	6100	MS	0.059	$48.70 \pm 0.10$
WASP-78	$1.33 \pm 0.09$	$2.20 \pm 0.12$	$7.2 \pm 0.8$	6100	S	0.095	$49.44 \pm 0.11$
WASP-79	$1.52 \pm 0.07$	$1.64 \pm 0.08$	$19.1 \pm 0.7$	6600	MS	0.039	$49.41 \pm 0.05$
WASP-80	$0.58 \pm 0.05$	$0.57 \pm 0.02$	$3.5 \pm 0.3$	4145	MS	0.156	$48.40 \pm 0.07$
WASP-103	$1.22 \pm 0.04$	$1.44 \pm 0.04$	$10.6 \pm 0.9$	6110	MS	0.054	$49.14 \pm 0.06$
WTS-1	$1.20 \pm 0.10$	$1.15 \pm 0.11$	$7.0 \pm 2.0$	6250	MS	0.055	$48.87 \pm 0.15$
xi Aql	$1.11 \pm 0.25$	$10.45 \pm 0.18$	2.0	4714	G	0.137	$49.64 \pm 0.19$
XO-1	$1.03 \pm 0.06$	$0.93 \pm 0.03$	$1.1 \pm 0.1$	5750	MS	0.069	$48.01 \pm 0.06$
XO-3	$1.41 \pm 0.00$	$2.08 \pm 0.07$	$18.3 \pm 1.3$	6429	MS	0.044	$49.51 \pm 0.06$
XO-5	$1.00 \pm 0.03$	$1.05 \pm 0.04$	$1.8 \pm 0.5$	5510	MS	0.071	$48.27 \pm 0.13$

## Appendix D

# Planetary Properties

The columns of Table D.1, from left to right, are: star name; planet designation; planet mass in Jupiter masses, with uncertainties; reference to explanation of how the planetary mass was determined (see below); semi-major axis in AU, with uncertainties; eccentricity,  $e$ , when known; angle of inclination of orbital plane,  $i_p$ , in degrees, when known (mostly for transiting planets); projected angle of obliquity,  $\lambda$ , in degrees; code identifying whether a planet is a hot Jupiter (J), hot Neptune (N), and/or whether the system is transiting (T); and log of calculated planetary angular momentum for each planet in  $\text{g} \cdot \text{cm}^2 \cdot \text{s}^{-1}$ , with uncertainties. See Equation 4.7 for method of calculation of log-uncertainties.

The planet mass reference codes correspond to the following methods of mass determination: (1) mass was calculated from  $m \sin i_p$  and  $i_p$ ; (2) mass was set to  $m \sin i_p$ , as  $i_p$  is unknown; (3) mass was estimated from the radius, per EOD documentation (Wright et al., 2011); (4) mass set to 0.8 of the upper bound reported in field MASSUPPER; (5) mass set to 0.8 of the upper bound reported in field MSINIUPPER; (6) mass obtained from a specific source (see EOD for full references): CoRoT-7 b (Haywood, 2014); CoRoT-25 b (Almenara, 2013); HD 97658 b (Dragomir, 2013); Kepler-10 c (Dumusque, 2014);

Kepler-11 b-f (Lissauer, 2013); Kepler-18 b-d (Cochran, 2011); Kepler-25 b-c, Kepler-48 b-c, Kepler-93 b, Kepler-94 b, Kepler-100 b, Kepler-102 d-f, and Kepler-103 b-c (Marcy, 2014); Kepler-30 b,d (Sanchis-Ojeda, 2012); Kepler-30 c (Fabrycky, 2012) ; OGLE-TR-10 b Torres, 2008); Kepler-68 b,c (Gilliland, 2013); TrES-3 b and TrES-4 b (Sozzetti, 2009); WASP-1 b (Simpson, 2011); WASP-75 b (Gomez, 2013).

The following planets had incorrect or inconsistent parameters reported by EOD. The corrections or adjustments are detailed in Section 3.4: Data Cleaning.

Kepler-10 b      Kepler-26 d,e    Kepler-37 b-d    Kepler-62 b-f    Kepler-100 c  
 Kepler-102 b,f    Kepler-407 b    WASP-33 b      WASP-71 b

TABLE D.1: Planetary Parameters

Host Star	Planet	Mass ( $M_J$ )	Ref	$a$ (AU)	$e$	$i_p$ ( $^\circ$ )	$\lambda$ ( $^\circ$ )	Code	$\log J_p$ (g cm <sup>2</sup> /s)
11 UMi	b	11.087 ± 1.109	2	1.535 ± 0.071	0.08				51.19 ± 0.06
14 And	b	4.684 ± 0.226	2	0.823 ± 0.019	0				50.72 ± 0.03
14 Her	b	5.215 ± 0.298	2	2.934 ± 0.084	0.37				50.86 ± 0.04
24 Sex	b	1.836 ± 0.108	2	1.412 ± 0.024	0.18				50.39 ± 0.03
	c	1.517 ± 0.200	2	2.240 ± 0.051	0.41				50.37 ± 0.06
47 UMa	b	2.546 ± 0.096	2	2.101 ± 0.035	0.03				50.51 ± 0.02
	c	0.546 ± 0.071	2	3.572 ± 0.111	0.10				49.95 ± 0.07
51 Peg	b	0.461 ± 0.016	2	0.052 ± 0.001	0.01			J	48.96 ± 0.02
6 Lyn	b	2.209 ± 0.135	2	2.186 ± 0.056	0.06				50.57 ± 0.04
61 Vir	b	0.016 ± 0.002	2	0.050 ± 0.001	0.12			N	47.47 ± 0.05
	c	0.033 ± 0.004	2	0.217 ± 0.004	0.14				48.10 ± 0.05
	d	0.072 ± 0.009	2	0.475 ± 0.008	0.35				48.58 ± 0.06
7 CMa	b	2.432 ± 0.269	2	1.803 ± 0.064	0.14				50.50 ± 0.06
70 Vir	b	7.461 ± 0.252	2	0.484 ± 0.008	0.40				50.63 ± 0.02
75 Cet	b	2.760 ± 0.212	2	1.977 ± 0.056	0.12				50.68 ± 0.04
81 Cet	b	4.311 ± 0.363	2	2.281 ± 0.093	0.21				50.85 ± 0.05
91 Aqr	b	3.070	2	0.688 ± 0.040	0.03				50.39 ± 0.11
alpha Ari	b	1.717 ± 0.193	2	1.130 ± 0.062	0.25				50.24 ± 0.07
BD -08 2823	b	0.046 ± 0.003	2	0.056 ± 0.002	0.15			N	47.89 ± 0.04
	c	0.328 ± 0.033	2	0.679 ± 0.022	0.19				49.29 ± 0.05
BD -10 3166	b	0.430 ± 0.017	2	0.044 ± 0.001	0.02			J	48.86 ± 0.02
BD +14 4559	b	1.519 ± 0.188	2	0.776 ± 0.045	0.29				50.00 ± 0.07
BD +20 2457	b	11.888 ± 1.610	2	1.050 ± 0.069	0.15				51.02 ± 0.08
	c	6.902 ± 0.967	2	1.457 ± 0.098	0.18				50.85 ± 0.09

Continued on next page

Host Star	Planet	Mass ( $M_J$ )	Ref	$a$ (AU)	$e$	$i_p$ ( $^\circ$ )	$\lambda$ ( $^\circ$ )	Code	$\log J_p$ ( $\text{g cm}^2/\text{s}$ )
BD +48 738	b	$1.265 \pm 0.201$	2	$1.112 \pm 0.075$	0.20				$50.08 \pm 0.09$
CoRoT-1	b	$1.030 \pm 0.124$	1	$0.025 \pm 0.001$	0	85.1	77.0	TJ	$49.13 \pm 0.07$
CoRoT-2	b	$3.275 \pm 0.171$	1	$0.028 \pm 0.001$	0.01	88.1	7.2	TJ	$49.66 \pm 0.03$
CoRoT-3	b	$21.855 \pm 0.992$	1	$0.057 \pm 0.001$	0	85.9	-37.6	TJ	$50.72 \pm 0.03$
CoRoT-4	b	$0.717 \pm 0.072$	1	$0.090 \pm 0.002$	0	90.0		TJ	$49.29 \pm 0.05$
CoRoT-5	b	$0.463 \pm 0.040$	1	$0.050 \pm 0.001$	0.09	85.8		TJ	$48.94 \pm 0.04$
CoRoT-6	b	$2.954 \pm 0.331$	1	$0.085 \pm 0.001$	0	89.1		TJ	$49.87 \pm 0.05$
CoRoT-7	b	$0.014 \pm 0.003$	6	$0.017 \pm 0.000$	0	80.1		TN	$47.18 \pm 0.10$
CoRoT-8	b	$0.216 \pm 0.034$	1	$0.063 \pm 0.001$	0	88.4		TJ	$48.64 \pm 0.07$
CoRoT-10	b	$2.755 \pm 0.160$	1	$0.105 \pm 0.002$	0.53	88.5		T	$49.78 \pm 0.03$
CoRoT-11	b	$2.348 \pm 0.342$	1	$0.044 \pm 0.001$	0	83.2	0.1	TJ	$49.67 \pm 0.07$
CoRoT-12	b	$0.919 \pm 0.071$	1	$0.040 \pm 0.001$	0.07	85.5		TJ	$49.21 \pm 0.04$
CoRoT-13	b	$1.311 \pm 0.077$	1	$0.051 \pm 0.001$	0	88.0		TJ	$49.42 \pm 0.03$
CoRoT-14	b	$7.695 \pm 0.453$	1	$0.027 \pm 0.001$	0	79.6		TJ	$50.06 \pm 0.03$
CoRoT-16	b	$0.538 \pm 0.088$	1	$0.062 \pm 0.002$	0.33	85.0		TJ	$49.05 \pm 0.07$
CoRoT-17	b	$2.460 \pm 0.277$	1	$0.048 \pm 0.002$	0	88.3		TJ	$49.67 \pm 0.06$
CoRoT-18	b	$3.487 \pm 0.376$	1	$0.030 \pm 0.002$	0.04	86.5	10.0	TJ	$49.69 \pm 0.07$
CoRoT-19	b	$1.108 \pm 0.064$	1	$0.052 \pm 0.001$	0.05	88.0	-52.0	TJ	$49.37 \pm 0.03$
CoRoT-23	b	$3.085 \pm 0.313$	1	$0.048 \pm 0.001$	0.16	85.7		TJ	$49.78 \pm 0.05$
CoRoT-25	b	$0.270 \pm 0.040$	6	$0.058 \pm 0.001$	0	84.5		TJ	$48.76 \pm 0.07$
CoRoT-26	b	$0.479 \pm 0.073$	1	$0.052 \pm 0.001$	0	86.8		TJ	$48.99 \pm 0.07$
CoRoT-27	b	$10.388 \pm 0.769$	1	$0.047 \pm 0.002$	0	86.7		TJ	$50.29 \pm 0.04$
epsilon CrB	b	$6.049 \pm 0.513$	2	$1.237 \pm 0.052$	0.11				$50.83 \pm 0.05$
epsilon Eri	b	$1.054 \pm 0.188$	2	$3.376 \pm 0.322$	0.25				$50.16 \pm 0.13$
epsilon Tau	b	$7.677 \pm 0.296$	2	$1.936 \pm 0.034$	0.15				$51.17 \pm 0.02$
eta Cet	b	2.549	2	$1.284 \pm 0.026$	0.16				$50.50 \pm 0.10$
	c	3.287	2	$1.920 \pm 0.038$	0.02				$50.70 \pm 0.10$
HAT-P-2	b	$8.871 \pm 0.406$	1	$0.068 \pm 0.001$	0.52	86.7	9.0	TJ	$50.28 \pm 0.03$
HAT-P-3	b	$0.596 \pm 0.025$	1	$0.039 \pm 0.001$	0	87.2		TJ	$48.98 \pm 0.02$
HAT-P-6	b	$1.060 \pm 0.052$	1	$0.052 \pm 0.001$	0	85.5	165.0	TJ	$49.37 \pm 0.03$
HAT-P-7	b	$1.792 \pm 0.063$	1	$0.038 \pm 0.001$	0	83.1	-177.5	TJ	$49.56 \pm 0.02$
HAT-P-8	b	$1.293 \pm 0.054$	1	$0.045 \pm 0.001$	0	87.8	-9.7	TJ	$49.42 \pm 0.02$
HAT-P-9	b	$0.777 \pm 0.089$	1	$0.053 \pm 0.002$	0	86.5	16.0	TJ	$49.23 \pm 0.06$
HAT-P-11	b	$0.083 \pm 0.009$	1	$0.053 \pm 0.001$	0.20	88.5	103.0	TN	$48.15 \pm 0.05$
HAT-P-12	b	$0.211 \pm 0.013$	1	$0.038 \pm 0.001$	0	89.0		TJ	$48.47 \pm 0.03$
HAT-P-13	b	$0.857 \pm 0.035$	1	$0.043 \pm 0.001$	0.01	83.4	1.9	TJ	$49.22 \pm 0.03$
	c	$14.270 \pm 0.691$	2	$1.226 \pm 0.025$	0.66				$51.04 \pm 0.03$
HAT-P-14	b	$2.236 \pm 0.081$	1	$0.061 \pm 0.001$	0.11	83.5	-170.9	TJ	$49.74 \pm 0.02$
HAT-P-15	b	$1.952 \pm 0.076$	1	$0.096 \pm 0.002$	0.19	89.1		TJ	$49.70 \pm 0.02$
HAT-P-16	b	$4.202 \pm 0.142$	1	$0.041 \pm 0.001$	0.04	86.6	10.0	TJ	$49.90 \pm 0.02$
HAT-P-17	b	$0.530 \pm 0.020$	1	$0.088 \pm 0.001$	0.35	89.2	19.0	TJ	$49.06 \pm 0.02$
HAT-P-18	b	$0.197 \pm 0.013$	1	$0.056 \pm 0.001$	0.08	88.8		TJ	$48.54 \pm 0.03$
HAT-P-19	b	$0.292 \pm 0.018$	1	$0.047 \pm 0.001$	0.07	88.2		TJ	$48.69 \pm 0.03$
HAT-P-20	b	$7.290 \pm 0.247$	1	$0.036 \pm 0.001$	0.02	86.8		TJ	$50.01 \pm 0.02$
HAT-P-21	b	$4.078 \pm 0.173$	1	$0.049 \pm 0.001$	0.23	87.2		TJ	$49.86 \pm 0.02$
HAT-P-22	b	$2.151 \pm 0.077$	1	$0.041 \pm 0.001$	0.02	86.9		TJ	$49.55 \pm 0.02$

Continued on next page

Host Star	Planet	Mass ( $M_J$ )	Ref	$a$ (AU)	$e$	$i_p$ ( $^\circ$ )	$\lambda$ ( $^\circ$ )	Code	$\log J_p$ ( $\text{g cm}^2/\text{s}$ )
HAT-P-23	b	$2.096 \pm 0.122$	1	$0.023 \pm 0.000$	0.11	85.1	15.0	TJ	$49.46 \pm 0.03$
HAT-P-24	b	$0.686 \pm 0.036$	1	$0.047 \pm 0.001$	0.07	88.6	20.0	TJ	$49.13 \pm 0.03$
HAT-P-25	b	$0.567 \pm 0.026$	1	$0.047 \pm 0.001$	0.03	87.6		TJ	$49.02 \pm 0.02$
HAT-P-26	b	$0.059 \pm 0.007$	1	$0.048 \pm 0.001$	0.12	88.6		TN	$47.99 \pm 0.06$
HAT-P-27	b	$0.617 \pm 0.030$	1	$0.040 \pm 0.001$	0	85.0	24.2	TJ	$49.00 \pm 0.03$
HAT-P-28	b	$0.628 \pm 0.038$	1	$0.043 \pm 0.001$	0.05	88.0		TJ	$49.05 \pm 0.03$
HAT-P-29	b	$0.779 \pm 0.064$	1	$0.067 \pm 0.001$	0.10	87.1		TJ	$49.27 \pm 0.04$
HAT-P-30	b	$0.711 \pm 0.035$	1	$0.042 \pm 0.001$	0.04	83.6	73.5	TJ	$49.14 \pm 0.03$
HAT-P-31	b	$2.169 \pm 0.091$	1	$0.061 \pm 0.001$	0.24	87.1		TJ	$49.69 \pm 0.03$
HAT-P-33	b	$0.763 \pm 0.103$	1	$0.050 \pm 0.001$	0	87.2		TJ	$49.23 \pm 0.06$
HAT-P-34	b	$3.334 \pm 0.242$	1	$0.068 \pm 0.001$	0.44	87.1	0.0	TJ	$49.89 \pm 0.03$
HAT-P-35	b	$1.054 \pm 0.040$	1	$0.050 \pm 0.001$	0.02	87.3		TJ	$49.34 \pm 0.02$
HAT-P-36	b	$1.839 \pm 0.100$	1	$0.024 \pm 0.000$	0.06	86.0		TJ	$49.38 \pm 0.03$
HAT-P-37	b	$1.174 \pm 0.105$	1	$0.038 \pm 0.001$	0.06	86.9		TJ	$49.27 \pm 0.04$
HAT-P-39	b	$0.599 \pm 0.100$	1	$0.051 \pm 0.001$	0	87.0		TJ	$49.13 \pm 0.07$
HAT-P-40	b	$0.620 \pm 0.082$	1	$0.061 \pm 0.004$	0	88.3		TJ	$49.20 \pm 0.08$
HAT-P-41	b	$0.800 \pm 0.104$	1	$0.043 \pm 0.001$	0	87.7		TJ	$49.22 \pm 0.06$
HAT-P-49	b	$1.730 \pm 0.208$	1	$0.044 \pm 0.001$	0	86.2		TJ	$49.58 \pm 0.05$
HATS-1	b	$1.865 \pm 0.252$	1	$0.044 \pm 0.001$	0.12	85.6		TJ	$49.52 \pm 0.06$
HATS-2	b	$1.349 \pm 0.152$	1	$0.023 \pm 0.000$	0	87.2		TJ	$49.21 \pm 0.05$
HD 1461	b	$0.024 \pm 0.005$	2	$0.064 \pm 0.001$	0.14			N	$47.71 \pm 0.10$
HD 1502	b	$2.907 \pm 0.172$	2	$1.272 \pm 0.032$	0.10				$50.52 \pm 0.03$
HD 1690	b	$6.526 \pm 1.339$	2	$1.362 \pm 0.089$	0.64				$50.73 \pm 0.11$
HD 2039	b	$5.925 \pm 0.978$	2	$2.198 \pm 0.058$	0.72				$50.74 \pm 0.08$
HD 2952	b	$1.620 \pm 0.229$	2	$1.228 \pm 0.021$	0.13				$50.38 \pm 0.06$
HD 4203	b	$2.082 \pm 0.116$	2	$1.165 \pm 0.022$	0.52				$50.24 \pm 0.03$
HD 4313	b	$2.172 \pm 0.123$	2	$1.133 \pm 0.023$	0.04				$50.38 \pm 0.03$
HD 4732	b	$2.377 \pm 0.235$	2	$1.192 \pm 0.039$	0.13				$50.46 \pm 0.05$
	c	$2.365 \pm 0.267$	2	$4.602 \pm 0.175$	0.23				$50.74 \pm 0.06$
HD 5319	b	$1.698 \pm 0.236$	2	$1.635 \pm 0.051$	0.12				$50.31 \pm 0.07$
HD 5388	b	$1.965 \pm 0.102$	2	$1.763 \pm 0.030$	0.40				$50.35 \pm 0.03$
HD 5608	b	$1.474 \pm 0.113$	2	$1.985 \pm 0.035$	0.19				$50.35 \pm 0.04$
HD 5891	b	$5.228 \pm 0.619$	2	$0.636 \pm 0.037$	0.07				$50.57 \pm 0.07$
HD 6718	b	$1.559 \pm 0.117$	2	$3.554 \pm 0.177$	0.10				$50.38 \pm 0.06$
HD 7924	b	$0.029 \pm 0.006$	2	$0.057 \pm 0.001$	0.17			N	$47.72 \pm 0.09$
HD 8535	b	$0.682 \pm 0.052$	2	$2.445 \pm 0.054$	0.15				$49.98 \pm 0.04$
HD 8574	b	$1.806 \pm 0.083$	2	$0.757 \pm 0.013$	0.30				$50.13 \pm 0.02$
HD 9446	b	$0.699 \pm 0.065$	2	$0.189 \pm 0.006$	0.20				$49.40 \pm 0.05$
	c	$1.815 \pm 0.172$	2	$0.654 \pm 0.022$	0.06				$50.09 \pm 0.05$
HD 10180	c	$0.042 \pm 0.002$	2	$0.064 \pm 0.001$	0.08			N	$47.96 \pm 0.03$
	d	$0.038 \pm 0.002$	2	$0.129 \pm 0.002$	0.14				$48.07 \pm 0.03$
	e	$0.080 \pm 0.004$	2	$0.270 \pm 0.004$	0.06				$48.56 \pm 0.03$
	f	$0.074 \pm 0.005$	2	$0.493 \pm 0.008$	0.13				$48.65 \pm 0.03$
	g	$0.067 \pm 0.009$	2	$1.423 \pm 0.029$	0				$48.85 \pm 0.06$
	h	$0.206 \pm 0.016$	2	$3.425 \pm 0.120$	0.15				$49.52 \pm 0.05$
HD 10647	b	$0.925 \pm 0.242$	2	$2.022 \pm 0.082$	0.16				$50.06 \pm 0.12$

Continued on next page

Host Star	Planet	Mass ( $M_J$ )	Ref	$a$ (AU)	$e$	$i_p$ ( $^\circ$ )	$\lambda$ ( $^\circ$ )	Code	$\log J_p$ ( $\text{g cm}^2/\text{s}$ )
HD 10697	b	$6.235 \pm 0.216$	2	$2.132 \pm 0.036$	0.10				$50.91 \pm 0.02$
HD 11506	b	$4.735 \pm 0.340$	2	$2.605 \pm 0.086$	0.30				$50.83 \pm 0.04$
HD 11977	b	$7.400 \pm 0.667$	2	$2.063 \pm 0.039$	0.40				$51.10 \pm 0.04$
HD 12661	b	$2.341 \pm 0.101$	2	$0.838 \pm 0.018$	0.38				$50.25 \pm 0.03$
	c	$1.949 \pm 0.092$	2	$2.919 \pm 0.064$	0.03				$50.48 \pm 0.03$
HD 13189	b	$7.123 \pm 1.025$	2	$1.252 \pm 0.083$	0.27				$50.85 \pm 0.09$
HD 13908	b	$0.865 \pm 0.035$	2	$0.154 \pm 0.003$	0.05				$49.51 \pm 0.02$
	c	$5.130 \pm 0.250$	2	$2.034 \pm 0.042$	0.12				$50.84 \pm 0.03$
HD 13931	b	$1.881 \pm 0.142$	2	$5.149 \pm 0.327$	0.02				$50.56 \pm 0.08$
HD 16175	b	$4.379 \pm 0.728$	2	$2.119 \pm 0.067$	0.60				$50.69 \pm 0.08$
HD 16417	b	$0.067 \pm 0.006$	2	$0.135 \pm 0.002$	0.20				$48.33 \pm 0.04$
HD 16760	b	$13.292 \pm 0.613$	2	$1.087 \pm 0.024$	0.07				$51.01 \pm 0.03$
HD 17156	b	$3.303 \pm 0.112$	1	$0.163 \pm 0.003$	0.68	87.8	10.0	T	$49.97 \pm 0.02$
HD 18742	b	$2.864 \pm 0.324$	2	$1.978 \pm 0.075$	0.12				$50.65 \pm 0.06$
HD 20794	b	$0.008 \pm 0.001$	2	$0.121 \pm 0.002$	0				$47.32 \pm 0.05$
	c	$0.007 \pm 0.001$	1	$0.204 \pm 0.003$	0	90.0			$47.38 \pm 0.08$
	d	$0.015 \pm 0.002$	1	$0.350 \pm 0.006$	0	90.0			$47.79 \pm 0.06$
HD 20868	b	$2.009 \pm 0.068$	2	$0.947 \pm 0.016$	0.75				$49.99 \pm 0.02$
HD 22781	b	$13.840 \pm 0.487$	2	$1.168 \pm 0.019$	0.82				$50.80 \pm 0.02$
HD 23079	b	$2.443 \pm 0.096$	2	$1.595 \pm 0.028$	0.10				$50.42 \pm 0.02$
HD 23127	b	$1.405 \pm 0.100$	2	$2.319 \pm 0.057$	0.44				$50.24 \pm 0.04$
HD 23596	b	$7.743 \pm 0.288$	2	$2.772 \pm 0.048$	0.27				$51.05 \pm 0.02$
HD 24040	b	$4.022 \pm 0.326$	2	$4.924 \pm 0.206$	0.04				$50.91 \pm 0.05$
HD 25171	b	$0.956 \pm 0.234$	2	$3.031 \pm 0.190$	0.08				$50.17 \pm 0.13$
HD 28678	b	$1.900 \pm 0.178$	2	$1.317 \pm 0.044$	0.17				$50.41 \pm 0.05$
HD 30177	b	$9.688 \pm 0.544$	2	$3.808 \pm 0.134$	0.19				$51.18 \pm 0.04$
HD 30562	b	$1.333 \pm 0.161$	2	$2.341 \pm 0.065$	0.76				$50.10 \pm 0.06$
HD 30856	b	$1.857 \pm 0.176$	2	$2.040 \pm 0.070$	0.12				$50.41 \pm 0.05$
HD 31253	b	$0.501 \pm 0.091$	2	$1.261 \pm 0.022$	0.30				$49.70 \pm 0.08$
HD 32518	b	$3.345 \pm 0.380$	2	$0.595 \pm 0.032$	0.01				$50.37 \pm 0.07$
HD 33142	b	$1.411 \pm 0.131$	2	$1.090 \pm 0.022$	0.12				$50.20 \pm 0.04$
HD 33283	b	$0.330 \pm 0.033$	2	$0.145 \pm 0.004$	0.48				$49.02 \pm 0.05$
HD 33636	b	$9.270 \pm 0.331$	2	$3.265 \pm 0.055$	0.48				$51.10 \pm 0.02$
HD 37124	b	$0.674 \pm 0.029$	2	$0.534 \pm 0.009$	0.05				$49.58 \pm 0.02$
	c	$0.648 \pm 0.055$	2	$1.710 \pm 0.029$	0.12				$49.82 \pm 0.04$
	d	$0.687 \pm 0.075$	2	$2.807 \pm 0.060$	0.16				$49.95 \pm 0.05$
HD 37605	b	$2.802 \pm 0.934$	2	$0.283 \pm 0.047$	0.68				$49.97 \pm 0.22$
	c	$3.366 \pm 1.124$	2	$3.818 \pm 0.638$	0.01				$50.75 \pm 0.22$
HD 38283	b	$0.338 \pm 0.040$	2	$1.024 \pm 0.017$	0.41				$49.44 \pm 0.05$
HD 38801	b	$10.011 \pm 0.430$	2	$1.647 \pm 0.032$	0				$51.08 \pm 0.03$
HD 39091	b	$10.088 \pm 0.376$	2	$3.347 \pm 0.104$	0.64				$51.09 \pm 0.04$
HD 43197	b	$0.597 \pm 0.141$	2	$0.918 \pm 0.015$	0.83				$49.42 \pm 0.11$
HD 44219	b	$0.589 \pm 0.104$	2	$1.187 \pm 0.022$	0.61				$49.63 \pm 0.08$
HD 45350	b	$1.836 \pm 0.096$	2	$1.944 \pm 0.038$	0.78				$50.15 \pm 0.03$
HD 45364	b	$0.187 \pm 0.008$	2	$0.682 \pm 0.014$	0.17				$49.07 \pm 0.03$
	c	$0.659 \pm 0.030$	2	$0.898 \pm 0.018$	0.10				$49.68 \pm 0.03$

Continued on next page

Host Star	Planet	Mass ( $M_J$ )	Ref	$a$ (AU)	$e$	$i_p$ ( $^\circ$ )	$\lambda$ ( $^\circ$ )	Code	$\log J_p$ ( $\text{g cm}^2/\text{s}$ )
HD 45652	b	0.468 $\pm$ 0.042	2	0.228 $\pm$ 0.005	0.38				49.20 $\pm$ 0.04
HD 47186	b	0.071 $\pm$ 0.003	2	0.050 $\pm$ 0.001	0.04			N	48.13 $\pm$ 0.02
	c	0.348 $\pm$ 0.076	2	2.387 $\pm$ 0.078	0.25				49.64 $\pm$ 0.10
HD 49674	b	0.102 $\pm$ 0.008	2	0.057 $\pm$ 0.001	0.09			J	48.31 $\pm$ 0.04
HD 50499	b	1.745 $\pm$ 0.140	2	3.872 $\pm$ 0.076	0.25				50.50 $\pm$ 0.04
HD 50554	b	4.399 $\pm$ 0.405	2	2.261 $\pm$ 0.040	0.44				50.71 $\pm$ 0.04
HD 52265	b	1.071 $\pm$ 0.090	2	0.500 $\pm$ 0.008	0.32				49.82 $\pm$ 0.04
HD 60532	b	1.035 $\pm$ 0.069	2	0.759 $\pm$ 0.018	0.28				49.94 $\pm$ 0.04
	c	2.463 $\pm$ 0.146	2	1.580 $\pm$ 0.040	0.02				50.50 $\pm$ 0.03
HD 63765	b	0.644 $\pm$ 0.046	2	0.940 $\pm$ 0.016	0.24				49.68 $\pm$ 0.03
HD 68988	b	1.800 $\pm$ 0.100	2	0.069 $\pm$ 0.002	0.12			J	49.62 $\pm$ 0.03
HD 69830	b	0.032 $\pm$ 0.002	2	0.078 $\pm$ 0.001	0.10			N	47.84 $\pm$ 0.03
	c	0.037 $\pm$ 0.003	2	0.185 $\pm$ 0.003	0.13				48.09 $\pm$ 0.03
	d	0.056 $\pm$ 0.005	2	0.627 $\pm$ 0.012	0.07				48.54 $\pm$ 0.04
HD 70642	b	1.909 $\pm$ 0.104	2	3.181 $\pm$ 0.066	0.03				50.46 $\pm$ 0.03
HD 72659	b	3.174 $\pm$ 0.148	2	4.754 $\pm$ 0.084	0.22				50.77 $\pm$ 0.03
HD 73267	b	3.063 $\pm$ 0.105	2	2.198 $\pm$ 0.038	0.26				50.54 $\pm$ 0.02
HD 73526	b	2.856 $\pm$ 0.172	2	0.647 $\pm$ 0.011	0.19				50.28 $\pm$ 0.03
	c	2.421 $\pm$ 0.167	2	1.028 $\pm$ 0.018	0.14				50.32 $\pm$ 0.03
HD 73534	b	1.068 $\pm$ 0.085	2	3.018 $\pm$ 0.075	0.07				50.23 $\pm$ 0.04
HD 74156	b	1.773 $\pm$ 0.090	2	0.292 $\pm$ 0.005	0.63				49.85 $\pm$ 0.03
	c	8.247 $\pm$ 0.357	2	3.900 $\pm$ 0.067	0.38				51.15 $\pm$ 0.02
HD 75898	b	2.515 $\pm$ 0.217	2	1.189 $\pm$ 0.042	0.10				50.42 $\pm$ 0.05
HD 76700	b	0.232 $\pm$ 0.020	2	0.051 $\pm$ 0.001	0.10			J	48.67 $\pm$ 0.04
HD 77338	b	0.050 $\pm$ 0.015	2	0.061 $\pm$ 0.001	0.09			N	48.00 $\pm$ 0.13
HD 81040	b	6.877 $\pm$ 0.482	2	1.937 $\pm$ 0.034	0.53				50.83 $\pm$ 0.03
HD 81688	b	2.691 $\pm$ 0.100	2	0.811 $\pm$ 0.014	0				50.47 $\pm$ 0.02
HD 82886	b	1.305 $\pm$ 0.140	2	1.581 $\pm$ 0.078	0.07				50.15 $\pm$ 0.07
HD 82943	b	1.685 $\pm$ 0.097	1	1.185 $\pm$ 0.022	0.20	70.6			50.21 $\pm$ 0.03
	c	1.589 $\pm$ 0.103	2	0.742 $\pm$ 0.013	0.42				50.05 $\pm$ 0.03
HD 83443	b	0.396 $\pm$ 0.018	2	0.040 $\pm$ 0.001	0.01			J	48.83 $\pm$ 0.02
HD 85390	b	0.132 $\pm$ 0.015	2	1.524 $\pm$ 0.041	0.41				49.04 $\pm$ 0.06
HD 86081	b	1.496 $\pm$ 0.050	2	0.035 $\pm$ 0.001	0.01			J	49.41 $\pm$ 0.02
HD 86264	b	6.627 $\pm$ 2.023	2	2.841 $\pm$ 0.085	0.70				50.90 $\pm$ 0.14
HD 87883	b	1.756 $\pm$ 0.282	2	3.576 $\pm$ 0.096	0.53				50.33 $\pm$ 0.08
HD 88133	b	0.296 $\pm$ 0.027	2	0.047 $\pm$ 0.001	0.13			J	48.77 $\pm$ 0.04
HD 89307	b	1.791 $\pm$ 0.150	2	3.266 $\pm$ 0.067	0.20				50.43 $\pm$ 0.04
HD 92788	b	3.564 $\pm$ 0.133	2	0.951 $\pm$ 0.016	0.33				50.46 $\pm$ 0.02
HD 95089	b	1.129 $\pm$ 0.114	2	1.386 $\pm$ 0.050	0.16				50.12 $\pm$ 0.06
HD 96063	b	1.142 $\pm$ 0.162	2	1.113 $\pm$ 0.031	0				50.08 $\pm$ 0.07
HD 96127	b	4.007 $\pm$ 0.849	2	1.421 $\pm$ 0.132	0.30				50.57 $\pm$ 0.13
HD 96167	b	0.685 $\pm$ 0.078	2	1.347 $\pm$ 0.045	0.71				49.73 $\pm$ 0.06
HD 97658	b	0.025 $\pm$ 0.002	6	0.080 $\pm$ 0.001	0.06	89.5		TN	47.71 $\pm$ 0.04
HD 98219	b	2.124 $\pm$ 0.137	2	1.324 $\pm$ 0.031	0				50.42 $\pm$ 0.04
HD 99109	b	0.504 $\pm$ 0.081	2	1.108 $\pm$ 0.021	0.09				49.64 $\pm$ 0.07
HD 99706	b	1.403 $\pm$ 0.176	2	2.134 $\pm$ 0.078	0.37				50.32 $\pm$ 0.07

Continued on next page

Host Star	Planet	Mass ( $M_J$ )	Ref	$a$ (AU)	$e$	$i_p$ ( $^\circ$ )	$\lambda$ ( $^\circ$ )	Code	$\log J_p$ ( $\text{g cm}^2/\text{s}$ )
HD 100655	b	$1.334 \pm 0.193$	2	$0.683 \pm 0.044$	0.08				$50.08 \pm 0.09$
HD 100777	b	$1.165 \pm 0.083$	2	$1.034 \pm 0.035$	0.36				$49.97 \pm 0.04$
HD 102117	b	$0.170 \pm 0.015$	2	$0.152 \pm 0.003$	0.12				$48.76 \pm 0.04$
HD 102195	b	$0.453 \pm 0.021$	2	$0.048 \pm 0.001$	0			J	$48.89 \pm 0.02$
HD 102329	b	$4.478 \pm 0.386$	2	$1.809 \pm 0.071$	0.21				$50.75 \pm 0.05$
HD 102365	b	$0.051 \pm 0.008$	2	$0.463 \pm 0.008$	0.34				$48.42 \pm 0.07$
HD 102956	b	$0.951 \pm 0.048$	2	$0.081 \pm 0.002$	0.05			J	$49.47 \pm 0.03$
HD 103197	b	$0.098 \pm 0.006$	2	$0.249 \pm 0.004$	0				$48.59 \pm 0.03$
HD 103774	b	$0.368 \pm 0.023$	2	$0.070 \pm 0.001$	0.09			J	$48.98 \pm 0.03$
HD 104067	b	$0.186 \pm 0.014$	2	$0.264 \pm 0.004$	0				$48.86 \pm 0.03$
HD 104985	b	$4.917 \pm 0.852$	2	$0.678 \pm 0.059$	0.09				$50.54 \pm 0.11$
HD 106252	b	$6.959 \pm 0.257$	2	$2.611 \pm 0.044$	0.48				$50.92 \pm 0.02$
HD 106270	b	$11.087 \pm 0.870$	2	$4.378 \pm 0.401$	0.40				$51.32 \pm 0.11$
HD 107148	b	$0.212 \pm 0.040$	2	$0.270 \pm 0.006$	0.05				$49.00 \pm 0.08$
HD 108147	b	$0.258 \pm 0.067$	2	$0.101 \pm 0.002$	0.53				$48.80 \pm 0.12$
HD 108863	b	$2.766 \pm 0.162$	2	$1.453 \pm 0.034$	0				$50.61 \pm 0.03$
HD 108874	b	$1.290 \pm 0.057$	2	$1.035 \pm 0.017$	0.13				$50.03 \pm 0.02$
	c	$1.028 \pm 0.054$	2	$2.720 \pm 0.052$	0.27				$50.13 \pm 0.03$
HD 109246	b	$0.768 \pm 0.064$	2	$0.328 \pm 0.012$	0.12				$49.57 \pm 0.05$
HD 113337	b	$2.830 \pm 0.240$	2	$1.033 \pm 0.035$	0.46				$50.41 \pm 0.05$
HD 114386	b	$1.364 \pm 0.079$	2	$1.727 \pm 0.035$	0.23				$50.12 \pm 0.03$
HD 114613	b	$0.506 \pm 0.042$	2	$5.311 \pm 0.131$	0.25				$50.05 \pm 0.04$
HD 114783	b	$1.105 \pm 0.049$	2	$1.160 \pm 0.020$	0.14				$49.96 \pm 0.02$
HD 116029	b	$1.908 \pm 0.193$	2	$1.649 \pm 0.049$	0				$50.38 \pm 0.05$
HD 117207	b	$1.819 \pm 0.089$	2	$3.738 \pm 0.074$	0.14				$50.48 \pm 0.03$
HD 117618	b	$0.177 \pm 0.035$	2	$0.175 \pm 0.003$	0.42				$48.77 \pm 0.09$
HD 118203	b	$2.136 \pm 0.078$	2	$0.070 \pm 0.001$	0.31			J	$49.70 \pm 0.02$
HD 120084	b	$4.477 \pm 3.448$	2	$4.269 \pm 1.352$	0.66				$50.96 \pm 1.43$
HD 125595	b	$0.042 \pm 0.004$	2	$0.081 \pm 0.001$	0			N	$47.94 \pm 0.05$
HD 128311	b	$1.457 \pm 0.152$	2	$1.086 \pm 0.018$	0.34				$50.04 \pm 0.05$
	c	$3.248 \pm 0.159$	2	$1.745 \pm 0.030$	0.23				$50.51 \pm 0.03$
HD 130322	b	$1.043 \pm 0.040$	2	$0.090 \pm 0.001$	0.01			J	$49.38 \pm 0.02$
HD 131496	b	$2.241 \pm 0.178$	2	$2.112 \pm 0.070$	0.16				$50.54 \pm 0.05$
HD 131664	b	$18.328 \pm 1.298$	2	$3.171 \pm 0.069$	0.64				$51.35 \pm 0.04$
HD 134987	b	$1.563 \pm 0.062$	2	$0.808 \pm 0.016$	0.23				$50.07 \pm 0.02$
	c	$0.805 \pm 0.046$	2	$5.825 \pm 0.331$	0.12				$50.22 \pm 0.07$
HD 136118	b	$11.681 \pm 0.419$	2	$2.333 \pm 0.039$	0.34				$51.19 \pm 0.02$
HD 136418	b	$1.994 \pm 0.126$	2	$1.291 \pm 0.030$	0.26				$50.33 \pm 0.03$
HD 141937	b	$9.475 \pm 0.411$	2	$1.501 \pm 0.025$	0.41				$50.96 \pm 0.02$
HD 142245	b	$1.890 \pm 0.219$	2	$2.776 \pm 0.095$	0				$50.53 \pm 0.06$
HD 142415	b	$1.662 \pm 0.093$	2	$1.061 \pm 0.018$	0.50				$50.11 \pm 0.03$
HD 145377	b	$5.782 \pm 0.224$	2	$0.450 \pm 0.008$	0.31				$50.52 \pm 0.02$
HD 147018	b	$2.127 \pm 0.076$	2	$0.239 \pm 0.004$	0.47				$49.87 \pm 0.02$
	c	$6.594 \pm 0.294$	2	$1.923 \pm 0.039$	0.13				$50.87 \pm 0.03$
HD 148156	b	$0.848 \pm 0.069$	2	$2.129 \pm 0.053$	0.52				$49.99 \pm 0.04$
HD 148427	b	$1.144 \pm 0.092$	2	$1.039 \pm 0.018$	0.16				$50.06 \pm 0.04$

Continued on next page

Host Star	Planet	Mass ( $M_J$ )	Ref	$a$ (AU)	$e$	$i_p$ ( $^\circ$ )	$\lambda$ ( $^\circ$ )	Code	$\log J_p$ ( $\text{g cm}^2/\text{s}$ )
HD 149026	b	$0.361 \pm 0.016$	1	$0.043 \pm 0.001$	0	84.5	12.0	TJ	$48.86 \pm 0.02$
HD 149143	b	$1.328 \pm 0.078$	2	$0.053 \pm 0.001$	0.02			J	$49.45 \pm 0.04$
HD 152581	b	$1.514 \pm 0.151$	2	$1.489 \pm 0.067$	0				$50.17 \pm 0.06$
HD 153950	b	$2.742 \pm 0.106$	2	$1.280 \pm 0.022$	0.34				$50.42 \pm 0.02$
HD 154345	b	$0.957 \pm 0.061$	2	$4.214 \pm 0.105$	0.04				$50.20 \pm 0.04$
HD 154672	b	$5.006 \pm 0.350$	2	$0.599 \pm 0.019$	0.61				$50.43 \pm 0.04$
HD 154857	b	$2.248 \pm 0.092$	2	$1.291 \pm 0.022$	0.46				$50.40 \pm 0.02$
	c	$2.579 \pm 0.148$	2	$5.356 \pm 0.141$	0.06				$50.82 \pm 0.04$
HD 156279	b	$9.785 \pm 0.533$	2	$0.495 \pm 0.008$	0.71				$50.60 \pm 0.03$
HD 156411	b	$0.733 \pm 0.051$	2	$1.875 \pm 0.038$	0.22				$49.96 \pm 0.04$
HD 156668	b	$0.013 \pm 0.002$	2	$0.050 \pm 0.001$	0			N	$47.34 \pm 0.06$
HD 158038	b	$1.794 \pm 0.202$	2	$1.498 \pm 0.039$	0.29				$50.36 \pm 0.05$
HD 159243	b	$1.130 \pm 0.050$	2	$0.110 \pm 0.002$	0.02				$49.53 \pm 0.02$
	c	$1.900 \pm 0.130$	2	$0.805 \pm 0.017$	0.08				$50.18 \pm 0.04$
HD 159868	b	$2.200 \pm 0.097$	2	$2.296 \pm 0.040$	0.01				$50.48 \pm 0.02$
	c	$0.730 \pm 0.050$	2	$1.026 \pm 0.017$	0.15				$49.82 \pm 0.03$
HD 162020	b	$15.214 \pm 0.508$	2	$0.076 \pm 0.001$	0.28			J	$50.48 \pm 0.02$
HD 163607	b	$0.769 \pm 0.041$	2	$0.359 \pm 0.006$	0.73				$49.44 \pm 0.03$
	c	$2.292 \pm 0.108$	2	$2.418 \pm 0.041$	0.12				$50.49 \pm 0.03$
HD 164509	b	$0.480 \pm 0.095$	2	$0.878 \pm 0.017$	0.26				$49.59 \pm 0.09$
HD 164922	b	$0.358 \pm 0.060$	2	$2.101 \pm 0.045$	0.05				$49.63 \pm 0.08$
HD 167042	b	$1.637 \pm 0.087$	2	$1.294 \pm 0.023$	0.09				$50.30 \pm 0.03$
HD 168443	b	$7.697 \pm 0.291$	2	$0.294 \pm 0.005$	0.53				$50.48 \pm 0.02$
	c	$17.386 \pm 0.581$	2	$2.853 \pm 0.048$	0.21				$51.38 \pm 0.02$
HD 169830	b	$2.889 \pm 0.102$	2	$0.813 \pm 0.014$	0.31				$50.40 \pm 0.02$
	c	$4.064 \pm 0.348$	2	$3.602 \pm 0.307$	0.33				$50.86 \pm 0.10$
HD 170469	b	$0.669 \pm 0.109$	2	$2.235 \pm 0.045$	0.11				$49.95 \pm 0.07$
HD 171028	b	$1.988 \pm 0.087$	2	$1.319 \pm 0.027$	0.59				$50.20 \pm 0.03$
HD 171238	b	$2.609 \pm 0.148$	2	$2.543 \pm 0.064$	0.40				$50.50 \pm 0.04$
HD 175541	b	$0.528 \pm 0.088$	2	$0.961 \pm 0.023$	0.33				$49.68 \pm 0.08$
HD 179079	b	$0.084 \pm 0.009$	2	$0.120 \pm 0.004$	0.12				$48.41 \pm 0.05$
HD 179949	b	$0.902 \pm 0.033$	2	$0.044 \pm 0.001$	0.02			J	$49.24 \pm 0.02$
HD 180902	b	$1.564 \pm 0.199$	2	$1.381 \pm 0.037$	0.09				$50.28 \pm 0.06$
HD 181342	b	$3.149 \pm 0.255$	2	$1.777 \pm 0.061$	0.18				$50.66 \pm 0.05$
HD 181433	b	$0.024 \pm 0.002$	2	$0.080 \pm 0.001$	0.40			N	$47.66 \pm 0.04$
	c	$0.640 \pm 0.027$	2	$1.756 \pm 0.034$	0.28				$49.78 \pm 0.03$
	d	$0.535 \pm 0.051$	2	$3.022 \pm 0.155$	0.48				$49.79 \pm 0.07$
HD 181720	b	$0.372 \pm 0.023$	2	$1.847 \pm 0.036$	0.26				$49.60 \pm 0.03$
HD 183263	b	$3.574 \pm 0.199$	2	$1.490 \pm 0.025$	0.36				$50.56 \pm 0.03$
	c	$3.476 \pm 0.309$	2	$4.295 \pm 0.125$	0.24				$50.80 \pm 0.05$
HD 187085	b	0.804	2	2.028	0.47				$49.96 \pm 0.11$
HD 187123	b	$0.510 \pm 0.017$	2	$0.042 \pm 0.001$	0.01			J	$48.95 \pm 0.02$
	c	$1.942 \pm 0.152$	2	$4.831 \pm 0.367$	0.25				$50.55 \pm 0.09$
HD 190228	b	$5.942 \pm 0.304$	2	$2.605 \pm 0.046$	0.53				$50.97 \pm 0.03$
HD 190647	b	$1.903 \pm 0.132$	2	$2.072 \pm 0.063$	0.18				$50.38 \pm 0.04$
HD 192263	b	$0.639 \pm 0.038$	2	$0.153 \pm 0.003$	0.06				$49.28 \pm 0.03$

Continued on next page

Host Star	Planet	Mass ( $M_J$ )	Ref	$a$ (AU)	$e$	$i_p$ ( $^\circ$ )	$\lambda$ ( $^\circ$ )	Code	$\log J_p$ ( $\text{g cm}^2/\text{s}$ )
HD 192699	b	$2.292 \pm 0.156$	2	$1.123 \pm 0.019$	0.13				$50.41 \pm 0.03$
HD 200964	b	$1.949 \pm 0.135$	2	$1.643 \pm 0.027$	0.04				$50.42 \pm 0.03$
	c	$0.946 \pm 0.201$	2	$2.001 \pm 0.034$	0.18				$50.14 \pm 0.09$
HD 202206	b	$16.824 \pm 0.680$	2	$0.812 \pm 0.016$	0.44				$51.08 \pm 0.02$
	c	$2.331 \pm 0.127$	2	$2.490 \pm 0.055$	0.27				$50.49 \pm 0.03$
HD 204313	b	$3.501 \pm 0.221$	2	$3.071 \pm 0.058$	0.23				$50.71 \pm 0.03$
	d	$1.606 \pm 0.281$	2	$3.945 \pm 0.154$	0.28				$50.42 \pm 0.09$
HD 205739	b	$1.487 \pm 0.128$	2	$0.895 \pm 0.020$	0.27				$50.10 \pm 0.04$
HD 206610	b	$1.971 \pm 0.155$	2	$1.537 \pm 0.052$	0.23				$50.36 \pm 0.05$
HD 207832	b	$0.564 \pm 0.065$	2	$0.570 \pm 0.020$	0.13				$49.54 \pm 0.06$
	c	$0.730 \pm 0.161$	2	$2.112 \pm 0.100$	0.27				$49.92 \pm 0.11$
HD 208487	b	$0.512 \pm 0.097$	2	$0.521 \pm 0.009$	0.24				$49.51 \pm 0.08$
HD 208527	b	$10.014 \pm 1.682$	2	$2.099 \pm 0.175$	0.08				$51.19 \pm 0.10$
HD 209458	b	$0.690 \pm 0.024$	1	$0.047 \pm 0.001$	0	86.7	-4.4	TJ	$49.13 \pm 0.02$
HD 210277	b	$1.273 \pm 0.051$	2	$1.131 \pm 0.019$	0.48				$50.00 \pm 0.02$
HD 210702	b	$1.865 \pm 0.126$	2	$1.172 \pm 0.020$	0.04				$50.35 \pm 0.03$
HD 212771	b	$2.700 \pm 0.375$	2	$1.165 \pm 0.022$	0.11				$50.48 \pm 0.06$
HD 215497	b	$0.021 \pm 0.002$	2	$0.047 \pm 0.001$	0.16			N	$47.55 \pm 0.05$
	c	$0.328 \pm 0.025$	2	$1.282 \pm 0.022$	0.49				$49.41 \pm 0.04$
HD 216437	b	$2.168 \pm 0.094$	2	$2.486 \pm 0.052$	0.32				$50.46 \pm 0.03$
HD 217786	b	$13.187 \pm 1.146$	2	$2.379 \pm 0.040$	0.40				$51.20 \pm 0.04$
HD 219828	b	$0.062 \pm 0.005$	2	$0.052 \pm 0.001$	0			N	$48.12 \pm 0.04$
HD 220074	b	$11.188 \pm 1.882$	2	$1.600 \pm 0.133$	0.14				$51.11 \pm 0.10$
HD 221287	b	$3.115 \pm 0.595$	2	$1.250 \pm 0.035$	0.08				$50.52 \pm 0.09$
HD 222155	b	$2.026 \pm 0.500$	2	$5.139 \pm 0.464$	0.16				$50.61 \pm 0.15$
HD 224693	b	$0.715 \pm 0.050$	2	$0.192 \pm 0.005$	0.05				$49.49 \pm 0.04$
HD 231701	b	$1.087 \pm 0.105$	2	$0.556 \pm 0.012$	0.10				$49.86 \pm 0.05$
HD 240210	b	$7.289 \pm 0.985$	2	$1.334 \pm 0.089$	0.15				$50.90 \pm 0.08$
HD 290327	b	$2.548 \pm 0.206$	2	$3.431 \pm 0.161$	0.08				$50.58 \pm 0.06$
HIP 2247	b	$5.123 \pm 0.179$	2	$1.339 \pm 0.022$	0.54				$50.56 \pm 0.02$
HIP 5158	b	$1.426 \pm 0.291$	2	$0.888 \pm 0.017$	0.52				$49.93 \pm 0.09$
HIP 14810	b	$3.874 \pm 0.129$	2	$0.069 \pm 0.001$	0.14			J	$49.93 \pm 0.02$
	c	$1.275 \pm 0.045$	2	$0.545 \pm 0.009$	0.15				$49.89 \pm 0.02$
	d	$0.581 \pm 0.036$	2	$1.886 \pm 0.036$	0.17				$49.82 \pm 0.03$
HIP 57274	b	$0.037 \pm 0.004$	2	$0.071 \pm 0.002$	0.19			N	$47.84 \pm 0.05$
	c	$0.410 \pm 0.020$	2	$0.178 \pm 0.004$	0.05				$49.10 \pm 0.03$
	d	$0.529 \pm 0.029$	2	$1.007 \pm 0.027$	0.27				$49.57 \pm 0.03$
HIP 91258	b	$1.068 \pm 0.038$	2	$0.057 \pm 0.001$	0.02			J	$49.32 \pm 0.02$
iota Hor	b	$2.047 \pm 0.202$	2	$0.924 \pm 0.016$	0.14				$50.25 \pm 0.05$
kappa CrB	b	$1.975 \pm 0.116$	2	$2.716 \pm 0.050$	0.12				$50.54 \pm 0.03$
Kepler-4	b	$0.077 \pm 0.013$	1	$0.046 \pm 0.001$	0	89.8		TN	$48.19 \pm 0.07$
Kepler-5	b	$2.117 \pm 0.075$	1	$0.051 \pm 0.001$	0	86.3		TJ	$49.67 \pm 0.02$
Kepler-6	b	$0.669 \pm 0.031$	1	$0.046 \pm 0.001$	0	86.8		TJ	$49.12 \pm 0.02$
Kepler-7	b	$0.438 \pm 0.096$	1	$0.062 \pm 0.001$	0	86.5		TJ	$49.03 \pm 0.10$
Kepler-8	b	$0.586 \pm 0.129$	1	$0.048 \pm 0.001$	0	84.1	5.0	TJ	$49.08 \pm 0.10$
Kepler-10	b	$0.010 \pm 0.002$	1	$0.017 \pm 0.000$	0	84.4		TN	$47.04 \pm 0.07$

Continued on next page

Host Star	Planet	Mass ( $M_J$ )	Ref	$a$ (AU)	$e$	$i_p$ ( $^\circ$ )	$\lambda$ ( $^\circ$ )	Code	$\log J_p$ ( $\text{g cm}^2/\text{s}$ )
Kepler-11	c	$0.054 \pm 0.012$	6	$0.240 \pm 0.005$		89.7		T	$48.33 \pm 0.10$
	b	$0.006 \pm 0.004$	6	$0.091 \pm 0.002$	0.04	89.6		TN	$47.18 \pm 0.32$
	c	$0.009 \pm 0.007$	6	$0.107 \pm 0.002$	0.03	89.6		T	$47.39 \pm 0.45$
	d	$0.023 \pm 0.004$	6	$0.155 \pm 0.003$	0.00	89.7		T	$47.87 \pm 0.07$
	e	$0.026 \pm 0.007$	6	$0.195 \pm 0.003$	0.01	88.9		T	$47.99 \pm 0.12$
	f	$0.007 \pm 0.005$	6	$0.250 \pm 0.004$	0.01	89.5		T	$47.48 \pm 0.41$
Kepler-12	g	$0.033 \pm 0.001$	3	$0.466 \pm 0.008$	0	89.9		T	$48.27 \pm 0.02$
	b	$0.432 \pm 0.042$	1	$0.056 \pm 0.001$	0	88.8		TJ	$48.97 \pm 0.04$
Kepler-14	b	$8.406 \pm 0.294$	1	$0.081 \pm 0.001$	0.04	90.0		TJ	$50.39 \pm 0.02$
Kepler-15	b	$0.662 \pm 0.079$	1	$0.057 \pm 0.001$	0.13	87.4		TJ	$49.13 \pm 0.05$
Kepler-17	b	$2.479 \pm 0.102$	1	$0.027 \pm 0.000$	0	87.2	0.0	TJ	$49.57 \pm 0.02$
Kepler-18	b	$0.022 \pm 0.011$	6	$0.045 \pm 0.001$	0	84.9		TN	$47.59 \pm 0.24$
	c	$0.054 \pm 0.006$	6	$0.075 \pm 0.001$	0.00	87.7		TN	$48.09 \pm 0.05$
Kepler-20	d	$0.052 \pm 0.004$	6	$0.117 \pm 0.002$	0.00	88.1		T	$48.17 \pm 0.04$
	b	$0.027 \pm 0.007$	1	$0.045 \pm 0.001$	0	86.5		TN	$47.66 \pm 0.11$
	c	$0.050 \pm 0.010$	1	$0.093 \pm 0.002$	0	88.4		TN	$48.08 \pm 0.09$
	d	$0.024 \pm 0.023$	1	$0.345 \pm 0.006$	0	89.6		T	$48.03 \pm 0.84$
	e	$0.002 \pm 0.001$	3	$0.063 \pm 0.001$	0	87.5		TN	$46.55 \pm 0.14$
	f	$0.003 \pm 0.001$	3	$0.138 \pm 0.002$	0	88.7		T	$46.98 \pm 0.16$
Kepler-21	b	$0.012 \pm 0.000$	3	$0.043 \pm 0.001$	0	82.6		TN	$47.39 \pm 0.02$
Kepler-22	b	$0.018 \pm 0.001$	3	$0.849 \pm 0.017$		89.8		T	$48.15 \pm 0.04$
Kepler-25	b	$0.022 \pm 0.001$	6	0.070	0			TN	$47.74 \pm 0.05$
	c	$0.090 \pm 0.003$	6	0.113	0			T	$48.45 \pm 0.05$
Kepler-26	b	$0.040 \pm 0.009$	3	$0.090 \pm 0.002$	0			TN	$47.91 \pm 0.10$
	c	$0.040 \pm 0.009$	3	$0.113 \pm 0.002$	0			T	$47.96 \pm 0.10$
	d	$0.004 \pm 0.001$	3	$0.039 \pm 0.001$				TN	$46.70 \pm 0.08$
Kepler-27	e	$0.019 \pm 0.002$	3	$0.220 \pm 0.004$				T	$47.78 \pm 0.04$
	b	$0.052 \pm 0.011$	3	$0.105 \pm 0.009$	0			T	$48.06 \pm 0.12$
	c	$0.079 \pm 0.017$	3	$0.168 \pm 0.014$	0			T	$48.35 \pm 0.12$
Kepler-29	b	$0.040 \pm 0.011$	3	$0.093 \pm 0.004$	0			TN	$48.01 \pm 0.13$
	c	$0.025 \pm 0.006$	3	$0.110 \pm 0.004$	0			T	$47.85 \pm 0.10$
Kepler-30	b	$0.036 \pm 0.004$	6	$0.186 \pm 0.005$	0.04	89.8	4.0	T	$48.11 \pm 0.06$
	c	$2.014 \pm 0.157$	6	$0.300 \pm 0.008$	0.01	89.7	4.0	T	$49.97 \pm 0.04$
	d	$0.073 \pm 0.008$	6	$0.534 \pm 0.014$	0.02	89.8	4.0	T	$48.65 \pm 0.06$
Kepler-37	b	$0.001 \pm 0.000$	1	$0.102 \pm 0.003$	0	88.6		T	$46.36 \pm 0.10$
	c	$0.002 \pm 0.001$	1	$0.140 \pm 0.004$	0.10	89.1		T	$46.82 \pm 0.10$
	d	$0.006 \pm 0.001$	1	$0.212 \pm 0.006$	0.10	89.3		T	$47.34 \pm 0.10$
Kepler-38	b	$0.062 \pm 0.003$	3	$0.430 \pm 0.009$	0	89.4		T	$48.53 \pm 0.03$
Kepler-39	b	$18.180 \pm 0.718$	1	$0.155 \pm 0.003$	0.12	88.8		T	$50.80 \pm 0.02$
Kepler-40	b	$2.177 \pm 0.336$	1	$0.081 \pm 0.001$	0	89.7		TJ	$49.80 \pm 0.07$
Kepler-41	b	$0.494 \pm 0.071$	1	$0.029 \pm 0.001$	0	88.3		TJ	$48.84 \pm 0.07$
Kepler-43	b	$3.231 \pm 0.184$	1	$0.045 \pm 0.001$	0	84.3		TJ	$49.82 \pm 0.03$
Kepler-44	b	$1.021 \pm 0.070$	1	$0.045 \pm 0.001$	0	83.8		TJ	$49.30 \pm 0.04$
Kepler-47	b	$0.026 \pm 0.002$	3	$0.268 \pm 0.005$	0	89.6		T	$48.07 \pm 0.04$
	c	$0.073 \pm 0.006$	3	$0.896 \pm 0.016$	0	89.8		T	$48.77 \pm 0.04$
Kepler-48	b	$0.012 \pm 0.007$	6	0.053	0			TN	$47.36 \pm 0.26$

Continued on next page

Host Star	Planet	Mass ( $M_J$ )	Ref	$a$ (AU)	$e$	$i_p$ ( $^\circ$ )	$\lambda$ ( $^\circ$ )	Code	$\log J_p$ ( $\text{g cm}^2/\text{s}$ )
	c	$0.046 \pm 0.007$	6	0.085				TN	$48.03 \pm 0.08$
	d	$0.015 \pm 0.001$	3	0.230	0			T	$47.76 \pm 0.05$
Kepler-62	b	$0.023 \pm 0.014$	5	$0.055 \pm 0.001$	0.07	89.2		TN	$47.58 \pm 0.31$
	c	$0.010 \pm 0.006$	5	$0.093 \pm 0.002$	0.19	89.7		TN	$47.34 \pm 0.31$
	d	$0.036 \pm 0.022$	5	$0.119 \pm 0.002$	0.09	89.7		T	$47.94 \pm 0.31$
	e	$0.093 \pm 0.057$	5	$0.426 \pm 0.007$	0.13	90.0		T	$48.63 \pm 0.31$
	f	$0.090 \pm 0.055$	5	$0.718 \pm 0.012$	0.09	89.9		T	$48.73 \pm 0.31$
Kepler-63	b	$0.125 \pm 0.008$	3	$0.087 \pm 0.001$		87.8	-110.0	TJ	$48.49 \pm 0.03$
Kepler-68	b	$0.026 \pm 0.006$	6	$0.062 \pm 0.001$	0	87.6		TN	$47.76 \pm 0.10$
	c	$0.015 \pm 0.010$	6	$0.091 \pm 0.002$	0	86.9		TN	$47.60 \pm 0.33$
	d	$0.810 \pm 0.038$	2	$1.396 \pm 0.033$	0.18				$49.92 \pm 0.03$
Kepler-74	b	$0.667 \pm 0.090$	1	$0.083 \pm 0.002$	0.29	85.5		TJ	$49.26 \pm 0.06$
Kepler-75	b	$9.985 \pm 0.498$	1	$0.081 \pm 0.002$	0.57	89.1		TJ	$50.27 \pm 0.03$
Kepler-77	b	$0.431 \pm 0.034$	1	$0.045 \pm 0.001$	0	88.0		TJ	$48.88 \pm 0.04$
Kepler-78	b	$0.005 \pm 0.002$	3	$0.009 \pm 0.000$		79.0		TN	$46.55 \pm 0.20$
Kepler-89	b	$0.029 \pm 0.012$	1	$0.051 \pm 0.001$	0.25	89.3		TN	$47.78 \pm 0.20$
	c	$0.064 \pm 0.013$	3	$0.101 \pm 0.002$	0.43	88.4		T	$48.25 \pm 0.09$
	d	$0.303 \pm 0.027$	1	$0.173 \pm 0.003$	0.02	89.9		T	$49.08 \pm 0.04$
	e	$0.099 \pm 0.064$	1	$0.305 \pm 0.005$	0.02	89.8		T	$48.72 \pm 0.33$
Kepler-93	b	$0.008 \pm 0.006$	6	0.053	0			TN	$47.18 \pm 0.45$
Kepler-94	b	$0.034 \pm 0.008$	6	0.034	0			TN	$47.68 \pm 0.11$
Kepler-95	b	$0.035 \pm 0.008$	3	0.102	0			T	$48.00 \pm 0.11$
Kepler-96	b	$0.026 \pm 0.006$	2	$0.125 \pm 0.003$	0			T	$47.89 \pm 0.10$
Kepler-97	b	0.011	2	0.036	0			TN	$47.22 \pm 0.11$
Kepler-98	b	0.010	2	0.026	0			TN	$47.14 \pm 0.11$
Kepler-99	b	0.020	2	0.050	0			TN	$47.53 \pm 0.11$
Kepler-100	b	$0.023 \pm 0.010$	6	0.073	0			TN	$47.74 \pm 0.21$
	c	$0.004 \pm 0.002$	5	0.110	0			T	$47.06 \pm 0.31$
Kepler-102	b	$0.002 \pm 0.001$	5	0.055	0			TN	$46.58 \pm 0.31$
	d	$0.006 \pm 0.003$	6	0.086	0			TN	$47.11 \pm 0.24$
	e	$0.028 \pm 0.006$	6	0.116	0			T	$47.86 \pm 0.11$
	f	$0.002 \pm 0.000$	6	0.165	0			T	$46.78 \pm 0.10$
Kepler-103	b	$0.031 \pm 0.027$	6	0.128	0			T	$47.98 \pm 0.62$
	c	$0.088 \pm 0.005$	6	0.641	0			T	$48.79 \pm 0.05$
Kepler-106	b	$0.001 \pm 0.001$	3	0.066	0			TN	$46.49 \pm 0.19$
	c	$0.020 \pm 0.003$	3	0.111	0			T	$47.74 \pm 0.09$
	e	$0.020 \pm 0.004$	3	0.243	0			T	$47.93 \pm 0.09$
Kepler-109	b	$0.018 \pm 0.001$	3	0.069	0			TN	$47.62 \pm 0.05$
	c	$0.020 \pm 0.001$	3	0.152	0			T	$47.83 \pm 0.05$
Kepler-113	b	$0.013 \pm 0.000$	3	0.050	0			TN	$47.34 \pm 0.05$
Kepler-131	b	0.050	2	0.126	0			T	$48.18 \pm 0.11$
	c	0.053	2	0.171	0			T	$48.27 \pm 0.11$
Kepler-406	b	0.020	2	0.036	0			TN	$47.52 \pm 0.11$
	c	0.009	2	0.056	0			TN	$47.25 \pm 0.11$
Kepler-407	b	$0.002 \pm 0.001$	5	$0.015 \pm 0.000$	0			TN	$46.22 \pm 0.31$
Kepler-412	b	$0.940 \pm 0.087$	1	$0.030 \pm 0.001$	0.00	80.9		TJ	$49.17 \pm 0.05$

Continued on next page

Host Star	Planet	Mass ( $M_J$ )	Ref	$a$ (AU)	$e$	$i_p$ ( $^\circ$ )	$\lambda$ ( $^\circ$ )	Code	$\log J_p$ ( $\text{g cm}^2/\text{s}$ )
KIC 11442793	b	$0.008 \pm 0.003$	3	$0.076 \pm 0.002$		89.4		TN	$47.28 \pm 0.17$
	c	$0.005 \pm 0.002$	3	$0.088 \pm 0.002$		89.7		TN	$47.17 \pm 0.16$
	d	$0.025 \pm 0.004$	3	$0.307 \pm 0.009$		89.7		T	$48.10 \pm 0.08$
	e	$0.022 \pm 0.003$	3	$0.424 \pm 0.012$		89.8		T	$48.12 \pm 0.07$
	f	$0.025 \pm 0.007$	3	$0.520 \pm 0.014$		89.8		T	$48.23 \pm 0.12$
	g	$0.218 \pm 0.058$	3	$0.736 \pm 0.020$		89.8		T	$49.24 \pm 0.12$
	h	$0.937 \pm 0.402$	3	$0.996 \pm 0.028$		89.6		T	$49.94 \pm 0.20$
mu Ara	b	$1.746 \pm 0.069$	2	$1.527 \pm 0.029$	0.13				$50.29 \pm 0.02$
	c	$1.889 \pm 0.223$	2	$5.341 \pm 0.402$	0.10				$50.60 \pm 0.10$
	d	$0.035 \pm 0.002$	2	$0.093 \pm 0.002$	0.17			N	$47.97 \pm 0.03$
	e	$0.543 \pm 0.030$	2	$0.940 \pm 0.018$	0.07				$49.68 \pm 0.03$
OGLE-TR-10	b	$0.620 \pm 0.140$	6	$0.043 \pm 0.001$	0	90.0		TJ	$49.07 \pm 0.10$
OGLE2-TR-L9	b	$4.574 \pm 1.509$	1	$0.041 \pm 0.001$	0	79.8		TJ	$49.99 \pm 0.15$
omega Ser	b	$1.701 \pm 0.180$	2	$1.077 \pm 0.041$	0.11				$50.34 \pm 0.06$
omicron CrB	b	$1.477 \pm 0.142$	2	$0.826 \pm 0.016$	0.19				$50.21 \pm 0.05$
omicron UMa	b	$4.096 \pm 0.294$	2	$3.950 \pm 0.087$	0.13				$51.08 \pm 0.04$
PH-2	b	$0.488 \pm 0.104$	3	$0.825 \pm 0.014$	0.41	89.8		T	$49.52 \pm 0.10$
Pr 201	b	$0.540 \pm 0.042$	2	$0.057 \pm 0.001$	0			J	$49.08 \pm 0.04$
Pr 211	b	$1.844 \pm 0.072$	2	$0.032 \pm 0.001$	0			J	$49.44 \pm 0.02$
Qatar-1	b	$1.090 \pm 0.085$	1	$0.023 \pm 0.000$	0	83.5	-8.4	TJ	$49.11 \pm 0.04$
Qatar-2	b	$2.484 \pm 0.087$	1	$0.022 \pm 0.000$	0	88.3		TJ	$49.42 \pm 0.02$
rho CrB	b	$1.064 \pm 0.053$	2	$0.226 \pm 0.004$	0.06				$49.62 \pm 0.03$
tau Gru	b	$1.215 \pm 0.115$	2	$2.518 \pm 0.092$	0.07				$50.26 \pm 0.05$
TrES-1	b	$0.752 \pm 0.048$	1	$0.039 \pm 0.001$	0	90.0	30.0	TJ	$49.07 \pm 0.03$
TrES-2	b	$1.201 \pm 0.052$	1	$0.036 \pm 0.001$	0	83.6	-9.0	TJ	$49.28 \pm 0.03$
TrES-3	b	$1.910 \pm 0.078$	6	$0.023 \pm 0.000$	0	81.8		TJ	$49.37 \pm 0.02$
TrES-4	b	$0.925 \pm 0.082$	6	$0.051 \pm 0.001$	0	82.8	7.3	TJ	$49.32 \pm 0.04$
TrES-5	b	$1.778 \pm 0.080$	1	$0.025 \pm 0.000$	0	84.5		TJ	$49.35 \pm 0.02$
WASP-1	b	$0.918 \pm 0.091$	6	$0.039 \pm 0.001$	0	88.7	-79.0	TJ	$49.22 \pm 0.05$
WASP-4	b	$1.223 \pm 0.047$	1	$0.023 \pm 0.000$	0	89.5	4.0	TJ	$49.18 \pm 0.02$
WASP-5	b	$1.624 \pm 0.055$	1	$0.027 \pm 0.000$	0	86.1	12.1	TJ	$49.36 \pm 0.02$
WASP-6	b	$0.521 \pm 0.020$	1	$0.043 \pm 0.001$	0.05	88.5	-11.0	TJ	$48.94 \pm 0.02$
WASP-7	b	$0.919 \pm 0.127$	1	$0.060 \pm 0.001$	0	89.6	86.0	TJ	$49.32 \pm 0.06$
WASP-10	b	$3.191 \pm 0.116$	1	$0.038 \pm 0.001$	0.05	88.5		TJ	$49.67 \pm 0.02$
WASP-11	b	$0.540 \pm 0.052$	1	$0.044 \pm 0.001$	0	89.8		TJ	$48.93 \pm 0.04$
WASP-12	b	$1.361 \pm 0.051$	1	$0.023 \pm 0.000$	0.05	82.5	59.0	TJ	$49.29 \pm 0.02$
WASP-13	b	$0.474 \pm 0.034$	1	$0.054 \pm 0.001$	0	85.4	8.0	TJ	$48.99 \pm 0.03$
WASP-14	b	$7.692 \pm 0.293$	1	$0.037 \pm 0.001$	0.09	84.3	-33.1	TJ	$50.15 \pm 0.02$
WASP-15	b	$0.543 \pm 0.021$	1	$0.050 \pm 0.001$	0	86.0	-139.6	TJ	$49.05 \pm 0.02$
WASP-16	b	$0.842 \pm 0.032$	1	$0.042 \pm 0.001$	0	85.2	-4.2	TJ	$49.16 \pm 0.02$
WASP-17	b	$0.509 \pm 0.030$	1	$0.050 \pm 0.001$	0	86.6	-148.5	TJ	$49.02 \pm 0.03$
WASP-18	b	$10.201 \pm 0.336$	1	$0.020 \pm 0.000$	0.01	80.6	4.0	TJ	$50.13 \pm 0.02$
WASP-19	b	$1.133 \pm 0.039$	1	$0.016 \pm 0.000$	0.00	79.4	4.6	TJ	$49.07 \pm 0.02$
WASP-21	b	$0.300 \pm 0.013$	1	$0.052 \pm 0.001$	0	88.8		TJ	$48.77 \pm 0.02$
WASP-22	b	$0.559 \pm 0.103$	1	$0.047 \pm 0.004$	0.02	89.2	22.0	TJ	$49.03 \pm 0.11$
WASP-23	b	$0.872 \pm 0.094$	1	$0.037 \pm 0.002$	0	88.4		TJ	$49.10 \pm 0.07$

Continued on next page

Host Star	Planet	Mass ( $M_J$ )	Ref	$a$ (AU)	$e$	$i_p$ ( $^\circ$ )	$\lambda$ ( $^\circ$ )	Code	$\log J_p$ ( $\text{g cm}^2/\text{s}$ )
WASP-24	b	$1.091 \pm 0.041$	1	$0.037 \pm 0.001$	0	83.6	-4.7	TJ	$49.28 \pm 0.02$
WASP-25	b	$0.578 \pm 0.045$	1	$0.047 \pm 0.001$	0	88.0	14.6	TJ	$49.03 \pm 0.04$
WASP-26	b	$1.017 \pm 0.224$	1	$0.040 \pm 0.001$	0	82.5	-34.0	TJ	$49.26 \pm 0.10$
WASP-29	b	$0.243 \pm 0.020$	1	$0.046 \pm 0.001$	0.03	88.8		TJ	$48.60 \pm 0.04$
WASP-32	b	$3.454 \pm 0.139$	1	$0.039 \pm 0.001$	0	85.1	-2.0	TJ	$49.78 \pm 0.02$
WASP-33	b	$3.361 \pm 2.050$	5	$0.026 \pm 0.000$	0	87.7	-108.8	TJ	$49.74 \pm 0.31$
WASP-34	b	$0.583 \pm 0.029$	1	$0.052 \pm 0.001$	0.04	85.2		TJ	$49.05 \pm 0.03$
WASP-35	b	$0.717 \pm 0.059$	1	$0.043 \pm 0.001$	0	88.0		TJ	$49.12 \pm 0.04$
WASP-36	b	$2.269 \pm 0.089$	1	$0.026 \pm 0.000$	0	83.7		TJ	$49.50 \pm 0.02$
WASP-37	b	$1.794 \pm 0.166$	1	$0.045 \pm 0.002$	0	88.8		TJ	$49.49 \pm 0.06$
WASP-38	b	$2.709 \pm 0.100$	1	$0.076 \pm 0.001$	0.03	89.5	7.5	TJ	$49.84 \pm 0.02$
WASP-39	b	$0.284 \pm 0.031$	1	$0.049 \pm 0.001$	0	87.8		TJ	$48.71 \pm 0.05$
WASP-41	b	$0.932 \pm 0.059$	1	$0.040 \pm 0.001$	0	87.7		TJ	$49.19 \pm 0.04$
WASP-42	b	$0.497 \pm 0.034$	1	$0.055 \pm 0.002$	0	88.3		TJ	$48.97 \pm 0.04$
WASP-43	b	$1.776 \pm 0.103$	1	$0.014 \pm 0.000$	0	82.6		TJ	$49.14 \pm 0.04$
WASP-44	b	$0.890 \pm 0.065$	1	$0.035 \pm 0.001$	0	86.0		TJ	$49.14 \pm 0.03$
WASP-45	b	$1.007 \pm 0.052$	1	$0.041 \pm 0.001$	0	84.5		TJ	$49.21 \pm 0.03$
WASP-46	b	$2.102 \pm 0.088$	1	$0.024 \pm 0.000$	0	82.6		TJ	$49.44 \pm 0.02$
WASP-47	b	$1.136 \pm 0.056$	1	$0.052 \pm 0.001$	0	89.2		TJ	$49.36 \pm 0.03$
WASP-48	b	$0.984 \pm 0.086$	1	$0.034 \pm 0.001$	0	80.1		TJ	$49.23 \pm 0.04$
WASP-49	b	$0.378 \pm 0.026$	1	$0.038 \pm 0.001$	0	84.9		TJ	$48.78 \pm 0.04$
WASP-50	b	$1.472 \pm 0.088$	1	$0.029 \pm 0.001$	0.01	84.0		TJ	$49.31 \pm 0.04$
WASP-52	b	$0.457 \pm 0.022$	1	$0.027 \pm 0.000$	0	85.3	24.0	TJ	$48.77 \pm 0.03$
WASP-54	b	$0.633 \pm 0.027$	1	$0.050 \pm 0.001$	0.07	85.0		TJ	$49.12 \pm 0.02$
WASP-55	b	$0.571 \pm 0.038$	1	$0.053 \pm 0.001$	0	89.6		TJ	$49.05 \pm 0.03$
WASP-56	b	$0.605 \pm 0.040$	1	$0.056 \pm 0.001$	0	88.5		TJ	$49.11 \pm 0.03$
WASP-57	b	$0.676 \pm 0.052$	1	$0.039 \pm 0.001$	0	88.0		TJ	$49.04 \pm 0.04$
WASP-58	b	$0.891 \pm 0.071$	1	$0.056 \pm 0.002$	0	87.4		TJ	$49.24 \pm 0.05$
WASP-59	b	$0.859 \pm 0.045$	1	$0.070 \pm 0.001$	0.10	89.3		TJ	$49.21 \pm 0.03$
WASP-60	b	$0.512 \pm 0.036$	1	$0.053 \pm 0.001$	0	87.9		TJ	$49.02 \pm 0.03$
WASP-61	b	$2.055 \pm 0.079$	1	$0.051 \pm 0.001$	0	89.3		TJ	$49.64 \pm 0.02$
WASP-62	b	$0.562 \pm 0.042$	1	$0.057 \pm 0.001$	0	88.3		TJ	$49.10 \pm 0.04$
WASP-63	b	$0.378 \pm 0.032$	1	$0.057 \pm 0.001$	0	87.8		TJ	$48.95 \pm 0.04$
WASP-64	b	$1.271 \pm 0.076$	1	$0.027 \pm 0.000$	0	86.6		TJ	$49.24 \pm 0.03$
WASP-66	b	$2.313 \pm 0.132$	1	$0.055 \pm 0.001$	0	85.9		TJ	$49.72 \pm 0.03$
WASP-67	b	$0.419 \pm 0.033$	1	$0.052 \pm 0.001$	0	85.8		TJ	$48.88 \pm 0.04$
WASP-71	b	$2.257 \pm 0.083$	1	$0.046 \pm 0.001$	0	84.2	19.8	TJ	$49.71 \pm 0.02$
WASP-72	b	$1.408 \pm 0.059$	1	$0.037 \pm 0.001$	0	86.8		TJ	$49.42 \pm 0.02$
WASP-75	b	$1.070 \pm 0.050$	6	$0.038 \pm 0.001$	0	82.0		TJ	$49.27 \pm 0.03$
WASP-78	b	$0.884 \pm 0.081$	1	$0.036 \pm 0.001$	0	83.2		TJ	$49.21 \pm 0.04$
WASP-79	b	$0.888 \pm 0.084$	1	$0.053 \pm 0.001$	0	85.4	-106.0	TJ	$49.33 \pm 0.04$
WASP-80	b	$0.552 \pm 0.035$	1	$0.034 \pm 0.001$	0	89.9		TJ	$48.82 \pm 0.04$
WASP-103	b	$1.488 \pm 0.096$	1	$0.020 \pm 0.000$	0	86.3		TJ	$49.29 \pm 0.03$
WTS-1	b	$3.999 \pm 0.359$	1	$0.047 \pm 0.001$	0.05	85.5		TJ	$49.90 \pm 0.05$
xi Aql	b	$1.779 \pm 0.271$	2	$0.538 \pm 0.040$	0				$50.07 \pm 0.09$
XO-1	b	$0.918 \pm 0.079$	1	$0.049 \pm 0.001$	0	88.8		TJ	$49.24 \pm 0.04$

Continued on next page

Host Star	Planet	Mass ( $M_J$ )	Ref	$a$ (AU)	$e$	$i_p$ ( $^\circ$ )	$\lambda$ ( $^\circ$ )	Code	$\log J_p$ ( $\text{g cm}^2/\text{s}$ )
XO-3	b	$13.285 \pm 0.444$	1	$0.048 \pm 0.001$	0.29	79.3	37.3	TJ	$50.45 \pm 0.02$
XO-5	b	$1.153 \pm 0.088$	1	$0.051 \pm 0.001$	0	86.9		TJ	$49.34 \pm 0.04$

## Appendix E

# System Properties

The columns of Table E.1, from left to right, are: star name; stellar mass in solar masses; stellar evolutionary classification (see Section 3.5 for method), MS = Main Sequence, S = Subgiant, and G = Giant; code identifying whether the system contains a hot Jupiter (J), hot Neptune (N), and/or whether the system is transiting (T); log of the stellar angular momentum in  $\text{g} \cdot \text{cm}^2 \cdot \text{s}^{-1}$ ; log of the sum of planetary angular momentum for the system in  $\text{g} \cdot \text{cm}^2 \cdot \text{s}^{-1}$ , with uncertainties; log of the system angular momentum in  $\text{g} \cdot \text{cm}^2 \cdot \text{s}^{-1}$ , with uncertainties; number of confirmed planets in the system (left blank for n=1); proportion of system angular momentum contained in the planet(s),  $K$ ; and log of the ratio of planetary to stellar angular momentum,  $\mathcal{L}$ . See Equation 4.7 for method of calculation of log-uncertainties.

TABLE E.1: System Parameters

Host Star Name	Mass $M_{\odot}$	Class	Code	$\log J_*$ ( $\text{g cm}^2/\text{s}$ )	$\log \sum J_p$ ( $\text{g cm}^2/\text{s}$ )	$\log J_{sys}$ ( $\text{g cm}^2/\text{s}$ )	n	$K$	$\mathcal{L}$
11 UMi	1.80	G		50.39	$51.19 \pm 0.06$	$51.26 \pm 0.06$		0.863	0.80
14 And	2.15	G		50.11	$50.72 \pm 0.03$	$50.82 \pm 0.04$		0.804	0.61
14 Her	1.07	MS		48.14	$50.86 \pm 0.04$	$50.86 \pm 0.04$		0.998	2.72
24 Sex	1.81	S		49.40	$50.68 \pm 0.03$	$50.70 \pm 0.03$	2	0.950	1.28
47 UMa	1.06	MS		48.48	$50.61 \pm 0.02$	$50.62 \pm 0.02$	2	0.993	2.13

Continued on next page

Host Star Name	Mass ( $M_{\odot}$ )	Class	Code	$\log J_*$ ( $\text{g cm}^2/\text{s}$ )	$\log \sum J_p$ ( $\text{g cm}^2/\text{s}$ )	$\log J_{sys}$ ( $\text{g cm}^2/\text{s}$ )	n	$K$	$\mathcal{L}$
51 Peg	1.05	S	J	48.59	$48.96 \pm 0.02$	$49.11 \pm 0.04$		0.703	0.37
6 Lyn	1.82	S		49.23	$50.57 \pm 0.04$	$50.59 \pm 0.03$		0.957	1.35
61 Vir	0.94	MS	N	48.34	$48.73 \pm 0.04$	$48.88 \pm 0.06$	3	0.710	0.39
7 CMa	1.34	S		48.67	$50.50 \pm 0.06$	$50.51 \pm 0.06$		0.985	1.83
70 Vir	1.10	MS		48.61	$50.63 \pm 0.02$	$50.63 \pm 0.02$		0.990	2.02
75 Cet	2.15	G		49.91	$50.68 \pm 0.04$	$50.75 \pm 0.04$		0.856	0.77
81 Cet	1.74	G		50.00	$50.85 \pm 0.05$	$50.91 \pm 0.05$		0.876	0.85
91 Aqr	1.32	G		50.05	$50.39 \pm 0.11$	$50.56 \pm 0.08$		0.688	0.34
alpha Ari	1.33	G		50.05	$50.24 \pm 0.07$	$50.46 \pm 0.08$		0.605	0.18
BD -08 2823	0.74	MS	N	48.30	$49.30 \pm 0.05$	$49.34 \pm 0.05$	2	0.909	1.00
BD -10 3166	0.92	MS	J	47.85	$48.86 \pm 0.02$	$48.90 \pm 0.03$		0.912	1.02
BD +14 4559	0.86	MS		48.28	$50.00 \pm 0.07$	$50.01 \pm 0.07$		0.981	1.72
BD +20 2457	1.06	G		49.82	$51.25 \pm 0.06$	$51.26 \pm 0.06$	2	0.964	1.43
BD +48 738	1.19	G		49.13	$50.08 \pm 0.09$	$50.13 \pm 0.08$		0.899	0.95
CoRoT-1	0.95	MS	TJ	48.77	$49.13 \pm 0.07$	$49.29 \pm 0.06$		0.699	0.37
CoRoT-2	0.97	MS	TJ	49.03	$49.66 \pm 0.03$	$49.75 \pm 0.03$		0.811	0.63
CoRoT-3	1.37	MS	TJ	49.36	$50.72 \pm 0.03$	$50.74 \pm 0.03$		0.958	1.36
CoRoT-4	1.16	MS	TJ	48.84	$49.29 \pm 0.05$	$49.42 \pm 0.04$		0.739	0.45
CoRoT-5	1.00	MS	TJ	48.07	$48.94 \pm 0.04$	$48.99 \pm 0.04$		0.881	0.87
CoRoT-6	1.05	MS	TJ	48.87	$49.87 \pm 0.05$	$49.91 \pm 0.05$		0.910	1.00
CoRoT-7	0.93	MS	TN	48.49	$47.18 \pm 0.10$	$48.51 \pm 0.15$		0.046	-1.32
CoRoT-8	0.88	MS	TJ	48.21	$48.64 \pm 0.07$	$48.77 \pm 0.08$		0.729	0.43
CoRoT-10	0.89	MS	T	48.21	$49.78 \pm 0.03$	$49.79 \pm 0.03$		0.974	1.57
CoRoT-11	1.27	MS	TJ	49.69	$49.67 \pm 0.07$	$49.98 \pm 0.05$		0.491	-0.02
CoRoT-12	1.08	MS	TJ	48.03	$49.21 \pm 0.04$	$49.24 \pm 0.04$		0.938	1.18
CoRoT-13	1.09	MS	TJ	48.58	$49.42 \pm 0.03$	$49.48 \pm 0.03$		0.872	0.83
CoRoT-14	1.13	MS	TJ	49.01	$50.06 \pm 0.03$	$50.09 \pm 0.03$		0.918	1.05
CoRoT-16	1.10	MS	TJ	47.75	$49.05 \pm 0.07$	$49.07 \pm 0.07$		0.952	1.30
CoRoT-17	1.04	MS	TJ	48.82	$49.67 \pm 0.06$	$49.73 \pm 0.05$		0.876	0.85
CoRoT-18	0.95	MS	TJ	48.91	$49.69 \pm 0.07$	$49.76 \pm 0.06$		0.859	0.79
CoRoT-19	1.21	MS	TJ	48.95	$49.37 \pm 0.03$	$49.51 \pm 0.03$		0.722	0.42
CoRoT-23	1.14	MS	TJ	49.13	$49.78 \pm 0.05$	$49.87 \pm 0.04$		0.817	0.65
CoRoT-25	1.09	MS	TJ	48.69	$48.76 \pm 0.07$	$49.03 \pm 0.05$		0.541	0.07
CoRoT-26	1.09	S	TJ	48.73	$48.99 \pm 0.07$	$49.18 \pm 0.10$		0.643	0.26
CoRoT-27	1.05	MS	TJ	48.62	$50.29 \pm 0.04$	$50.30 \pm 0.04$		0.979	1.67
epsilon CrB	1.44	G		50.31	$50.83 \pm 0.05$	$50.95 \pm 0.05$		0.769	0.52
epsilon Eri	0.82	MS		48.29	$50.16 \pm 0.13$	$50.16 \pm 0.13$		0.987	1.87
epsilon Tau	2.73	G		50.24	$51.17 \pm 0.02$	$51.22 \pm 0.03$		0.895	0.93
eta Cet	1.70	G		50.28	$50.91 \pm 0.07$	$51.00 \pm 0.06$	2	0.812	0.64
HAT-P-2	1.31	MS	TJ	49.44	$50.28 \pm 0.03$	$50.34 \pm 0.02$		0.874	0.84
HAT-P-3	0.93	MS	TJ	47.63	$48.98 \pm 0.02$	$49.00 \pm 0.02$		0.958	1.35
HAT-P-6	1.29	MS	TJ	49.05	$49.37 \pm 0.03$	$49.54 \pm 0.03$		0.675	0.32
HAT-P-7	1.50	MS	TJ	48.79	$49.56 \pm 0.02$	$49.63 \pm 0.02$		0.853	0.76
HAT-P-8	1.28	MS	TJ	49.21	$49.42 \pm 0.02$	$49.63 \pm 0.02$		0.620	0.21
HAT-P-9	1.28	MS	TJ	49.14	$49.23 \pm 0.06$	$49.49 \pm 0.05$		0.551	0.09
HAT-P-11	0.81	MS	TN	48.09	$48.15 \pm 0.05$	$48.42 \pm 0.08$		0.537	0.06

Continued on next page

Host Star Name	Mass ( $M_{\odot}$ )	Class	Code	$\log J_*$ ( $\text{g cm}^2/\text{s}$ )	$\log \sum J_p$ ( $\text{g cm}^2/\text{s}$ )	$\log J_{sys}$ ( $\text{g cm}^2/\text{s}$ )	n	$K$	$\mathcal{L}$
HAT-P-12	0.73	MS	TJ	47.60	$48.47 \pm 0.03$	$48.53 \pm 0.05$		0.883	0.88
HAT-P-13	1.22	S	TJ	48.87	$51.05 \pm 0.03$	$51.05 \pm 0.03$	2	0.993	2.18
HAT-P-14	1.39	MS	TJ	49.02	$49.74 \pm 0.02$	$49.81 \pm 0.02$		0.838	0.71
HAT-P-15	1.01	MS	TJ	48.33	$49.70 \pm 0.02$	$49.72 \pm 0.02$		0.960	1.38
HAT-P-16	1.22	MS	TJ	48.59	$49.90 \pm 0.02$	$49.92 \pm 0.02$		0.953	1.31
HAT-P-17	0.86	MS	TJ	47.42	$49.06 \pm 0.02$	$49.07 \pm 0.02$		0.978	1.64
HAT-P-18	0.77	MS	TJ	47.62	$48.54 \pm 0.03$	$48.59 \pm 0.03$		0.893	0.92
HAT-P-19	0.84	MS	TJ	47.79	$48.69 \pm 0.03$	$48.74 \pm 0.04$		0.889	0.90
HAT-P-20	0.76	MS	TJ	48.21	$50.01 \pm 0.02$	$50.02 \pm 0.02$		0.984	1.80
HAT-P-21	0.95	MS	TJ	48.59	$49.86 \pm 0.02$	$49.88 \pm 0.02$		0.949	1.27
HAT-P-22	0.92	MS	TJ	47.73	$49.55 \pm 0.02$	$49.56 \pm 0.02$		0.985	1.82
HAT-P-23	1.13	MS	TJ	48.96	$49.46 \pm 0.03$	$49.58 \pm 0.03$		0.758	0.50
HAT-P-24	1.19	MS	TJ	49.08	$49.13 \pm 0.03$	$49.41 \pm 0.03$		0.531	0.05
HAT-P-25	1.01	MS	TJ	47.67	$49.02 \pm 0.02$	$49.04 \pm 0.02$		0.957	1.34
HAT-P-26	0.82	MS	TN	48.18	$47.99 \pm 0.06$	$48.40 \pm 0.09$		0.389	-0.20
HAT-P-27	0.92	MS	TJ	47.73	$49.00 \pm 0.03$	$49.02 \pm 0.03$		0.949	1.27
HAT-P-28	1.02	MS	TJ	47.33	$49.05 \pm 0.03$	$49.06 \pm 0.03$		0.981	1.72
HAT-P-29	1.21	MS	TJ	48.64	$49.27 \pm 0.04$	$49.36 \pm 0.03$		0.811	0.63
HAT-P-30	1.24	MS	TJ	48.38	$49.14 \pm 0.03$	$49.21 \pm 0.03$		0.851	0.76
HAT-P-31	1.22	MS	TJ	47.79	$49.69 \pm 0.03$	$49.69 \pm 0.03$		0.987	1.90
HAT-P-33	1.38	MS	TJ	49.29	$49.23 \pm 0.06$	$49.56 \pm 0.04$		0.467	-0.06
HAT-P-34	1.39	MS	TJ	49.39	$49.89 \pm 0.03$	$50.01 \pm 0.03$		0.760	0.50
HAT-P-35	1.24	MS	TJ	47.81	$49.34 \pm 0.02$	$49.36 \pm 0.02$		0.972	1.53
HAT-P-36	1.02	MS	TJ	48.58	$49.38 \pm 0.03$	$49.45 \pm 0.03$		0.863	0.80
HAT-P-37	0.93	MS	TJ	48.44	$49.27 \pm 0.04$	$49.33 \pm 0.04$		0.871	0.83
HAT-P-39	1.40	MS	TJ	49.25	$49.13 \pm 0.07$	$49.49 \pm 0.04$		0.435	-0.11
HAT-P-40	1.51	S	TJ	49.47	$49.20 \pm 0.08$	$49.66 \pm 0.09$		0.348	-0.27
HAT-P-41	1.42	MS	TJ	49.45	$49.22 \pm 0.06$	$49.65 \pm 0.04$		0.373	-0.23
HAT-P-49	1.54	MS	TJ	49.38	$49.58 \pm 0.05$	$49.79 \pm 0.04$		0.613	0.20
HATS-1	0.99	MS	TJ	48.41	$49.52 \pm 0.06$	$49.55 \pm 0.06$		0.927	1.10
HATS-2	0.88	MS	TJ	48.15	$49.21 \pm 0.05$	$49.25 \pm 0.05$		0.921	1.06
HD 1461	1.03	MS	N	48.25	$47.71 \pm 0.10$	$48.36 \pm 0.13$		0.226	-0.53
HD 1502	1.47	S		49.36	$50.52 \pm 0.03$	$50.55 \pm 0.03$		0.935	1.16
HD 1690	1.18	G		50.23	$50.73 \pm 0.11$	$50.85 \pm 0.09$		0.762	0.50
HD 2039	1.12	S		48.76	$50.74 \pm 0.08$	$50.75 \pm 0.08$		0.990	1.98
HD 2952	2.54	G		50.05	$50.38 \pm 0.06$	$50.55 \pm 0.07$		0.683	0.33
HD 4203	1.13	MS		48.12	$50.24 \pm 0.03$	$50.24 \pm 0.03$		0.992	2.11
HD 4313	1.53	S		49.44	$50.38 \pm 0.03$	$50.43 \pm 0.03$		0.898	0.94
HD 4732	1.74	S		49.25	$50.92 \pm 0.04$	$50.93 \pm 0.04$	2	0.979	1.67
HD 5319	1.28	S		49.45	$50.31 \pm 0.07$	$50.37 \pm 0.06$		0.880	0.87
HD 5388	1.21	MS		48.69	$50.35 \pm 0.03$	$50.36 \pm \text{NA}$		0.978	1.65
HD 5608	1.66	S		49.20	$50.35 \pm 0.04$	$50.38 \pm 0.04$		0.933	1.14
HD 5891	1.09	S		49.95	$50.57 \pm 0.07$	$50.66 \pm 0.06$		0.807	0.62
HD 6718	0.96	MS		48.23	$50.38 \pm 0.06$	$50.39 \pm \text{NA}$		0.993	2.16
HD 7924	0.83	MS	N	48.04	$47.72 \pm 0.09$	$48.21 \pm 0.12$		0.324	-0.32
HD 8535	1.13	MS		48.14	$49.98 \pm 0.04$	$49.98 \pm \text{NA}$		0.986	1.84

Continued on next page

Host Star Name	Mass ( $M_{\odot}$ )	Class	Code	$\log J_*$ (g cm <sup>2</sup> /s)	$\log \sum J_p$ (g cm <sup>2</sup> /s)	$\log J_{sys}$ (g cm <sup>2</sup> /s)	n	$K$	$\mathcal{L}$
HD 8574	1.12	MS		48.78	50.13 ± 0.02	50.15 ± 0.02		0.957	1.35
HD 9446	1.00	MS		48.56	50.17 ± 0.04	50.18 ± 0.04	2	0.976	1.61
HD 10180	1.06	MS	N	48.20	49.70 ± 0.03	49.71 ± 0.03	6	0.969	1.49
HD 10647	1.09	MS		48.80	50.06 ± 0.12	50.08 ± 0.12		0.948	1.26
HD 10697	1.11	S		48.77	50.91 ± 0.02	50.91 ± 0.02		0.993	2.14
HD 11506	1.19	MS		48.76	50.83 ± 0.04	50.83 ± 0.04		0.991	2.07
HD 11977	2.31	G		49.96	51.10 ± 0.04	51.13 ± 0.04		0.932	1.14
HD 12661	1.14	MS		48.11	50.68 ± 0.02	50.68 ± 0.02	2	0.997	2.57
HD 13189	1.17	G		50.19	50.85 ± 0.09	50.93 ± 0.07		0.820	0.66
HD 13908	1.29	MS		48.79	50.86 ± 0.03	50.87 ± 0.03	2	0.992	2.07
HD 13931	1.02	MS		48.38	50.56 ± 0.08	50.57 ± 0.08		0.993	2.18
HD 16175	1.29	MS		48.71	50.69 ± 0.08	50.69 ± 0.08		0.990	1.98
HD 16417	1.12	MS		48.46	48.33 ± 0.04	48.70 ± 0.09		0.428	-0.13
HD 16760	0.78	MS		48.45	51.01 ± 0.03	51.02 ± 0.03		0.997	2.57
HD 17156	1.28	MS	T	48.57	49.97 ± 0.02	49.99 ± 0.02		0.962	1.40
HD 18742	1.73	S		49.57	50.65 ± 0.06	50.68 ± 0.06		0.924	1.08
HD 20794	0.70	MS		48.33	48.03 ± 0.04	48.50 ± NA	3	0.334	-0.30
HD 20868	0.78	S		48.19	49.99 ± 0.02	49.99 ± 0.02		0.984	1.79
HD 22781	0.75	MS		48.14	50.80 ± 0.02	50.80 ± 0.02		0.998	2.65
HD 23079	1.01	MS		48.53	50.42 ± 0.02	50.42 ± 0.02		0.987	1.88
HD 23127	1.13	MS		48.67	50.24 ± 0.04	50.25 ± 0.04		0.974	1.57
HD 23596	1.16	S		49.12	51.05 ± 0.02	51.06 ± 0.02		0.989	1.94
HD 24040	1.18	MS		48.40	50.91 ± 0.05	50.91 ± 0.05		0.997	2.51
HD 25171	1.09	MS		48.01	50.17 ± 0.13	50.17 ± 0.13		0.993	2.16
HD 28678	2.03	S		49.69	50.41 ± 0.05	50.49 ± 0.05		0.842	0.73
HD 30177	0.95	MS		48.56	51.18 ± 0.04	51.19 ± 0.04		0.998	2.63
HD 30562	1.28	MS		48.73	50.10 ± 0.06	50.12 ± 0.06		0.960	1.38
HD 30856	1.36	G		49.63	50.41 ± 0.05	50.48 ± 0.05		0.858	0.78
HD 31253	1.23	MS		48.75	49.70 ± 0.08	49.75 ± 0.07		0.899	0.95
HD 32518	1.13	G		49.80	50.37 ± 0.07	50.47 ± 0.06		0.787	0.57
HD 33142	1.62	G		49.63	50.20 ± 0.04	50.30 ± 0.04		0.788	0.57
HD 33283	1.24	MS		48.62	49.02 ± 0.05	49.16 ± 0.04		0.713	0.40
HD 33636	1.02	MS		48.49	51.10 ± 0.02	51.10 ± 0.02		0.998	2.60
HD 37124	0.85	MS		48.00	50.28 ± 0.03	50.29 ± 0.03	3	0.995	2.29
HD 37605	1.00	MS		47.66	50.81 ± 0.19	50.81 ± 0.19	2	0.999	3.16
HD 38283	1.08	MS		48.63	49.44 ± 0.05	49.50 ± 0.05		0.865	0.81
HD 38801	1.22	S		48.30	51.08 ± 0.03	51.08 ± 0.03		0.998	2.78
HD 39091	1.07	MS		48.54	51.09 ± 0.04	51.09 ± 0.04		0.997	2.56
HD 43197	0.96	MS		48.42	49.42 ± 0.11	49.46 ± NA		0.910	1.00
HD 44219	1.00	MS		48.48	49.63 ± 0.08	49.66 ± NA		0.935	1.16
HD 45350	1.05	S		48.38	50.15 ± 0.03	50.15 ± 0.03		0.983	1.77
HD 45364	0.82	MS		48.04	49.77 ± 0.02	49.78 ± 0.02	2	0.982	1.73
HD 45652	0.83	MS		48.39	49.20 ± 0.04	49.26 ± 0.04		0.868	0.82
HD 47186	0.99	MS	N	48.39	49.66 ± 0.10	49.68 ± 0.09	2	0.948	1.26
HD 49674	1.01	MS	J	47.56	48.31 ± 0.04	48.38 ± 0.04		0.850	0.75
HD 50499	1.28	MS		48.65	50.50 ± 0.04	50.51 ± 0.04		0.986	1.86

Continued on next page

Host Star Name	Mass ( $M_{\odot}$ )	Class	Code	$\log J_*$ ( $\text{g cm}^2/\text{s}$ )	$\log \sum J_p$ ( $\text{g cm}^2/\text{s}$ )	$\log J_{sys}$ ( $\text{g cm}^2/\text{s}$ )	n	$K$	$\mathcal{L}$
HD 50554	1.02	MS		48.68	$50.71 \pm 0.04$	$50.71 \pm 0.04$		0.991	2.03
HD 52265	1.17	MS		48.76	$49.82 \pm 0.04$	$49.85 \pm 0.04$		0.919	1.05
HD 60532	1.44	S		49.55	$50.60 \pm 0.03$	$50.64 \pm 0.03$	2	0.919	1.06
HD 63765	0.86	MS		48.22	$49.68 \pm 0.03$	$49.69 \pm 0.03$		0.966	1.46
HD 68988	1.12	MS	J	48.47	$49.62 \pm 0.03$	$49.65 \pm 0.03$		0.934	1.15
HD 69830	0.85	MS	N	47.43	$48.73 \pm 0.03$	$48.75 \pm 0.03$	3	0.952	1.30
HD 70642	1.00	MS		47.48	$50.46 \pm 0.03$	$50.46 \pm 0.03$		0.999	2.97
HD 72659	1.07	MS		48.45	$50.77 \pm 0.03$	$50.77 \pm 0.03$		0.995	2.32
HD 73267	0.89	MS		48.30	$50.54 \pm 0.02$	$50.55 \pm 0.02$		0.994	2.24
HD 73526	1.01	MS		48.57	$50.60 \pm 0.02$	$50.61 \pm 0.02$	2	0.991	2.03
HD 73534	1.17	S		48.36	$50.23 \pm 0.04$	$50.23 \pm 0.04$		0.987	1.87
HD 74156	1.24	MS		48.72	$51.17 \pm 0.02$	$51.17 \pm 0.02$	2	0.996	2.45
HD 75898	1.28	MS		48.79	$50.42 \pm 0.05$	$50.43 \pm 0.05$		0.977	1.62
HD 76700	1.13	MS	J	48.19	$48.67 \pm 0.04$	$48.80 \pm 0.05$		0.751	0.48
HD 77338	0.93	MS	N	48.32	$48.00 \pm 0.13$	$48.49 \pm 0.06$		0.324	-0.32
HD 81040	0.96	MS		48.27	$50.83 \pm 0.03$	$50.83 \pm 0.03$		0.997	2.56
HD 81688	2.10	G		50.03	$50.47 \pm 0.02$	$50.61 \pm \text{NA}$		0.737	0.45
HD 82886	1.06	S		48.39	$50.15 \pm 0.07$	$50.16 \pm 0.07$		0.983	1.77
HD 82943	1.13	MS		48.14	$50.44 \pm 0.02$	$50.44 \pm 0.02$	2	0.995	2.30
HD 83443	0.99	MS	J	48.08	$48.83 \pm 0.02$	$48.90 \pm 0.03$		0.849	0.75
HD 85390	0.76	MS		48.03	$49.04 \pm 0.06$	$49.08 \pm \text{NA}$		0.911	1.01
HD 86081	1.21	MS	J	48.66	$49.41 \pm 0.02$	$49.48 \pm 0.02$		0.851	0.76
HD 86264	1.40	MS		49.20	$50.90 \pm 0.14$	$50.91 \pm 0.14$		0.980	1.70
HD 87883	0.80	MS		48.26	$50.33 \pm 0.08$	$50.33 \pm 0.08$		0.991	2.07
HD 88133	1.18	S	J	48.83	$48.77 \pm 0.04$	$49.10 \pm 0.08$		0.461	-0.07
HD 89307	0.99	MS		48.56	$50.43 \pm 0.04$	$50.43 \pm 0.04$		0.986	1.86
HD 92788	1.08	MS		47.30	$50.46 \pm 0.02$	$50.46 \pm 0.02$		0.999	3.16
HD 95089	1.38	S		49.45	$50.12 \pm 0.06$	$50.20 \pm 0.05$		0.823	0.67
HD 96063	1.41	S		48.77	$50.08 \pm 0.07$	$50.10 \pm 0.07$		0.953	1.31
HD 96127	0.91	G		48.98	$50.57 \pm 0.13$	$50.58 \pm 0.12$		0.975	1.59
HD 96167	1.31	MS		48.82	$49.73 \pm 0.06$	$49.78 \pm 0.05$		0.891	0.91
HD 97658	0.75	MS	TN	47.59	$47.71 \pm 0.04$	$47.96 \pm 0.07$		0.564	0.11
HD 98219	1.62	S		48.26	$50.42 \pm 0.04$	$50.42 \pm 0.03$		0.993	2.15
HD 99109	0.94	MS		48.26	$49.64 \pm 0.07$	$49.66 \pm 0.07$		0.959	1.37
HD 99706	1.72	S		49.01	$50.32 \pm 0.07$	$50.35 \pm 0.06$		0.954	1.31
HD 100655	1.71	G		49.72	$50.08 \pm 0.09$	$50.24 \pm 0.11$		0.700	0.37
HD 100777	1.00	MS		48.28	$49.97 \pm 0.04$	$49.98 \pm 0.04$		0.980	1.69
HD 102117	1.08	MS		47.98	$48.76 \pm 0.04$	$48.83 \pm 0.05$		0.859	0.78
HD 102195	0.87	MS	J	48.41	$48.89 \pm 0.02$	$49.02 \pm \text{NA}$		0.754	0.49
HD 102329	1.30	G		49.69	$50.75 \pm 0.05$	$50.79 \pm 0.05$		0.921	1.07
HD 102365	0.89	MS		47.78	$48.42 \pm 0.07$	$48.51 \pm 0.06$		0.812	0.64
HD 102956	1.68	S	J	48.34	$49.47 \pm 0.03$	$49.50 \pm 0.03$		0.931	1.13
HD 103197	0.90	MS		48.32	$48.59 \pm 0.03$	$48.78 \pm \text{NA}$		0.652	0.27
HD 103774	1.34	MS	J	49.01	$48.98 \pm 0.03$	$49.29 \pm 0.08$		0.484	-0.03
HD 104067	0.79	MS		48.18	$48.86 \pm 0.03$	$48.94 \pm 0.04$		0.826	0.68
HD 104985	1.04	G		49.36	$50.54 \pm 0.11$	$50.57 \pm 0.10$		0.938	1.18

Continued on next page

Host Star Name	Mass ( $M_{\odot}$ )	Class	Code	$\log J_*$ ( $\text{g cm}^2/\text{s}$ )	$\log \sum J_p$ ( $\text{g cm}^2/\text{s}$ )	$\log J_{sys}$ ( $\text{g cm}^2/\text{s}$ )	n	$K$	$\mathcal{L}$
HD 106252	1.01	MS		48.33	$50.92 \pm 0.02$	$50.92 \pm 0.02$		0.997	2.59
HD 106270	1.33	S		49.17	$51.32 \pm 0.11$	$51.32 \pm 0.11$		0.993	2.15
HD 107148	1.14	MS		47.85	$49.00 \pm 0.08$	$49.03 \pm 0.08$		0.933	1.15
HD 108147	1.17	MS		48.86	$48.80 \pm 0.12$	$49.14 \pm 0.06$		0.466	-0.06
HD 108863	2.08	G		49.51	$50.61 \pm 0.03$	$50.64 \pm 0.03$		0.926	1.10
HD 108874	0.95	MS		48.40	$50.38 \pm 0.02$	$50.39 \pm 0.02$	2	0.990	1.98
HD 109246	1.01	MS		48.47	$49.57 \pm 0.05$	$49.60 \pm 0.05$		0.926	1.10
HD 113337	1.40	MS		48.91	$50.41 \pm 0.05$	$50.42 \pm 0.05$		0.969	1.50
HD 114386	0.78	MS		47.62	$50.12 \pm 0.03$	$50.12 \pm 0.03$		0.997	2.50
HD 114613	1.36	S		48.97	$50.05 \pm 0.04$	$50.08 \pm \text{NA}$		0.923	1.08
HD 114783	0.85	MS		47.88	$49.96 \pm 0.02$	$49.97 \pm 0.02$		0.992	2.08
HD 116029	1.33	G		48.79	$50.38 \pm 0.05$	$50.39 \pm 0.05$		0.975	1.59
HD 117207	1.03	S		48.16	$50.48 \pm 0.03$	$50.48 \pm 0.03$		0.995	2.32
HD 117618	1.07	MS		48.55	$48.77 \pm 0.09$	$48.97 \pm 0.06$		0.622	0.22
HD 118203	1.23	S	J	49.22	$49.70 \pm 0.02$	$49.83 \pm 0.05$		0.752	0.48
HD 120084	2.39	G		50.11	$50.96 \pm 1.43$	$51.02 \pm 0.59$		0.877	0.85
HD 125595	0.76	MS	N	48.24	$47.94 \pm 0.05$	$48.41 \pm 0.10$		0.336	-0.30
HD 128311	0.83	MS		48.36	$50.63 \pm 0.02$	$50.64 \pm 0.02$	2	0.995	2.28
HD 130322	0.84	MS	J	48.23	$49.38 \pm 0.02$	$49.41 \pm 0.02$		0.935	1.16
HD 131496	1.61	S		48.66	$50.54 \pm 0.05$	$50.54 \pm 0.05$		0.987	1.88
HD 131664	1.10	MS		48.47	$51.35 \pm 0.04$	$51.35 \pm 0.04$		0.999	2.88
HD 134987	1.05	MS		48.39	$50.46 \pm 0.04$	$50.46 \pm 0.04$	2	0.992	2.07
HD 136118	1.19	MS		49.07	$51.19 \pm 0.02$	$51.19 \pm 0.02$		0.992	2.12
HD 136418	1.33	S		49.05	$50.33 \pm 0.03$	$50.35 \pm 0.03$		0.950	1.28
HD 141937	1.05	MS		48.29	$50.96 \pm 0.02$	$50.96 \pm 0.02$		0.998	2.68
HD 142245	1.69	S		49.41	$50.53 \pm 0.06$	$50.57 \pm 0.06$		0.930	1.12
HD 142415	1.06	MS		48.57	$50.11 \pm 0.03$	$50.12 \pm 0.03$		0.972	1.55
HD 145377	1.12	MS		48.56	$50.52 \pm 0.02$	$50.52 \pm 0.02$		0.989	1.96
HD 147018	0.93	MS		48.22	$50.91 \pm 0.03$	$50.91 \pm 0.02$	2	0.998	2.69
HD 148156	1.22	MS		48.70	$49.99 \pm 0.04$	$50.02 \pm \text{NA}$		0.952	1.30
HD 148427	1.36	S		49.17	$50.06 \pm 0.04$	$50.11 \pm 0.04$		0.885	0.89
HD 149026	1.29	S	TJ	49.15	$48.86 \pm 0.02$	$49.33 \pm 0.07$		0.339	-0.29
HD 149143	1.20	S	J	49.04	$49.45 \pm 0.04$	$49.60 \pm 0.04$		0.719	0.41
HD 152581	0.93	S		48.41	$50.17 \pm 0.06$	$50.18 \pm 0.06$		0.983	1.76
HD 153950	1.12	MS		48.51	$50.42 \pm 0.02$	$50.42 \pm 0.02$		0.988	1.91
HD 154345	0.89	MS		48.10	$50.20 \pm 0.04$	$50.20 \pm 0.04$		0.992	2.10
HD 154672	1.06	S		48.02	$50.43 \pm 0.04$	$50.43 \pm 0.04$		0.996	2.41
HD 154857	1.72	MS		48.35	$50.96 \pm 0.03$	$50.96 \pm 0.03$	2	0.998	2.61
HD 156279	0.93	MS		48.39	$50.60 \pm 0.03$	$50.60 \pm 0.03$		0.994	2.21
HD 156411	1.24	S		49.01	$49.96 \pm 0.04$	$50.01 \pm 0.04$		0.901	0.96
HD 156668	0.77	MS	N	47.60	$47.34 \pm 0.06$	$47.79 \pm 0.07$		0.350	-0.27
HD 158038	1.65	G		49.47	$50.36 \pm 0.05$	$50.41 \pm 0.05$		0.885	0.88
HD 159243	1.12	MS		48.60	$50.27 \pm 0.03$	$50.28 \pm 0.03$	2	0.979	1.67
HD 159868	1.16	MS		48.56	$50.57 \pm 0.02$	$50.57 \pm 0.02$	2	0.990	2.01
HD 162020	0.80	MS	J	48.12	$50.48 \pm 0.02$	$50.49 \pm 0.02$		0.996	2.36
HD 163607	1.09	S		48.58	$50.53 \pm 0.02$	$50.54 \pm 0.02$	2	0.989	1.95

Continued on next page

Host Star Name	Mass ( $M_{\odot}$ )	Class	Code	$\log J_*$ ( $\text{g cm}^2/\text{s}$ )	$\log \sum J_p$ ( $\text{g cm}^2/\text{s}$ )	$\log J_{sys}$ ( $\text{g cm}^2/\text{s}$ )	n	$K$	$\mathcal{L}$
HD 164509	1.13	MS		48.38	$49.59 \pm 0.09$	$49.62 \pm 0.08$		0.943	1.22
HD 164922	0.93	MS		48.23	$49.63 \pm 0.08$	$49.64 \pm 0.07$		0.961	1.40
HD 167042	1.63	G		49.33	$50.30 \pm 0.03$	$50.35 \pm 0.03$		0.904	0.98
HD 168443	1.00	MS		48.54	$51.43 \pm 0.02$	$51.44 \pm 0.02$	2	0.999	2.90
HD 169830	1.41	MS		48.77	$50.99 \pm 0.07$	$50.99 \pm 0.07$	2	0.994	2.22
HD 170469	1.14	S		48.51	$49.95 \pm 0.07$	$49.97 \pm 0.07$		0.965	1.44
HD 171028	1.01	S		48.85	$50.20 \pm 0.03$	$50.21 \pm 0.03$		0.957	1.35
HD 171238	0.94	MS		48.20	$50.50 \pm 0.04$	$50.50 \pm 0.04$		0.995	2.30
HD 175541	1.34	S		49.20	$49.68 \pm 0.08$	$49.80 \pm 0.06$		0.752	0.48
HD 179079	1.09	S		48.00	$48.41 \pm 0.05$	$48.55 \pm 0.06$		0.716	0.40
HD 179949	1.18	MS	J	48.90	$49.24 \pm 0.02$	$49.40 \pm 0.02$		0.687	0.34
HD 180902	1.53	G		49.54	$50.28 \pm 0.06$	$50.35 \pm 0.05$		0.846	0.74
HD 181342	1.70	G		49.77	$50.66 \pm 0.05$	$50.71 \pm 0.05$		0.885	0.89
HD 181433	0.78	MS	N	48.22	$50.09 \pm 0.04$	$50.09 \pm 0.04$	3	0.987	1.87
HD 181720	0.92	MS		48.28	$49.60 \pm 0.03$	$49.62 \pm \text{NA}$		0.954	1.32
HD 183263	1.12	S		48.43	$51.00 \pm 0.03$	$51.00 \pm 0.03$	2	0.997	2.57
HD 187085	1.14	MS		48.79	$49.96 \pm 0.11$	$49.99 \pm 0.10$		0.936	1.17
HD 187123	1.04	MS	J	48.38	$50.56 \pm 0.09$	$50.57 \pm 0.09$	2	0.994	2.18
HD 190228	1.82	S		48.87	$50.97 \pm 0.03$	$50.97 \pm 0.03$		0.992	2.10
HD 190647	1.10	MS		48.51	$50.38 \pm 0.04$	$50.38 \pm 0.04$		0.987	1.87
HD 192263	0.80	MS		48.32	$49.28 \pm 0.03$	$49.32 \pm 0.03$		0.900	0.95
HD 192699	1.58	S		49.14	$50.41 \pm 0.03$	$50.43 \pm 0.03$		0.948	1.26
HD 200964	1.57	S		49.24	$50.61 \pm 0.04$	$50.62 \pm 0.04$	2	0.958	1.36
HD 202206	1.07	MS		48.34	$51.18 \pm 0.02$	$51.18 \pm 0.02$	2	0.999	2.84
HD 204313	1.04	MS		48.24	$50.89 \pm 0.04$	$50.89 \pm 0.04$	2	0.998	2.65
HD 205739	1.22	MS		48.77	$50.10 \pm 0.04$	$50.12 \pm 0.04$		0.955	1.33
HD 206610	1.30	S		49.45	$50.36 \pm 0.05$	$50.41 \pm 0.04$		0.891	0.91
HD 207832	0.94	MS		48.44	$50.07 \pm 0.08$	$50.08 \pm 0.08$	2	0.977	1.64
HD 208487	1.11	MS		48.72	$49.51 \pm 0.08$	$49.57 \pm 0.07$		0.859	0.79
HD 208527	1.60	G		50.69	$51.19 \pm 0.10$	$51.31 \pm 0.09$		0.761	0.50
HD 209458	1.13	MS	TJ	48.69	$49.13 \pm 0.02$	$49.26 \pm 0.02$		0.735	0.44
HD 210277	0.99	MS		48.23	$50.00 \pm 0.02$	$50.01 \pm 0.02$		0.983	1.77
HD 210702	1.71	S		49.28	$50.35 \pm 0.03$	$50.38 \pm 0.03$		0.921	1.07
HD 212771	1.51	S		49.45	$50.48 \pm 0.06$	$50.52 \pm 0.06$		0.915	1.03
HD 215497	0.87	MS	N	48.29	$49.41 \pm 0.04$	$49.44 \pm 0.04$	2	0.930	1.13
HD 216437	1.12	S		48.82	$50.46 \pm 0.03$	$50.47 \pm 0.03$		0.978	1.64
HD 217786	1.02	MS		48.20	$51.20 \pm 0.04$	$51.20 \pm 0.04$		0.999	3.00
HD 219828	1.24	S	N	48.85	$48.12 \pm 0.04$	$48.92 \pm \text{NA}$		0.159	-0.72
HD 220074	1.20	G		50.58	$51.11 \pm 0.10$	$51.23 \pm 0.09$		0.773	0.53
HD 221287	1.25	MS		48.61	$50.52 \pm 0.09$	$50.52 \pm 0.09$		0.988	1.91
HD 222155	1.13	MS		48.70	$50.61 \pm 0.15$	$50.62 \pm 0.15$		0.988	1.91
HD 224693	1.33	MS		48.55	$49.49 \pm 0.04$	$49.53 \pm 0.03$		0.895	0.93
HD 231701	1.14	MS		48.67	$49.86 \pm 0.05$	$49.89 \pm 0.04$		0.940	1.20
HD 240210	1.25	G		49.62	$50.90 \pm 0.08$	$50.92 \pm 0.08$		0.949	1.27
HD 290327	0.90	MS		48.17	$50.58 \pm 0.06$	$50.58 \pm \text{NA}$		0.996	2.41
HIP 2247	0.74	MS		48.26	$50.56 \pm 0.02$	$50.56 \pm 0.02$		0.995	2.30

Continued on next page

Host Star Name	Mass ( $M_{\odot}$ )	Class	Code	$\log J_*$ ( $\text{g cm}^2/\text{s}$ )	$\log \sum J_p$ ( $\text{g cm}^2/\text{s}$ )	$\log J_{sys}$ ( $\text{g cm}^2/\text{s}$ )	n	$K$	$\mathcal{L}$
HIP 5158	0.78	MS		48.23	$49.93 \pm 0.09$	$49.94 \pm 0.09$		0.981	1.70
HIP 14810	0.99	MS	J	47.85	$50.36 \pm 0.01$	$50.36 \pm 0.01$	3	0.997	2.51
HIP 57274	0.73	MS	N	47.59	$49.70 \pm 0.03$	$49.70 \pm 0.03$	3	0.992	2.11
HIP 91258	0.95	MS	J	48.55	$49.32 \pm 0.02$	$49.39 \pm 0.02$		0.856	0.77
iota Hor	1.15	MS		48.86	$50.25 \pm 0.05$	$50.26 \pm 0.04$		0.960	1.38
kappa CrB	1.58	S		49.19	$50.54 \pm 0.03$	$50.55 \pm 0.03$		0.957	1.35
Kepler-4	1.22	MS	TN	48.45	$48.19 \pm 0.07$	$48.64 \pm 0.15$		0.353	-0.26
Kepler-5	1.37	MS	TJ	48.87	$49.67 \pm 0.02$	$49.74 \pm 0.02$		0.865	0.81
Kepler-6	1.21	MS	TJ	48.58	$49.12 \pm 0.02$	$49.23 \pm 0.04$		0.778	0.54
Kepler-7	1.35	S	TJ	49.14	$49.03 \pm 0.10$	$49.39 \pm 0.07$		0.439	-0.11
Kepler-8	1.21	MS	TJ	49.15	$49.08 \pm 0.10$	$49.42 \pm 0.06$		0.459	-0.07
Kepler-10	0.90	MS	TN	47.74	$48.35 \pm 0.09$	$48.44 \pm 0.08$	2	0.803	0.61
Kepler-11	0.96	MS	TN	47.63	$48.63 \pm 0.04$	$48.67 \pm 0.04$	6	0.909	1.00
Kepler-12	1.17	MS	TJ	48.04	$48.97 \pm 0.04$	$49.02 \pm 0.05$		0.895	0.93
Kepler-14	1.51	S	TJ	49.50	$50.39 \pm 0.02$	$50.45 \pm 0.02$		0.887	0.89
Kepler-15	1.02	MS	TJ	48.29	$49.13 \pm 0.05$	$49.19 \pm 0.05$		0.873	0.84
Kepler-17	1.16	MS	TJ	48.77	$49.57 \pm 0.02$	$49.63 \pm 0.03$		0.864	0.80
Kepler-18	0.97	MS	TN	47.65	$48.49 \pm 0.04$	$48.55 \pm 0.04$	3	0.875	0.85
Kepler-20	0.91	MS	TN	47.59	$48.46 \pm 0.17$	$48.51 \pm 0.15$	5	0.880	0.87
Kepler-21	1.34	S	TN	49.41	$47.39 \pm 0.02$	$49.41 \pm 0.10$		0.010	-2.02
Kepler-22	0.97	MS	T	47.77	$48.15 \pm 0.04$	$48.30 \pm 0.04$		0.705	0.38
Kepler-25	1.19	MS	TN	49.06	$48.52 \pm 0.04$	$49.17 \pm 0.12$	2	0.226	-0.53
Kepler-26	0.65	MS	TN	48.12	$48.38 \pm 0.05$	$48.57 \pm 0.04$	4	0.640	0.25
Kepler-27	0.65	MS	T	48.29	$48.53 \pm 0.09$	$48.72 \pm 0.12$	2	0.634	0.24
Kepler-29	1.00	MS	TN	48.58	$48.24 \pm 0.09$	$48.74 \pm 0.17$	2	0.313	-0.34
Kepler-30	0.99	MS	T	48.26	$49.99 \pm 0.04$	$50.00 \pm 0.04$	3	0.982	1.73
Kepler-37	0.80	MS	T	47.96	$47.49 \pm 0.07$	$48.09 \pm 0.12$	3	0.250	-0.48
Kepler-38	0.95	S	T	48.76	$48.53 \pm 0.03$	$48.96 \pm 0.08$		0.367	-0.24
Kepler-39	1.10	S	T	49.53	$50.80 \pm 0.02$	$50.82 \pm 0.02$		0.949	1.27
Kepler-40	1.48	S	TJ	49.57	$49.80 \pm 0.07$	$50.00 \pm 0.07$		0.633	0.24
Kepler-41	0.94	MS	TJ	48.64	$48.84 \pm 0.07$	$49.05 \pm 0.08$		0.610	0.19
Kepler-43	1.32	S	TJ	49.13	$49.82 \pm 0.03$	$49.90 \pm 0.04$		0.830	0.69
Kepler-44	1.19	S	TJ	48.99	$49.30 \pm 0.04$	$49.48 \pm 0.08$		0.673	0.31
Kepler-47	1.04	MS	T	48.58	$48.85 \pm 0.03$	$49.04 \pm 0.03$	2	0.647	0.26
Kepler-48	0.88	MS	TN	47.67	$48.27 \pm 0.06$	$48.37 \pm 0.06$	3	0.801	0.60
Kepler-62	0.69	MS	TN	47.47	$49.04 \pm 0.17$	$49.05 \pm 0.17$	5	0.974	1.57
Kepler-63	0.98	MS	TJ	48.70	$48.49 \pm 0.03$	$48.91 \pm 0.05$		0.382	-0.21
Kepler-68	1.08	MS	TN	47.77	$49.92 \pm 0.03$	$49.93 \pm 0.03$	3	0.993	2.15
Kepler-74	1.40	MS	TJ	48.81	$49.26 \pm 0.06$	$49.40 \pm 0.06$		0.741	0.46
Kepler-75	0.88	MS	TJ	48.51	$50.27 \pm 0.03$	$50.28 \pm 0.03$		0.983	1.76
Kepler-77	0.95	MS	TJ	48.18	$48.88 \pm 0.04$	$48.96 \pm 0.06$		0.834	0.70
Kepler-78	0.81	MS	TN	48.28	$46.55 \pm 0.20$	$48.29 \pm 0.12$		0.018	-1.73
Kepler-89	1.28	MS	TN	48.99	$49.29 \pm 0.08$	$49.47 \pm 0.06$	4	0.666	0.30
Kepler-93	0.91	MS	TN	47.67	$47.18 \pm 0.45$	$47.80 \pm 0.15$		0.243	-0.49
Kepler-94	0.81	MS	TN	47.61	$47.68 \pm 0.11$	$47.95 \pm 0.09$		0.537	0.06
Kepler-95	1.08	MS	T	47.97	$48.00 \pm 0.11$	$48.29 \pm 0.09$		0.513	0.02

Continued on next page

Host Star Name	Mass ( $M_{\odot}$ )	Class	Code	$\log J_*$ ( $\text{g cm}^2/\text{s}$ )	$\log \sum J_p$ ( $\text{g cm}^2/\text{s}$ )	$\log J_{sys}$ ( $\text{g cm}^2/\text{s}$ )	n	$K$	$\mathcal{L}$
Kepler-96	1.00	MS	T	47.70	$47.89 \pm 0.10$	$48.11 \pm 0.09$		0.609	0.19
Kepler-97	0.94	MS	TN	47.70	$47.22 \pm 0.11$	$47.82 \pm 0.12$		0.251	-0.47
Kepler-98	0.99	MS	TN	47.74	$47.14 \pm 0.11$	$47.84 \pm 0.13$		0.202	-0.60
Kepler-99	0.79	MS	TN	47.60	$47.53 \pm 0.11$	$47.87 \pm 0.10$		0.462	-0.07
Kepler-100	1.08	MS	TN	48.72	$47.82 \pm 0.18$	$48.77 \pm 0.14$	2	0.112	-0.90
Kepler-102	0.80	MS	TN	47.60	$47.98 \pm 0.09$	$48.13 \pm 0.08$	4	0.702	0.37
Kepler-103	1.09	MS	T	48.53	$48.86 \pm 0.07$	$49.03 \pm 0.07$	2	0.677	0.32
Kepler-106	1.00	MS	TN	47.49	$48.16 \pm 0.06$	$48.24 \pm 0.06$	3	0.823	0.67
Kepler-109	1.04	MS	TN	48.11	$48.03 \pm 0.03$	$48.37 \pm 0.09$	2	0.458	-0.07
Kepler-113	0.75	MS	TN	47.49	$47.34 \pm 0.05$	$47.72 \pm 0.09$		0.416	-0.15
Kepler-131	1.02	MS	T	47.61	$48.53 \pm 0.08$	$48.58 \pm 0.07$	2	0.893	0.92
Kepler-406	1.07	MS	TN	47.61	$47.71 \pm 0.08$	$47.96 \pm 0.08$	2	0.554	0.09
Kepler-407	1.00	MS	TN	48.30	$46.22 \pm 0.31$	$48.30 \pm 0.16$		0.008	-2.08
Kepler-412	1.17	MS	TJ	48.77	$49.17 \pm 0.05$	$49.32 \pm 0.04$		0.713	0.40
KIC 11442793	1.20	MS	TN	48.70	$50.04 \pm 0.16$	$50.06 \pm 0.15$	7	0.956	1.33
mu Ara	1.15	S		48.78	$50.80 \pm 0.06$	$50.81 \pm 0.06$	4	0.991	2.02
OGLE-TR-10	1.14	MS	TJ	48.52	$49.07 \pm 0.10$	$49.17 \pm 0.11$		0.781	0.55
OGLE2-TR-L9	1.52	MS	TJ	49.70	$49.99 \pm 0.15$	$50.17 \pm 0.10$		0.662	0.29
omega Ser	2.17	G		50.01	$50.34 \pm 0.06$	$50.51 \pm 0.06$		0.683	0.33
omicron CrB	2.13	G		50.02	$50.21 \pm 0.05$	$50.43 \pm 0.07$		0.610	0.20
omicron UMa	3.09	G		50.52	$51.08 \pm 0.04$	$51.18 \pm 0.04$		0.785	0.56
PH-2	0.94	MS	T	48.16	$49.52 \pm 0.10$	$49.54 \pm 0.09$		0.958	1.36
Pr 201	1.23	MS	J	48.99	$49.08 \pm 0.04$	$49.34 \pm 0.03$		0.553	0.09
Pr 211	0.95	MS	J	48.62	$49.44 \pm 0.02$	$49.50 \pm 0.02$		0.866	0.81
Qatar-1	0.85	MS	TJ	48.26	$49.11 \pm 0.04$	$49.17 \pm 0.04$		0.877	0.85
Qatar-2	0.74	MS	TJ	48.35	$49.42 \pm 0.02$	$49.46 \pm 0.02$		0.922	1.07
rho CrB	0.96	MS		48.24	$49.62 \pm 0.03$	$49.64 \pm 0.03$		0.961	1.39
tau Gru	1.24	MS		48.91	$50.26 \pm 0.05$	$50.28 \pm 0.05$		0.957	1.35
TrES-1	0.88	MS	TJ	48.94	$49.07 \pm 0.03$	$49.31 \pm 0.03$		0.575	0.13
TrES-2	0.98	MS	TJ	48.30	$49.28 \pm 0.03$	$49.32 \pm 0.04$		0.905	0.98
TrES-3	0.92	MS	TJ	47.92	$49.37 \pm 0.02$	$49.38 \pm 0.02$		0.966	1.45
TrES-4	1.39	MS	TJ	49.17	$49.32 \pm 0.04$	$49.55 \pm 0.04$		0.586	0.15
TrES-5	0.89	MS	TJ	48.53	$49.35 \pm 0.02$	$49.41 \pm 0.02$		0.867	0.81
WASP-1	1.20	MS	TJ	48.90	$49.22 \pm 0.05$	$49.39 \pm 0.04$		0.677	0.32
WASP-4	0.91	MS	TJ	48.32	$49.18 \pm 0.02$	$49.23 \pm 0.03$		0.879	0.86
WASP-5	1.01	MS	TJ	48.54	$49.36 \pm 0.02$	$49.42 \pm 0.02$		0.869	0.82
WASP-6	0.93	MS	TJ	48.09	$48.94 \pm 0.02$	$49.00 \pm 0.04$		0.876	0.85
WASP-7	1.20	MS	TJ	49.28	$49.32 \pm 0.06$	$49.60 \pm 0.05$		0.522	0.04
WASP-10	0.79	MS	TJ	48.36	$49.67 \pm 0.02$	$49.69 \pm 0.02$		0.954	1.31
WASP-11	0.80	MS	TJ	47.60	$48.93 \pm 0.04$	$48.95 \pm 0.04$		0.955	1.33
WASP-12	1.28	MS	TJ	48.50	$49.29 \pm 0.02$	$49.36 \pm 0.05$		0.860	0.79
WASP-13	1.09	MS	TJ	48.90	$48.99 \pm 0.03$	$49.24 \pm 0.03$		0.552	0.09
WASP-14	1.31	MS	TJ	48.75	$50.15 \pm 0.02$	$50.17 \pm 0.02$		0.962	1.40
WASP-15	1.18	MS	TJ	48.73	$49.05 \pm 0.02$	$49.22 \pm 0.08$		0.673	0.31
WASP-16	1.00	MS	TJ	48.45	$49.16 \pm 0.02$	$49.24 \pm 0.03$		0.839	0.72
WASP-17	1.19	MS	TJ	49.00	$49.02 \pm 0.03$	$49.31 \pm 0.05$		0.515	0.03

Continued on next page

Host Star Name	Mass ( $M_{\odot}$ )	Class	Code	$\log J_*$ (g cm <sup>2</sup> /s)	$\log \sum J_p$ (g cm <sup>2</sup> /s)	$\log J_{sys}$ (g cm <sup>2</sup> /s)	n	K	$\mathcal{L}$
WASP-18	1.22	MS	TJ	49.08	50.13 ± 0.02	50.17 ± 0.02		0.918	1.05
WASP-19	0.93	MS	TJ	48.61	49.07 ± 0.02	49.20 ± 0.06		0.745	0.47
WASP-21	1.01	MS	TJ	48.19	48.77 ± 0.02	48.87 ± 0.04		0.789	0.57
WASP-22	1.10	MS	TJ	48.57	49.03 ± 0.11	49.16 ± 0.09		0.741	0.46
WASP-23	0.78	MS	TJ	48.27	49.10 ± 0.07	49.16 ± 0.06		0.871	0.83
WASP-24	1.18	MS	TJ	48.93	49.28 ± 0.02	49.44 ± 0.03		0.692	0.35
WASP-25	1.00	MS	TJ	48.44	49.03 ± 0.04	49.13 ± 0.04		0.796	0.59
WASP-26	1.12	S	TJ	48.69	49.26 ± 0.10	49.36 ± 0.09		0.787	0.57
WASP-29	0.82	MS	TJ	48.11	48.60 ± 0.04	48.72 ± 0.05		0.754	0.49
WASP-32	1.07	MS	TJ	48.61	49.78 ± 0.02	49.81 ± 0.02		0.936	1.17
WASP-33	1.50	MS	TJ	50.03	49.74 ± 0.31	50.21 ± 0.10		0.340	-0.29
WASP-34	1.01	MS	TJ	48.11	49.05 ± 0.03	49.10 ± 0.03		0.898	0.95
WASP-35	1.07	MS	TJ	48.40	49.12 ± 0.04	49.19 ± 0.04		0.839	0.72
WASP-36	1.02	MS	TJ	48.47	49.50 ± 0.02	49.54 ± 0.03		0.914	1.03
WASP-37	0.92	MS	TJ	48.39	49.49 ± 0.06	49.52 ± 0.06		0.926	1.10
WASP-38	1.23	MS	TJ	48.96	49.84 ± 0.02	49.90 ± 0.02		0.884	0.88
WASP-39	0.93	MS	TJ	48.11	48.71 ± 0.05	48.81 ± 0.06		0.800	0.60
WASP-41	0.95	MS	TJ	48.16	49.19 ± 0.04	49.23 ± 0.04		0.914	1.03
WASP-42	0.88	MS	TJ	48.38	48.97 ± 0.04	49.07 ± 0.04		0.794	0.59
WASP-43	0.58	MS	TJ	48.48	49.14 ± 0.04	49.22 ± 0.03		0.821	0.66
WASP-44	0.95	MS	TJ	48.48	49.14 ± 0.03	49.22 ± 0.04		0.821	0.66
WASP-45	0.91	MS	TJ	48.35	49.21 ± 0.03	49.27 ± 0.03		0.880	0.86
WASP-46	0.96	MS	TJ	48.24	49.44 ± 0.02	49.46 ± 0.03		0.940	1.19
WASP-47	1.08	MS	TJ	48.52	49.36 ± 0.03	49.42 ± 0.03		0.874	0.84
WASP-48	1.19	S	TJ	48.83	49.23 ± 0.04	49.37 ± 0.05		0.714	0.40
WASP-49	0.94	MS	TJ	47.95	48.78 ± 0.04	48.84 ± 0.04		0.871	0.83
WASP-50	0.89	MS	TJ	48.36	49.31 ± 0.04	49.35 ± 0.03		0.899	0.95
WASP-52	0.87	MS	TJ	48.32	48.77 ± 0.03	48.90 ± 0.05		0.742	0.46
WASP-54	1.21	S	TJ	49.08	49.12 ± 0.02	49.40 ± 0.06		0.524	0.04
WASP-55	1.01	MS	TJ	48.51	49.05 ± 0.03	49.16 ± 0.04		0.776	0.54
WASP-56	1.11	MS	TJ	48.20	49.11 ± 0.03	49.16 ± 0.04		0.890	0.91
WASP-57	0.95	MS	TJ	48.49	49.04 ± 0.04	49.15 ± 0.05		0.779	0.55
WASP-58	0.94	MS	TJ	48.52	49.24 ± 0.05	49.32 ± 0.05		0.839	0.72
WASP-59	0.72	MS	TJ	48.21	49.21 ± 0.03	49.25 ± 0.04		0.910	1.00
WASP-60	1.08	MS	TJ	48.57	49.02 ± 0.03	49.15 ± 0.04		0.737	0.45
WASP-61	1.22	MS	TJ	49.10	49.64 ± 0.02	49.75 ± 0.02		0.775	0.54
WASP-62	1.25	MS	TJ	49.00	49.10 ± 0.04	49.36 ± 0.03		0.559	0.10
WASP-63	1.32	S	TJ	48.96	48.95 ± 0.04	49.26 ± 0.06		0.490	-0.02
WASP-64	1.00	MS	TJ	48.55	49.24 ± 0.03	49.32 ± 0.03		0.832	0.69
WASP-66	1.30	MS	TJ	49.32	49.72 ± 0.03	49.86 ± 0.03		0.716	0.40
WASP-67	0.87	MS	TJ	48.28	48.88 ± 0.04	48.98 ± 0.04		0.797	0.59
WASP-71	1.57	S	TJ	49.64	49.71 ± 0.02	49.98 ± 0.05		0.539	0.07
WASP-72	1.33	MS	TJ	48.95	49.42 ± 0.02	49.55 ± 0.03		0.745	0.47
WASP-75	1.14	MS	TJ	48.70	49.27 ± 0.03	49.38 ± 0.03		0.787	0.57
WASP-78	1.33	S	TJ	49.44	49.21 ± 0.04	49.65 ± 0.07		0.371	-0.23
WASP-79	1.52	MS	TJ	49.41	49.33 ± 0.04	49.67 ± 0.04		0.454	-0.08

Continued on next page

Host Star Name	Mass ( $M_{\odot}$ )	Class	Code	$\log J_*$ (g cm <sup>2</sup> /s)	$\log \sum J_p$ (g cm <sup>2</sup> /s)	$\log J_{sys}$ (g cm <sup>2</sup> /s)	n	$K$	$\mathcal{L}$
WASP-80	0.58	MS	TJ	48.40	$48.82 \pm 0.04$	$48.96 \pm 0.03$		0.723	0.42
WASP-103	1.22	MS	TJ	49.14	$49.29 \pm 0.03$	$49.52 \pm 0.03$		0.587	0.15
WTS-1	1.20	MS	TJ	48.87	$49.90 \pm 0.05$	$49.94 \pm 0.04$		0.916	1.04
xi Aql	1.11	G		49.64	$50.07 \pm 0.09$	$50.21 \pm 0.08$		0.726	0.42
XO-1	1.03	MS	TJ	48.01	$49.24 \pm 0.04$	$49.27 \pm 0.04$		0.945	1.24
XO-3	1.41	MS	TJ	49.51	$50.45 \pm 0.02$	$50.49 \pm 0.02$		0.896	0.94
XO-5	1.00	MS	TJ	48.27	$49.34 \pm 0.04$	$49.38 \pm 0.03$		0.922	1.07

# References

- Allen, C. W. 1963, *Allen's Astrophysical Quantities*, London: Athlone Press, 2nd edition, doi:10.1063/1.1325201
- Alves, S., Do Nascimento Jr, J. D., and De Medeiros, J. R. 2010, "On the rotational behaviour of parent stars of extrasolar planets," *Mon. Not. R. Astron. Soc.*, 408, 1770–1777, doi:10.1111/j.1365-2966.2010.17243.x
- Armstrong, J. C. and Larson, S. L. 2007, "Specific Angular Momenta of Extrasolar Planetary Systems," *Bulletin of the American Astronomical Society*, 39, 105
- Armstrong, J. C., Larson, S. L., and Zollinger, R. R. 2011, "Specific Angular Momentum of Extrasolar Planetary Systems," *arXiv.org*, arXiv:0708.1771v2 [astro-ph]
- Barclay, T., Rowe, J. F., Lissauer, J. J., Huber, D., Fressin, F., Howell, S. B., Bryson, S. T., Chaplin, W. J., Désert, J.-M., Lopez, E. D., Marcy, G. W., Mullally, F., Ragozzine, D., Torres, G., Adams, E. R., Agol, E., Barrado, D., Basu, S., Bedding, T. R., Buchhave, L. A., Charbonneau, D., Christiansen, J. L., Christensen-Dalsgaard, J. r., Ciardi, D., Cochran, W. D., Dupree, A. K., Elsworth, Y., Everett, M., Fischer, D. a., Ford, E. B., Fortney, J. J., Geary, J. C., Haas, M. R., Handberg, R., Hekker, S., Henze, C. E., Horch, E., Howard, A. W., Hunter, R. C., Isaacson, H., Jenkins, J. M., Karoff, C., Kawaler, S. D., Kjeldsen, H., Klaus, T. C., Latham, D. W., Li, J., Lillo-Box, J., Lund, M. N., Lundkvist, M., Metcalfe, T. S., Miglio, A., Morris, R. L., Quintana, E. V., Stello, D., Smith, J. C., Still, M., and Thompson, S. E. 2013, "A sub-Mercury-sized exoplanet," *Nature*, 494, 452–454, doi:10.1038/nature11914
- Barnes, J. W., van Eyken, J. C., Jackson, B. K., Ciardi, D. R., and Fortney, J. J. 2013, "Measurement of Spin-Orbit Misalignment and Nodal Precession for the Planet Around Pre-Main-Sequence Star Ptf0 8-8695 From Gravity Darkening," *Astrophys. J.*, 774, 53, doi:10.1088/0004-637X/774/1/53

- Barnes, S. A. 2001, “An assessment of the rotation rates of the host stars of extrasolar planets,” *Astrophys. J.*, 561, 1095
- Barnes, S. A. 2007, “Ages for Illustrative Field Stars Using Gyrochronology: Viability, Limitations, and Errors,” *Astrophys. J.*, 669, 1167–1189, doi:10.1086/519295
- Batalha, N. M., Rowe, J. F., Bryson, S. T., Barclay, T., Burke, C. J., Caldwell, D. A., Christiansen, J. L., Mullally, F., Thompson, S. E., Brown, T. M., Dupree, A. K., Fabrycky, D. C., Ford, E. B., Fortney, J. J., Gilliland, R. L., Isaacson, H., Latham, D. W., Marcy, G. W., Quinn, S. N., Ragozzine, D., Shporer, A., Borucki, W. J., Ciardi, D. R., Gautier, T. N., Haas, M. R., Jenkins, J. M., Koch, D. G., Lissauer, J. J., Rapin, W., Basri, G. S., Boss, A. P., Buchhave, L. A., Carter, J. A., Charbonneau, D., Christensen-Dalsgaard, J., Clarke, B. D., Cochran, W. D., Demory, B.-O., Desert, J.-M., Devore, E., Doyle, L. R., Esquerdo, G. A., Everett, M., Fressin, F., Geary, J. C., Girouard, F. R., Gould, A., Hall, J. R., Holman, M. J., Howard, A. W., Howell, S. B., Ibrahim, K. A., Kinemuchi, K., Kjeldsen, H., Klaus, T. C., Li, J., Lucas, P. W., Meibom, S. r., Morris, R. L., Prša, A., Quintana, E., Sanderfer, D. T., Sasselov, D., Seader, S. E., Smith, J. C., Steffen, J. H., Still, M., Stumpe, M. C., Tarter, J. C., Tenenbaum, P., Torres, G., Twicken, J. D., Uddin, K., Van Cleve, J., Walkowicz, L., and Welsh, W. F. 2013, “Planetary Candidates Observed By Kepler. III. Analysis of the First 16 Months of Data,” *Astrophys. J. Suppl. Ser.*, 204, 24, doi:10.1088/0067-0049/204/2/24
- Berget, D. and Durrance, S. 2010, “Angular Momentum in Extrasolar Planetary Systems,” *J. Southeast. Assoc. Res. Astron.*, 3, 32–35
- Bodenheimer, P. 1995, “Angular Momentum Evolution of Young Stars and Disks,” *Annu. Rev. Astron. Astrophys.*, 33, 199–238, doi:10.1146/annurev.aa.33.090195.001215
- Brosche, P. 1963, “Über das Masse-Drehimpuls-Diagramm von Spiralnebeln und anderen Objekten,” *Zeitschrift für Astrophys.*, 57, 143–155
- Brosche, P. 1969, “The distribution of angular momentum in planetary systems,” *Obs.*, 89, 206
- Brosche, P. 1980, “Mass Angular Momentum Diagram of Astronomical Objects,” in P. G. Bergmann and V. D. Sabbata eds. *Cosmol. Gravit. spin, torsion, rotation, supergravity*, 375–382
- Brosche, P. 1986, “Angular momentum versus mass,” *Comments Astrophys.*, 11, 213

- Carrasco, L., Roth, M., and Serrano, A. 1982, “Density scaling of the angular momentum versus mass universal relationship,” *Astron. Astrophys.*, 106, 89–93
- Carroll, B. W. and Ostlie, D. A. 2006, *An Introduction to Modern Astrophysics*, 1, San Francisco: Pearson, Addison-Wesley, 2nd edition
- Claret, A. 1995, “Stellar models for a wide range of initial chemical compositions until helium burning. I. From  $X=0.60$  to  $X=0.80$  for  $Z=0.02$ ,” doi:10.1051/aas:1998452
- Claret, A. 2004, “New grids of stellar models including tidal-evolution constants up to carbon burning,” *Astron. Astrophys.*, 424, 919–925, doi:10.1051/0004-6361:20040470
- Claret, A. 2012, “Gravity-darkening exponents and apsidal-motion constants for pre-main-sequence models,” *Astron. Astrophys.*, 541, A113, doi:10.1051/0004-6361/201218881
- Claret, A. and Giménez, A. 1989, “The moment of inertia of main sequence stars,” *Astron. Astrophys. Suppl. Ser.*, 81, 37–45
- Claret, A. and Giménez, A. 1990, “The moment of inertia of low mass stars,” *Astrophys. Space Sci.*, 169, 215–217, doi:10.1007/BF00640716
- Cox, A. N. 2000, *Allen’s Astrophysical Quantities*, London: Athlone Press, 1st edition, doi:10.1063/1.1325201
- Criss, R. E. and Hofmeister, A. M. 2015, “Analytical representations for simple and composite polytropes and their moments of inertia,” *New Astron.*, 36, 26–31, doi:10.1016/j.newast.2014.09.012
- Cumming, A., Butler, R. P., Marcy, G. W., Vogt, S. S., Wright, J. T., and Fischer, D. a. 2008, “The Keck Planet Search: Detectability and the Minimum Mass and Orbital Period Distribution of Extrasolar Planets,” *Publ. Astron. Soc. Pacific*, 120, 531–554, doi:10.1086/588487
- Dumusque, X., Bonomo, A. S., Haywood, R. D., Malavolta, L., Ségransan, D., Buchhave, L. a., Cameron, A. C., Latham, D. W., Molinari, E., Pepe, F., Udry, S., Charbonneau, D., Cosentino, R., Dressing, C. D., Figueira, P., Fiorenzano, A. F. M., Gettel, S., Harutyunyan, A., Horne, K., Lopez-Morales, M., Lovis, C., Mayor, M., Micela, G., Motalebi, F., Nascimbeni, V., Phillips, D. F., Piotto, G., Pollacco, D., Queloz, D., Rice, K., Sasselov, D., Sozzetti, A., Szentgyorgyi, A., and Watson, C. 2014, “The Kepler-10 Planetary System Revisited by HARPS-N: A Hot Rocky World and a Solid Neptune-Mass Planet,” *Astrophys. J.*, 789, 154, doi:10.1088/0004-637X/789/2/154

- Duquennoy, A. and Mayor, M. 1991, “Multiplicity among solar-type stars in the solar neighbourhood. II - Distribution of the orbital elements in an unbiased sample,” *Astronomy and Astrophysics*, 248, 485–524
- EOD, “Exoplanet Orbit Database,” URL: <http://exoplanets.org>, accessed on 5 Dec 2014
- Fabrycky, D. C. and Winn, J. N. 2009, “Exoplanetary Spin-Orbit Alignment: Results from the Ensemble of Rossiter-McLaughlin Observations,” *Astrophys. J.*, 696, 1230, doi:10.1088/0004-637X/696/2/1230
- Feuersänger, C. 2010, *Manual for Package pgfplots*, 1–163
- Fischer, D. A. and Valenti, J. 2005, “The Planet-Metallicity Correlation,” *Astrophys. J.*, 622, 1102–1117, doi:10.1086/428383
- Fukuda, I. 1982, “A statistical study of rotational velocities of the stars,” *Publ. Astron. Soc. Pacific*, 94, 271, doi:10.1086/130977
- Giguere, M. J., Fischer, D. A., Howard, A. W., Johnson, J. A., Henry, G. W., Wright, J. T., Marcy, G. W., Isaacson, H. T., Hou, F., and Spronck, J. 2012, “A High-eccentricity Component in the Double-planet System around HD 163607 and a Planet around HD 164509,” *Astrophys. J.*, 744, 4, doi:10.1088/0004-637X/744/1/4
- Gillon, M., Doyle, A. P., Lendl, M., Maxted, P. F. L., Triaud, A. H. M. J., Anderson, D. R., Barros, S. C. C., Bento, J., Collier Cameron, A., Enoch, B., Faedi, F., Hellier, C., Jehin, E., Magain, P., Montalbán, J., Pepe, F., Pollacco, D., Queloz, D., Smalley, B., Segransan, D., Smith, A. M. S., Southworth, J., Udry, S., West, R. G., and Wheatley, P. J. 2011, “WASP-50b: a hot Jupiter transiting a moderately active solar-type star,” *Astron. Astrophys.*, 88, 9, doi:10.1051/0004-6361/201117198
- Godłowski, W., Szydlowski, M., Flin, P., and Biernacka, M. 2003, “Rotation of the Universe and the Angular Momenta of Celestial Bodies,” *Gen. Relativ. Gravit.*, 35, 907–913, doi:10.1023/A:1022959523795
- Gonzalez, G. 1997, “The stellar metallicity-giant planet connection,” *Mon. Not. R. Astron. Soc. Notices of the Royal Astronomical Society*, 285, 403–412
- Hadden, S. and Lithwick, Y. 2014, “Densities and Eccentricities of 139 Kepler Planets from Transit Time Variations,” *Astrophys. J.*, 787, 80, doi:<http://dx.doi.org/10.1088/0004-637X/787/1/80>

- Han, E., Wang, S. X., Wright, J. T., Feng, Y. K., Zhao, M., Brown, J. I., and Hancock, C. 2014, “The Exoplanet Orbit Database II: Updates to exoplanets.org,” *Publ. Astron. Soc. Pacific*, 126, 827
- Hansen, C. J., Kawaler, S. D., and Trimble, V. 2004, *Stellar Interiors: Physical Principles, Structure, and Evolution*, New York: Springer-Verlag, 2nd edition, 526
- Herbst, W., Eisloffel, J., Mundt, R., and Scholz, A. 2007, “The Rotation of Young Low-Mass Stars and Brown Dwarfs,” in B. Reipurth, D. Jewitt, and K. Keil eds. *Protostars Planets V*, Tucson: University of Arizona Press, 297–311
- van den Heuvel, E. P. J. 1966, “The distribution of angular momentum in planetary systems,” *Obs.*, 86, 113–115
- Ilin, V. B. 1985, “Models of zero-age main sequence stars from 0.15 to 125 solar masses,” *Trudy*, 40, 25–41
- Kawaler, S. D. 1987, “Angular momentum in stars: The Kraft curve revisited,” *Publ. Astron. Soc. Pacific*, 99, 1322, doi:10.1086/132120
- Kawaler, S. D. 1988, “Angular momentum loss in low-mass stars,” *Astrophys. J.*, 333, 236, doi:10.1086/166740
- KOI, “Kepler Objects of Interest Catalog,” URL: [http://archive.stsci.edu/kepler/confirmed\\_planets](http://archive.stsci.edu/kepler/confirmed_planets), accessed on 2015-07-01
- Kraft, R. P. 1965, “Studies of Stellar Rotation. I. Comparison of Rotational Velocities in the Hyades and Coma Clusters,” *Astrophys. J.*, 142, 681–702
- Kraft, R. P. 1967, “Studies of Stellar Rotation. V. The Dependence of Rotation on Age among Solar-Type Stars,” *Astrophys. J.*, 150, 551, doi:10.1086/149359
- Kraft, R. P. 1970, “Stellar Rotation,” in G. Herbig ed. *Spectrosc. Astrophys. An Assess. Contrib. Otto Struve*, Berkeley; Los Angeles; London: University of California Press, Ch. 10, 385–422
- Larson, R. B. 1981, “Turbulence and star formation in molecular clouds,” *Mon. Not. R. Astron. Soc.*, 194, 809–826
- Liu, Y.-Z., Deng, Z.-G., and Cao, S.-L. 1985, “Characteristic actions  $h^{(s)}$  in the structure of the universe,” *Astrophys. Space Sci.*, 116, 215–224

- Lovis, C., Ségransan, D., Mayor, M., Udry, S., Benz, W., Bertaux, J.-L., Bouchy, F., Correia, A. C. M., Laskar, J., Lo Curto, G., Mordasini, C., Pepe, F., Queloz, D., and Santos, N. C. 2011, “The HARPS search for southern extra-solar planets. XXVIII. Up to seven planets orbiting HD 10180: probing the architecture of low-mass planetary systems,” *Astron. Astrophys.*, 528, A112, doi:10.1051/0004-6361/201015577
- Marcy, G. W., Isaacson, H., Howard, A. W., Rowe, J. F., Jenkins, J. M., Bryson, S. T., Latham, D. W., Howell, S. B., Gautier, T. N., Batalha, N. M., Rogers, L., Ciardi, D., Fischer, D. A., Gilliland, R. L., Kjeldsen, H., Christensen-Dalsgaard, J. r., Huber, D., Chaplin, W. J., Basu, S., Buchhave, L. A., Quinn, S. N., Borucki, W. J., Koch, D. G., Hunter, R., Caldwell, D. A., Van Cleve, J., Kolbl, R., Weiss, L. M., Petigura, E., Seager, S., Morton, T., Johnson, J. A., Ballard, S., Burke, C., Cochran, W. D., Endl, M., MacQueen, P., Everett, M. E., Lissauer, J. J., Ford, E. B., Torres, G., Fressin, F., Brown, T. M., Steffen, J. H., Charbonneau, D., Basri, G. S., Sasselov, D. D., Winn, J., Sanchis-Ojeda, R., Christiansen, J., Adams, E., Henze, C., Dupree, A., Fabrycky, D. C., Fortney, J. J., Tarter, J., Holman, M. J., Tenenbaum, P., Shporer, A., Lucas, P. W., Welsh, W. F., Orosz, J. A., Bedding, T. R., Campante, T. L., Davies, G. R., Elsworth, Y., Handberg, R., Hekker, S., Karoff, C., Kawaler, S. D., Lund, M. N., Lundkvist, M., Metcalfe, T. S., Miglio, A., Aguirre, V. S., Stello, D., White, T. R., Boss, A., Devore, E., Gould, A., Prsa, A., Agol, E., Barclay, T., Coughlin, J., Brugamyer, E., Mullally, F., Quintana, E. V., Still, M., Thompson, S. E., Morrison, D., Twicken, J. D., Désert, J.-M., Carter, J., Crepp, J. R., Hébrard, G., Santerne, A., Moutou, C., Sobeck, C., Hudgins, D., Haas, M. R., Robertson, P., Lillo-Box, J., and Barrado, D. 2014, “Masses, Radii, and Orbits of Small Kepler Planets: the Transition From Gaseous To Rocky Planets,” *Astrophys. J. Suppl. Ser.*, 210, doi:10.1088/0067-0049/210/2/20
- Mayor, M. and Queloz, D. 1995, “A Jupiter-mass companion to a solar-type star,” *Nature*, 378, 355–359, doi:10.1038/378355a0
- McNally, D. 1965, “The distribution of angular momentum among main sequence stars,” *Obs.*, 85, 166–169
- Mestel, L. 1968, “Magnetic braking by a stellar wind-I,” *Mon. Not. R. Astron. Soc.*, 138, 359
- Motz, L. 1952, “On the Radius of Gyration of Stars,” *Astrophys. J.*, 115, 562, doi:10.1086/145570

- NASA, “NASA Exoplanet Archive,” URL: <http://exoplanetarchive.ipac.caltech.edu>, accessed on 9 Jan 2015
- Ochsenbein, F., Bauer, P., and Marcout, J. 2000, “The VizieR database of astronomical catalogues,” *Astron. Astrophys. Suppl. Ser.*, 143, 23–32
- Ohta, Y., Taruya, A., and Suto, Y. 2005, “The Rossiter-McLaughlin Effect and Analytic Radial Velocity Curves for Transiting Extrasolar Planetary Systems,” *Astrophys. J.*, 622, 1118–1135, doi:10.1086/428344
- de Pater, I. and Lissauer, J. J. 2001, *Planetary Sciences*, Cambridge, UK: Cambridge University Press, 544
- Paz-Chinchón, F., Leão, I. C., Bravo, J. P., de Freitas, D. B., Ferreira Lopes, C. E., Alves, S., Catelan, M., Canto Martins, B. L., and de Medeiros, J. R. 2015, “The rotational behavior of Kepler stars with planets,” *Astron. J.*
- Pinsonneault, M. H., Kawaler, S. D., and Demarque, P. 1990, “Rotation of low-mass stars: A new probe of stellar evolution,” *Astrophys. J. Suppl. Ser.*, 74, 501, doi:10.1086/191507
- Ray, T. 2012, “Losing spin: the angular momentum problem,” *Astron. Geophys.*, 53, 5.19–5.22, doi:10.1111/j.1468-4004.2012.53519.x
- Rein, H. 2012, “A proposal for community driven and decentralized astronomical databases and the Open Exoplanet Catalogue,” *arXiv.org*, arXiv:1211.7121v2 [astro-ph.EP]
- Ruciński, S. M. 1988, “Rotational properties of composite polytrope models,” *Astron. J.*, 95, 1895, doi:10.1086/114784
- Schatzman, E. 1962, “A theory of the role of magnetic activity during star formation,” *Annales d’Astrophysique*, 25
- Schlaufman, K. C. 2010, “Evidence of Possible Spin-Orbit Misalignment Along the Line of Sight in Transiting Exoplanet Systems,” *Astrophys. J.*, 719, 602–611, doi:10.1088/0004-637X/719/1/602
- Sigurdsson, S., Richer, H. B., Hansen, B. M., Stairs, I. H., and Thorsett, S. E. 2003, “A Young White Dwarf Companion to Pulsar B1620-26: Evidence for Early Planet Formation,” *Science*, 301, 193–196, doi:10.1126/science.1086326
- Skumanich, A. 1972, “Time Scales for CA II Emission Decay, Rotational Braking, and Lithium Depletion,” *Astrophys. J.*, 171, 565, doi:10.1086/151310

- Smith, A. M. S., Anderson, D. R., Bouchy, F., Collier Cameron, A., Doyle, A. P., Fumel, A., Gillon, M., Hébrard, G., Hellier, C., Jehin, E., Lendl, M., Maxted, P. F. L., Moutou, C., Pepe, F., Pollacco, D., Queloz, D., Santerne, A., Segransan, D., Smalley, B., Southworth, J., Triaud, A. H. M. J., Udry, S., and West, R. G. 2013, “WASP-71b: a bloated hot Jupiter in a 2.9-day, prograde orbit around an evolved F8 star,” *Astron. Astrophys.*, 552, A120, doi:10.1051/0004-6361/201220727
- Stauffer, J. R. and Hartmann, L. W. 1986, “The rotational velocities of low-mass stars,” *Publ. Astron. Soc. Pacific*, 98, 1233
- Steffen, J. H., Fabrycky, D. C., Ford, E. B., Carter, J. A., Désert, J.-M., Fressin, F., Holman, M. J., Lissauer, J. J., Moorhead, A. V., Rowe, J. F., Ragozzine, D., Welsh, W. F., Batalha, N. M., Borucki, W. J., Buchhave, L. A., Bryson, S., Caldwell, D. A., Charbonneau, D., Ciardi, D. R., Cochran, W. D., Endl, M., Everett, M. E., Gautier, T. N., Gilliland, R. L., Girouard, F. R., Jenkins, J. M., Horch, E., Howell, S. B., Isaacson, H., Klaus, T. C., Koch, D. G., Latham, D. W., Li, J., Lucas, P., MacQueen, P. J., Marcy, G. W., McCauliff, S., Middour, C. K., Morris, R. L., Mullally, F. R., Quinn, S. N., Quintana, E. V., Shporer, A., Still, M., Tenenbaum, P., Thompson, S. E., Twicken, J. D., and Van Cleve, J. 2012, “Transit timing observations from Kepler - III. Confirmation of four multiple planet systems by a Fourier-domain study of anticorrelated transit timing variations,” *Mon. Not. R. Astron. Soc.*, 421, 2342–2354, doi:10.1111/j.1365-2966.2012.20467.x
- Tarafdar, S. P. and Vardya, M. S. 1971, “On the variation of specific angular momentum among Main Sequence stars,” *Astrophys. Space Sci.*, 13, 234–248, doi:10.1007/BF00656330
- Tassoul, J. L. 2000, *Stellar Rotation*, New York: Cambridge University Press
- Tuomi, M. 2012, “Evidence for nine planets in the HD 10180 system,” *Astron. Astrophys.*, 543, A52, doi:10.1051/0004-6361/201118518
- Valsecchi, F. and Rasio, F. A. 2014, “Tidal Dissipation and Obliquity Evolution in Hot Jupiter Systems,” *Astrophys. J.*, 786, 102, doi:10.1088/0004-637X/786/2/102
- Walpole, R. E., Myers, R. H., Myers, S. L., and Ye, K. 2007, *Probability and Statistics for Engineers and Scientists*, Upper Saddle River, NJ: Pearson Prentice Hall, 8th edition
- Wesson, P. S. 1979, “Self-similarity and the angular momenta of astronomical systems: A basic rule in astronomy,” *Astron. Astrophys.*, 80, 296

- Wesson, P. S. 1983, "Clarification of the angular momentum/mass relation ( $J = pM$ -squared) for astronomical objects," *Astron. Astrophys.*, 119, 313–314
- Wilson, O. C. 1963, "A Probable Correlation Between Chromospheric Activity and Age in Main-Sequence Stars," *Astrophys. J.*, 138, 832, doi:10.1086/147689
- Wolff, S. C. and Simon, T. 1997, "The Angular Momentum of Main-Sequence Stars and its Relation to Stellar Activity," *Publ. Astron. Soc. Pacific*, 109, 759–775
- Wolff, S. C., Strom, S. E., and Hillenbrand, L. A. 2004, "The angular momentum evolution of 0.1-10 M stars from the birth line to the main sequence," *Astrophys. J.*, 601, 979–999, doi:10.1086/380503
- Wolszczan, A. and Frail, D. A. 1992, "A planetary system around the millisecond pulsar PSR1257 + 12," *Nature*, 355, 145–147, doi:10.1038/355145a0
- Wright, J., Fakhouri, O., Marcy, G., Han, E., Feng, Y., Johnson, J., Howard, A., Valenti, J., Anderson, J., and Piskunov, N. 2011, "The Exoplanet Orbit Database," *Publ. Astron. Soc. Pacific*, 123, 412–422, doi:10.1086/659427
- Xiao, X., White, E. P., Hooten, M. B., and Durham, S. L. 2011, "On the use of log-transformation vs. nonlinear regression for analyzing biological power laws," *Ecology*, 92, 1887–1894, doi:10.1890/11-0538.1
- Yoder, C. F. 1995, "Astrometric and Geodetic Properties of Earth and the Solar System," in T. J. Ahrens ed. *Glob. Earth Phys. A Handb. Phys. Constants*, 1 of AGU Reference Shelf: American Geophysical Union, Ch. 1, 1
- Zoghbi, J.-P. A. 2013, "Quantization of Planetary Systems and its Dependency on Stellar Rotation," *Publ. Astron. Soc. Aust.*, 28, 177–201, doi:10.1071/AS09062